#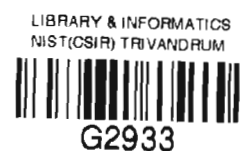 OLIGO(*P*-PHENYLENEVINYLENE) DERIVED π-GELS: MODULATION OF OPTICAL PROPERTIES AND APPLICATION AS EXCITATION ENERGY DONOR SCAFFOLDS

THESIS SUBMITTED TO
THE UNIVERSITY OF KERALA
FOR THE DEGREE OF
DOCTOR OF PHILOSOPHY
IN CHEMISTRY
UNDER THE FACULTY OF SCIENCE

By

PRAVEEN V. K.

PHOTOSCIENCES AND PHOTONICS GROUP
CHEMICAL SCIENCES AND TECHNOLOGY DIVISION
REGIONAL RESEARCH LABORATORY (CSIR)
TRIVANDRUM 695 019
KERALA, INDIA
APRIL 2007

Dedicated To . . .

My Beloved Parents and Brother

DECLARATION

I hereby declare that the matter embodied in the thesis entitled: **"Oligo(*p*-phenylenevinylene) Derived π-Gels: Modulation of Optical Properties and Application as Excitation Energy Donor Scaffolds"** is the result of the investigations carried out by me at the Photosciences and Photonics Group, Chemical Sciences and Technology Division, Regional Research Laboratory (CSIR), Trivandrum, under the supervision of Dr. A. Ajayaghosh and the same has not been submitted elsewhere for any other degree.

In keeping with the general practice of reporting scientific observations, due acknowledgement has been made wherever the work described is based on the findings of other investigators.

Praveen V. K.

PHOTOSCIENCES AND PHOTONICS GROUP
CHEMICAL SCIENCES AND TECHNOLOGY DIVISION
REGIONAL RESEARCH LABORATORY (CSIR)
TRIVANDRUM-695 019, INDIA

Dr. A. AJAYAGHOSH, F.A. Sc.
SCIENTIST and HEAD

Phone: 91-471-2515306
Fax: 91-471-2490186, 2491712
E. mail: aajayaghosh@rediffmail.com

April 02, 2007

CERTIFICATE

This is to certify that the work embodied in the thesis entitled:

"Oligo(*p*-phenylenevinylene) Derived π-Gels: Modulation of Optical Properties and Application as Excitation Energy Donor Scaffolds" has been carried out by Mr. Praveen V. K. under my supervision at the Photosciences and Photonics Group of the Regional Research Laboratory (CSIR), Trivandrum and the same has not been submitted elsewhere for a degree.

A. Ajayaghosh
(Thesis Supervisor)

ACKNOWLEDGEMENTS

CONTENTS

CHAPTER-4 *Molecular Wire Encapsulated π-Organogels: A New Design of Efficient Supramolecular Light Harvesting Antenna*

PREFACE

Excitation energy transfer within and between molecular assemblies plays a key role in natural photosynthesis. The remarkable efficiency and directionality with which this process occurs in natural light harvesting assemblies is matchless. Inspired by nature, researchers have been attempting to mimic such process with the help of synthetic molecular architectures. The sustained efforts to unravel the processes involved in the natural light harvesting assemblies have not only helped to design artificial light harvesting assemblies but also to the development of nanoscale opto-electronic and photonic devices. A challenging task in this area is the organization of chromophores with precise control on distance and orientation, which is an indispensable criterion for efficient energy transfer process. Several strategies have been adopted for this purpose. Among them supramolecular organization of chromophores has attracted considerable interest, particularly of linear π-conjugated systems, due to the importance in the emerging field of molecular and supramolecular electronics.

Among the various class of π-conjugated systems, oligo(p-phenylene-vinylene)s (OPVs) are one of the well studied class of compounds because of their wide ranging application in opto-electronic devices. The optical and electronic properties of these molecules strongly depend upon structural features and hence can be modulated by variation in conjugation length and donor-acceptor substitution. An alternative approach to the modulation of the electronic properties is by inducing intermolecular interactions using weak noncovalent forces. Among these interactions hydrogen bonding and π-stacking are widely exploited for the self-assembly of OPVs. Recently, it has been recognized that appropriately functionalized OPVs self-assemble to form gel in organic solvents. It has been observed that the gelation of OPVs has remarkable influence in modulating the optical properties of the parent chromophores. The above mentioned aspects of gelation of OPVs are highly attractive for the design of light harvesting assemblies with tunable optical properties.

The present thesis entitled "**Oligo(*p*-phenylenevinylene) Derived π-Gels: Modulation of Optical Properties and Application as Excitation Energy Donor Scaffolds**" embodies the results of our attempt towards achieving this goal.

The thesis is comprised of four chapters. In the first chapter, a review on excitation energy transfer in molecular self-assemblies and organogels is described. Emphasis is given for energy transfer in OPV self-assemblies. At the beginning of the chapter, a brief description of natural light harvesting assemblies and theories of energy transfer is given. Attention has been paid to have a discussion on various supramolecular methods in organizing phenylenevinylene donors and various acceptors. The subsequent section deals with use of organogels as medium to organize donor-acceptor chromophores to facilitate energy transfer process. At the end of the first chapter, the aim and the outline of the thesis are also presented.

The second chapter of the thesis describes the design, synthesis and properties of a few donor-acceptor substituted oligo(*p*-phenylenevinylene)s derived π-organogels.[1] The design strategy involves the functionalization of the rigid π-conjugated backbone of OPVs with dipolar end functional groups and long hydrocarbon side chains. These molecules are analogous to quadrupolar systems with A-D-D-D-A type substitution pattern, which are reported to have large two photon absorption crossection. Detailed optical studies in polar solvents revealed the role of end functional groups in modulating the optical properties of OPVs. The OPV derivatives with nonconjugated ester, conjugated ester, ester cyano and dicyano end functional groups showed blue, green, orange and red fluoresce respectively. However, in aliphatic nonpolar solvents, these molecules exhibited a strong tendency to form aggregates which is clear from their optical properties. Interestingly, when the concentration of OPVs is increased above a critical value, self-supporting gels are formed in nonpolar solvents except in the case of OPV with dicyano moiety. Gelation of OPVs resulted in remarkable change in the emission properties when compared to that

in polar solvents. The blue emission of the OPV with a nonconjugated ester moiety is shifted to green in the gel state. Similarly the green and orange emission of OPVs with conjugated ester and ester cyano moiety are shifted to yellow and red, respectively. Thus a combined molecular and supramolecular approach is shown to be effective for the modulation of the optoelectronic properties of A-D-D-D-A type OPVs that form molecular aggregates to self-assembled gels.

In the third chapter, selective energy transfer from self-assembled oligo(p-phenylenevinylene) in the gel state to entrapped Rhodamine B is described.[2,3] The emission of OPV is shifted significantly to long wavelength region which matches with absorption of Rhodamine B thereby facilitating energy transfer. The efficiency of fluorescence resonance energy transfer (FRET) is considerably influenced by the ability of the OPVs to form self-assembled aggregates and hence could be controlled by structural variation of the molecules and polarity of the solvent. This aspect is demonstrated with the help of OPVs with different end functional groups such as –OH, –OMe, –COOC$_2$H$_5$ and –COOH. The edges of the H-bonded nanotapes formed by the self-assembly of OPVs could be polar due to the presence of free –COOH and –OH groups. Therefore, the polar acceptor molecules may preferably localized on the edges of the tape. FRET occurs exclusively from the self-assembled OPVs to the physically attached acceptors and not from the individual donor molecules. Most importantly, FRET could be controlled by temperature due to the thermally reversible self-assembly process. Energy transfer efficiency from an OPV xerogel to the dye in the solid state is higher than that in the solution state. The present study illustrates that the self-assembly of chromophores facilitates temperature and solvent controlled FRET within the supramolecular tapes.

In the fourth chapter, we demonstrate a novel approach to create light harvesting supramolecular self-assembly in which oligo(p-phenylenevinylene) based π-organogels act as an energy donor and entrapped molecular wires as energy trap. Pyrrolenevinylene-co-phenylenevinylene (PYPV) based oligomer

(average molecular weight (M_n) of ~ 4358 g/mol and polydispersity index = 1.2) was used as the energy acceptor. Encapsulation of PYPV in small concentration as low as < 2 mol% to the OPV gel facilitate efficient FRET (rate of energy transfer, k_{ET} = 2.99 x 10^9 s^{-1}) which is evident from the strong quenching of the OPV emission with concomitant formation of the oligomer emission. Time resolved emission, anisotropy and wavelength dependent lifetime studies provided evidence for energy migration (rate of energy migration, k_{EM} = 1.28 x 10^{10} s^{-1}) in donor scaffold which ultimately facilitate funneling of excitation energy from a long distance of the donor scaffold to a few encapsulated molecular wires. Energy transfer is feasible only in the case of gel and occurs exclusively from the donor (OPV) self-assembly to the molecular wires.

In summary, we have carried out a systematic investigation on the gelation behavior of OPVs and their application as scaffolds for excitation energy transfer to suitable acceptors. Using rationale molecular and supramolecular approaches we could design organogelators with tunable emission. Encapsulation of a molecular wire into these gels facilitated efficient energy funneling due to fast exciton migration. We hope these studies will open new avenues for π-organogels in the realm of advanced functional materials especially in the emerging area of supramolecular electronics.

References

1. A. Ajayaghosh, V. K. Praveen, S. Srinivasan, R. Varghese, *Adv. Mater.* **2007**, *19*, 411–415.
2. V. K. Praveen, S. J. George, R. Varghese, C. Vijayakumar, A. Ajayaghosh, *J. Am. Chem. Soc.* **2006**, *128*, 7542–7550.
3. A. Ajayaghosh, S. J. George, V. K. Praveen, *Angew. Chem., Int. Ed.* **2003**, *42*, 332–335.

Chapter 1

Molecular Self-Assemblies and Organogels as Excitation Energy Transfer Scaffolds: An Overview

H-bond assemblies

Vesicles or Nanoparticles

Excitation Energy Transfer in Molecular Self-Assemblies

Donor

FRET

Acceptor

Helical structures

Organogels
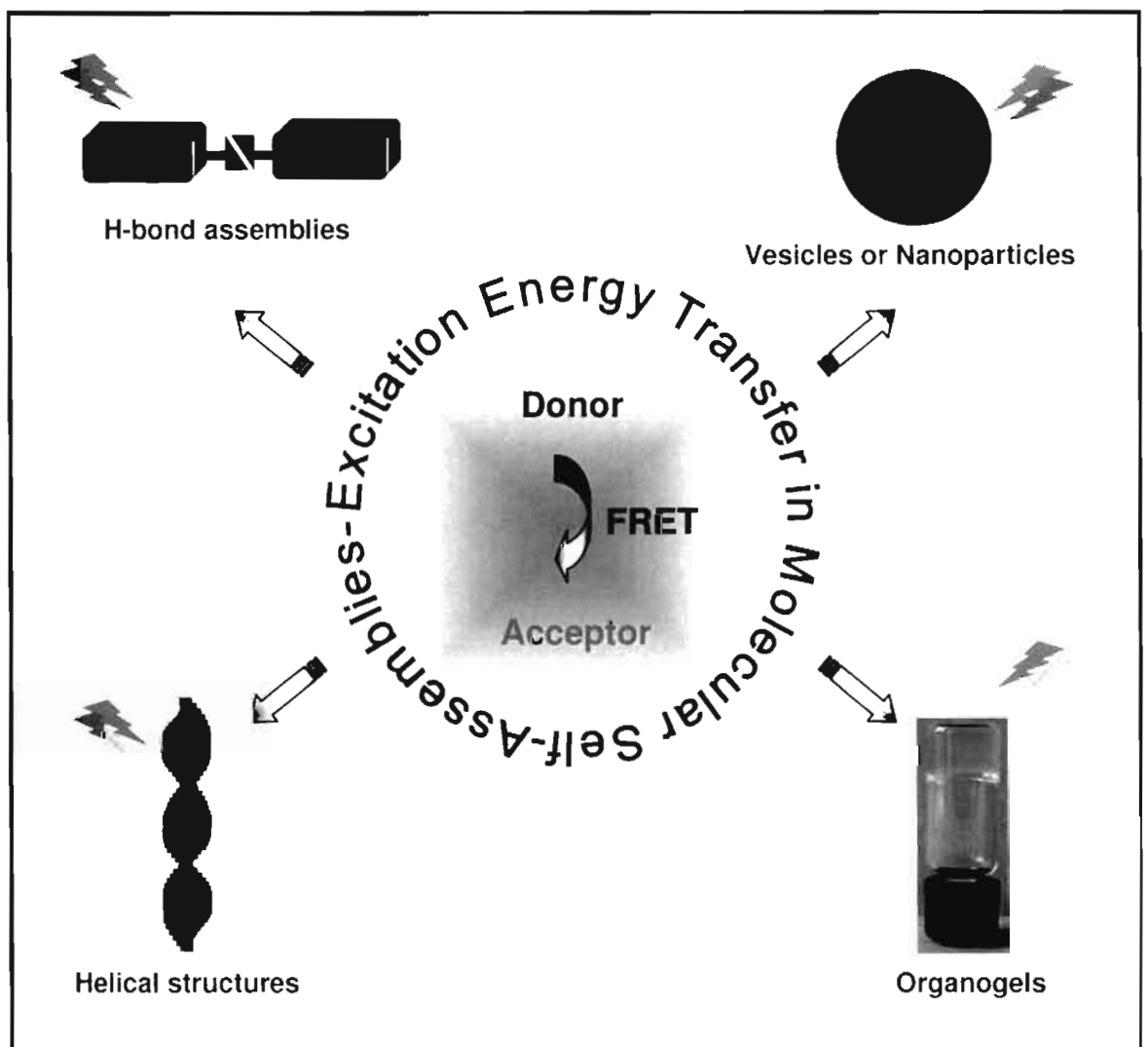
1.1. Abstract

Understanding of the fundamental principles and mechanism of natural light harvesting processes has helped chemists to create artificial molecular self-assemblies for light harvesting applications. A challenging task in this area is the organization of chromophores with precise control on distance and orientation, which is an indispensable criterion for efficient light harvesting. In recent years self-assembly of chromophores has been recognized as an efficient strategy for this purpose. Moreover, self-assembly of chromophores especially those of linear π-conjugated systems have paramount importance in the emerging field of molecular and supramolecular electronics. In the present chapter an overview on excitation energy transfer in oligo(p-phenylenevinylene) (OPV) self-assemblies is presented. Different supramolecular approaches in organizing OPV donors and various acceptors that facilitate the efficient energy transfer processes are discussed. Attention has been paid on discussing excitation energy transfer in organogels, a novel supramolecular scaffold for the organization of donor and acceptor chromophores. Finally the aim and outline of the thesis is presented.

1.2. Introduction

Nature's most sophisticated and important solar energy storage system is found in photosynthetic organisms including plants, algae and photosynthetic bacteria. It is through photosynthesis, these organisms convert the energy harvested from sunlight into increasingly more stable forms of energy.[1,2] In order to facilitate this process in an efficient manner, photosynthetic organisms share some common features despite the wide variety of their structures and functions. Pigments (chlorophylls and carotenoids) are the primary components of light harvesting systems, responsible for converting the energy of an absorbed photon into an electronic excitation. This excitation energy is then used for the transport of electrons across the cell membrane resulting in a voltage gradient. Most pigments are not directly involved in the charge separation process; instead their excitation energy is transferred eventually to a reaction center.

In contrast to reaction centers, antennae complexes of photosynthetic organisms display an amazing diversity according to the growth conditions such as light intensity and temperature. A typical example is the light harvesting complex of purple bacteria photosynthetic unit.[1] The photosynthetic membrane of purple bacteria contains two types of light harvesting complex, namely LHI and LHII (Figure 1.1). The small peripheral LHII comprise of two rings of bacteriochlorophylls (BChls)–a set of sixteen molecules oriented perpendicular to the membrane plane is arranged in almost face-to-face manner like a turbine wheel

(upper ring), and another set of eight molecules is located in the lower ring of LHII with their tetrapyrrol rings nearly parallel to the membrane plane. Because of different chemical environments, the two sets of BChl molecules have different absorption and photophysical properties. The sixteen Bchl molecules belong to the upper ring of LHII have the absorption maximum at 850 nm (and are therefore named B850) and the eight BChl molecules located in the lower ring have the absorption maximum at 800 nm (B800 nm).
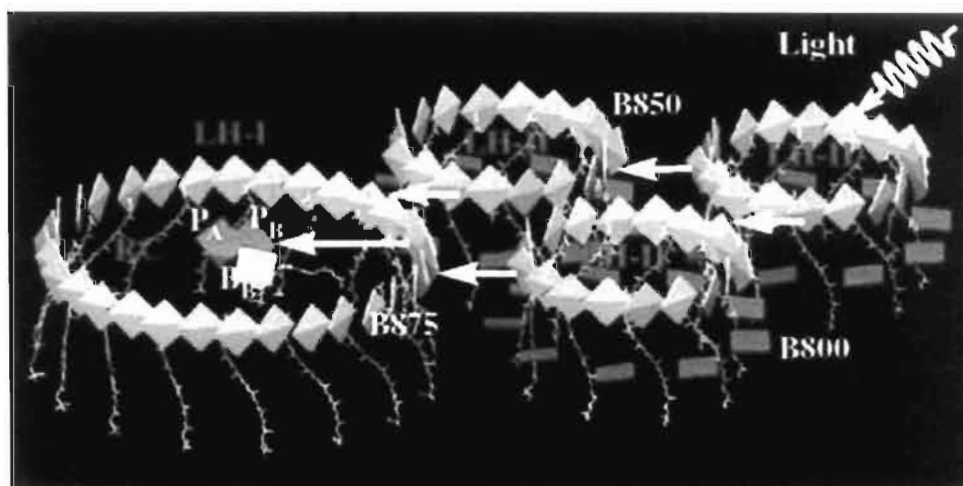
FIGURE 1.1. Excitation energy transfer in the purple bacterial photosynthetic unit. LHII contains two types of BChls, B800 (dark blue) and B850 (green) and LHI contains B875 (green) BChl molecules. P_A and P_B refer to the RC special pair BChls, and B_A, B_B refer to the accessory BChls in the RC. The figure demonstrates the coplanar arrangement of the B850 BChl ring in LHII, the B875 BChl ring of LHI, and the RC BChls P_A, P_B, B_A, B_B. (adapted from ref. 1d)

There are other significant differences between these two sets of pigments-the B800 species are largely monomeric whereas the B850 species are strongly exciton-coupled with exciton state delocalized over several (presumably four)

BChl molecules. Carotenoids are also associated within the LHII structure with the dual function of the contributing light harvesting and protecting systems against photoxidation, by quenching the singlet oxygen molecules produced by photosensitization. All these pigment molecules are maintained in a fixed spatial relationship by the surrounding polypeptides. The light absorbed by the B800 array is transferred to B850 wheel within 1 ps. Energy migration among the different exciton states of B850 then occurs on the 300 fs timescale.

The energy collected by the LHII antennae is then transferred to another antennae complex, LHI, which surrounds the reaction center (RC). The RC is the final destination of the collected energy and is the site where charge separation occurs. The structure of LHI is not known at the same level of definition as that of LHII. LHI is formed from 32 BChl molecules arranged as the B850 molecules of LHII, so that LHI wheel is much larger. LHI absorbs at 875 nm (B875 nm). LHI and LHII are in close contact (estimated to be close than 30 Å) and hence LHII to LHI energy transfer is quiet fast (3 ps). The rate of successive energy transfer from LHI to RC is more than ten times slower (35 ps). Since the molecules of the LHI wheel are exciton coupled like those of B850, such an energy transfer process should occur from approximately eight sites of LHI, each comprising four delocalized BChl subunits to RC. These energy transfer processes are believed to occur by a Förster type mechanism. The different mechanisms involved in energy transfer processes are discussed below.

1.3. Theories of Excitation Energy Transfer

Other than by self-relaxation, excited states of molecules may relax to the ground state by transferring the energy to other molecules present in the system by a bimolecular process (Equation 1.1).[3,4]

$$D^* + A \longrightarrow D + A^* \qquad \text{- - - - (1.1)}$$
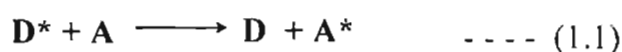
where D is the energy donor, A is the energy acceptor and * denotes an excited state. The general requirements for excitation energy transfer is that (1) the energy of D* is higher than the energy of A* and (2) rate of energy transfer is more rapid than the decay rate of D*. Two different mechanisms for energy transfer can be distinguished: Dexter and Förster energy transfer, the details of these will be discussed below.

1.3.1. Dexter Mechanism

This mechanism also known as collisional or exchange mechanism, is represented schematically as in Figure 1.2.[3c,4a] The exchange interaction (double solid arrows) represents a double electron substitution reaction, i.e., the electron initially on D* jumps to A, simultaneously with the jump of an electron on A to D*. The exchange resonance interaction occurs via overlap of electron clouds and requires physical contact between the interaction partners.
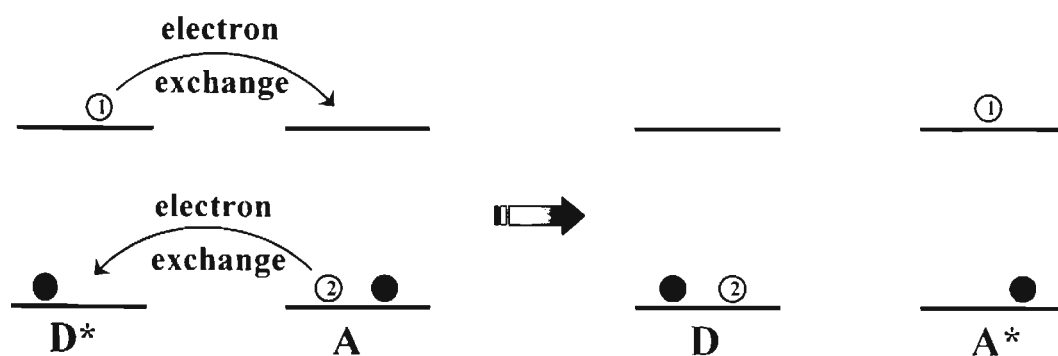
FIGURE 1.2. Schematic representation of exchange (Dexter) energy transfer mechanism. The solid circles represent "passive" electrons whose interactions with other electrons are assumed to be roughly constant during the energy transfer step. (adapted from ref. 3c)

The rate constant for this process is described by equation 1.2.

$$k_{ET} = KJ(\lambda)\exp(-2R_{DA}/L) \qquad \text{- - - - (1.2)}$$

where K is related to the specific orbital interactions, R_{DA} is the donor–acceptor separation relative to their van der Waals radii (L) and $J(\lambda)$ is the spectral overlap integral. The overlap integral $J(\lambda)$ express the degree of spectral overlap between the donor emission and acceptor absorption (Figure 1.3) and is given by equation 1.3,

$$J(\lambda) = \int_{0}^{\infty} F_D(\lambda)\, \varepsilon_A(\lambda)\, \lambda^4\, d\lambda \qquad \text{- - - - (1.3)}$$

where $F_D(\lambda)$ is the corrected fluorescence intensity of the donor in the wavelength range $\lambda + \Delta\lambda$, with the total intensity (area under the curve) normalized to unity; $\varepsilon_A(\lambda)$ is the extinction coefficient of the acceptor at λ.
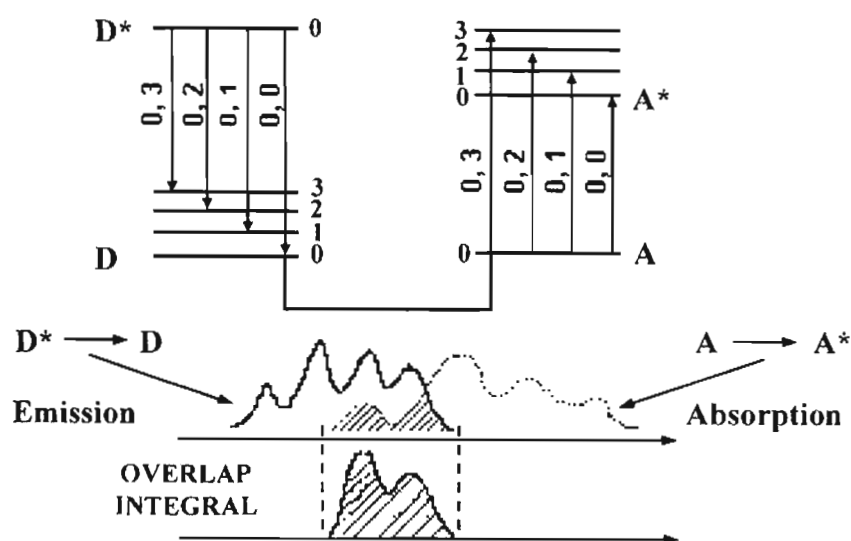
FIGURE 1.3. Schematic representation of the spectral overlap integral $J(\lambda)$ (equation 1.3) and its relation to an experimental emission and absorption spectrum. The shaded region corresponds to the overlap of the emission spectrum of D* and the absorption spectrum of A (adapted from ref. 3c).

The rate of exchange-induced transfer decreases as $\exp(-2R_{DA}/L)$ i.e., rate drops to negligibly small values (relative to the donor life time) as R_{DA} increases more than on the order of one or two molecular diameters. The rate of energy transfer is found to be diffusion controlled and depends on the temperature and the viscosity of the solvent. Both singlet-singlet and triplet-triplet energy transfer processes are allowed and this is in fact the dominant mechanism in triplet-triplet energy transfer.

1.3.2. Förster Mechanism

In contrast to the Dexter mechanism, the Förster type energy transfer does not require electron exchange and operates rather a through-space dipole–dipole

interaction. Hence this mechanism is also known as dipole-dipole or columbic

mechanism and can be represented schematically as in Figure 1.4.[3a,4b]
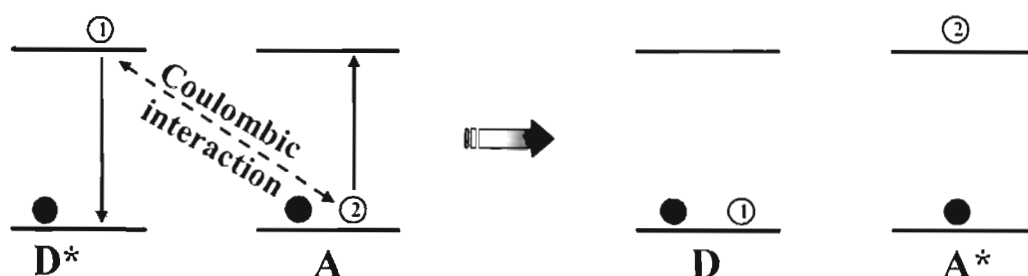
FIGURE 1.4. Schematic representation of columbic (Förster) energy transfer mechanism. The solid circles represent "passive" electrons whose interactions with other electrons are assumed to be roughly constant during the energy transfer step. (adapted from ref. 3c)

The columbic interaction (dotted double arrow) represents "an action at

distance," i.e., the electrons initially on D* stay on D while the electrons initially

on A stay on A*. The columbic resonance interaction occurs via the

electromagnetic field and does not require physical contact of the interacting

partners. The basic mechanism involves the induction of a dipole oscillation in A

by D*. As opposed to the exchange energy transfer, only singlet-singlet energy

transfer is allowed.

The rate of energy transfer in this case is given by,

$$k_{EN} = \frac{1}{\tau_D} \left(\frac{R_0}{R} \right)^6 \qquad \text{---- (1.4)}$$

where τ_D is the lifetime of the donor in the absence of acceptor, R is the distance

between the donor and the acceptor, the rate of energy transfer being inversely

proportional to R^6. R_0 is the Förster distance, at which the energy transfer rate k_{EN} is equal to the decay rate of the donor in the absence of acceptor (τ_D^{-1}) and is described by equation 1.5. Förster distance is typically in the range of 20 to 60 Å and can be as large as 100 Å for efficient acceptors.

$$R_0^6 = \frac{9000(\ln 10)\, K^2\, \Phi_D}{128\, \pi^5\, N\, n^4}\, J(\lambda) \qquad \text{- - - - (1.5)}$$

where K^2 is the orientation factor (related to the relative orientation of the donor and the acceptor transition dipole moments), Φ_D is the donor quantum yield in the absence of the acceptor, n is the index of refraction of the solvent, N is Avogadro's number and $J(\lambda)$ is the spectral overlap integral.

1.4. Photoinduced Energy Transfer in Molecular Architectures and Self-Assemblies

Energy transfer in donor-acceptor systems can be facilitated by integrating them in a single molecular structure or by inducing the self-assembly between them. Linear π-conjugated molecules with different HOMO-LUMO energy levels are widely used as donor-acceptor molecules. Among a plethora of π-conjugated systems known oligo(*p*-phenylenevinylene)s (OPV)s have received significant attention, mainly due to the well-defined molecular structures and novel optical properties.[5-9] Control of energy transfer in these systems are extremely important for optoelectronic device applications. An approach towards the modulation of

optical and electronic properties of π-conjugated systems utilizes the self-assembly of molecules with the help of directional noncovalent interactions.[10] Moreover, self-assembly of OPVs is at the center stage of research due to their interesting optical and electronic properties which are sensitive to intermolecular interactions and molecular organization.[11-13] Apart from this, photoinduced energy transfer from OPVs to various acceptors have generated enormous interest owing to their possible application in molecular and supramolecular electronic devices.[5,6] In the context of the present work, it is appropriate to have an overview of energy transfer studies in noncovalent assemblies of OPVs.

1.4.1. OPVs as Energy Donors

OPVs are known to be efficient energy donors to different acceptors when excited at a suitable wavelength and has been exploited for various applications. A large number of molecular dyads of acceptor linked OPVs has been reported in the literature.[14-16] Among them OPV-fullerene systems have been extensively studied due to their possible application in photovoltaic devices (PVDs) (Chart 1.1).[14b,15f] A characteristic feature in all these dyads is an ultrafast energy transfer from the lowest singlet excited state of the OPV unit to populate the fullerene singlet. This event can be followed by an electron transfer depending on the donating ability of the oligomer, on structural factors and on the solvent polarity.
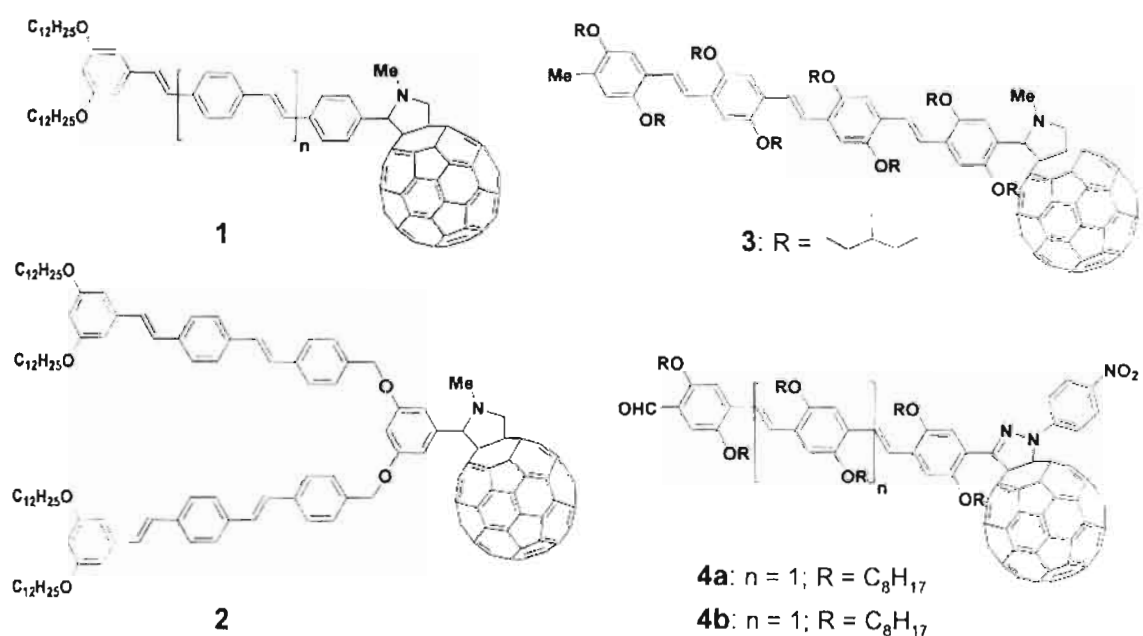
CHART 1.1. Molecular structures of OPV-fullerene molecular dyads.

In addition, energy transfer from poly(p-phenylenevinylene)s (PPVs) and OPVs to doped or covalently linked organic dye molecules has been investigated in great detail with a view of tuning the optical properties for the application in light emitting devices (LEDs).[17,18] An earlier report pertaining to energy transfer from the OPV to doped organic dyes is reported by Meijer and co-workers.[18a] Very recently, Stupp and co-workers have demonstrated energy transfer in nanostructured OPV/silicate hybrid film, loaded with Rhodamine B dye molecules.[18b] The details of these studies will be discussed in the introduction section of Chapter 3 of the thesis.

Though the energy transfer process in various molecular dyads has been studied extensively, a challenging task is the control of the direction of energy

transfer in such a molecular system. Recently, this has been addressed with the help of an OPV-phenanthroline molecular dyad which is a proton triggered molecular switch based on directional energy transfer (Figure 1.5).[19] The electronic energy level of OPV is intermediate in energy relative to the level of phenanthroline (Phen) and protonated phenanthroline, (Phen.H⁻). Thus, Phen can act as an energy transfer donor in OPV-Phen dyad (**5**) and Phen.H⁺ act as an acceptor in OPV-Phen.H⁺ dyad (**6**). As a result, the direction of energy transfer process could be controlled by means of the reversible protonation-deprotonation reaction of Phen unit, which is signaled by the on/off switching of the intense OPV fluorescence.
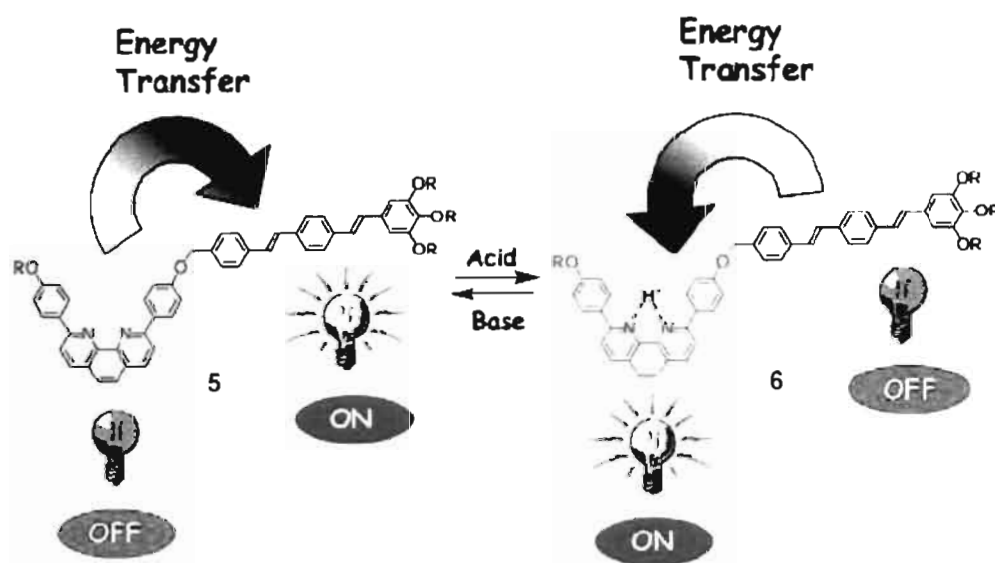
FIGURE 1.5. Schematic representation showing the functioning of the OPV-phenanthroline molecular switch. (adapted from ref. 19b)

1.4.2. Energy Transfer in Hydrogen Bonded Assemblies of OPVs

Among various noncovalent interactions, H-bonding has emerged as the most powerful and useful techniques to organize donor-acceptor chromophores in photoinduced energy transfer process.[20,21] Due to their tunable strength (between 4–120 kJmol[-1]), directionality and specificity, H-bonding is considered as the favorite noncovalent interaction to the creation of molecular architectures. The research groups of Meijer and Janssen have extensively studied the energy transfer processes in H-bonded OPV self-assemblies. An interesting case is the quadruple hydrogen bonded donor-acceptor dyad, 7 (Chart 1.2a) which is constructed by attaching the self-complementary 2-ureido-4[1H]-pyrimidinone (UP) unit to an OPV donor and C_{60} acceptor.[22a,b] Detailed steady state emission studies revealed that singlet energy transfer from the excited OPV unit to fullerene results in a strong quenching of the donor emission (quenching factor, $Q_{max} \geq 90$). This is attributed to the high association constant of the quadruple H-bonded hetero-dimers. Later, the same concept has been used for energy transfer in an OPV-perylene bisimide dyad, 8 (Chart 1.2b).[22c] In contrast to the previous examples in which self-complementary nature of H-bonding motif resulted in statistical mixture of homo- and heterodimers, the dyad 9 (Chart 1.2c) showed preferential formation of hydrogen bonded heterodimers as evidenced by ^{1}H NMR studies.[22d] Fluorescence studies of the dyad 9 revealed that the excitation energy transfer occurs from the photoexcited OPV to C_{60} moiety. The absence of electron transfer

in the above systems is attributed to the weak electronic coupling between the donor and the acceptor in the excited state due to the long distance between the chromophores.[22]
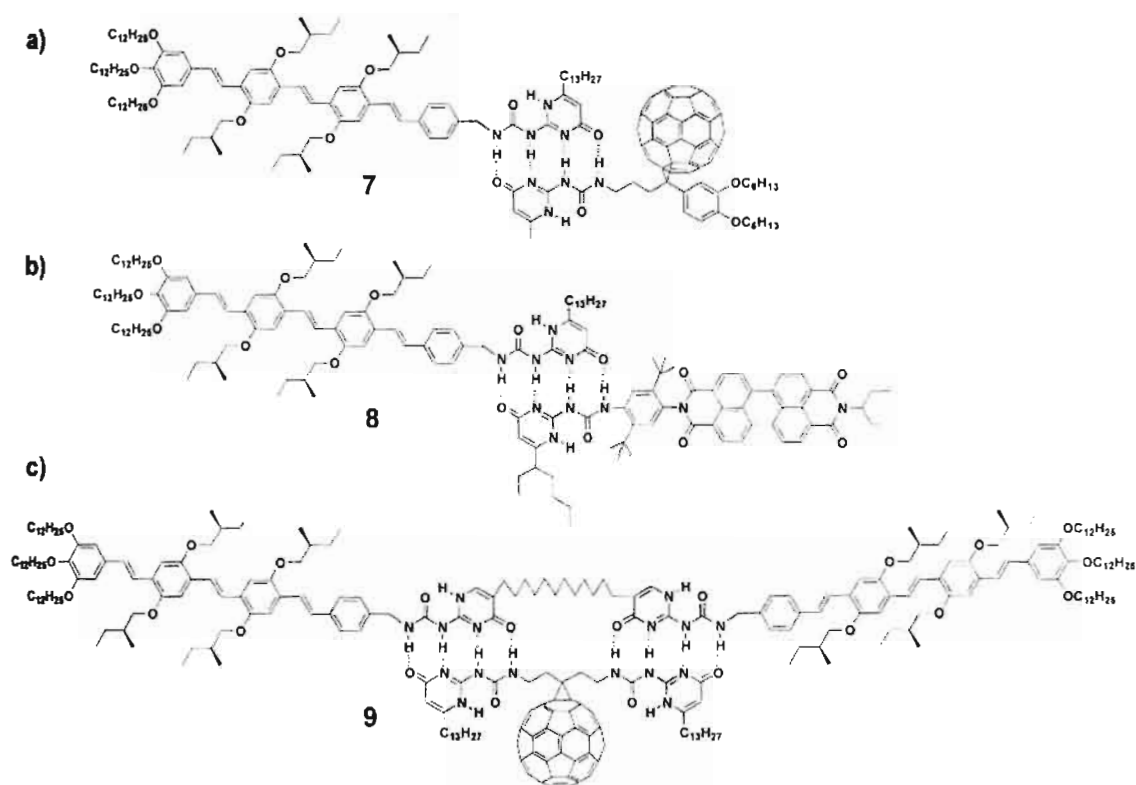
CHART 1.2. Quadruple H-bonded heterodimers formed by energy donor OPVs and acceptors functionalized with 2-ureido-4[1*H*]-pyrimidinone (UP) unit. a) OPV-fullerene dyad **7** b) OPV-perylene bisimide dyad **8** and c) OPV-fullerene dyad **9**, which formed a cyclic heterodimer.

Schenning, Meijer and co-workers have successfully demonstrated energy transfer in H-bonded helical co-assembly of OPVs **10** and **11** of different conjugation length bearing identical ureido-*s*-triazine (UT) motif (Chart 1.3).[23] Fast and efficient energy transfer from shorter (**10**) to longer (**11**) oligomers which are self-assembled in helical stacks is observed on increasing the concentration of
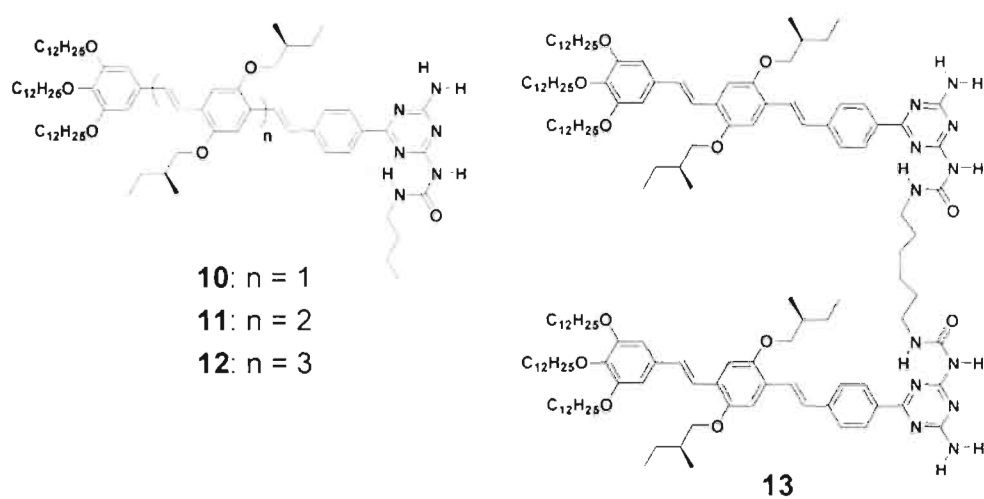
CHART 1.3. Molecular structures of ureido-*s*-triazine H-bonding motif functionalized OPVs.
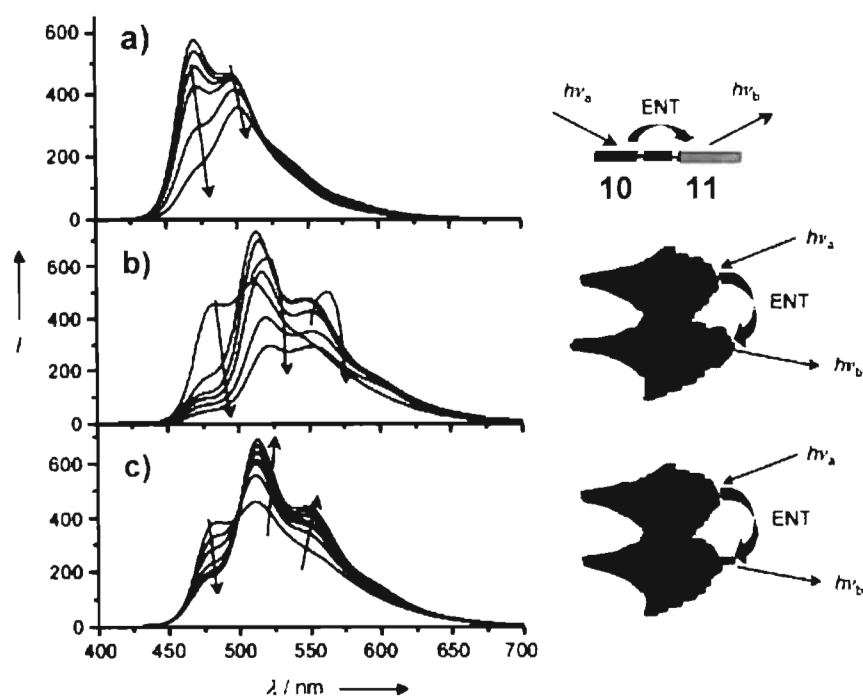
FIGURE 1.6. Photoluminescence spectra for mixtures of **10** and **11** in dodecane solution ($\lambda_{ex} = 412$ nm). The concentration of **10** is fixed at 1.9×10^{-5} M: a) 0-30 mol% **11** at 80 °C b) 0-30 mol% **11** at 10 °C and c) 0-1.2 mol% **11** at 10 °C. (adapted from ref. 23a)

the acceptor molecules as evident from the decrease in the fluorescence intensity of the donor (Figure 1.6). Up to about 2 mol%, the acceptor molecules exist only as isolated energy traps, but at higher concentrations clustering of acceptor molecules occur as evident from its quenched and red shifted fluorescence after energy transfer.

A recent theoretical study suggests that the rate of energy transfer process in multichromophoric systems can be controlled by chromophore arrangements.[24] This is experimentally proved by Meijer and co-workers using ordered and disordered assemblies of OPVs.[25] When compared to the well ordered assembly of **10**, the bifunctional analogue **13** form disordered polymeric aggregates owing to the presence of connecting hexyl spacer between the H-bonding motifs (Figure 1.7). Detailed fluorescence titration studies with compound **12** as an energy acceptor revealed that the quenching efficiency at comparable amounts of acceptor is significantly higher for the well-ordered stacks of **10** when compared to that of the disordered aggregates of **13**.[25a] Detailed time resolved fluorescence studies indicates that for ordered helical assembly of **10** a fast initial fluorescence depolarization and excitation transfer to dopant occurs, which is in agreement with semi-coherent exciton diffusion along the chiral stacks of **10**. For disordered polymeric assemblies of **13**, both depolarization and energy transfer dynamics take place on a much longer time scale which is attributed to weak electronic coupling

of chromophoric units that result in slow incoherent motion of excitations along the stacks of **13**.[25c]
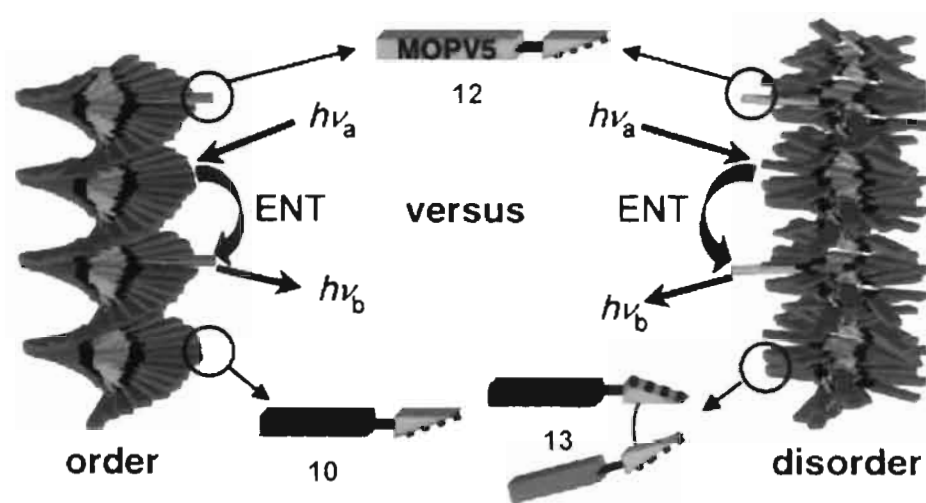
FIGURE 1.7. Energy transfer in helically ordered and disordered assemblies of **10** and **13**, respectively. (adapted from ref. 25a)

Energy transfer is reported to occur in ureido-*s*-triazine (UT) functionalized OPV-perylene bisimide dyad **14**, in which the perylene bisimide unit is covalently attached to the ureido moiety of the OPV-UT through a flexible linker.[26] Emission studies of mixed assemblies formed by OPV-perylene bisimide dyad (**14**) and OPV-UTs (**10** or **11**) in chloroform or dodecane showed strong quenching of the OPV-UTs emission with concomitant formation of perylene bisimide luminescence. This observation indicates the occurrence of energy transfer in heterodimer, formed by **14** with **10** or **11**. Furthermore, in dodecane, incorporation of **14** into the columnar aggregates of pure OPV-UTs (**10** or **11**) resulted in more effective energy transfer from OPVs to perylene bisimide unit.

14
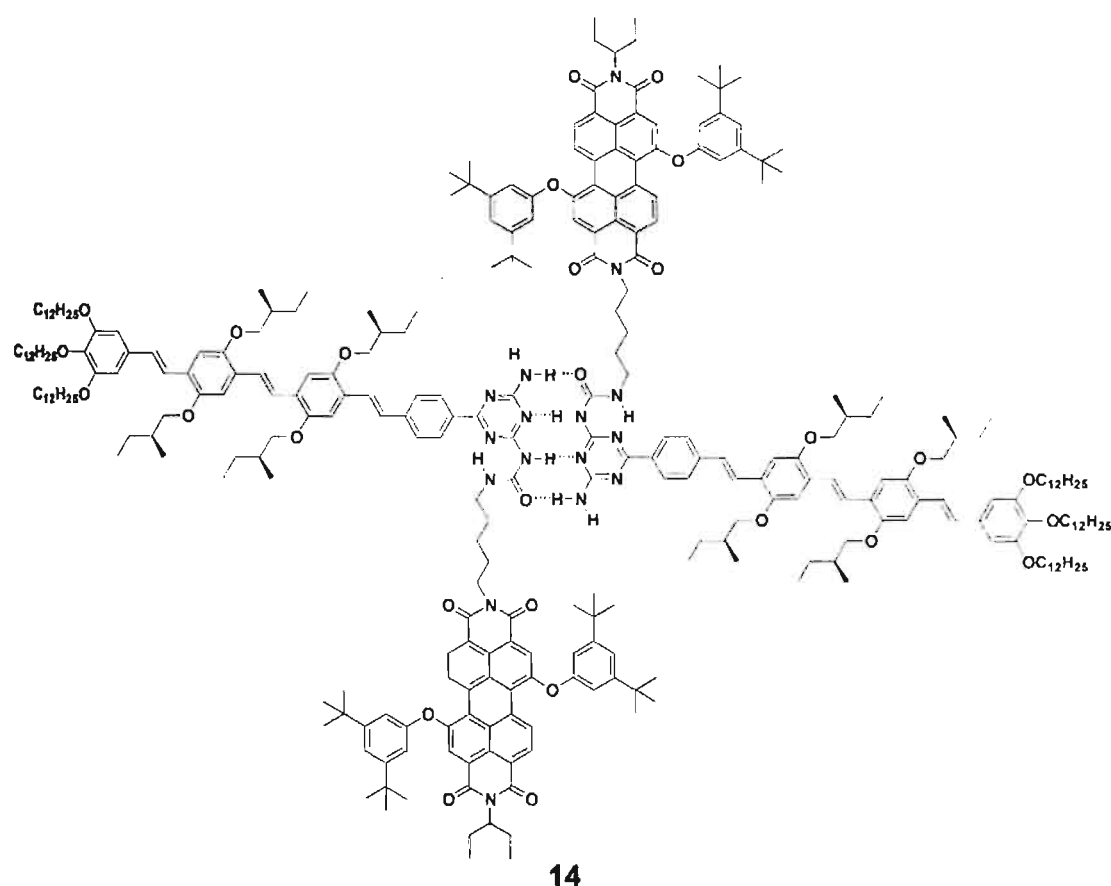
The advantage of the strength and directionality of triple H-bonding array of melamine and cyanuric acid, has been utilized to the self-assembly of OPV-porphyrin donor-acceptor system, **15**.[27] The porphyrin unit functionalized with cyanuric acid motif ensures two sites for hydrogen bonding with the OPVs with *s*-triazine units (OPV*n*Ts). Addition of the porphyrin derivative to OPV*n*Ts results in a H-bonded complex **15** in which quenching of the OPV emission is observed due to aggregation as well as energy transfer. Detailed optical and chiro-optical studies provided ample evidence for the formation of chiral co-assemblies which is facilitated by the additional π-π interaction provided by the porphyrin unit.

15: n = 1 or 2
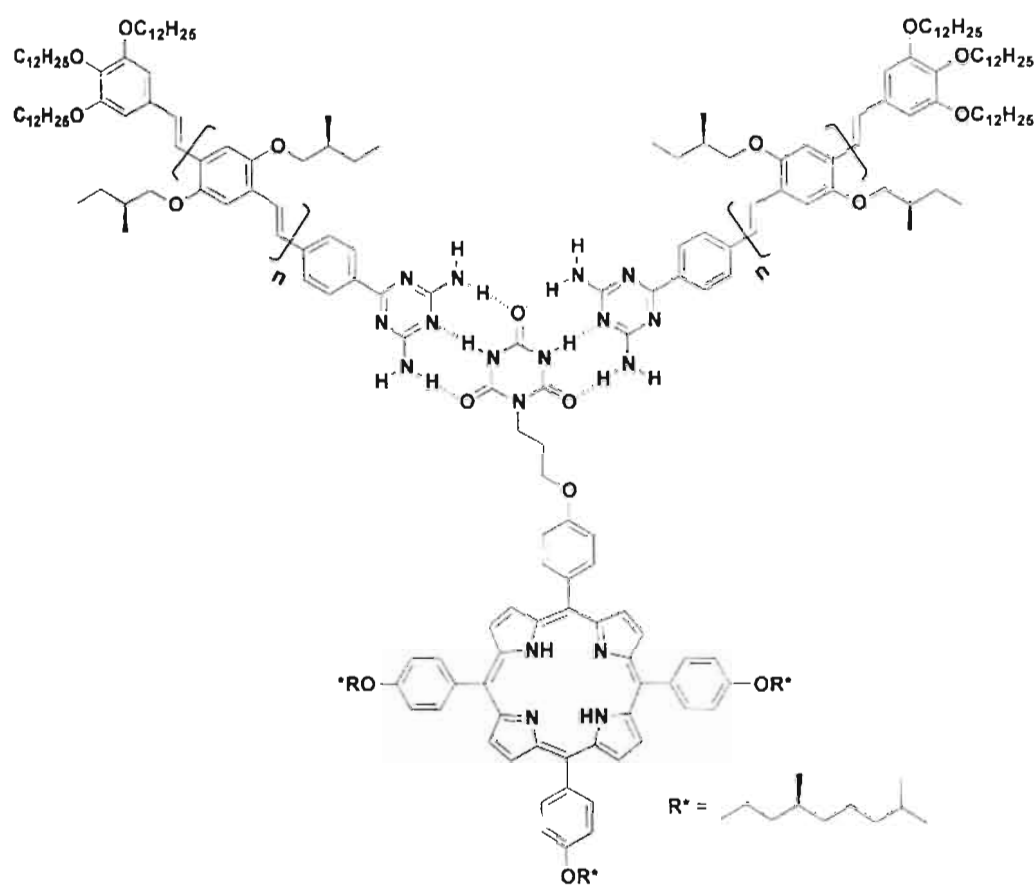
1.4.3. Energy Transfer in Self-Assembled Triblock and Diblock Systems

Rod-coil type block copolymers comprising of electronically active π-conjugated molecules as a rigid rod segment are known to self-organize to form architectures of different size and shape.[28] Incorporation of suitable donor-acceptor molecules to such systems facilitate energy transfer process.[28-31] The advantage of such an approach to the design of electronically active functional supramolecular architectures is mainly based on the characteristic microphase

segregating properties of the diblock polymers. For instance, Hadziioannou et al. have illustrated the formation of a honeycomb like morphology from a phenylenevinylene–C_{60} based rod-coil diblock copolymers.[28b-d] In addition to this interesting morphological feature, an efficient electron transfer process at the donor-acceptor interface has been observed, which makes these supramolecular materials ideal for photovoltaic device application.
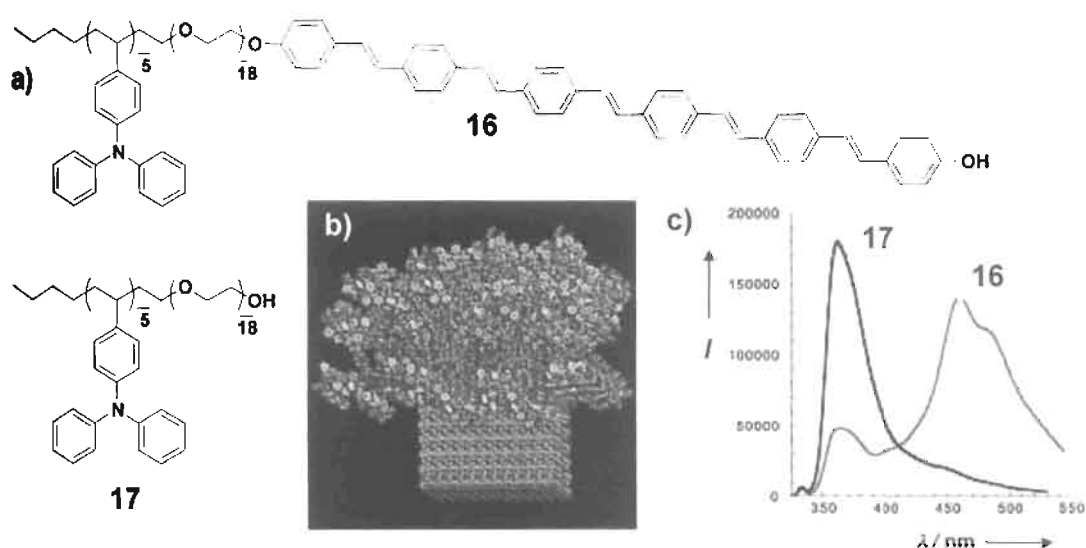
FIGURE 1.8. a) Chemical structures of the rod-coil triblock molecule **16** and the model compound **17**. b) A cartoon of the supramolecular aggregate formed by **16**. c) Emission spectra from **16** and **17** at the same optical density using 302 nm as the excitation wavelength. The emission spectra suggest energy transfer between the coil and the rod segments. (adapted from ref. 29b)

Stupp and co-workers have extensively studied the formation of nanostructured supramolecular architectures with triblock rod-coil systems.[29] In an attempt to design supramolecular materials with optical functionality, they have synthesized a triblock molecule containing a diblock coil of oligo-4-

diphenylaminostyryl-ethylene oxide and an oligomer of phenylenevinylene, (16) (Figure 1.8a).[29b] Detailed morphological analysis showed that these molecules self-organize into discrete mushroom-shaped nanostructures (Figure 1.8b). Interestingly, selective excitation of the triphenylamine (TPA) moiety (λ_{ex} = 302 nm) of 16 showed substantial emission from the phenylenevinylene segments (λ_{em} = 460 nm) in comparison with the emission of an oligo-TPA derivative 17 (λ_{em} = 368 nm, Figure 1.8c). The energy transfer process from the coils to rod blocks is further verified by monitoring the excitation spectrum of 16 at 460 nm which indicates an emission for the coil.

In comparison to the extensive studies of the rod-coil type diblock copolymers, studies related to rod-rod conjugated diblock copolymers is very less. An interesting example in this category is from Yu and co-workers.[30] They have synthesized a few rod-rod type co-oligomers consisting of liquid crystalline rigid rod phenylenevinylene and amorphous thiophene blocks, 18a-c (Figure 1.9a). Detailed morphological and XRD studies revealed that composition of diblock copolymers significantly affect the morphology of the resulting self-assembly (Figure 1.9b-d). Emission studies showed that excitation of OPV segments results in strong emission from the thiophene block. Excitation and time resolved spectroscopy unambiguously proved the occurrence of intramolecular energy transfer from OPV segments to thiophene block. The rod-rod diblock oligomers based strategy is found to be applicable to other type of π-conjugated molecules

with distinct electronic and structural properties. Such materials are expected to be useful to the design of photovoltaic and molecular electronic devices.
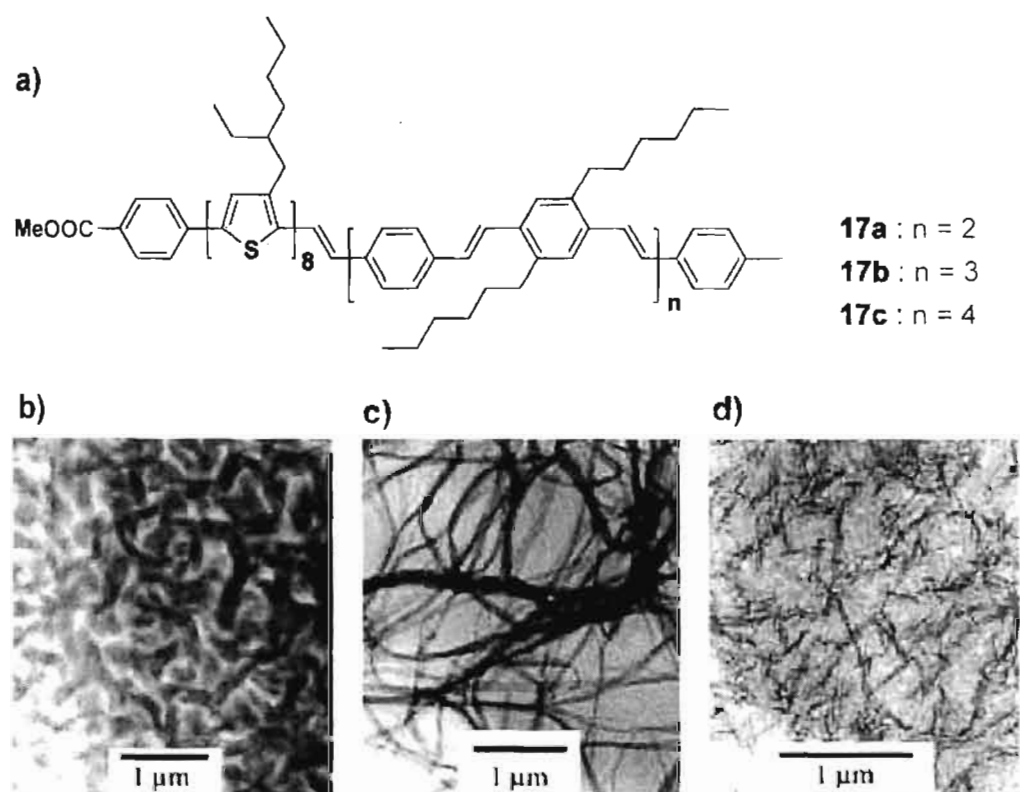
FIGURE 1.9. a) Chemical structures of rod-rod diblock molecules containing thiophene and OPV blocks (18a-c). Transmission Electron Microscopic (TEM) images of the films of the copolymers showing different morphology depending upon the composition of OPV block; b) 18a, interwoven network, c) 18b, layered stripes and d) 18c, lamella. (adapted from ref. 30)

The novel donor-bridge-acceptor system. 19 reported by Janssen et al. is an excellent example of supramolecularly controlled photoinduced energy and electron transfer processes (Figure 1.10).[31] For this purpose an OPV donor and a perylene (PERY) acceptor chromophores are attached to the opposite ends of a long foldable *m*-phenyleneethynylene oligomer (FOLD). In good solvents the

oligomer bridge adapts a random coil conformation (A). Photoexcitation in random coil conformation, where the interaction between the donor and acceptor chromophores is small, results only in long range intramolecular energy transfer. Upon addition of poor solvent, *m*-phenyleneethynylene bridge will adapt a folded conformation (B). Under this condition the donor and acceptor are closer enough for sufficient interaction and favor the formation of charge separated states upon photoexcitation.
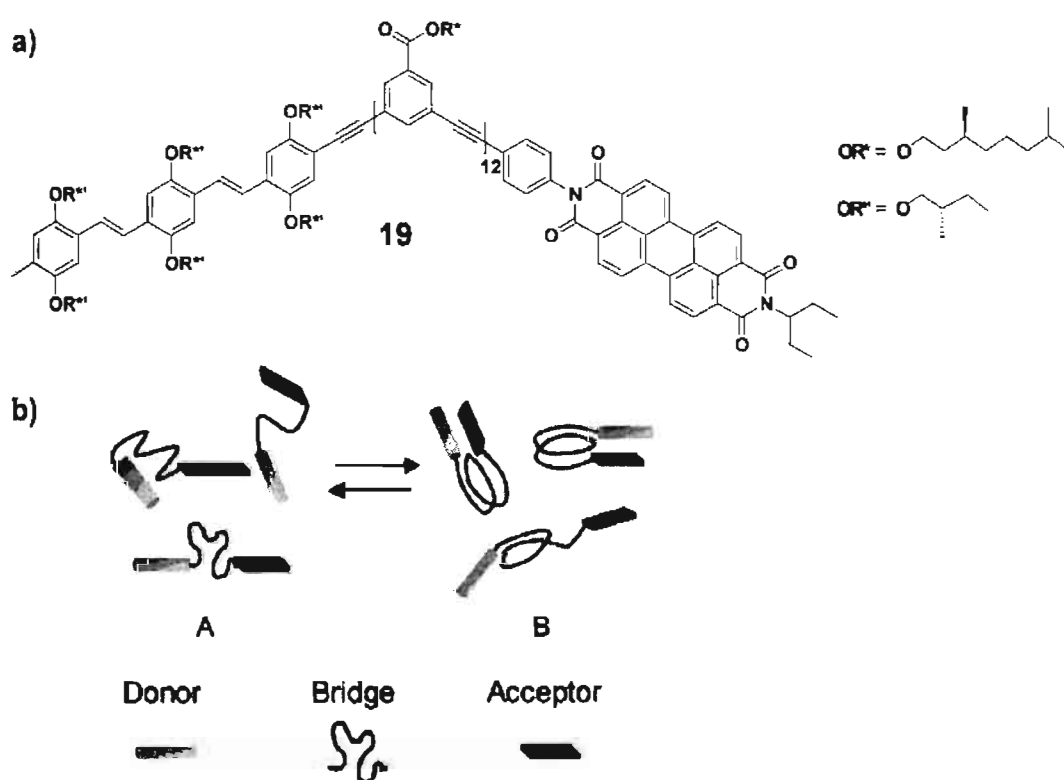
FIGURE 1.10. a) Molecular structure of OPV-FOLD-PERY donor-bridge-acceptor system, **19.** b) Schematic representation of the different conformational states of **19,** A: random coil; B: folded (helical) conformation. (adapted from ref. 31)

1.4.4. Energy Transfer in Self-Assembled OPV Nanoparticles

Energy transfer studies in OPV nanoparticles doped with oligomers having longer conjugation length were successfully demonstrated by Oelkrug, Hanack and co-workers.[32] The doped nanoparticles of OPV were prepared by co-precipitation of **20** (host) and **21** (guest) from methanolic solutions by the addition of water and were characterized by dynamic light scattering (DLS) technique (diameter 20-200 nm). The close intermolecular contacts and parallel orientation of **20** in the nanoparticles makes them suitable for excitation energy transfer to lower energy fluorescence centers (OPVs having higher conjugation length). Excitation of **20** in the presence of small amount of dopant **21** showed typical fluorescence of the latter. Additionally, the excitation spectrum of the guest molecule is found to be identical to the absorption spectrum of **20**. These observations indicated efficient energy transfer from host to entrapped guest molecules (Figure 1.11). Similar results were obtained when an oligothiophene derivative **22** was used as the energy trap. Detailed steady state emission and anisotropy studies showed that the nanoparticle matrix of **20** provide an anisotropic and highly ordered environment for the guest molecules.[32b,c] The parallel alignment of guest molecules with the host preserves a high degree of fluorescence polarization during the transfer of the excitation energy from the host to the guest molecules, which involves energy diffusion in the host lattice.
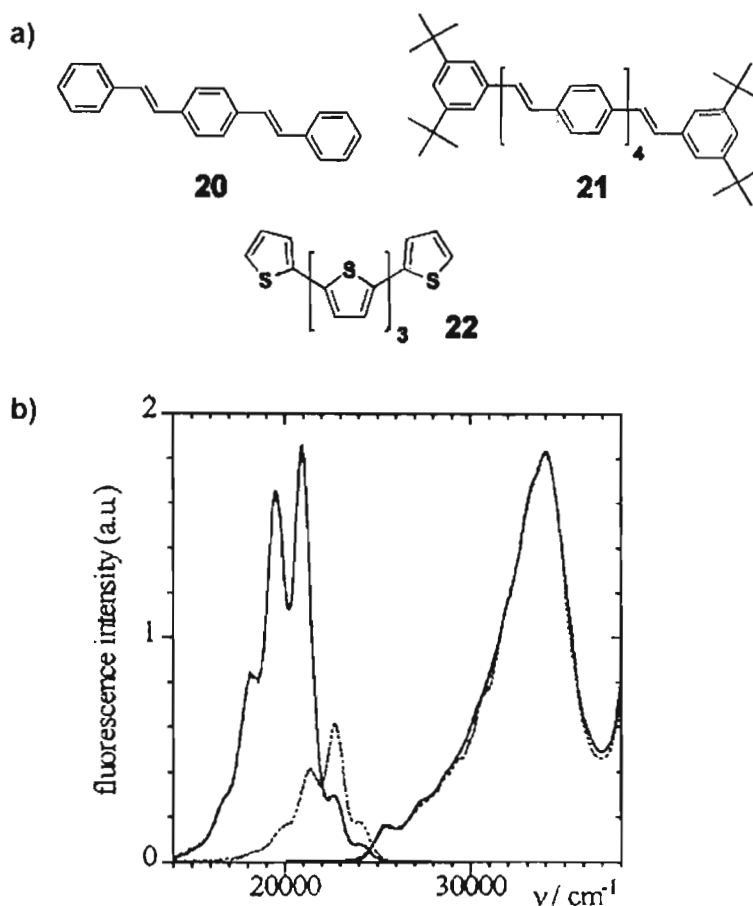
FIGURE 1.11. a) Molecular structures of the energy transfer donor (20) and acceptors (21 and 22). b) The emission and excitation spectra of nanoparticle suspensions of 20: undoped (dashed lines), excitation spectrum scanned for fluorescence at 22000 cm⁻¹, doped with 21 (solid lines), excitation spectrum scanned for fluorescence at 17500 cm⁻¹. (adapted from ref. 32a)

1.4.5. Energy Transfer in Amphiphilic OPV Self-Assemblies

The rationally designed amphiphilic OPVs 23 and 24 (Figure 1.12a) form vesicular assemblies in aqueous medium as evident from DLS and scanning confocal microscopy studies.[33] Since the cyano substituted derivative 24 has low HOMO-LUMO energy gap when compared to that of the parent derivative 23. it serves as an energy acceptor when coassembled with the latter (Figure 1.12b).

This is proved in a mixed vesicular assembly of **23** and **24**. The energy transfer process at single vesicle level is probed by using scanning confocal microscopy which revealed that the properties of individual vesicles are different from those of the bulk solution (Figure 1.12c).
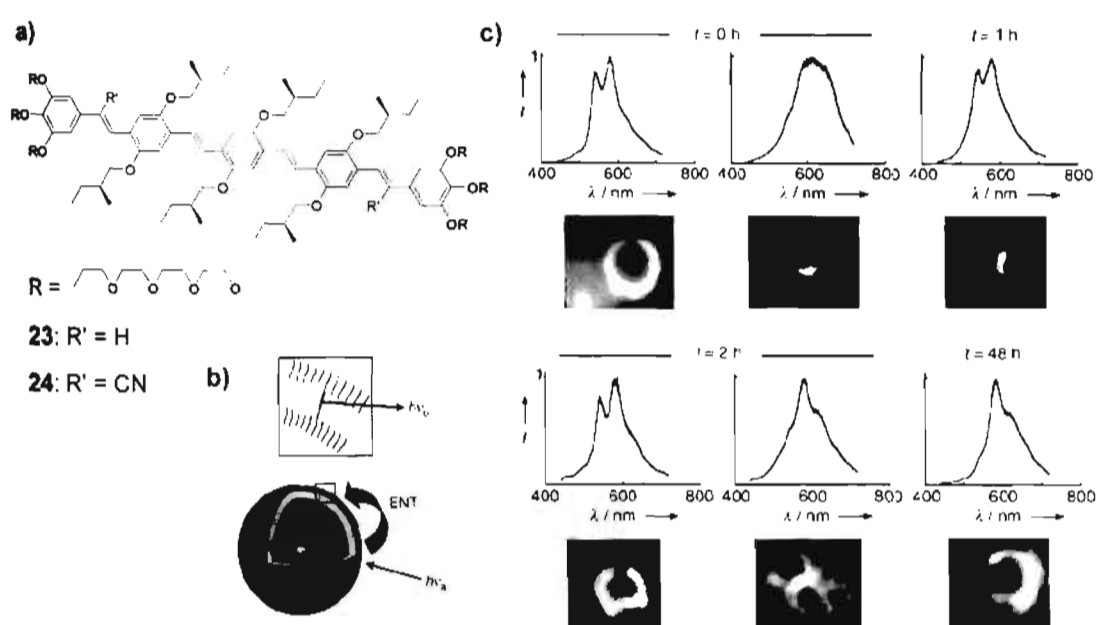
FIGURE 1.12. a) The structure of the molecules and b) the schematic representation of the vesicular self-assembly. c) Scanning confocal microscopy images and normalized fluorescence (λ_{exc} = 411 nm) of single vesicles showing the transition from nonmixed to mixed vesicles on prolonged heating of a 2 mol% solution of **24** at 35 °C. At t = 0 h (and t = 1 h), vesicles of **23** and some vesicles of **24** predominate. At t = 2 h some vesicles show energy transfer (ENT). After 48 h all the vesicles are mixed and show the acceptor OPV luminescence. (adapted from ref. 33)

Sequential energy and electron transfer in mixed π-conjugated assemblies have been demonstrated using mixed assemblies of (OPV)$_4$-porphyrins **25** and **26** in water (Figure 1.13a).[34] Selective excitation of OPV unit in these mixed assemblies results in the transfer of excitation energy from OPV via Zn-porphyrin

to free-base porphyrin. Apart from this, incorporation of C_{60} into mixed aggregates of **25** and **26** showed an additional electron transfer step to C_{60} (Figure 1.13b).

25: M = 2H
26: M = Zn
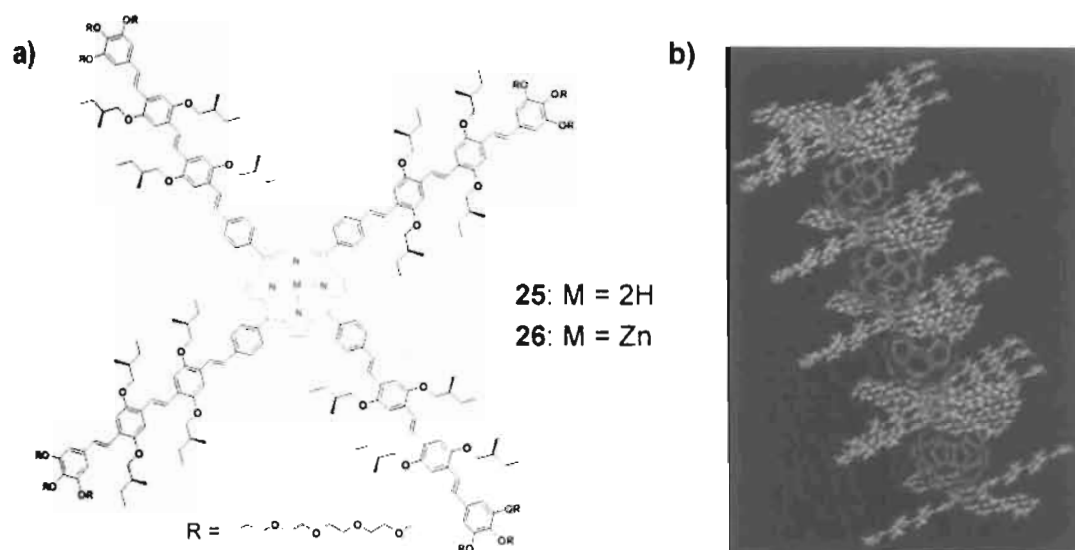
FIGURE 1.13. (a) Molecular structure of (OPV)4-H2-porphyrin (**25**) and (OPV4)4-Zn-porphyrin (**26**). (b) Proposed molecular picture of a co-aggregate of **25** and C60. (adapted from ref. 34)

Recently, efficient one-dimensional energy/electron transfer in acceptor-donor-acceptor (A-D-A) type linear chain chromophores based on amphiphilic OPVs as a donor (D) and several electron/energy (A) acceptors which are encapsulated within the helical structures of amylose has been reported by Kim et al. (Figure 1.14).[35] Detailed photoinduced electron/energy transfer studies of the chromophores in the presence and absence of the helical encapsulation showed that the efficiency of these processes are highly depend upon the D-A distance and the acceptor strength. For example, excitation of a helically encapsulated OPV-based chromophore **29b** at 375 nm in water exhibited > 99% quenching of the

OPV fluorescence in comparison with a weak acceptor **27c** ($\lambda_{em} = 432$ nm).

Energy transfer from OPV unit to the acceptor (DASP) brings about > 10-fold

increase of the acceptor fluorescence when compared to that by selective

excitation of the acceptor unit at 480 nm. In the absence of amylose, excitation of

either OPV or DASP showed no measurable difference in the intensity. These

observations reveal the importance of helix encapsulation in energy transfer
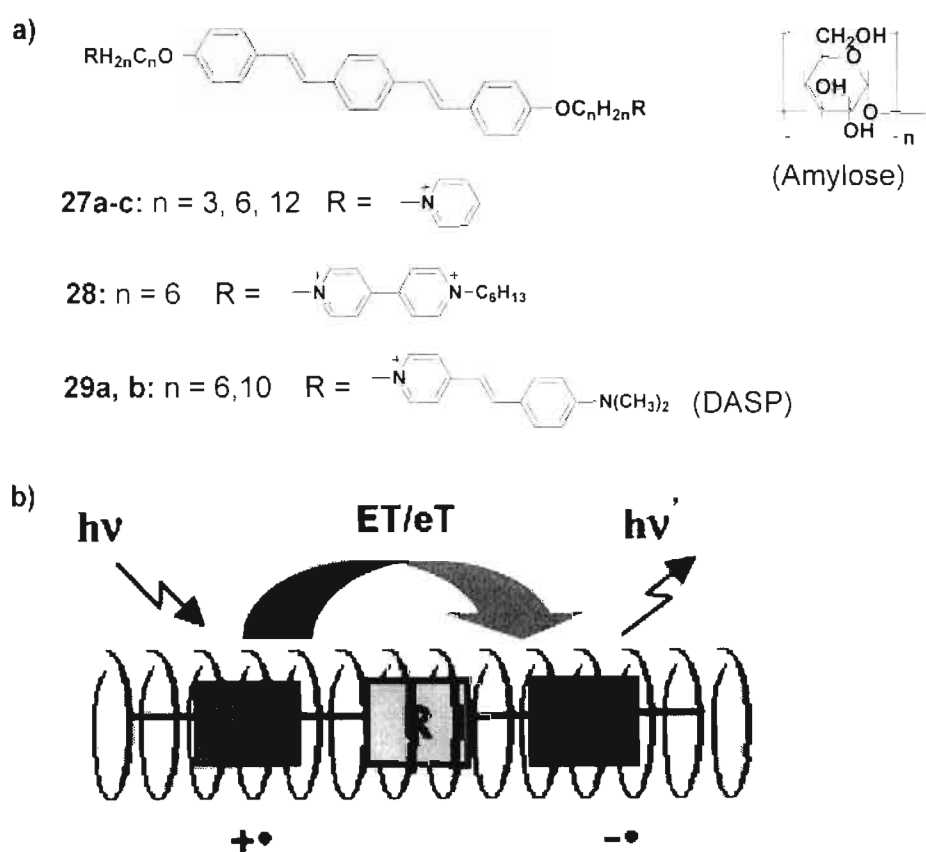
process.

FIGURE 1.14. a) Molecular structure of amphiphilic OPVs substituted with electron (**27** and **28**) and energy acceptor (**29**) chromophores. b) Schematic representation of one dimensional electron and energy transfer process in amylose encapsulated A-OPV-A chromophores. (adapted from ref. 35)

1.5. Light Harvesting Gels

Certain organic molecules spontaneously self-assemble to form soft solid-like mass called 'gel' by entrapping a large volume of the solvent within the self-assembled structures.[36] Among a variety of low molecular weight organogelators known in the literature, those based on functional chromophores and dyes have attracted immense interest as novel functional materials for optoelectronic applications.[21,36d] Gelation in many cases are known to facilitate the alignment of chromophores. Such organized arrays of chromophores are conducive for directional energy or electron transport processes. There are several reports pertaining to fluorescence resonance energy transfer (FRET) in organized assemblies. In this context organogels are attracting considerable attention as scaffold for efficient energy transfer between donor-acceptor chromophores.
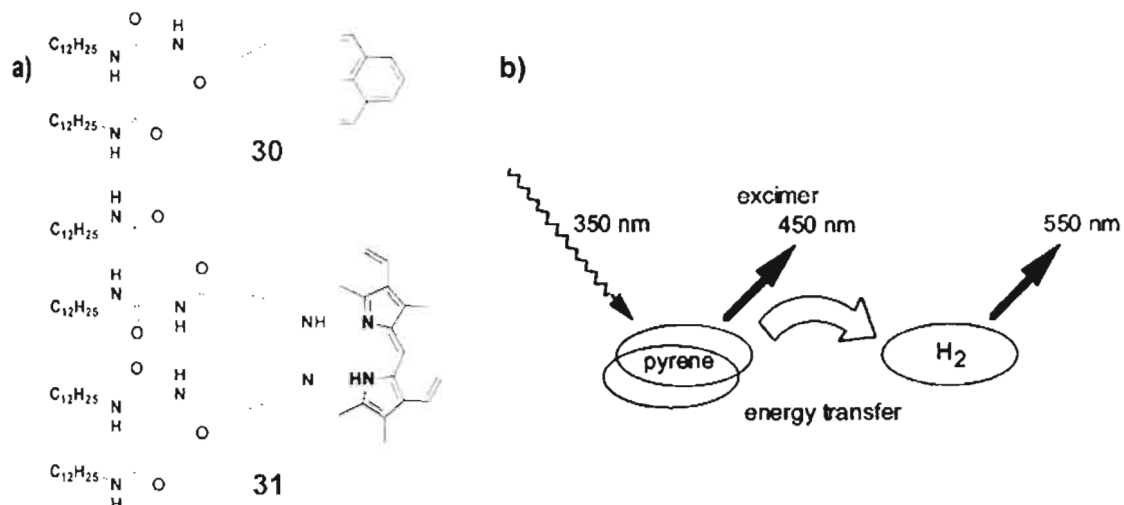
FIGURE 1.15. Didodecyl L-glutamic acid substituted pyrene (**30**) and porphyrin (**31**) form mixed assemblies in benzene, the energy transfer process in these assemblies is schematically depicted. (adapted from ref. 37)

One of the early examples of a light harvesting gel is reported by Sagawa et al.[37] They have synthesized pyrene and porphyrin functionalized L-glutamate derivatives (30 and 31). Detailed gelation studies showed that the pyrene derivative (30) forms physical gel in benzene and cyclohexane whereas the porphyrin derivative (31) failed to gelate any of the solvent tried. Spectroscopic studies revealed that these molecules form ordered co-facial chiral aggregates even in the solution state. Energy transfer studies in the mixed assemblies of 30 and 31 provided evidence for singlet-singlet energy migration from pyrene excimers to the ground state. free base porphyrin (Figure 1.15).

Nakashima and Kimizuka, have prepared light harvesting hydrogels by electrostatically incorporating the anionic naphthalene, 32 (energy donor) and the anthracene derivative 33 (energy acceptor) into the fibrous assemblies of cationic L-glutamate derivatives (34 or 35).[38] The regular packing of the glutamate chains into the bilayer assemblies ensures ordered chromophoric assembly. Consequently efficient energy transfer from the naphthalene donors to the anthracene acceptors has been observed (Figure 1.16). Moreover it is found that the efficiency of energy transfer process in the gel state is high when compared to that in the solution state. demonstrating the importance of gel matrix in organizing donor-acceptor chromophores.

a)

32

33

34: R = Octyl
35: R = Isopropyl

b)

50 – 200 nm (AFM)

ca. 8 nm (TEM)

light-harvesting
supramolecular
hydrogels

bundle of nano-fibers

self-assembled 1-NaphSO₃⁻ complexes
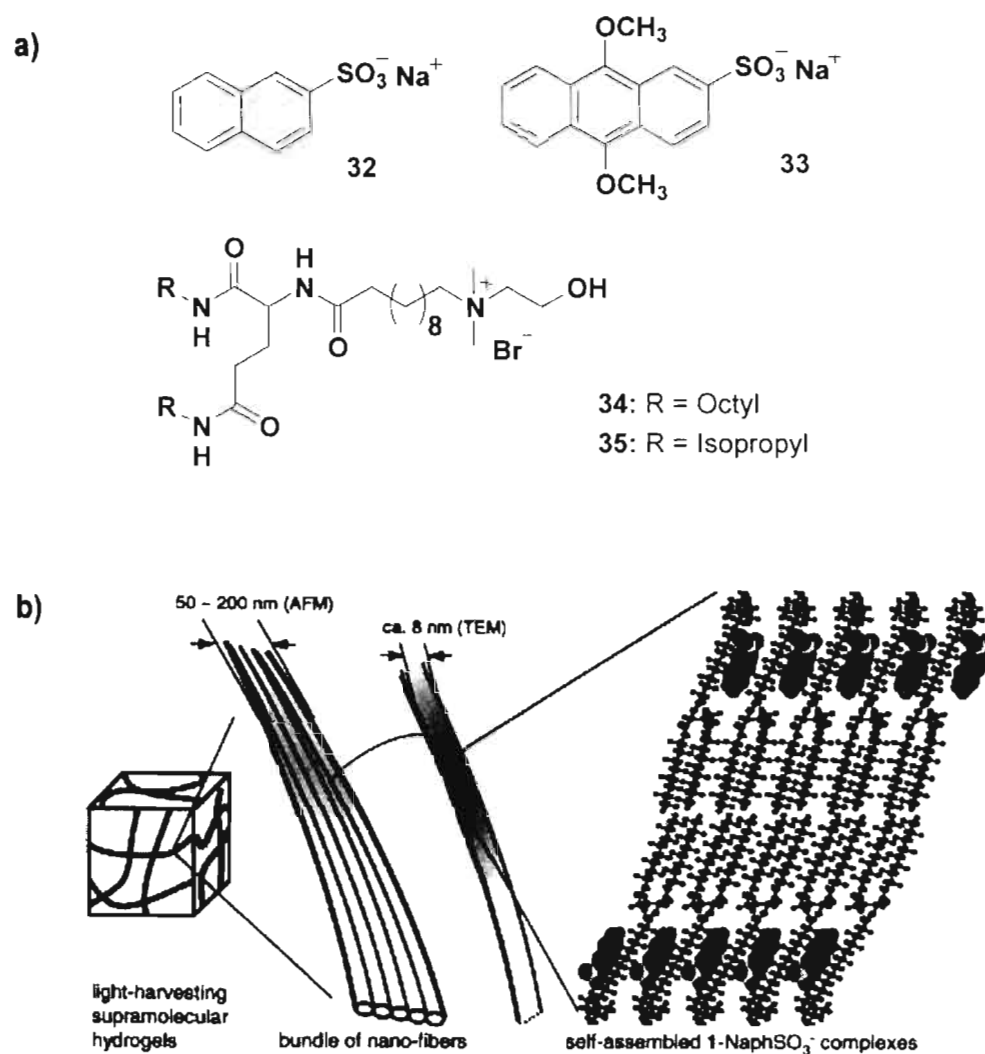
FIGURE 1.16. a) Molecular structures of energy transfer donor (**32**), acceptor (**33**) and the cationic L-glutamate derivatives (**34**, **35**). b) Cartoon representation of the self-assembly of the anionic naphthalene (**32**) and anthracene (**33**) within the cationic glutamate (**34** or **35**) derivatives resulting in supramolecular hydrogels. (adapted from ref. 38)

Shinkai and co-workers have reported a light harvesting energy transfer cascade in co-assembled organogels of cholesterol functionalized perylene bisimide gelators **36a-d** (Chart 1.4).[39a] For this purpose, four perylene bisimides were prepared, the absorption maximum of which could be tuned across the

visible spectrum by attaching different substituents at the bay positions of the perylene moiety.

36 a-d

36a: R = —H

36c: R = ⬡

36b: R = —O⬡—⟨

36d: R = —N⬡O
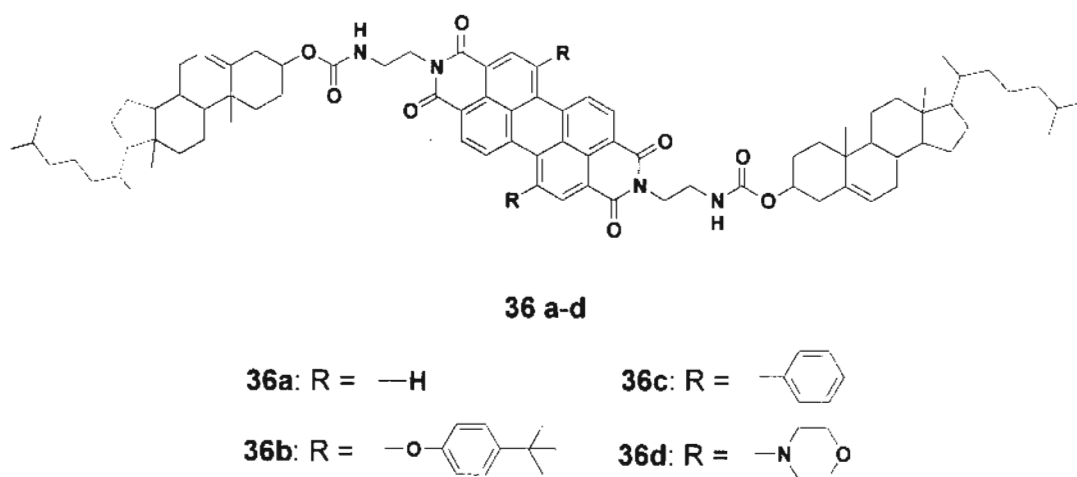
CHART 1.4. Molecular structures of cholesterol functionalized perylene derivatives (**36a-d**).

Various binary, ternary and quaternary perylene gels were prepared and subjected to energy transfer studies. Selective excitation of **36a** at 457 nm resulted in the quenching of its emission at λ_{em} = 544 nm with efficiencies of 68% for **33b**, 53% for **36c** and 34% for **36d**, consistent with decreasing donor-acceptor spectral overlap (Figure 1.17). The perylene derivative **36d** acts as an energy sink because of its low emissive nature which arises from the twisted intramolecular charge transfer (TICT) state. These trends are visually shown in the inset in Figure 1.17. It is interesting to note that the supramolecular organization of the chromophores in the gel state guarantees the success of this cascade transfer process, whereas in solution the mentioned effects are not observed.
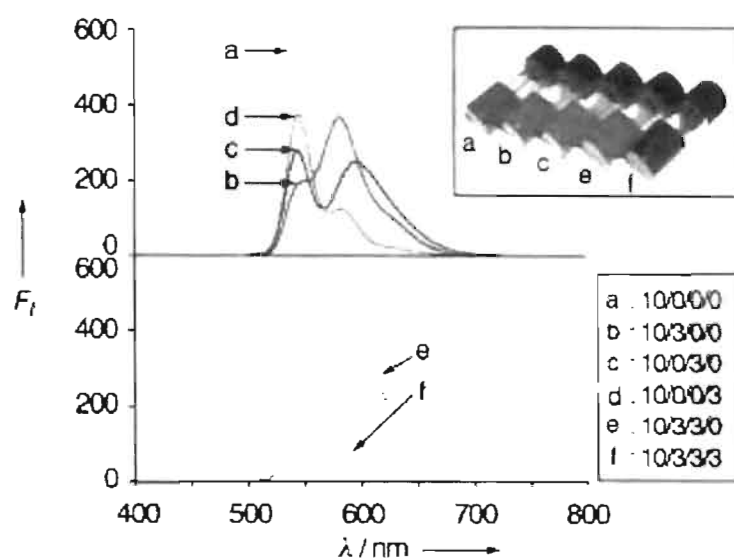
FIGURE 1.17. Fluorescence spectra of mixed perylene gels. The numbers in the inset denote the molar ratios for **36a/36b/36c/36d**. The corresponding photographs of the mixed gels are also shown in the inset. (adapted from ref. 39a)
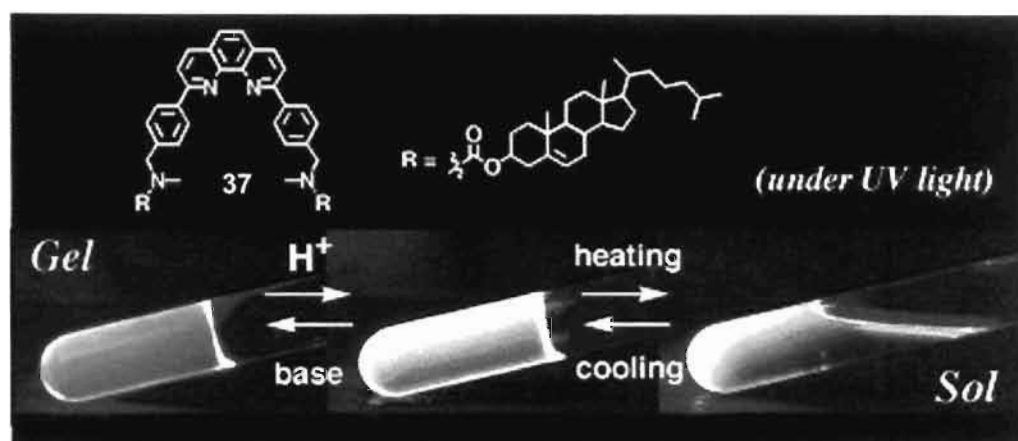
FIGURE 1.18. Emission changes in the phenanthroline-appended cholesterol based gelator **37** upon protonation. (adapted from ref. 39b)

The cholesterol appended 1,10-phenanthroline based gelator **37** is an example of a proton sensitive energy transfer system (Figure 1.18).[39b] In the presence of two equivalents of trifluoroacetic acid (TFA), the purple emission

(360 nm) of the gel phase of **37** is quenched completely, with the appearance of

the yellow emission (530 nm) corresponding to the protonated form of **37**, due to

energy transfer from the neutral to the protonated form. However, when the gel

was converted into the solution phase at 90 °C in the presence of TFA, a blue

emission with bimodal maximum was obtained indicating the absence of energy

transfer.
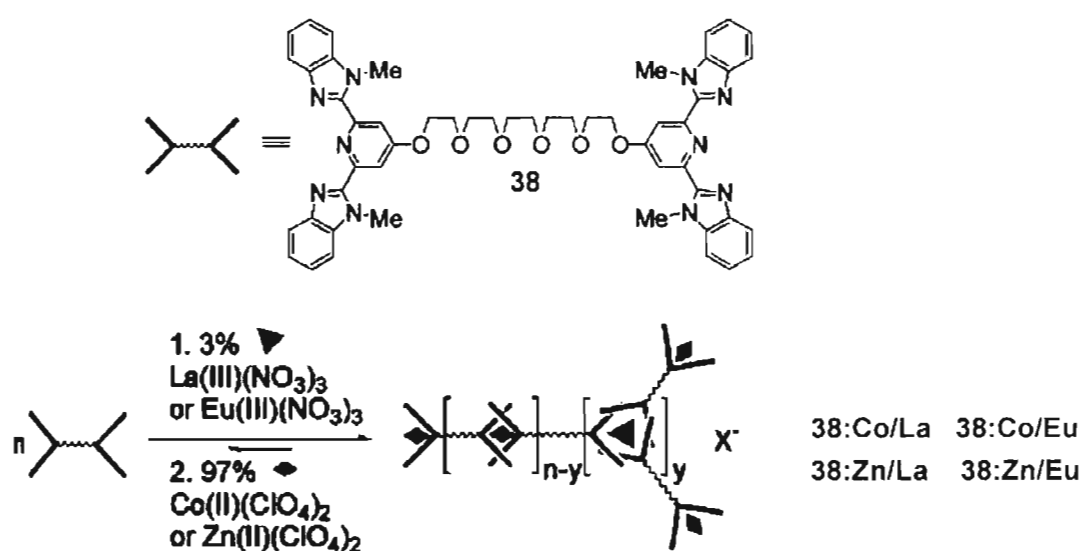
FIGURE 1.19. Schematic representation of the formation of a metallo-supramolecular gel like material using a combination of lanthanoid and transition metal ions mixed with monomer **38**. (adapted from ref. 40)

The metallo-supramolecular gel of compound **38** which responds to metal-

ligand interactions is an example of stimuli responsive gel.[40] The different binding

modes of the tridentate ligand bis(2,6-bis(1'-methylbenzimidazolyl)-4-

hydroxypyridine) (BIP) with transition metal ions (2:1 complex) and lanthanide

ions (3:1 complex) are advantageous to the formation of a supramolecular gel

(Figure 1.19). Compound **38** spontaneously forms gel upon addition of the lanthanoid(III) nitrate (3 mol%) followed by the transition metal ion perchlorate (97 mol%) to a solution of **38** in $CHCl_3/CH_3CN$.
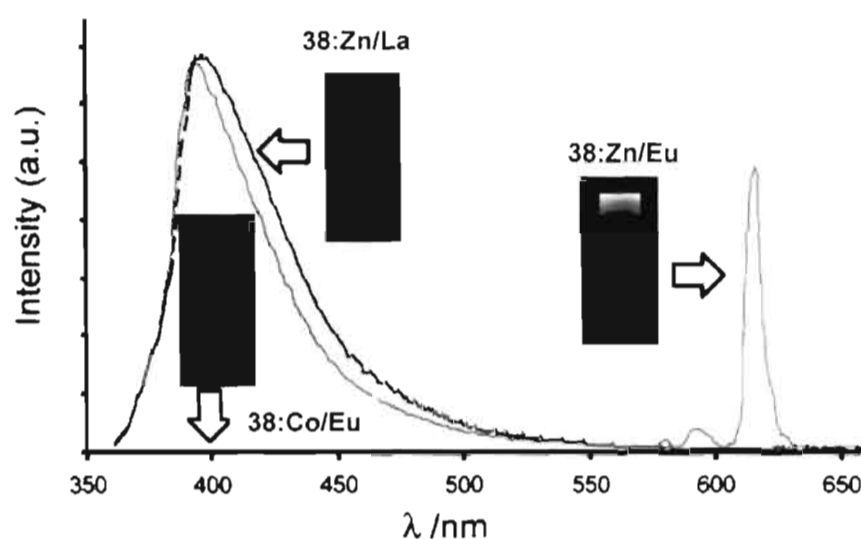
FIGURE 1.20. Photoluminescent spectra of metallo-supramolecular gels prepared in acetonitrile (excited at 340 nm). **38**:Co/Eu shows no photoluminescence and lies essentially along the baseline. The insets show the gels under UV light (365 nm). (adapted from ref. 40)

Excitation (λ_{ex} = 340 nm) of **38**:Zn/Eu system results in intense emission from Eu(III) ions (Figure 1.20). The emission is due to efficient ligand to metal energy transfer process. While **38**:Zn/La displayed emission from metal-bound ligand (λ_{ex} = 397 nm), **38**:Co/Eu did not emit at all, probably due to the presence of low energy metal centered levels which facilitate radiationless decay process. Addition of small amount of formic acid to the luminescent gel of **38**:Zn/Eu results in the disruption of the gel and a strong quenching of Eu(III) emission. This could be due to the displacement of the BIP ligand by formate ions, which

eventually 'switch off' the antenna effect. This process could be reversed by the evaporation of the solvent followed by reswelling of the material with CH_3CN, which will restore the Eu(III) emission.
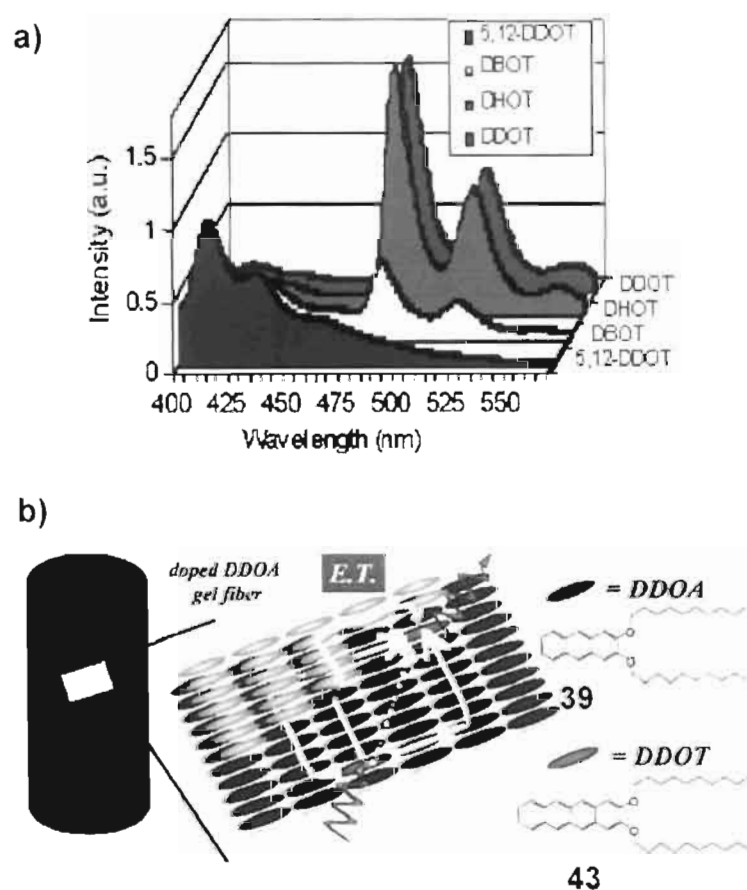
FIGURE 1.21. a) Emission spectra of doped DDOA (39) gels in DMSO at 293 K, with 1 mol% of 5,12-DDOT (40), DBOT (41), DHOT (42), and DDOT (43) respectively. b) Schematic representation of energy transfer process in DDOA gel fiber. Energy transfer pathways are depicted by yellow arrows. (adapted from ref. 41c)

Recently, Del Guerzo et al. have demonstrated the versatility of anthracene based organogels as a medium to study the energy transfer process.[41] They have used 2,3-*n*-didecyloxyanthracene (DDOA, 39) as the excitation energy donor and

2,3-*n*-dialkoxytetracene derivatives (D*n*OTs, **40-43**) as the acceptors. The doping of DDOA gels with D*n*OTs facilitated energy transfer from excited anthracenes to the tetracene derivatives (Figure 1.21a). Detailed energy transfer studies showed that the efficiency of the process is highly influenced by the structural and chemical similarity between tetracene acceptors and DDOA. In this case, the energy transfer is found to be highly efficient, as the acceptor is required in very small quantities. The high energy transfer efficiency of the present system indicates the involvement of exciton migration in addition to the direct energy transfer from the closest donor molecules (Figure 1.21b).

44

45
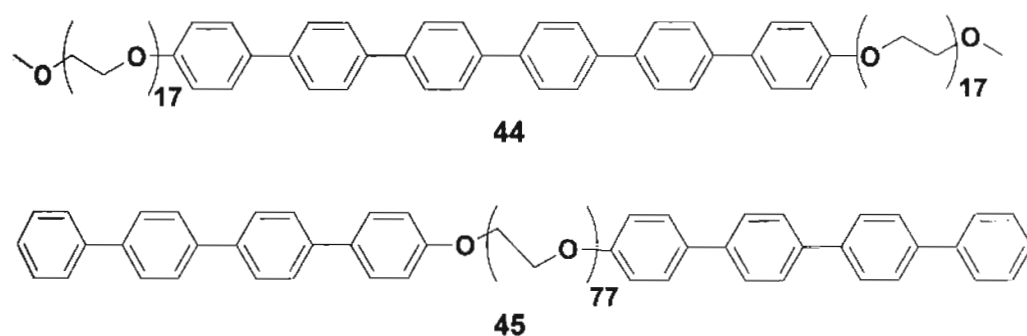
CHART 1.5. Molecular structure of the coil-rod-coil molecule **44** and the rod-coil-rod molecule **45**.

Recently Lee et al. have shown the self-assembly of the amphiphilic triblock coil-rod-coil molecule **44** and the rod-coil-rod molecule **45** in aqueous solution to cylindrical micellar structures (Chart 1.5).[42] Addition of small amount of **45** as a bridging agent to **44** resulted in the formation of a reversible nematic gel (Figure 1.22a). Detailed morphological studies showed that these dynamic

interconnections lead to stiff bundles composed of cylindrical micelles that are responsible for the formation of the nematic gel. More importantly under this condition excitation of the co-assembly at 290 nm, where most of the radiation is absorbed by **45**, resulted in strong emission from **44** at 431 nm (Figure 1.22b). These results indicate that energy transfer takes place from **45** to **44**, which is an additional evidence for the formation of the co-assembly between **44** and **45**.
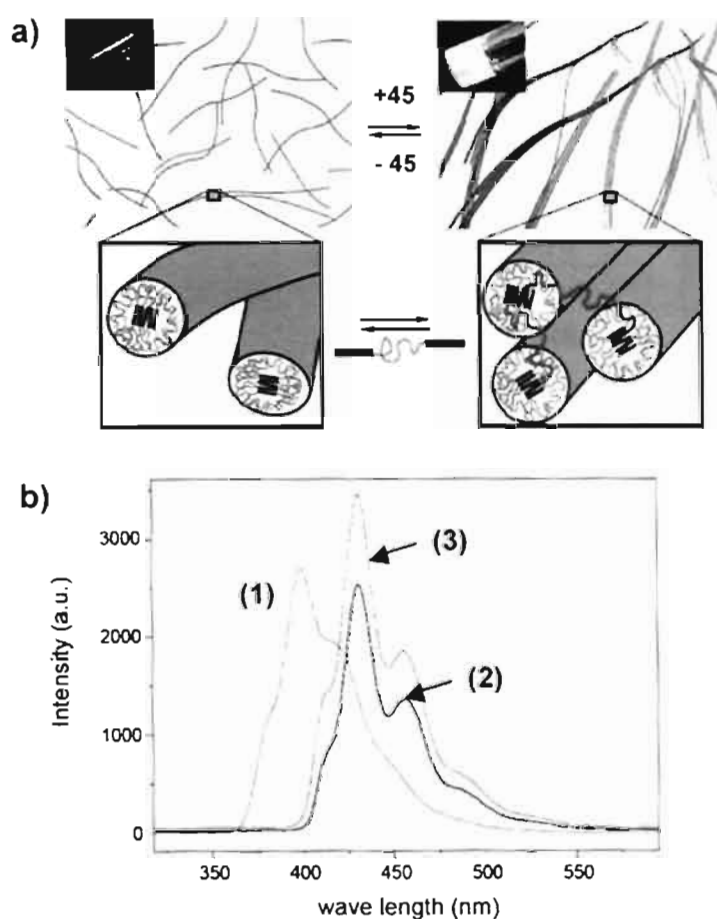
FIGURE 1.22. a) Cartoon representation of the reversible bridging between the isotropic fluid and the nematic gel of the supramolecular nanocylinders. b) Fluorescence spectra (λ_{ex} = 290 nm) of the aqueous solution of **45** (1), **44** (2) and **44+45** (3). (adapted from ref. 42)

Recently, Hamachi and co-workers have successfully demonstrated energy transfer between artificial receptors and suitable acceptors which are noncovalently immobilized in a semi-wet supramolecular hydrogel.[43] This system is useful for the detection and discrimination of biologically important phosphate derivatives. A glycosylated amino acetate type hydrogelator **46** (Chart 1.6) is found to be effective for this purpose.
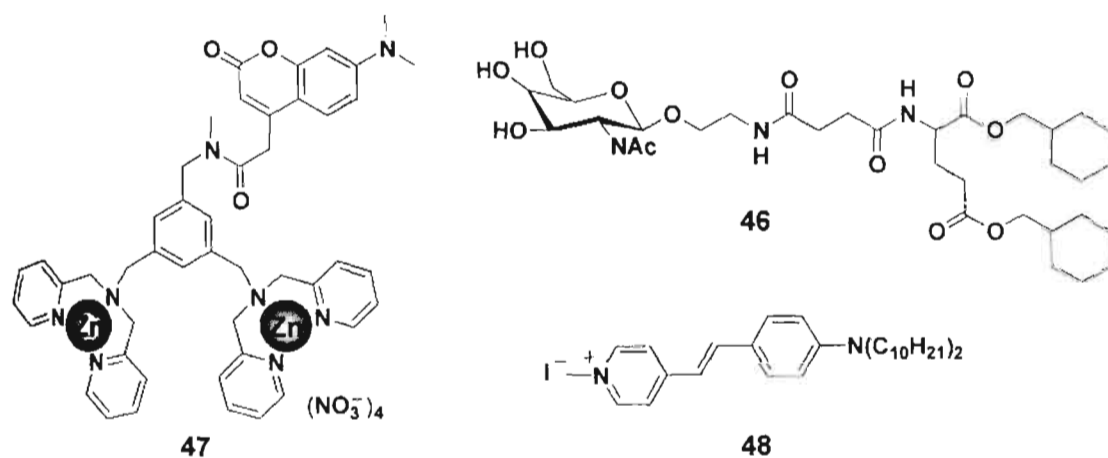
CHART 1.6. Molecular structures of the glycosylated amino acetate type hydrogelator **46**, coumarin-appended phosphate receptor **47** (energy transfer donor) and styryl dye **48** (energy transfer acceptor).

The guest (phosphate derivatives) dependent redistribution of the artificial receptor in the hydrophobic and hydrophilic domain of the supramolecular hydrogel results in substantial difference in the FRET efficiency (Figure 1.23a). A semi-wet molecular recognition (MR) chip for the rapid and high-throughput sensing could be developed based on the above system (Figure 1.23b).

a) **FRET cancelled**   **FRET enhanced**

hydrophilic phosphate   hydrophobic phosphate

gel fiber

b) 47,48 + Anion

c) 47 + Anion

receptor only	Phosphate	PhP	phospho-Tyr	ATP	Me₂P
Ph₂P	cAMP	Sulfate	Carbonate	Nitrate	Acetate
Fluoride	Chloride	Bromide	Azide	Glucose	Acetyl choline
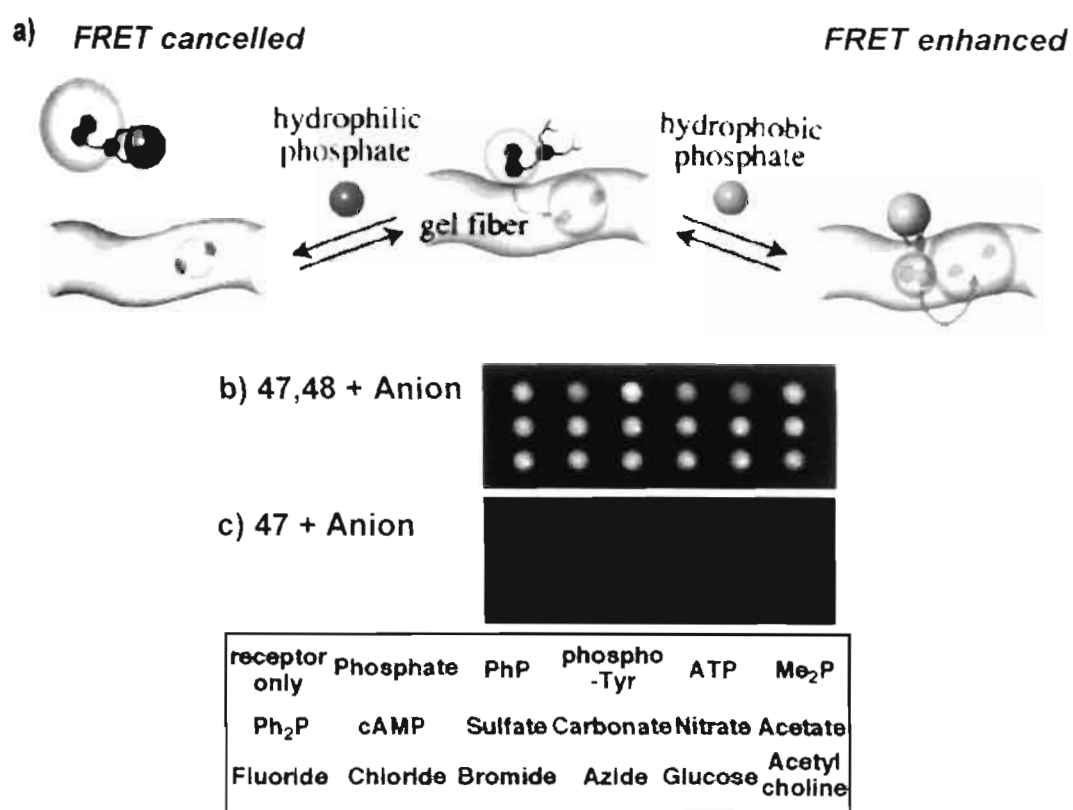
FIGURE 1.23. a) Illustration of the guest-dependent FRET system using **47** and **48** by the addition of PhP or ATP in a hydrogel matrix. Digital camera photographs of the sensing patterns of semi-wet molecular recognition (MR) chips of the hydrogel **46** containing b) the coumarin-appended receptor **47** with the styryl dye **48** and c) **47** without **48** in the presence of various anions. The spotted position of anions is shown in the bottom of the figure. (adapted from ref. 43)

1,3,5-Cyclohexyltricarboxamide based hydrogelator (**49**) comprising of two hydrophilic moieties and one hydrophobic substituent containing a naphthalenic group is a good excitation energy donor to the dansyl fluorophore **50** (Figure 1.24).[44] The formation of H-type aggregates of the naphthalene moiety favors very fast energy migration in the gel scaffold. Addition of 1% of the dansyl fluorophore **50**, results in 50% quenching of the emission of the gel with strong emission at

490 nm. A 5-fold higher concentration of **50** enhances the energy transfer efficiency to 75%. Under this condition both entrapped and free acceptors are present. The emission maximum of the entrapped **50** (λ_{em} – 490 nm, λ_{ex} = 290 nm) after energy transfer indicates that the fluorophore is surrounded by a nonaqueous environment of the donor molecules within the water medium (Figure 1.24b). On the other hand, direct excitation of **50** (λ_{ex} = 365 nm) results in the shift of the emission maximum to 535 nm due to the combined emission from molecules existing in the gel fiber (λ_{em} = 490 nm) and in the solution (λ_{em} = 560 nm, Figure 1.24c). Detailed steady state and time resolved fluorescence spectroscopic studies revealed that around 30% of the total dansyl fluorophore (**50**) gets incorporated into the gel fiber and participated in the light harvesting process.
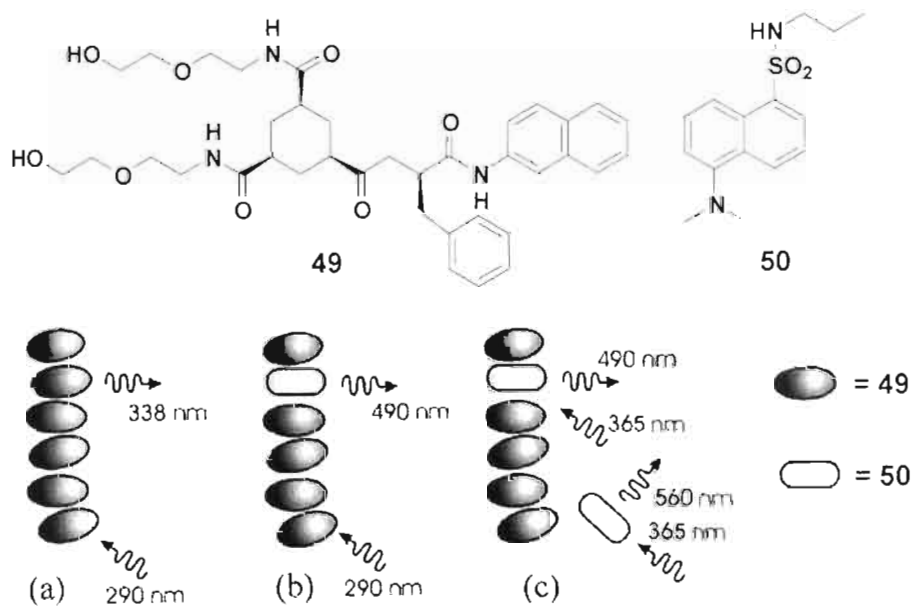
FIGURE 1.24. Representation of the energy transfer process in 1,3,5-cyclohexyltricarboxamide based hydrogelator **49** doped with dansyl fluorophore **50**. (adapted from ref. 44)

1.6. Origin, Objectives and Approach to the Thesis

Self-assembly of small molecules into nanosized architectures, using the principles of supramolecular chemistry is a topic of considerable importance. In this context, self-organization of linear π-conjugated molecules with the aid of weak noncovalent associations are of extreme importance. Linearly conjugated molecules, by virtue of their delocalized π-electrons, are the integral part of organic electronic devices.[5,6] Detailed studies revealed that, electron and energy transport properties in these molecules are strongly influenced by the proper alignment of the chromophores within the self-assembly.[10] Oligo(*p*-phenylenevinylene)s are one of the extensively studied class of molecules due to interesting opto-electronic properties.[7-9] The strong π-π interaction provided by the rigid OPV π-conjugated backbone is highly useful to derive self-assembled nanostructured materials from these molecules. Therefore a large number of reports pertaining to the self-assembling properties of tailor made OPVs is known in the literature.[11]

Recent studies from our group revealed a rational approach to the design of self-assembled organogels of OPVs (Figure 1.25).[45] Self-assembly of these molecules induce gelation of hydrocarbon solvents at very low concentrations (< 1 mM) resulting in high aspect ratio nanostructures. Detailed morphological studies revealed the formation of twisted and entangled supramolecular nanotapes of

several micrometers in length scale. These structures are responsible for the gelation of OPVs and are found to be distinctly different from the nanostructures created by directional multiple H-bonded assemblies[11] and diblock polymers.[29,30] The hierarchical growth of the entangled tapes and the consequent gelation is attributed to the lamellar type packing of the molecules, facilitated by co-operative H-bonding, π-stacking and van der Waal's interactions of the OPV units resulting in network structures (Figure 1.25c).[46]
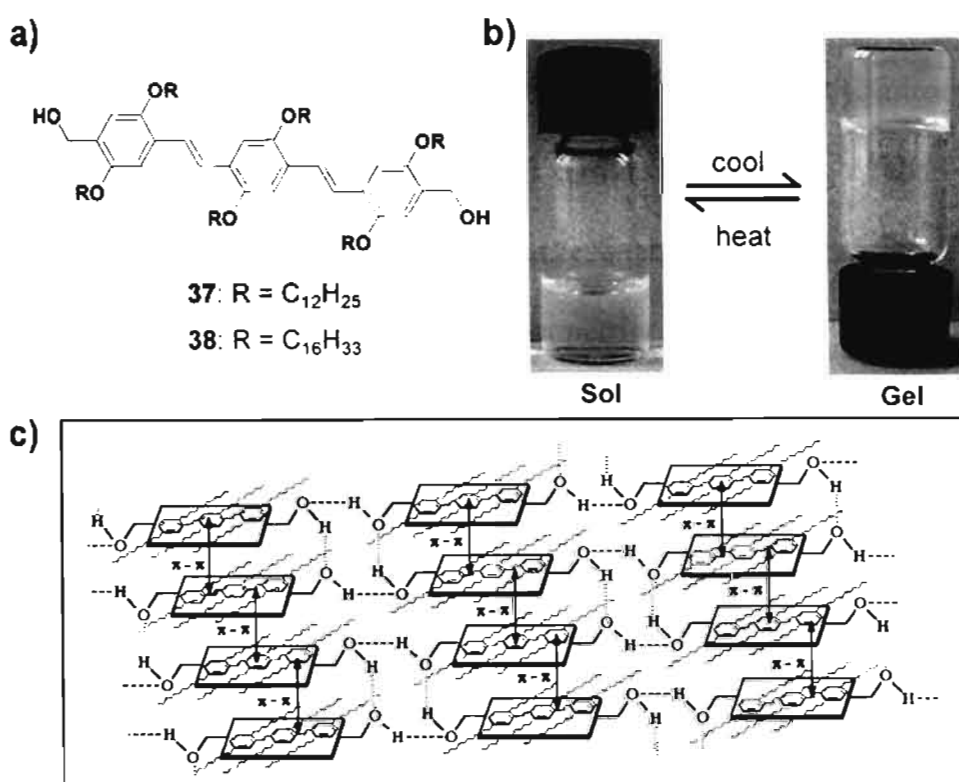
FIGURE 1.25. a) Structures of the gel forming OPVs. b) Photograph of **37** in cyclohexane before and after gelation. c) Probable self-assembly of OPVs, depicting the H-bond and π-stack induced three dimensional network formations.

Gelation of OPVs induces remarkable changes in the absorption and emission properties. The modulation of emission in the gel state is more predominant than that in the simple aggregates.[46a,c] The interesting optical properties particularly remarkable modulation in the emission properties of OPVs during the gelation is highly attractive and warrant further investigation. More importantly, OPV self-assemblies are potential excitation energy donors. The present thesis aims at exploring these interesting properties of OPVs for the designing of functional π-organogels with tunable emission properties. For this purpose we have selected two different approaches. The first approach is based on the modulation of the optical properties of OPV chromophore by introducing donor-acceptor substitution. The second one is based on the tuning of the optical properties of OPV derived gels by fluorescence resonance energy transfer (FRET) to suitable acceptors having desired emission properties.

In order to fulfill the above mentioned objectives, the design and synthesis of a variety of OPVs with appropriate structural variations were planned. To accomplish the first objective we set out a design principle which involves the functionalization of OPV backbone with dipolar end functional groups (acceptor, A) and sufficient number of alkoxy side chains (donor, D) in a A-D-D-D-A type substitution pattern. We anticipated that these functional groups will serve as self-assembling motifs to induce gelation. At the same time they could influence the electronic properties of the parent chromophore. In such an event the optical

properties of OPVs could be modulated both in molecular and supramolecular level. Therefore, we planned to conduct a detailed investigation on the optical properties of OPVs in the molecularly dissolved and gel state using different spectroscopic techniques such as UV/Vis absorption, steady state and time resolved emission. In addition, it was planned to conduct a detailed morphological ananlyses of OPV self-assembly using advanced microscopic techniques. Apart from this, the potential use of these gels to the design of light harvesting was aimed. Detailed investigation to understand the energy migration properties of the OPV donor scaffold using different time resolved spectroscopic techniques were also planned. The present thesis is a detailed and systematic approach to the realization of the above objectives which are presented in the subsequent three chapters.

1.7. References

1. (a) *Energy Harvesting Materials* (Ed.: D. L. Andrews) World Scientific: Singapore, **2005**. (b) T. Ritz, A. Damjanović, K. Schulten, *ChemPhysChem* **2002**, *3*, 243. (c) A. M. van Oijen, M. Ketelaars, J. Köhler, T. J. Aartsma, J. Schmidt, *Science* **1999**, *285*, 400. (d) X. Hu, A. Damjanović, T. Ritz, K. Schulten, *Proc. Natl. Acad. Sci. U. S. A.* **1998**, *95*, 5935.

2. (a) S. Bahatyroval, R. N. Frese, C. A. Siebert, J. D. Olsen, K. O. van der Werf, R. van Grondelle, R. A. Niederman, P. A. Bullough, C. Otto, C. N. Hunter, *Nature* **2004**, *430*, 1058. (b) W. Kühlbrandt, *Nature* **1995**, *374*, 497.

(c) G. McDermott, S. M. Prince, A. A. Freer, A. M. Hawthornthwaite-Lawless, M. Z. Papiz, R. J. Cogdell, N. W. Isaacs, *Nature* **1995**, *374*, 517. (d) W. Kühlbrandt, D. N. Wang, *Nature* **1991**, *350*, 130.

3. (a) J. R. Lakowicz, *Principles of Fluorescence Spectroscopy* (2nd ed.), Kluwer Academic/Plenum Publishers: New York **1999**. (b) B. W. Van Der Meer, G. Coker III, S.-Y. S. Chen, *Resonance Energy Transfer, Theory and Data*, VCH: New York, **1994**. (c) N. J. Turro, *Modern Molecular Photochemistry*, University Science Books: Sausalito, **1991**.

4. (a) D. L. Dexter, *J. Chem. Phys.* **1953**, *21*, 836. (b) T. Förster, *Ann. Phys.* **1948**, *2*, 55.

5. (a) S. R. Forrest, *Nature* **2004**, *428*, 911. (b) J. M. Tour, *Molecular Electronics: Commercial Insights, Chemistry, Devices, Architectures and Programming*, World Scientific: River Edge, New Jersey, **2003**. (c) R. L. Carroll, C. B. Gorman, *Angew. Chem., Int. Ed.* **2002**, *41*, 4378. (d) A. Kraft, A. C. Grimsdale, A. B. Holmes, *Angew. Chem., Int. Ed.* **1998**, *37*, 402. (e) *Electronic Materials: The Oligomer Approach* (Eds: K. Müllen, G. Wegner), VCH: Weinheim, **1998**.

6. (a) A. P. H. J. Schenning, E. W. Meijer, *Chem. Commun.* **2005**, 3245. (b) M. Van Der Auweraer, F. C. De Schryver, *Nat. Mater.* **2004**, *3*, 507. (c) E. W. Meijer, A. P. H. J. Schenning, *Nature* **2002**, *419*, 353.

7. For reviews of oligo(*p*-phenylenevinylene)s based π-conjugated systems, see: (a) S. R. Marder, *Chem. Commun.* **2006**, 131. (b) H. Meier, *Angew. Chem., Int. Ed.* **2005**, *44*, 2482. (c) J. L. Segura, N. Martín *J. Mater. Chem.* **2000**, *10*, 2403. (d) U. Scherf, *Top. Curr. Chem.* **1999**, *201*, 163. (e) P. F. van Hutten,
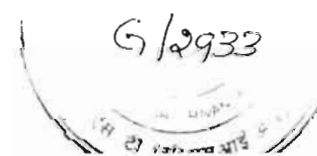
V. V. Krasnikov, G. Hadziioannou, *Acc. Chem. Res.* **1999**, *32*, 257. (f) H. Meier, U. Stalmach, H. Kolshorn, *Acta Polym.* **1997**, *48*, 379. (g) A. Greiner, B. Bolle, P. Hesemann, J. M. Oberski, R. Sander, *Macromol. Chem. Phys.* **1996**, *197*, 113. (h) K. Müllen, *Pure Appl. Chem.* **1993**, *65*, 89.

8. (a) B. R. Crenshaw, C. Weder, *Adv. Mater.* **2005**, *17*, 1471. (b) F. He, H. Xu, B. Yang, Y. Duan, L. Tian, K. Huang, Y. Ma, S. Liu, S. Feng, J. Shen *Adv. Mater.* **2005**, *17*, 2710. (c) H. Y. Woo, B. Liu, B. Kohler, D. Korystov, A. Mikhailovsky, G. C. Bazan, *J. Am. Chem. Soc.* **2005**, *127*, 14721. (d) J. N. Wilson, M. D. Smith, V. Enkelmann, U. H. F. Bunz, *Chem. Commun.* **2004**, 1700. (e) C.-L. Li, S.-J. Shieh, S.-C. Lin, R.-S. Liu, *Org. Lett.* **2003**, *5*, 1131.

9. (a) S. Wang, W. J. Oldham Jr., R. A. Hudack, Jr., G. C. Bazan, *J. Am. Chem. Soc.* **2000**, *122*, 5695. (b) E. Peeters, A. M. Ramos, S. C. J. Meskers, R. A. J. Janssen, *J. Chem. Phys.* **2000**, *112*, 9445. (c) B. Strehmel, A. M. Sarker, J. H. Malpert, V. Strehmel, H. Seifert, D. C. Neckers, *J. Am. Chem. Soc.* **1999**, *121*, 1226. (d) M. Albota, D. Beljonne, J.-L. Brédas, J. E. Ehrlich, J.-Y. Fu, A. A. Heikal, S. E. Hess, T. Kogej, M. D. Levin, S. R. Marder, D. McCord-Maughon, J. W. Perry, H. Röckel, M. Rumi, G. Subramaniam, W. W. Webb, S.-L. Wu, C. Xu, *Science* **1998**, *281*, 1653. (e) T. Maddux, W. Li, L. Yu, *J. Am. Chem. Soc.* **1997**, *119*, 844.

10. For recent reviews of supramolecular organization of chromophores, see: (a) F. J. M. Hoeben, P. Jonkheijm, E. W. Meijer, A. P. H. J. Schenning, *Chem. Rev.* **2005**, *105*, 1491. (b) *Supramolecular Dye Chemistry* (Ed.: F. Würthner), Topics in Current Chemistry: Springer Berlin/Newyork, *258*, **2005**.

11. (a) R. W. Sinkeldam, F. J. M. Hoeben, M. J. Pouderoijen, I. De Cat, J. Zhang, S. Furukawa, S. De Feyter, J. A. J. M. Vekemans, E. W. Meijer, *J. Am. Chem. Soc.* **2006**, *128*, 13298. (b) C. R. L. P. N. Jeukens, P. Jonkheijm, F. J. P. Wijnen, J. C. Gielen, P. C. M. Christianen, A. P. H. J. Schenning, E. W. Meijer, J. C. Maan, *J. Am. Chem. Soc.* **2005**, *127*, 8280. (c) P. Jonkheijm, A. Miura, M. Zdanowska, F. J. M. Hoeben, S. De Feyter, A. P. H. J. Schenning, F. C. De Schryver, E. W. Meijer, *Angew. Chem., Int. Ed.* **2004**, *43*, 74. (d) P. Jonkheijm, F. J. M. Hoeben, R. Kleppinger, J. van Herrikhuyzen, A. P. H. J. Schenning, E. W. Meijer, *J. Am. Chem. Soc.* **2003**, *125*, 15941. (e) A. P. H. J. Schenning, P. Jonkheijm, E. Peeters, E. W. Meijer, *J. Am. Chem. Soc.* **2001**, *123*, 409. (f) A. El-ghayoury, A. P. H. J. Schenning, P. A. van Hal, J. K. J. van Duren, R. A. J. Janssen, E. W. Meijer, *Angew. Chem., Int. Ed.* **2001**, *40*, 3660.

12. (a) J. F. Hulvat, M. Sofos, K. Tajima, S. I. Stupp, *J. Am. Chem. Soc.* **2005**, *127*, 366. (b) B. W. Messmore, J. F. Hulvat, E. D. Sone, S. I. Stupp, *J. Am. Chem. Soc.* **2004**, *126*, 14452. (c) G. N. Tew, M. U. Pralle, S. I. Stupp, *J. Am. Chem. Soc.* **1999**, *121*, 9852. (d) G. N. Tew, L. Li, S. I. Stupp, *J. Am. Chem. Soc.* **1998**, *120*, 5601.

13. (a) O. J. Dautel, G. Wantz, R. Almairac, D. Flot, L. Hirsch, J.-P. Lere-Porte, J.-P. Parneix, F. Serein-Spirau, L. Vignau, J. J. E. Moreau, *J. Am. Chem. Soc.* **2006**, *128*, 4892. (b) U. Hahn, M. Elhabiri, A. Trabolsi, H. Herschbach, E. Leize, A. Van Dorsselaer, A.-M. Albrecht-Gary, J.-F. Nierengarten, *Angew. Chem., Int. Ed.* **2005**, *44*, 5338. (c) H. Wang, W. You, P. Jiang, L. Yu, H. H. Wang, *Chem. –Eur. J.* **2004**, *10*, 986. (d) F. Cacialli, J. S. Wilson, J. J.

Michels, C. Daniel, C. Silva, R. H. Friend, N. Severin, P. Samorì, J. P. Rabe, M. J. O'Connell, P. N. Taylor, H. L. Anderson, *Nat. Mater.* **2002**, *1*, 160.

14. (a) N. Armaroli in *Fullerenes: From Synthesis to Optoelectronic Properties* (Eds.: D. M. Guldi, N. Martin), Kluwer Academic Publishers: Dordrecht, **2002**, pp. 137. (b) N. Armaroli, G. Accorsi, Y. Rio, J.-F. Nierengarten, J.-F. Eckert, M. J. Gómez-Escalonilla, F. Langa, *Synth. Met.* **2004**, *147*, 19 and references therein. (c) M. Gutierrez-Nava, G. Accorsi, P. Masson, N. Armaroli, J.-F. Nierengarten, *Chem. –Eur. J.* **2004**, *10*, 5076. (d) F. Langa, M. J. Gómez-Escalonilla, J.-M. Rueff, T. M. F. Duarte, J.-F. Nierengarten, V. Palermo, P. Samorì, Y. Rio, G. Accorsi, N. Armaroli, *Chem. –Eur. J.* **2005**, *11*, 4405. (e) N. Armaroli, G. Accorsi, J. N. Clifford, J.-F. Eckert, J.-F. Nierengarten, *Chem. –Asian. J.* **2006**, *1*, 564. (f) T. M. Figueira-Duarte, A. Gégout, J.-F. Nierengarten, *Chem. Commun.* **2007**, 109.

15. (a) D. M. Guldi, A. Swartz, C. Luo, R. Gómez, J. L. Segura, N. Martín, *J. Am. Chem. Soc.* **2002**, *124*, 10875. (b) F. Giacalone, J. L. Segura, N. Martín, J. Ramey, D. M. Guldi, *Chem. –Eur. J.* **2005**, *11*, 4819.

16. (a) E. E. Neuteboom, P. A. van Hal, R. A. J. Janssen, *Chem. –Eur. J.* **2004**, *10*, 3907. (b) E. E. Neuteboom, S. C. J. Meskers, P. A. van Hal, J. K. J. van Duren, E. W. Meijer, R. A. J. Janssen, H. Dupin, G. Pourtois, J. Cornil, R. Lazzaroni, J.-L. Brédas, D. Beljonne, *J. Am. Chem. Soc.* **2003**, *125*, 8625. (c) A. M. Ramos, S. C. J. Meskers, P. A. van Hal, J. Knol, J. C. Hummelen, R. A. J. Janssen, *J. Phys. Chem. A* **2003**, *107*, 9269 (d) P. A. van Hal, R. A. J. Janssen, G. Lanzani, G. Cerullo, M. Zavelani-Rossi, S. De Silvestri, *Phys. Rev. B* **2001**, *64*, 075206/1.

17. (a) K. Brunner, J. A. E. H. van Haare, B. M. W. Langeveld-Voss, H. F. M. Schoo, J. W. Hofstraat, A. van Dijken, *J. Phys. Chem. B* **2002**, *106*, 6834. (b) J. Morgado, F. Cacialli, R. Iqbal, S. C. Moratti, A. B. Holmes, G. Yahioglu, L. R. Milgrom, R. H. Friend, *J. Mater. Chem.* **2001**, *11*, 278. (c) J. Morgado, F. Cacialli, R. H. Friend, R. Iqbal, G. Yahioglu, L. R. Milgrom, S. C. Moratti, A. B. Holmes, *Chem. Phys. Lett.* **2000**, *325*, 552. (d) P. H. Bolivar , G. Wegmann, R. Kersting, M. Deussen, U. Lemmer, R. E. Mahrt, H. Bässler, E. O. Göbel, H. Kurz, *Chem. Phys. Lett.* **1995**, *245*, 534.

18. (a) A. P. H. J. Schenning, E. Peeters, E. W. Meijer, *J. Am. Chem. Soc.* **2000**, *122*, 4489. (b) K. Tajima, L.-s. Li, S. I. Stupp, *J. Am. Chem. Soc.* **2006**, *128*, 5488.

19. (a) N. Armaroli, J.-F. Eckert, J.-F. Nierengarten, *Chem. Commun.* **2000**, 2105. (b) N. Armaroli, *Photochem. Photobiol. Sci.* **2003**, *2*, 73. (c) N. Armaroli, G. Accorsi, Y. Rio, J.-F. Nierengarten, J.-F. Eckert, M. J. Gomez-Escalonilla, F. Langa, *Synth. Met.* **2004**, *147*, 19. (d) N. Armaroli, G. Accorsi, J.-P. Gisselbrecht, M. Gross, J.-F. Eckert, J.-F. Nierengarten, *New J. Chem.* **2003**, *27*, 1470.

20. For reviews on H-bonded assemblies based energy transfer systems, see: (a) L. S. Sánchez, N. Martín, D. M. Guldi, *Angew. Chem., Int. Ed.* **2005**, *44*, 5374. (b) M. D. Ward, *Chem. Soc. Rev.* **1997**, *26*, 365.

21. A. Ajayaghosh, S. J. George, A. P. H. J. Schenning, *Top. Curr. Chem.* **2005**, *258*, 83 and references therein.

22. (a) E. H. A. Beckers, P. A. van Hal, A. P. H. J. Schenning, A. El-ghayoury, E. Peeters, M. T. Rispens, J. C. Hummelen, E. W. Meijer, R. A. J. Janssen,

J. Mater. Chem. **2002**, *12*, 2054. (b) M. T. Rispens, L. Sanchez, E. H. A. Beckers, P. A. van Hal, A. P. H. J. Schenning, A. El-ghayoury, E. Peeters, E. W. Meijer, R. A. J. Janssen, J. C. Hummelen, *Synth. Met.* **2003**, *135-136*, 801. (c) E. E. Neuteboom, E. H. A. Beckers, S. C. J. Meskers, E. W. Meijer, R. A. J. Janssen, *Org. Biomol. Chem.* **2003**, *1*, 198. (d) E. H. A. Beckers, A. P. H. J. Schenning, P. A. van Hal, A. El-ghayoury, L. Sánchez, J. C. Hummelen, E. W. Meijer, R. A. J. Janssen, *Chem. Commun.* **2002**, 2888.

23. (a) F. J. M. Hoeben, L. M. Herz, C. Daniel, P. Jonkheijm, A. P. H. J. Schenning, C. Silva, S. C. J. Meskers, D. Beljonne, R. T. Phillips, R. H. Friend, E. W. Meijer, *Angew. Chem., Int. Ed.* **2004**, *43*, 1976. (b) C. Daniel, L. M. Herz, D. Beljonne, F. J. M. Hoeben, P. Jonkheijm, A. P. H. J. Schenning, E. W. Meijer, R. T. Phillips, C. Silva, *Synth. Met.* **2004**, *147*, 29. (c) D. Beljonne, E. Hennebicq, C. Daniel, L. M. Herz, C. Silva, G. D. Scholes, F. J. M. Hoeben, P. Jonkheijm, A. P. H. J. Schenning, S. C. J. Meskers, R. T. Phillips, R. H. Friend, E. W. Meijer, *J. Phys. Chem. B* **2005**, *109*, 10594.

24. S. Jang, M. Newton, R. J. Silbey, *Phys. Rev. Lett.* **2004**, *92*, 218301/1.

25. (a) F. J. M. Hoeben, A. P. H. J. Schenning, E. W. Meijer, *ChemPhysChem* **2005**, *6*, 2337. (b) C. Daniel, F. Makereel, L. M. Herz, F. J. M. Hoeben, P. Jonkheijm, A. P. H. J. Schenning, E. W. Meijer, *J. Chem. Phys.* **2005**, *123*, 084902/1. (c) M. H. Chang, F. J. M. Hoeben, P. Jonkheijm, A. P. H. J. Schenning, E. W. Meijer, C. Silva, L. M. Herz, *Chem. Phys. Lett.* **2006**, *418*, 196.

26. J. Zhang, F. J. M. Hoeben, M. J. Pouderoijen, A. P. H. J. Schenning, E. W. Meijer, F. C. D. Schryver, S. D. Feyter, *Chem. –Eur. J.* **2006**, *12*, 9046.

27. F. J. M. Hoeben, M. J. Pouderoijen, A. P. H. J. Schenning, E. W. Meijer, *Org. Biomol. Chem.* **2006**, *4*, 4460.

28. (a) M. Lee, B. K. Cho, W. C. Zin, *Chem. Rev.* **2001**, *101*, 3869 and references therein. (b) U. Stalmach, B. de Boer, C. Videlot, P. F. van Hutten, G. Hadziioannou, *J. Am. Chem. Soc.* **2000**, *122*, 5464. (c) B. de Boer, U. Stalmach, P. F. van Hutten, C. Melzer, V. V. Krasnikov, G. Hadziioannou, *Polymer* **2001**, *42*, 9097. (d) B. de Boer, U. Stalmach, C. Melzer, G. Hadziioannou, *Synth. Met.* **2001**, *121*, 1541.

29. (a) S. I. Stupp, V. Lebonheur, K. Walker, L. S. Li, K. E. Huggins, M. Keser, A. Amstutz, *Science* **1997**, *276*, 384. (b) G. N. Tew, M. U. Pralle, S. I. Stupp, *Angew. Chem., Int. Ed.* **2000**, *39*, 517.

30. H. Wang, M.-K. Ng, L. Wang, L. Yu, B. Lin, M. Meron, Y. Xiao, *Chem. –Eur. J.* **2002**, *8*, 3246.

31. A. M. Ramos, S. C. J. Meskers, E. H. A. Beckers, R. B. Prince, L. Brunsveld, R. A. J. Janssen, *J. Am. Chem. Soc.* **2004**, *126*, 9630.

32. (a) D. Oelkrug, A. Tompert, J. Gierschner, H. J. Egelhaaf, M. Hanack, M. Hohloch, E. Steinhuber, *J. Phys. Chem. B* **1998**, *102*, 1902. (b) J. Gierschner, H.-J. Egelhaaf, D. Oelkrug, K. Müllen, *J. Fluorescence* **1998**, *8*, 37. (c) H. J. Egelhaaf, J. Gierschner, D. Oelkrug, *Synth. Met.* **2002**, *127*, 221.

33. F. J. M. Hoeben, I. O. Shklyarevskiy, M. J. Pouderoijen, H. Engelkamp, A. P. H. J. Schenning, P. C. M. Christianen, J. C. Maan, E. W. Meijer, *Angew. Chem., Int. Ed.* **2006**, *45*, 1232.

34. M. Wolffs, F. J. M. Hoeben, E. H. A. Beckers, A. P. H. J. Schenning, E. W. Meijer, *J. Am. Chem. Soc.* **2005**, *127*, 13484.

35. O. K. Kim, J. Je, J. S. Melinger, *J. Am. Chem. Soc.* **2006**, *128*, 4532.

36. For reviews of low molecular weight organogels, see: (a) P. Terech, R. G. Weiss, *Chem. Rev.* **1997**, *97*, 3133. (b) N. M. Sangeetha, U. Maitra, *Chem. Soc. Rev.* **2005**, *34*, 821. (c) *Molecular Gels, Materials with Self-Assembled Fibrillar Networks* (Eds.: R. G. Weiss, P. Terech), Kluwer Press: Dordrecht, **2005** (d) T. Ishi-i, S. Shinkai, *Top. Curr. Chem.* **2005**, *258*, 119.

37. T. Sagawa, S. Fukugawa, T. Yamada, H. Ihara, *Langmuir* **2002**, *18*, 7223.

38. T. Nakashima, N. Kimizuka, *Adv. Mater.* **2002**, *14*, 1113.

39. (a) K. Sugiyasu, N. Fujita, S. Shinkai, *Angew. Chem., Int. Ed.* **2004**, *43*, 1229. (b) K. Sugiyasu, N. Fujita, M. Takeuchi, S. Yamada, S. Shinkai, *Org. Biomol. Chem.* **2003**, *1*, 895.

40. J. B. Beck, S. J. Rowan, *J. Am. Chem. Soc.* **2003**, *125*, 13922.

41. (a) J.-P. Desvergne, A. G. L. Olive, N. M. Sangeetha, J. Reichwagen, H. Hopf, A. Del Guerzo, *Pure. Appl. Chem.* **2006**, *78*, 2333. (b) J.-P. Desvergne, A. Del Guerzo, H. Bouas-Laurent, C. Belin, J. Reichwagen, H. Hopf, *Pure. Appl. Chem.* **2006**, *78*, 707. (c) A. Del Guerzo, A. G. L. Olive, J. Reichwagen, H. Hopf, J.-P. Desvergne, *J. Am. Chem. Soc.* **2005**, *127*, 17984.

42. J.-H. Ryu, M. Lee, *J. Am. Chem. Soc.* **2005**, *127*, 14170.

43. S. Yamaguchi, I. Yoshimura, T. Kohira, S.-i. Tamaru, I. Hamachi, *J. Am. Chem. Soc.* **2005**, *127*, 11835.

44. M. Montalti, L. S. Dolci, L. Prodi, N. Zaccheroni, M. C. A. Stuart, K. J. C. Van Bommel, A. Friggeri, *Langmuir* **2006**, *22*, 2299.

45. (a) S. J. George, A. Ajayaghosh, *Chem. –Eur. J.* **2005**, *11*, 3217. (b) S. J. George, A. Ajayaghosh, P. Jonkheijm, A. P. H. J. Schenning, E. W. Meijer, *Angew. Chem., Int. Ed.* **2004**, *43*, 3422. (c) A. Ajayaghosh, S. J. George, *J. Am. Chem. Soc.* **2001**, *123*, 5148.

Quadrupolar π-Gels: Sol-Gel Tunable Red-Green-Blue (RGB) Emission in Donor-Acceptor Type Oligo(p-phenylenevinylene)s
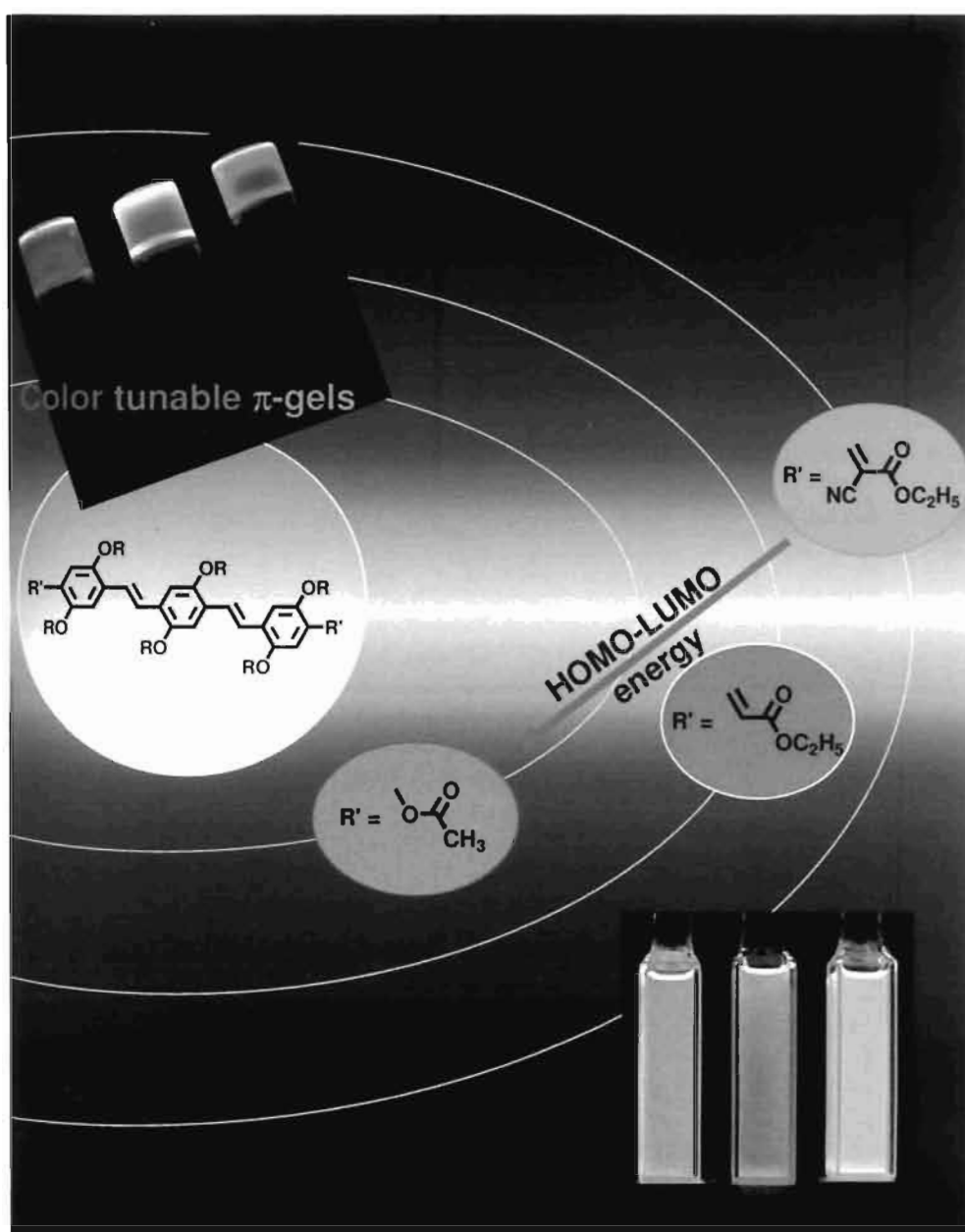
2.1. Abstract

*A-D-D-D-A type oligo(p-phenylenevinylene)s (OPVs) having terminal ester and dicyano moieties were synthesized and characterized. These molecules are analogous to quadrupolar systems which are reported to have large two-photon absorption cross section. **OPV1** with insulated ester moiety exhibited strong blue fluorescence in dichloromethane while **OPV2** having a conjugated ester group showed bright green fluorescence. However, **OPV3** with a —CN group on the ester moiety had orange emission and **OPV4** with dicyano terminal groups resulted in strong red fluorescence. Interestingly, in aliphatic hydrocarbon solvents, **OPV1-4** exhibited significant thermoreversible shift in the emission. Above a critical concentration, **OPV1-3** form fluorescent organogels in these solvents whereas **OPV4** fails to gel although resulted in weakly fluorescing aggregates. These molecules are examples of quadrupolar chromophores that form gels with tunable RGB emission. Thus, a combined molecular and supramolecular approach is shown to be effective for the modulation of the optoelectronic properties of rationally designed A-D-D-D-A type OPVs that form molecular aggregates to self-assembled gels.*

2.2. Introduction

The quest for the design of advanced materials with intriguing properties is a never ending process from fundamental as well as technological view points. This is particularly relevant to the design of organic materials for optoelectronic applications.[1-5] An important requirement to this end is the modulation of the HOMO-LUMO gap of conjugated molecules which could be achieved either by increasing the conjugation length[4c,d,5-8] or by introducing electron donor-acceptor functional groups.[7a-e,9-11] In the first approach, the convergence of absorption and emission due to limited electron delocalization with increasing conjugation length results in an optical limit though there are exceptions.[8a] On the other hand, the second strategy allows the design of conjugated molecules that emit virtually at any wavelength of the visible spectrum.

Among different classes of π-conjugated systems, monodispersed oligo(p-phenylenevinylene)s (OPVs) have attracted considerable attention due to their wide-range of applications in electrooptical devices.[3a,4c,12] Meier and coworkers have significantly contributed to the fundamental understanding of the effect of conjugation length and donor-acceptor interaction to the optical and electronic properties of OPVs and related π-conjugated systems.[7] For instance, through a systematic UV/Vis absorption study of a series of OPV derivatives **1a-j** (Figure 2.1a) and their correlation with the oligomer length, they have successfully

answered the question of effective conjugation length in phenylenevinylenes (Figure 2.1b and c).[7b,f,h]
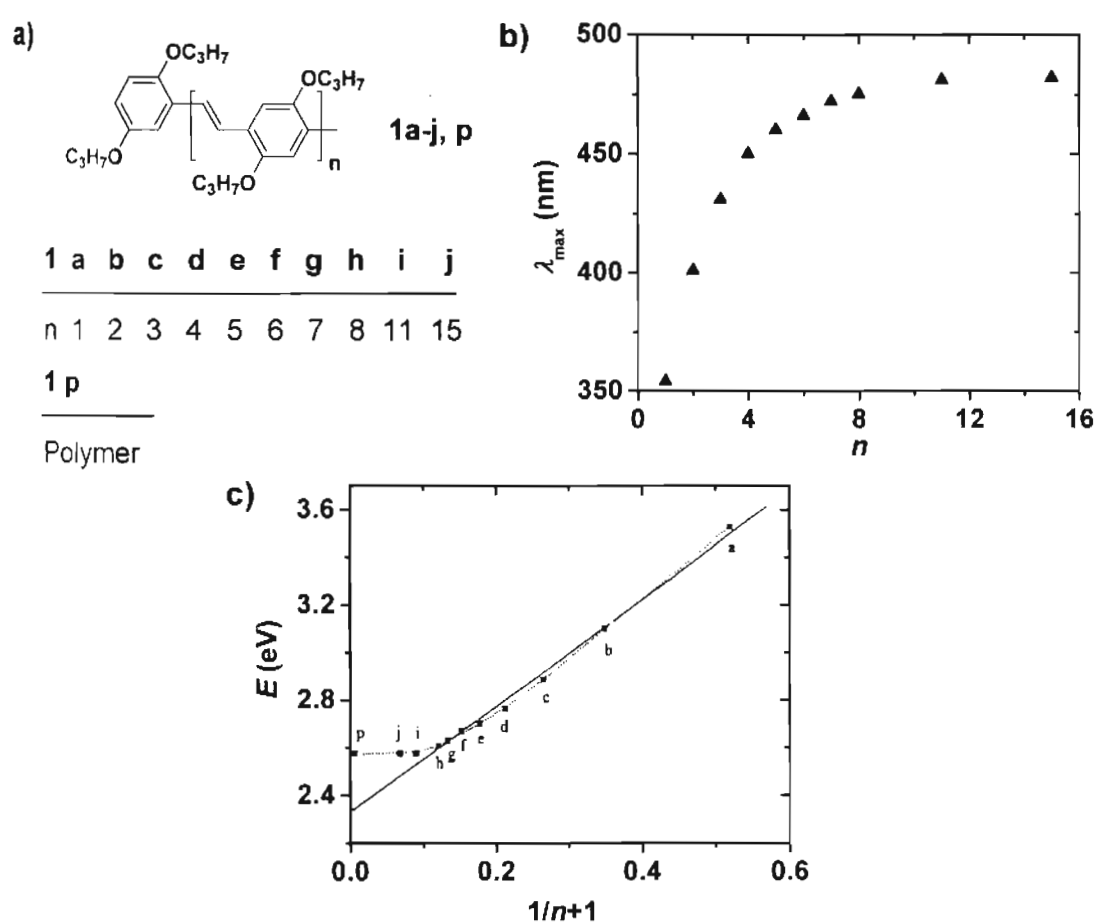
FIGURE 2.1. a) Molecular structure of the OPV derivatives **1a-j** and the polymer **1p**. b) Plot of the absorption maxima (λ_{max}) as a function of the number of repeating units (*n*). c) Plot of the energies of the long wavelength absorption maxima as a function of $(n+1)^{-1}$, the dotted line in the figure represents experimental fit function which approaches the values of the corresponding polymer **1p**. The linear function $(n+1)^{-1}$ furnishes an erroneous limiting value. (adapted from ref. 7b)

Yu and co-workers investigated the aforementioned aspect with a different series of OPV derivatives, **2a-e** (Chart 2.1).[6b] A careful analysis of λ_{max} values of OPVs **2a-e** indicates a tendency to converge to a value similar to that of OPV **1a-j**. However, it should be noted that OPV **2a-e** and **1a-j** have different substitution patterns, rendering a more accurate comparison difficult.
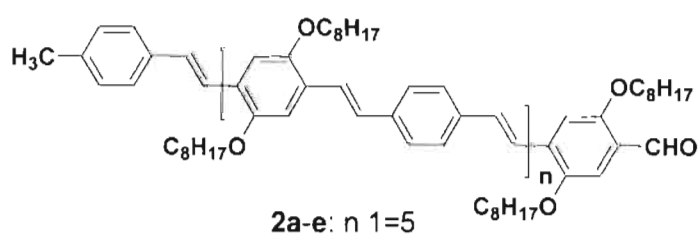
CHART 2..1.

It is well known that push-pull effect has a strong influence on the long wavelength electronic transition in conjugated oligomers with terminal donor-acceptor substituents. Recently Meier et al., reported that some OPV derivatives with strong donor and acceptor groups at the terminal positions (D-OPV-A) showing a monotonous decrease in λ_{max} values with increase in conjugation length (Figure 2.2).[7b-e] To be precise, the length of the chromophores strongly affects the intramolecular charge transfer (ICT)–an effect which superimposes upon the extension of the conjugation.
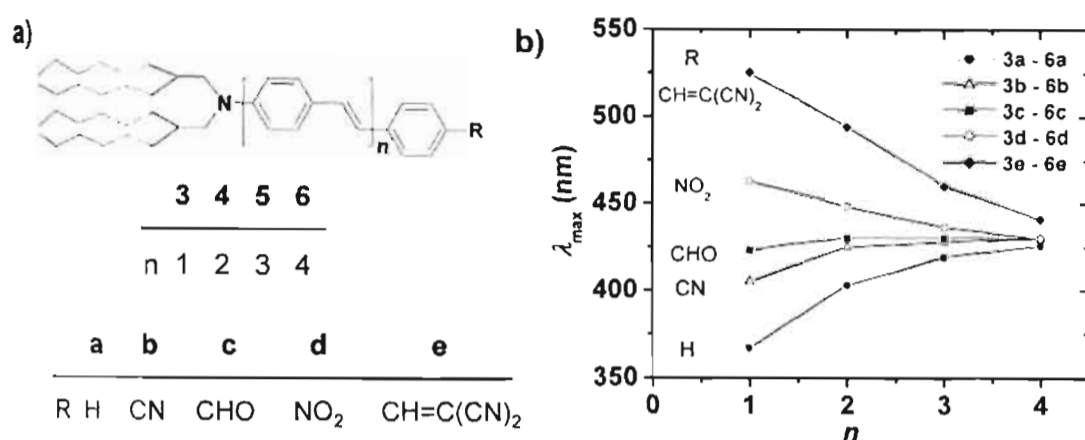
FIGURE 2.2. a) Molecular structure of OPV derivatives **3-6(a-e)**. b) Plot of the long wavelength absorption maxima (λ_{max}) of OPV series **3-6(a-e)** as a function of the number of repeating units (n). (adapted from ref. 7b)

Detailed absorption studies (Figure 2.2b) revealed that an increase in the number of repeating units (n) causes an overall bathochromic shift for the purely donor-substituted series **3a-6a** and the series **3b-6b** with −CN as a weak acceptor. The two effects annihilate each other in the series **3c-6c** with terminal −CHO groups, so that the absorption maxima are almost independent of the length of the chromophore. A hypsochromic shift is observed for the series **3d-6d** having terminal −NO$_2$ group, and an even stronger hypsochromic effect for **3e-6e** which contains the stronger acceptor group −CH=(CN)$_2$. This anomaly disappeared on protonation of the dialkylamino group since the push-pull effect disappears in the ammonium salts. Detailed semi empirical quantum mechanical (AM1, INDO/S) calculations showed that when the distance between donor and acceptor is

increased the HOMO-LUMO transition, which is mainly responsible for the ICT, becomes less important in the $S_0 \longrightarrow S_1$ electronic transitions.

One of the reasons to the design of conjugated systems with strong absorption and emission is concerned with the application as multiphoton-absorbing materials.[3a] Two-photon absorption (TPA) is a process whereby molecules simultaneously absorb two photons and is inherently weak at normal light intensities. TPA allows for the excitation of molecules with precise three-dimensional (3D) spatial confinement. It has been shown that π-conjugated molecules that undergo large changes in quadrupole moment upon excitation can show large TPA cross sections (δ).[13] It has been shown that OPVs with quadrupolar arrangements of donor and acceptor moieties result in nonlinear optical properties, dual fluorescence and large TPA cross sections (δ). Subsequently, numerous groups have successfully implemented this strategy and now a large variety of quadrupolar OPV derivatives with different substitution patterns are known in the literature. Some of the structures of quadrupolar OPV derivatives which are relevant to the present study are shown in Chart 2.2.[13-15] Though the optoelectronic properties of OPVs are well-understood on a molecular level, a supramolecular approach to the problem needs attention in the context of the emerging applications of π-conjugated oligomers in nanodevices and supramolecular electronics.[16]
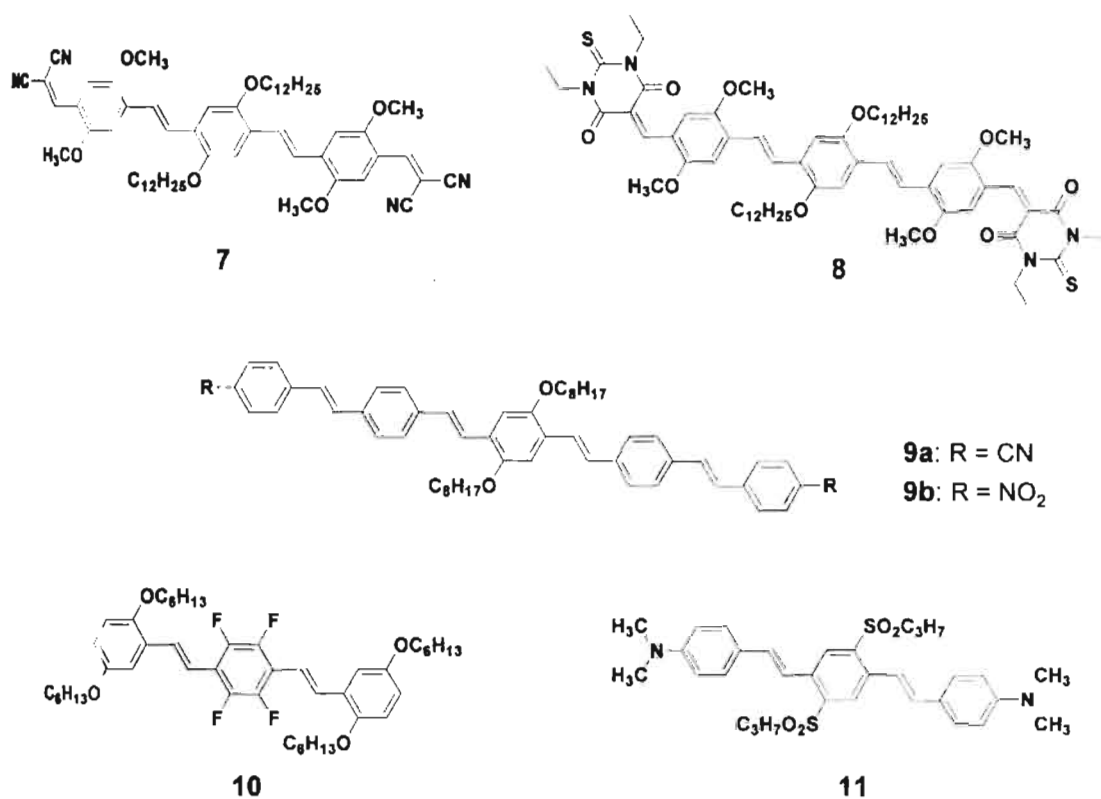
CHART 2.2. Molecular structures of centrosymmetric quadrupolar OPVs.

We were interested in the optical band gap modulation of OPVs mainly due to three reasons. In the first place, we were interested in the design of OPV based organogelators with tunable emission. We have already shown that OPVs have the ability to form nano- to micrometer sized self-assemblies leading to organogels when functionalized with hydrogen bonding end groups and long hydrocarbon side chains.[17,18] These OPV gels exhibit yellow emission whereas the corresponding aggregates in solution have green emission.[17b] However, OPV based π-gels with green and red emission have not been reported. Secondly, we were interested in exploring the ability of dipolar groups to induce the gelation of

OPVs, in place of the commonly used hydrogen bonding moieties.[19] This will provide an opportunity to explore the potential of ester moieties with different polarizabilities that facilitate the tuning of the HOMO-LUMO gap and thereby the optoelectronic properties. Finally, there is significant interest in quadrupolar type donor-acceptor substituted OPVs due to their widespread applications in optoelectronics, photonics and other areas of nanotechnologies.[3a,13-15] Nevertheless, organogels of such chromophores have not been reported. In the present chapter we report a combined molecular and supramolecular approach to quadrupolar π-systems that form organogels with tunable RGB emission.

2.3. Results and Discussion

2.3.1. The Design Strategy

The actual cause of gelation of organic molecules is still a matter of debate though it is known that supramolecular noncovalent organization leading to entangled structures, which are different from simple molecular aggregates, are mainly responsible.[20] However, gelation can be considered as a delicate balance between crystallization, precipitation and solubility of noncovalently interacting molecules in a suitable solvent. Keeping this fact in mind, we set to design π-conjugated molecules in such a way that they satisfy the conditions necessary for the formation of an extended self-assembly required for gelation (Figure 2.3). In this design. an appropriate π-conjugated system is equipped with two dipolar end

functional groups and sufficient number of long hydrocarbon side chains. The presence of the two dipolar end functional groups will allow the molecules to self-assemble via weak dipole-dipole interactions. The presence of long hydrocarbon side chains facilitates the packing of the molecules, assisted by weak van der Waals interaction. These interactions will be reinforced by π-stacking of the rigid aromatic OPV backbone. A cooperative interaction of all these forces will eventually lead the molecules to form entangled nanoscopic structures which are able to hold large amount of appropriate solvent molecules within the self-assembly, thereby forming a gel.
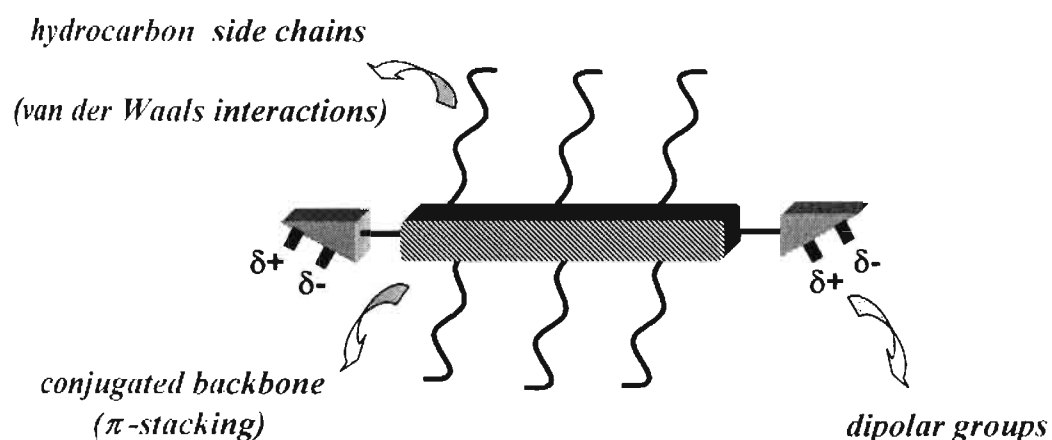
FIGURE 2.3. Design features of the OPV based organogelators showing various noncovalent interactions.

Based on the above mentioned design strategy, we have synthesized **OPV1-4** with all-*trans* configuration, the structures of which are shown in Figure 2.4. The rationale for the choice of these molecules is that they have the A-D-D-D-

A type backbone where 'A' represents dipolar acceptor end groups with tunable polarizability, and 'D' represents the donor-substituted phenyl ring. In **OPV1** the ester groups are insulated from the conjugated backbone whereas in **OPV2-3**, the ester groups are in conjugation with the OPV unit. In **OPV4** instead of the ester moiety, electron withdrawing dicyano groups are present. These molecules are examples of quadrupolar systems where the electron donor-acceptor groups are symmetrically tailored on the π-conjugated backbone.[13b,14a,15b] The color of these molecules in the powder form exhibit significant variation with the end functional groups (Figure 2.4) which clearly indicate their role in modulating the properties of the parent chromophore unit.
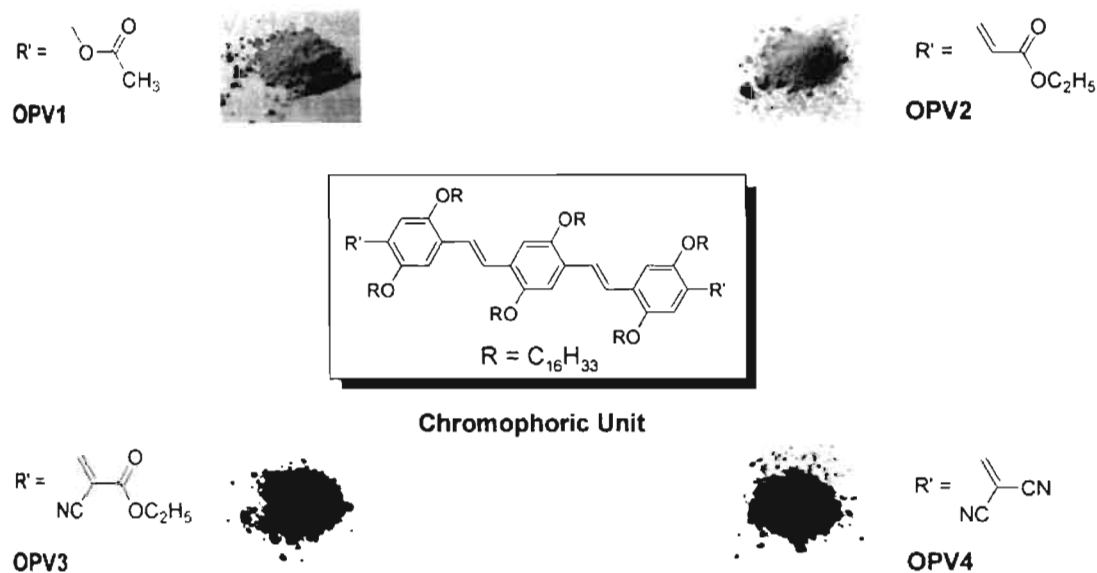
FIGURE 2.4. The chemical structures and the corresponding colors of OPV derivatives as prepared.

2.3.2. Synthesis of OPVs

The OPV derivatives **OPV1-4** were synthesized from a bisformyl OPV derivative (**16**), which is prepared according to a known procedure as shown in Scheme 2.1.[17b,21a] The 1,4-hydroquinone **12** on reaction with 1-bromo hexadecane in DMF in the presence of NaOH readily afforded 1,4-(hexadecyloxy)benzene **13** in a 63% yield. Subsequent bromomethylation of **13**, as per a general bromomethylation procedure[21b] with paraformaldehyde and HBr in acetic acid provided the bisbromomethyl derivative **14** in a 90% yield. Compound **14** on acetylation with potassium acetate (**15**, 88% yield) followed by hydrolysis with KOH, gave the bisalcohol **16** in a 90% yield. Oxidation of the bisalcohol with PCC gave the corresponding bisaldehyde **17** in a 92% yield.

The double Wittig reaction of **17** with bisphosphonium salt **18**, which were prepared *in situ* by the reaction of corresponding bisbromo derivate **14** with PPh$_3$, yielded a mixture of *trans*- and *cis*-vinylene isomers of the conjugated bisaldehyde **19**. These isomeric mixtures were converted to the all-*trans* derivative by treating with iodine in dichloromethane at room temperature, in a 71% yield. The high efficiency of these synthetic transformations ensures the ease of isolation and purification of the products at each step.
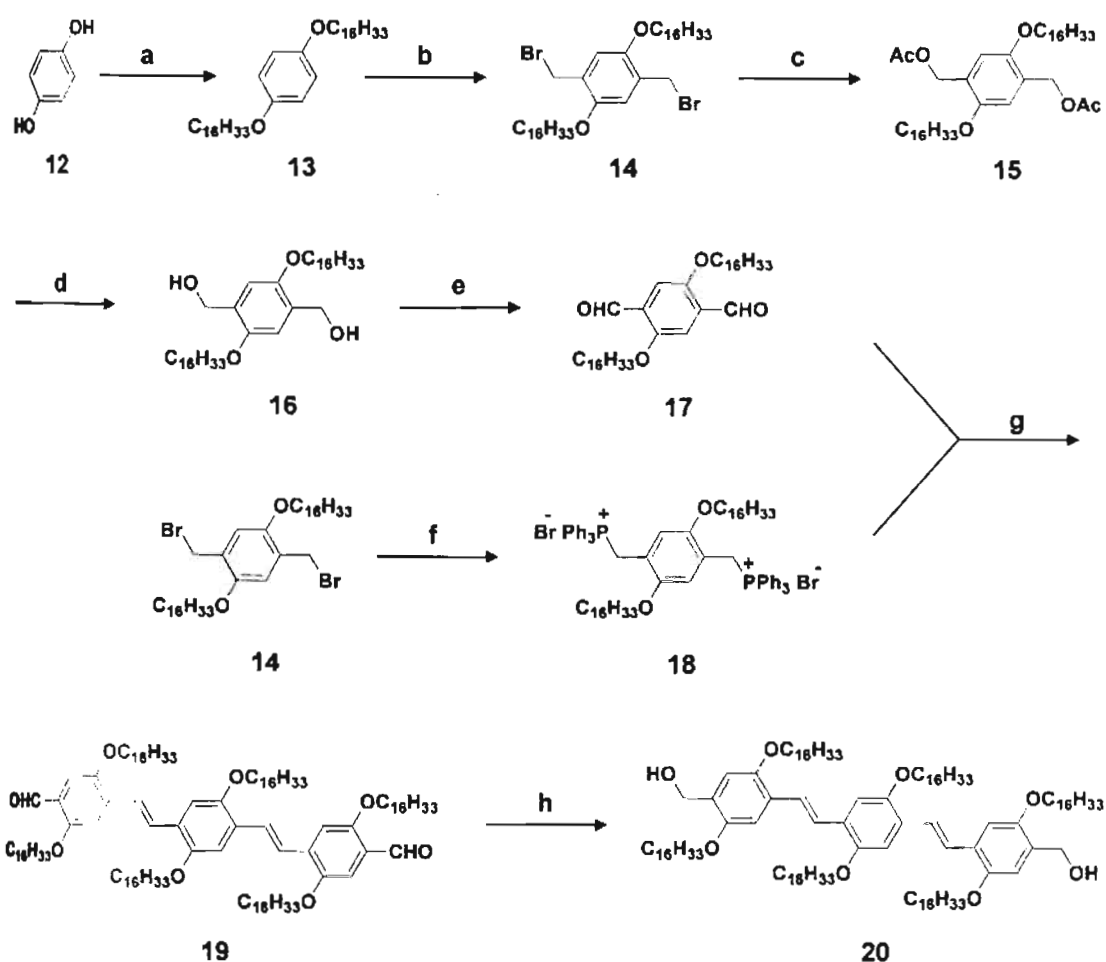
SCHEME 2.1. Reagents and conditions: a) 1-Bromohexadecane, NaOH, DMF, 100 °C, 24 h (63%). b) Paraformaldehyde, 33% HBr in CH₃COOH, glacial CH₃COOH , 70 °C, 4 h (90%). c) KOAc, TBAB, CH₃CN/CHCl₃, reflux, 12 h (88%). d) KOH (5N)/CH₃OH, distilled THF, reflux, 4 h (90%). e) PCC, CH₂Cl₂, 27 °C, 3 h (92%). f) PPh₃, dry C₆H₆, reflux, 4 h. g) i) LiOEt, dry CH₂Cl₂, 27 °C, 15 min; ii) I₂, CH₂Cl₂, rt, 12h (in dark) (71 %). h) NaBH₄, CH₃OH, CH₂Cl₂, 27 °C, 30 min (92 %).

The introduction of different end functional groups in the OPV backbone is achieved by adapting three different synthetic strategies (Scheme 2.2.). **OPV1**, the ester analogue of the bisalcohol **20** was prepared by a simple acylation using acetic anhydride (63% yield). The Wittig-Horner reaction of the bisaldehyde **19**

with the phosphonate **21** which is derived from ethyl bromoacetate using Michaelis-Arbuzov reaction, afforded **OPV2** in a 71% yield. Preparation of **OPV3** and **OPV4** were accomplished by the condensation reaction of bisaldehyde **19** with ethyl cyanoacetate (**22**) and malononitrile (**23**), respectively in 95% yields. All OPV derivatives under investigation were fully characterized by IR, ^{1}H and ^{13}C NMR and MALDI-TOF mass spectral analyses.
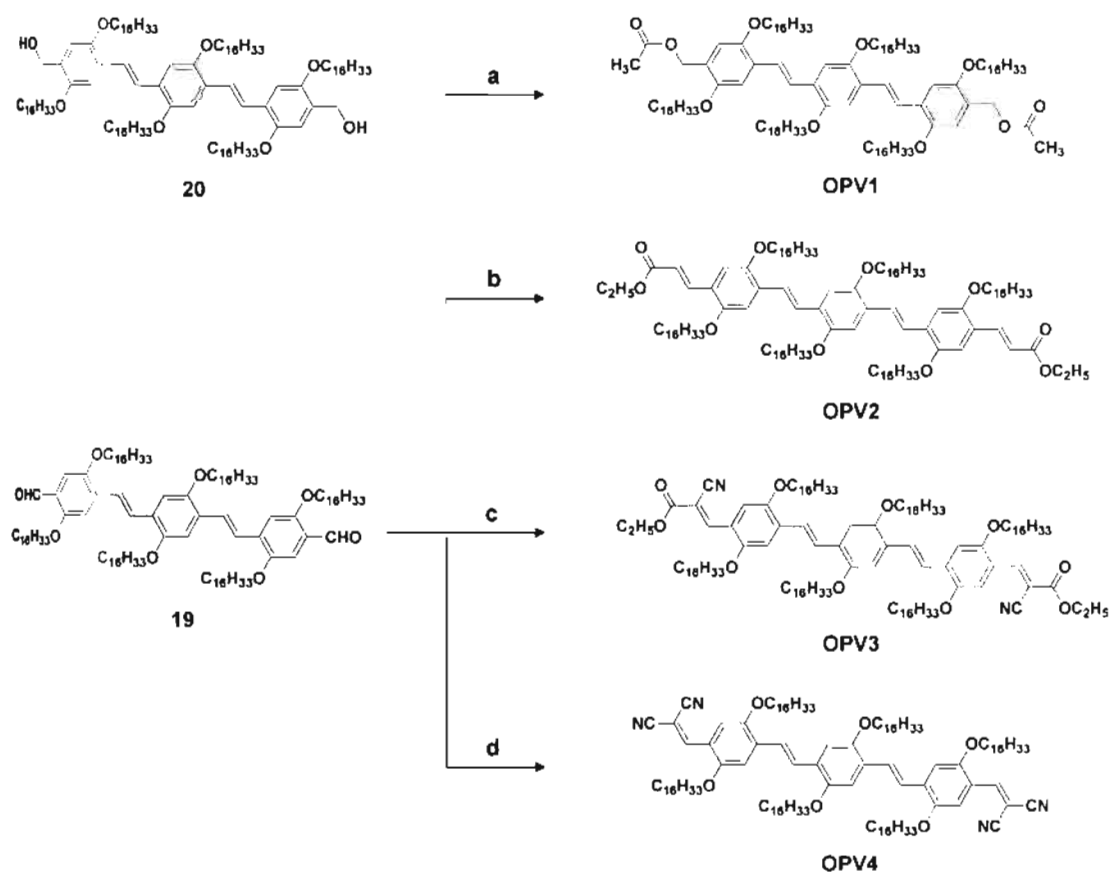
SCHEME 2.2. Reagents and conditions: a) (CH$_3$CO)$_2$O, DMAP, dry CHCl$_3$, 27 °C, 12 h (63%). b) C$_2$H$_5$CO$_2$CH$_2$PO(OC$_2$H$_5$)$_2$ (**21**), NaH, THF, 70 °C, 8 h (71%). c) C$_2$H$_5$CO$_2$CH$_2$CN (**22**), NH$_4$OAc, CH$_3$COOH, toluene, 80 °C, 4 h (95%). d) CH$_2$(CN)$_2$ (**23**), NH$_4$OAc, CH$_3$COOH, toluene, 80 °C, 4 h (95%).

2.3.3. Absorption and Emission Properties in Dichloromethane

The UV/Vis absorption and emission spectra of **OPV1-4** in dichloromethane (1×10^{-5} M) are shown in Figure 2.5. These molecules exhibit strong fluorescence in CH_2Cl_2, providing the three fundamental RGB emission colors (Figure 2.5c). Between **OPV1** and **OPV4**, a 110 nm red-shift in the absorption and a 179 nm red-shift in the emission could be observed. The emission spectrum of **OPV1** is structured whereas **OPV2-4** exhibited broad structureless emission.

The details of the absorption and emission characteristics of **OPV1-4** in dichloromethane together with the quantum yield (Φ_f), lifetimes (τ), radiative rate constants (k_r) and nonradiative rate constants (k_d) are shown in Table 2.1. Since k_r and k_d values are related to the corresponding emission quantum yields and life times they can be calculated by using the following relations,[22]

$$\Phi_f = k_r / \tau \qquad\qquad \text{- - - - (2.1)}$$

$$k_r + k_d = \tau^{-1} \qquad\qquad \text{- - - - (2.2)}$$
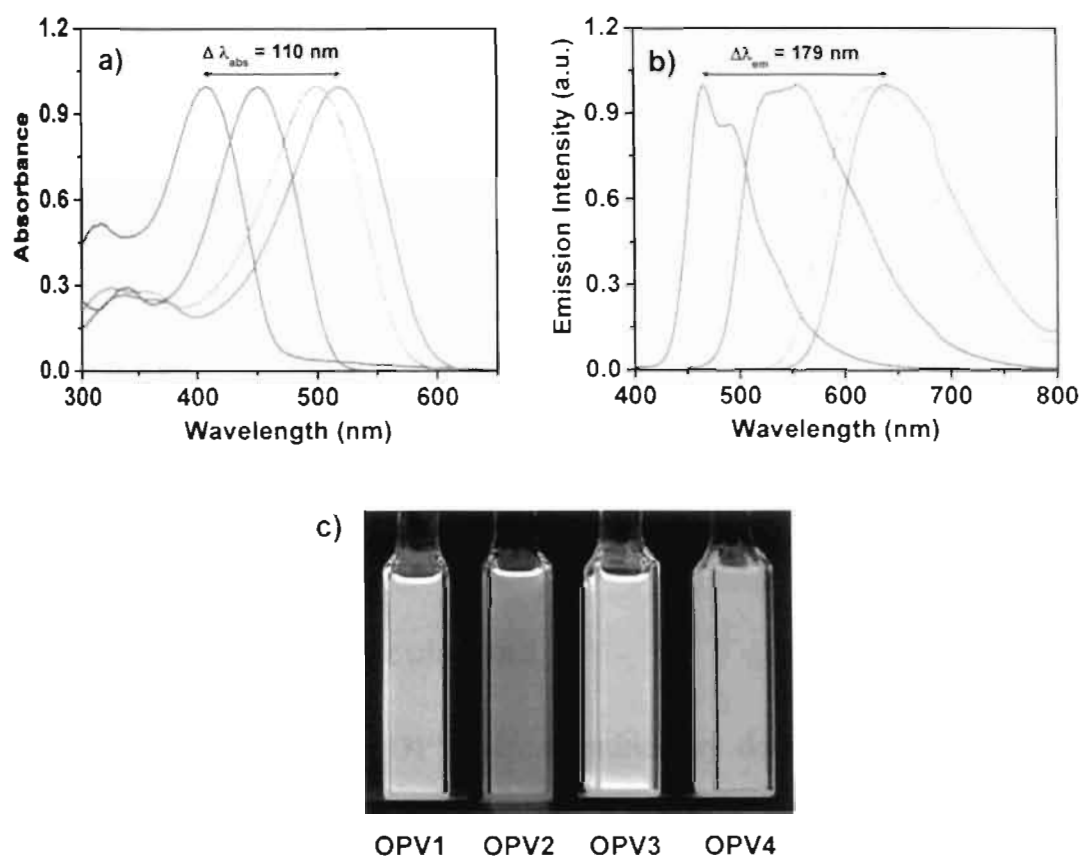
FIGURE 2.5. Optical properties of OPV derivatives in CH_2Cl_2. Normalized a) absorption and b) emission spectra of **OPV1-4** [1 x 10⁻⁵ M]. **OPV1** (   ) λ_{ex} = 390 nm, **OPV2** (   ) λ_{ex} = 440 nm, **OPV3** (   ) λ_{ex} = 480 nm and **OPV4** (   ) λ_{ex} = 500 nm. c) Photographs of the emission colors of OPVs in dichloromethane solution [1 x 10⁻⁵ M] under illumination at 365 nm.

These data reveal that **OPV2** with a conjugated ester moiety has higher quantum yield (Φ_f = 0.74, k_r/k_d = 2.84) when compared to those of **OPV1** with insulated ester moiety (Φ_f = 0.67, k_r/k_d = 2.03). The quantum yields are decreased as the electron withdrawing ability of the end functional groups are increased, thus having the lowest Φ_f for **OPV4** (0.52, k_r/k_d = 1.08).

TABLE 2.1. Optical properties of **OPV1-4** in CH_2Cl_2.

Compound	λ_{abs} (nm)	$\log \varepsilon$	λ_{em} (nm)	$\Delta\nu_{St}$ (cm^{-1})[a]	Φ_f	τ (ns)	k_r (s^{-1})	k_d (s^{-1})	k_r/k_d
OPV1	410	4.40	466, 495	2931	0.67[b]	1.71	3.92×10^8	1.93×10^8	2.03
OPV2	451	4.80	528, 558	3233	0.74[c]	7.63[d]	9.69×10^7	3.41×10^7	2.84
OPV3	499	4.84	626	4065	0.71[c]	8.76[d]	8.10×10^7	3.30×10^7	2.45
OPV4	520	4.70	645	3726	0.52[c]	9.14[d]	5.69×10^7	5.25×10^7	1.08

[a] $\Delta\nu_{St} = \nu_{abs} - \nu_{em}$, Stokes shift. Fluorescence quantum yields ($\pm5\%$ error) were determined using [b] quinine sulphate as the standard ($\Phi_f = 0.546$ in 0.1 N H_2SO_4). [c] Rhodamine 6G as the standard ($\Phi_f = 0.9$ in ethanol). [d] Average lifetime (τ_{av}) of the biexponential decay.[22]

2.3.4. Molecular Orbital Calculations

The frontier orbitals of **OPV1-4** determined by density functional theory (DFT) B3YLP/631-G* level single point energy calculations (TITAN software, Wavefunction, Inc.) exhibit specific patterns of electron localizations. Representative examples of these are shown for **OPV1** and **OPV4** in Figure 2.6. Electron density of the HOMO in both cases is localized on the three phenyl rings through the vinyl linkages. The LUMO of **OPV1** is mainly localized on the central aromatic ring. However, the electron density of the LUMO of **OPV4** is localized at the terminal phenyl rings and on the end functional groups through the vinylic linkage. The symmetric charge transfer from the middle to the end (or vice versa) is characteristic of quadrupolar type chromophores with large TPA cross section (δ).[13b,14,23] Similar is the case with **OPV3**. Therefore, the excited states of **OPV3**

and **OPV4** are expected to have a polar nature. Under this situation, intramolecular charge transfer (ICT) plays a dominant role in the optical properties of these OPVs.
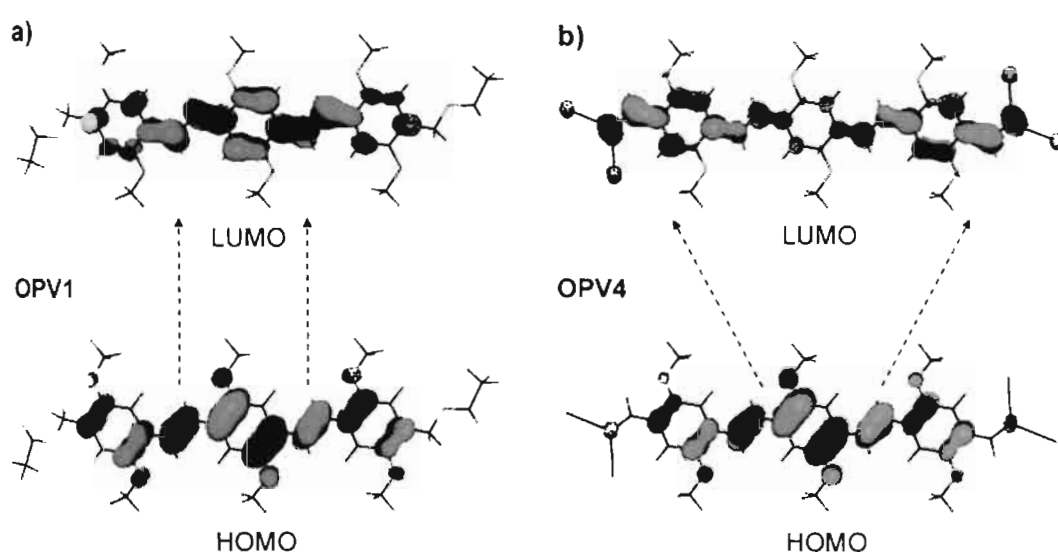
FIGURE 2.6. Frontier orbitals of a) **OPV1** and b) **OPV4** obtained by DFT B3YLP/631-G* level single point energy calculations. Geometries of OPVs were optimized using AM1 semiemperical quantum mechanical method. For computation, the hexadecyloxy side chains in the OPV structure were replaced with methoxy groups. Arrows indicate extend of charge localization.

2.3.5. Absorption and Emission Properties in *n*-Hexane

The photophysical properties of **OPV1-4** in *n*-hexane are summarized in Table 2.2. The absorption spectra of **OPV1-4** in *n*-hexane (1×10^{-5} M) at 20 °C showed a long wavelength absorbing shoulder band in addition to the π-π^* transition band (Figure 2.7). At higher temperature (60 °C) the long wavelength absorbing shoulder is disappeared with an increase in intensity of the π-π^* transition band. Under this condition the absorption spectra matches well with that

in dichloromethane solution except for slight changes in the maxima. This latter effect could be due to the change in the solvent polarity. These molecules exhibited structured emission in *n*-hexane at 20 °C with considerable decrease in the emission intensity (Figure 2.8). However at 60 °C, the emission maximum is shifted towards shorter wavelength with considerable increase in the intensity. Detailed analysis of the emission properties of OPVs in *n*-hexane revealed that among **OPV1-4**, **OPV2** has higher quantum yield ($\Phi_f = 0.50$, $k_r/k_d = 0.99$). In the case of **OPV4** in *n*-hexane at lower temperature, a dramatic quenching in the emission properties was observed ($\Phi_f = 0.09$, $k_r/k_d = 0.10$) when compared to that of other OPVs.

TABLE 2.2. Optical properties of **OPV1-4** in *n*-hexane.

Compound	λ_{abs} (nm)	λ_{em} (nm)	Φ_f^a	τ (ns)^b	k_r (s^{-1})	k_d (s^{-1})	k_r/k_d
OPV1	397, 470	454, 481, 514, 554, 609	0.31	3.54	8.75×10^7	1.95×10^8	0.45
OPV2	423, 514	448, 487, 529, 567, 620	0.50	2.27	2.20×10^8	2.21×10^8	0.99
OPV3	465, 560	583, 623, 683	0.43	7.60	5.67×10^7	7.43×10^7	0.76
OPV4	502, 583	510, 562, 611, 652	0.09	7.04	1.27×10^7	1.29×10^8	0.10

[a] Fluorescence quantum yields (±5% error) were determined using Rhodamine 6G as the standard ($\Phi_f = 0.9$ in ethanol). [b] Average lifetime (τ_{av}) of the biexponential decay.[22]

FIGURE 2.7. Absorption spectra of **OPV1-4** in *n*-hexane [1 x 10⁻⁵ M] at 20 °C (——) and 60 °C (- - -) that show the aggregation behavior of OPVs. a) **OPV1**, b) **OPV2**, c) **OPV3** and d) **OPV4**.

Temperature dependent absorption and emission studies of **OPV1-4** in *n*-hexane indicate the aggregation of these molecules with a significant modulation in optical properties. As a representative case, variable temperature absorption and emission spectra of **OPV1** in *n*-hexane is shown in Figure 2.9. Temperature dependent UV/Vis and fluorescence spectra of **OPV1** in *n*-hexane showed a transition from the self-assembled species to the molecularly dissolved species as the temperature is increased from 10 °C to 50 °C (Figure 2.9).
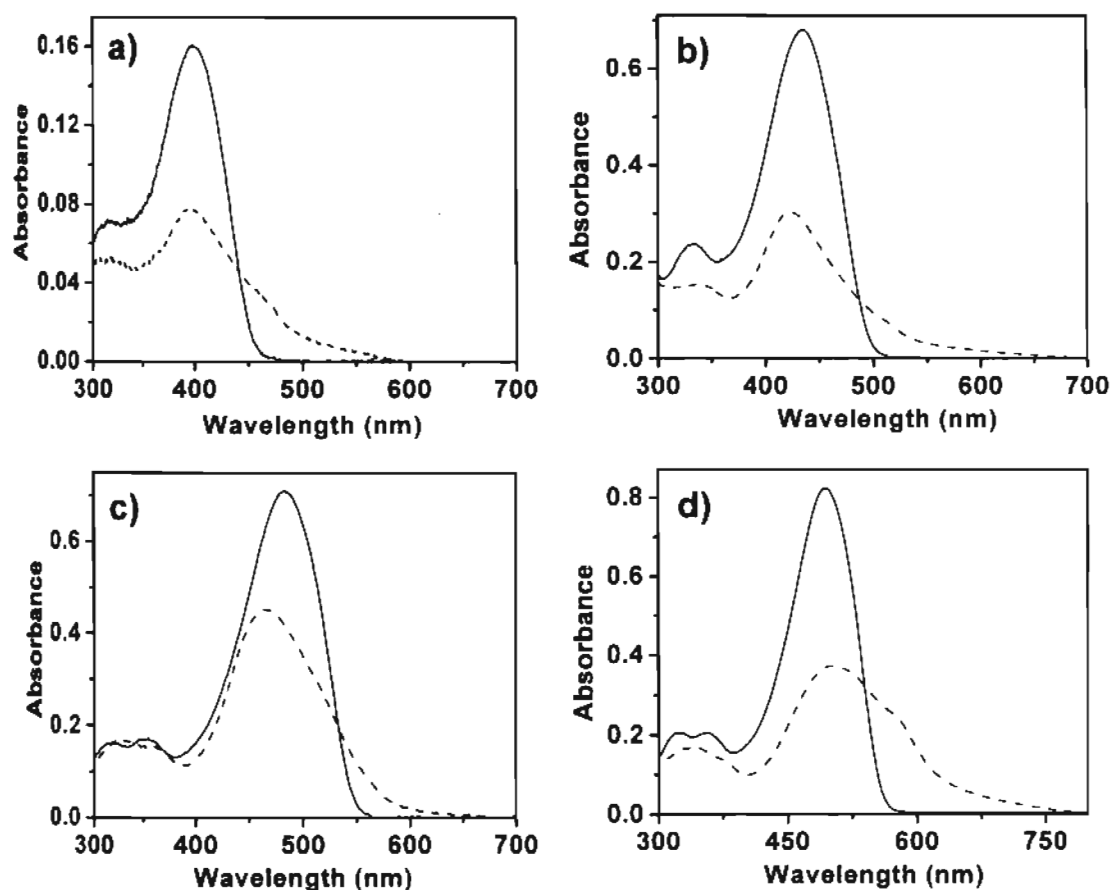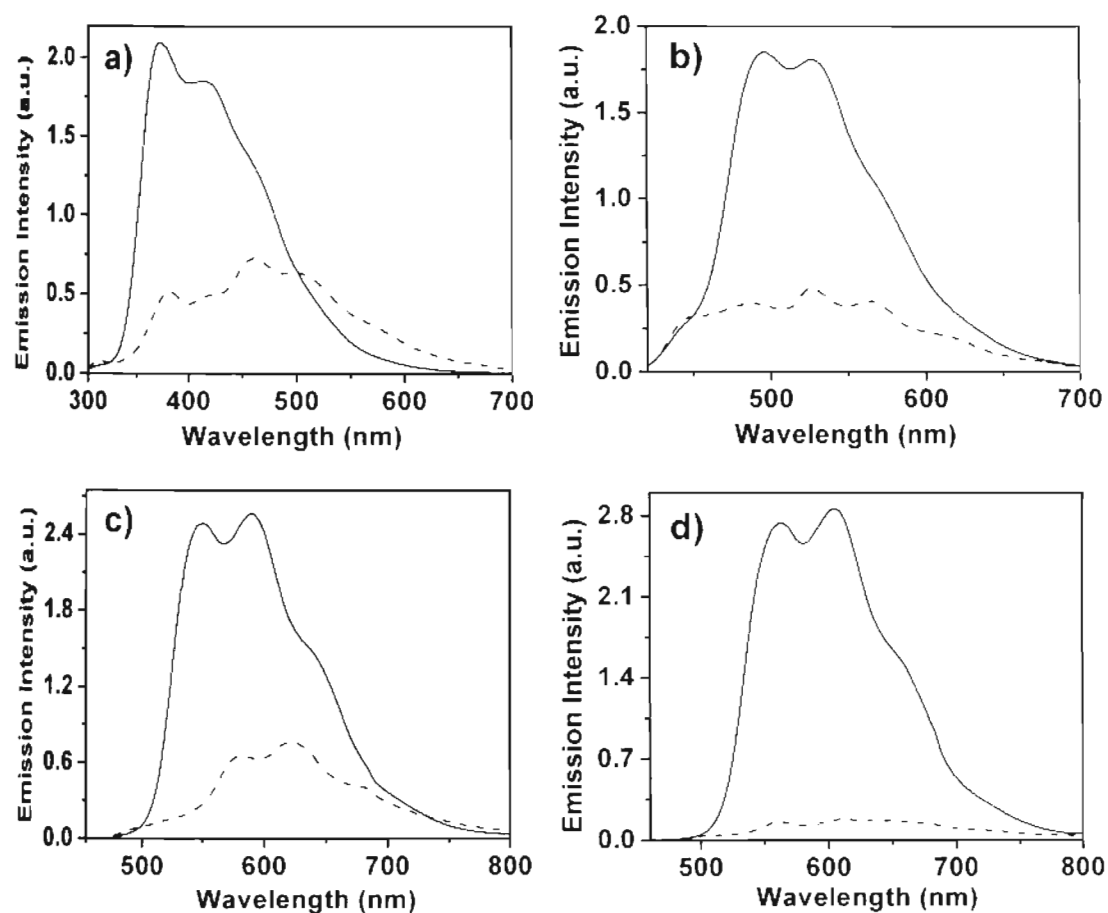
FIGURE 2.8. Emission spectra of **OPV1-4** in *n*-hexane [1 x 10⁻⁵ M] at 20 °C (——) and 60 °C (- - -) that show the aggregation behavior of OPVs. a) **OPV1** (λ_{ex} = 380 nm), b) **OPV2** (λ_{ex} = 410 nm), c) **OPV3** (λ_{ex} = 450 nm) and d) **OPV4** (λ_{ex} = 480 nm).

In the UV/Vis spectra, an increase in the intensity of the absorption maximum at 397 nm was observed with increase in the temperature. This is accompanied by a concomitant decrease in the intensity of the shoulder band at 470 nm through an isosbestic point at 440 nm (Figure 2.9a). Similarly, in the fluorescence spectra (λ_{ex} − 380 nm), the intensity of the long wavelength maxima at 514 and 554 nm decreases with the simultaneous increase in the intensity of the

emission bands at 447 nm and 483 nm (Figure 2.9b) when the temperature is increased from 10-50 °C. These observations clearly show the existence of at least two different species of **OPV1** in *n*-hexane, the self-assembled species at room temperature and the non-assembled species at elevated temperatures.
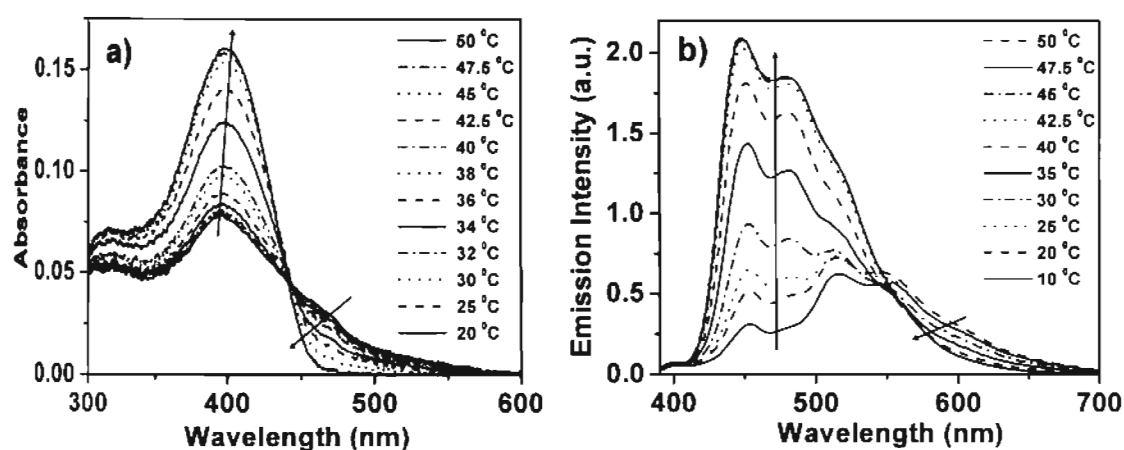
FIGURE 2.9. Temperature dependent a) absorption and b) fluorescence spectra (λ_{ex} = 380 nm) of **OPV1** in *n*-hexane [1 x 10^{-5} M].

2.3.6. Gelation Studies

Gelation behavior of **OPV1-4** was examined in a range of organic solvents by dissolving different amounts of the required molecule in a specific volume (1 mL) of the solvent under heating and cooling. It has been observed that either gelation, precipitation or a clear solution could be obtained depending upon the solvent and structural characteristics of the compound. Gel formation could be detected readily by the failure of the resultant mass to flow when the vial was tilted upside down and also from the soft and transparent appearance.

TABLE 2.3. Critical gelator concentrations (mM)ᵃ **OPV1-4** in different solvents.

Solvent	OPV1	OPV2	OPV3	OPV4
n-Decane	1.61 (s, tr)	1.04 (s, tr)	1.49 (s, tr)	P
n-Hexane	3.21 (s, tr)	2.08 (s, tr)	2.13 (s, tr)	P
Cyclohexane	4.01 (s, tr)	2.60 (s, tr)	3.90 (s, tr)	P
Methylcyclo-hexane	4.11 (s, tr)	2.69 (s, tr)	3.99 (s, tr)	P
Toluene	4.28 (th, tr)	3.38 (th, tr)	8.80 (th, tr)	P
p-Xylene	4.32 (th, tr)	3.41 (th, tr)	8.86 (th, tr)	P
Dichloromethane	S	S	S	S

ᵃCGC = Critical gelator concentration, which is the minimum concentration required for the formation of a stable gel at room temperature. In parenthesis, s = stable, tr = transparent, th = thixotropic, S = soluble, P = precipitation.

Interestingly, when the concentrations of **OPV1-3** are increased above a threshold value, self-supporting gels are formed in aliphatic and aromatic hydrocarbon solvents. Surprisingly, **OPV4** failed to gelate any of the solvents despite its strong tendency for aggregation. The results of gelation experiments are summarized in Table 2.3., which revealed that **OPV2** has better gelation efficiency in aliphatic and aromatic hydrocarbon solvents when compared to other OPVs.

The critical gelator concentrations (CGC) of **OPV2** in n-decane, n-hexane, cyclohexane and methyl- cyclohexane were 1.04, 2.08, 2.60 and 2.69 mM, respectively. The small CGC value of **OPV2** in n-decane indicates that it can entrap approximately 5000 molecules of decane per gelator molecule. It is observed that the nature of the solvent has considerable influence on the gelation behavior of **OPV1-3**. For example, CGC values of **OPV2** in aromatic hydrocarbon solvents are high when compared to that in aliphatic hydrocarbon solvents. The CGC value of **OPV2** in toluene and p-xylene is 3.38 and 3.49, respectively. Moreover, **OPV2** gel in toluene and p-xylene is found to be unstable and breaks upon shaking (thixotropic). Similar observations were made in the case of **OPV2** and **OPV3** also. Detailed gelation studies of **OPV1-3** in different solvents revealed that the gelation ability is in the order **OPV2** > **OPV3** > **OPV1** in aliphatic hydrocarbon solvents whereas in aromatic hydrocarbon solvents the order is **OPV2** > **OPV1** > **OPV3**. The change in the gelation behavior of **OPV1** and **OPV2** in aliphatic and aromatic hydrocarbon solvents may be due to the better solubility of **OPV2** in aromatic hydrocarbon solvents. In polar solvents like dichloromethane all OPV derivatives were failed to form gel even at higher concentration. The results of gelation studies indicate that in combination with π-staking and van der Waals forces, the dipolar interaction provided by the end functional groups plays a crucial role in the gelation of **OPV1-3**.
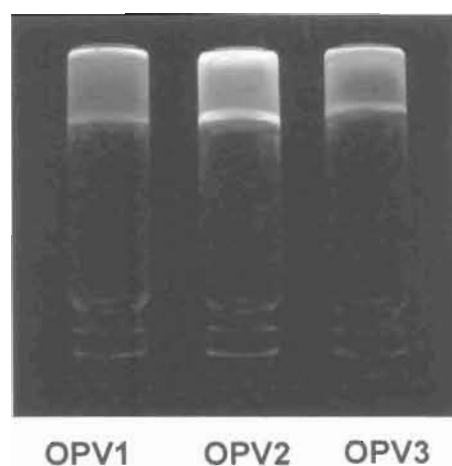
FIGURE 2.10. Photographs of the *n*-hexane gels of **OPV1-3** under illumination at 365 nm.
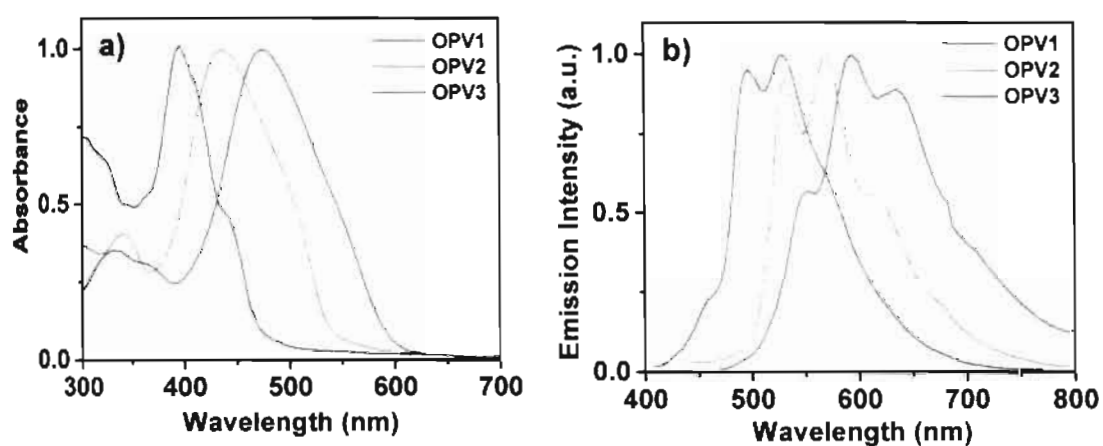
FIGURE 2.11. Normalized a) absorption b) emission spectra of **OPV1-3** in the *n*-hexane gel state [3 x 10^{-4} M], *l* = 1 mm, **OPV1** λ_{ex} = 390 nm, **OPV2** λ_{ex} = 420 nm and **OPV3** λ_{ex} = 460 nm.

Photographs of **OPV1-3** gels from *n*-hexane under illumination (λ_{ex} = 365 nm) are shown in Figure 2.10. As observed, the end functional groups play considerable role in the gelation and the emission properties of the OPVs. **OPV1** showed green emission, **OPV2** yellow and **OPV3** red emission. The absorption and emission spectra of **OPV1-3** in the gel state is shown in Figure 2.11. The

emission of the molecules in the gel state was shifted remarkably towards the long wavelength region. For example, the blue (λ_{max} = 466 nm, in dichloromethane) emission of **OPV1** is shifted to green (λ_{max} = 530 nm) in the gel state. Similarly, the green and orange emission of **OPV2** and **OPV3** are shifted to yellow and red, respectively in *n*-hexane gels.

Comparison of the absorption spectra of **OPV1-3** in *n*-hexane solution (1 x 10^{-5} M) (Figure 2.7) and in the gel state (3 x 10^{-4} M) revealed that the red shifted long wavelength shoulder band of the absorption spectrum becomes more prominent in the latter case (Figure 2.11a). This observation indicates the presence of large number of low energy (higher order) aggregates in the gel state. The presence of these aggregates determines the emission properties of OPVs in the gel state.[17b,24,25a] In the gel state due to efficient exciton migration within the aggregates of different HOMO-LUMO levels, emission occurs mainly from the lower energy (higher order) aggregates resulting in a red shift in the wavelength (Figure 2.11b). This aspect of OPV gels will be discussed in details in Chapter 4.

2.3.7. Stability of OPV Self-Assemblies

Stability of the OPV self-assembly under different experimental conditions was established from the plots of the aggregate fraction (α) against temperature (Figure 2.12) which is obtained by monitoring the temperature dependent changes in the UV/Vis absorption spectra. Figure 2.12a shows the temperature transition

plots of **OPV1-3** in *n*-hexane (1×10^{-5} M) which revealed that aggregates of

OPV2 have better thermal stability (melting transition temperature, $T_m = 41$ °C)

when compared to that of **OPV1** ($T_m = 37$ °C) and **OPV3** ($T_m = 33$ °C).
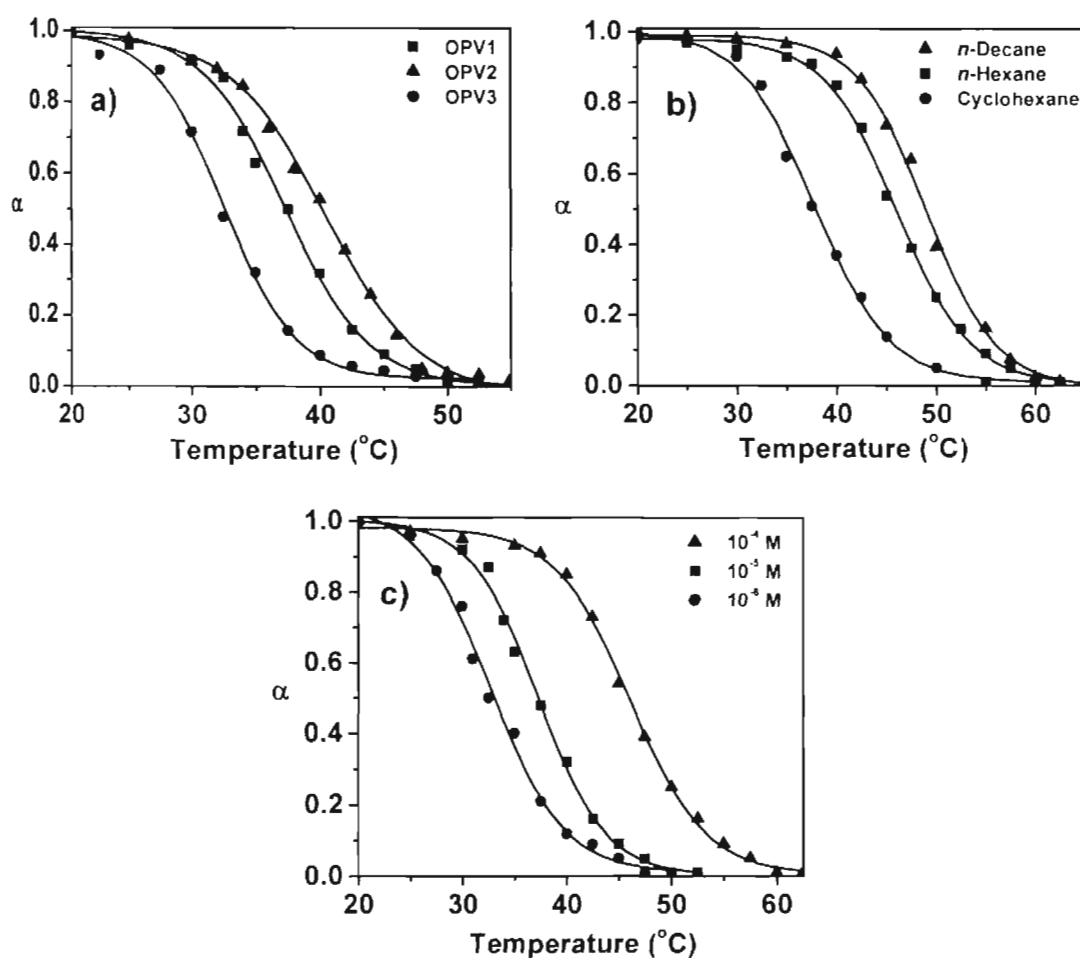
FIGURE 2.12. Plots of the fraction of aggregate (α) versus temperature a) **OPV1-3** in *n*-hexane [1×10^{-5} M], b) **OPV2** in different solvents [1×10^{-5} M] and c) **OPV2** in different concentration in *n*-hexane. The data points were acquired by monitoring absorption spectral changes at 470 nm (**OPV1**), 507 nm (**OPV2**) and 560 nm for **OPV3**, corresponding to the lower energy band in the absorption spectra at ambient conditions.

Figure 2.12b and 2.12c show the temperature transition plots of **OPV3** as a function of solvent and concentration respectively. As expected for a non-covalent self-assembly, the transition temperatures of **OPV2** self-assembly increase on changing the solvent from cyclohexane to hexane and decane. It is observed that the stability of the self-assembled molecules increases by 10-15 °C, per an order of the increase in concentration (Figure 2.12c). In all the experiments, transitions from the self-assembly to isotropic state are sigmoidal in nature and occurred within short temperature range (~ 10 °C), which are characteristic of co-operative noncovalent interactions during the self-assembly process.[17b,25]

The thermotropic behavior of the gels formed by **OPV1-3** were investigated by the dropping ball method.[17a,b] Phase diagrams of the gels of **OPV1-3** in *n*-hexane were obtained by plotting the T_{gel} at different concentrations. The phase above each curve is solution, whereas the phase below is gel. The phase diagrams of **OPV1-3** exhibited a regular increase in T_{gel} with increasing concentration of the gelator molecule (Figure 2.13). The observed trend of T_{gel} is in accordance with the trend in T_m which is in the order **OPV2** > **OPV1** > **OPV3**. The enhanced gel stability **OPV2** could be associated with the better polarizability of the ester group which in turn may enhance the π-stacking of the OPV backbone. **OPV1** with the insulated ester moiety and **OPV3** with cyanoester moiety are less polarizable than the conjugated ester moiety of **OPV2**.
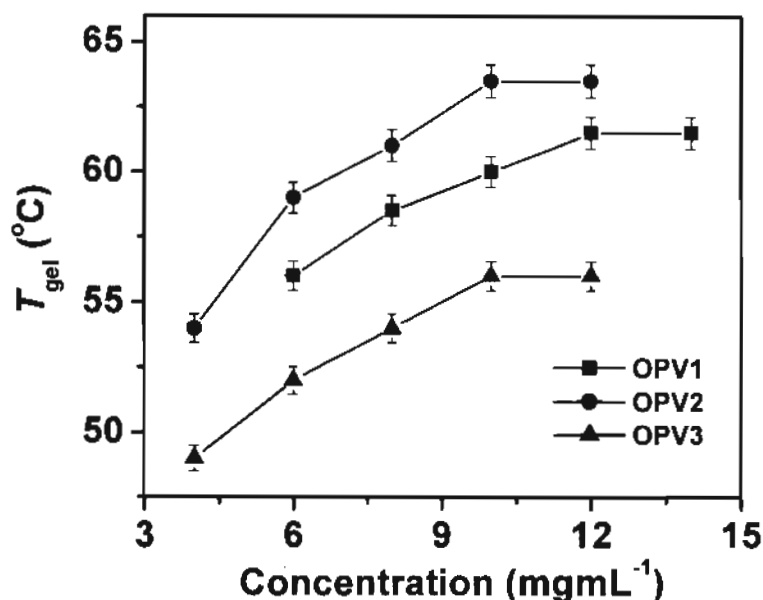
FIGURE 2.13. Plots of T_{gel} versus concentration of OPVs (data points are obtained by dropping ball method).

2.3.8. Morphological Features

Atomic force microscopy (AFM) tapping mode height images of the self-assemblies of **OPV1-4** from toluene (5×10^{-5} M) are shown in Figure 2.14. The gel forming molecules **OPV1-3** exhibited nano- to micrometer sized extended tapes. The smallest fiber has a width of 95-115 nm with a height of 12 ± 2 nm. The observed morphology of these gels is analogous to that of the previously reported hydrogen bonded OPV gels.[17b,18] The AFM images reveal that the weak dipolar interaction of the ester groups is good enough to facilitate the extended self-assembly of the OPVs. The nongelling **OPV4** exhibits isolated rod like structures with 20-47 nm width, 2.85 ± 0.5 nm in height and a few micrometers in length. In

addition, bundles of the rods could also be seen which are incapable of gelating any of the solvent tested.

FIGURE 2.14. Morphological features of OPV derivatives. AFM tapping mode height images and the corresponding section analysis of a) **OPV1**, b) **OPV2**, c) **OPV3** and d) **OPV4**. In all experiments [OPV] = 5 x 10^{-5} M in toluene. The actual width of the self-assemblies is estimated by subtracting the tip broadening factor from the measured size.[26]
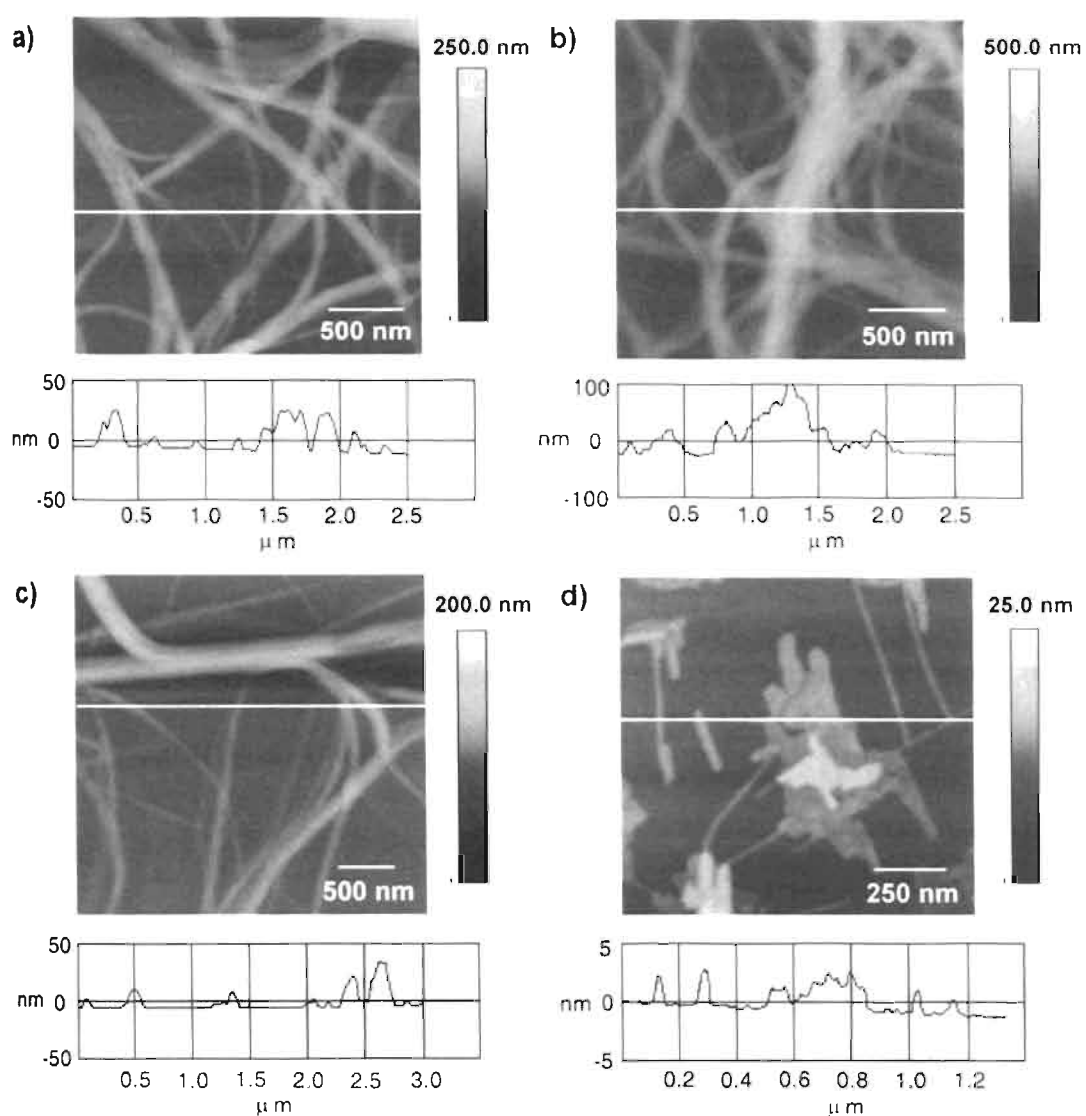
These results reveal that dipolar interactions in combination with π-stacking and van der Waals forces are able to assist the self-assembly of conjugated molecules[19] resulting in entangled supramolecular architectures that are responsible for gelation. These molecules form a new class of nonhydrogen-bonded π-organogels based on quadrupolar OPVs.

2.4. Conclusions

In conclusion, the rational choice of the dipolar end functional groups in OPVs allows the tuning of the emission in the molecular level and the modulation of the gelation behavior at the supramolecular level. A combination of these two strategies facilitates the design of π-gels with sol-gel tunable RGB emission. The dipolar ester moieties play a crucial role in providing tunable electronic character to the molecules, which also facilitate the gelation. Furthermore, in place of the commonly used hydrogen bonding motifs, dipolar interaction of the terminal ester groups in cooperation with π-stacking and van der Waals forces are shown to be effective in inducing the self-assembly of OPVs, resulting in strongly fluorescent organogels. These quadrupolar π-gels are ideal scaffolds for the design of supramolecular light harvesting assemblies[27] and are potential two photon absorbing materials[28] which open the window to a novel class of electronically active soft organic materials with tunable optical properties.

2.5. Experimental Section

2.5.1. Synthesis and Characterization

Unless otherwise stated, all starting materials and reagents were purchased from commercial suppliers and used without further purification. The solvents used were purified and dried by standard methods prior to use. Melting points were determined with a Mel-Temp-II melting point apparatus and are uncorrected. ^{1}H and ^{13}C NMR spectra were measured on a 300 MHz Bruker Avance DPX spectrometer using TMS as internal standard. FT-IR spectra were recorded on a Shimadzu IRPrestige-21 Fourier Transform Infrared Spectrophotometer. High Resolution Mass Spectral (HRMS) analysis was done on a JEOL JMS600 instrument. Matrix-assisted laser desorption ionization time-of-flight (MALDI-TOF) mass spectra were obtained on a Perseptive Biosystems Voyager DE-Pro MALDI-TOF mass spectrometer using α-Cyano-4-hydroxy cinnamic acid as the matrix.

1,4-Bis(hexadecyloxy)benzene (13). A suspension of 1,4-hydroquinone **12** (75 mmol), 1-bromohexadecane (150 mmol) and NaOH (187 mmol) in 50 mL dimethyl formamide was heated at 100 °C for 24 h. After cooling, the reaction mixture was poured into water and the precipitate formed was collected by filtration. Recrystallization of the crude product from hot ethanol provided **13** as a white solid.
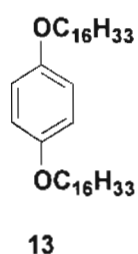
Yield: 63%; mp: 80-81 °C; FT-IR (KBr) v_{max}: 540, 725,

771, 825, 771, 825, 1006, 1033, 1111, 1242, 1290, 1394,

1467, 1516, 2848, 2920, 2953 cm^{-1}; ^{1}H NMR (300 MHz,

CDCl$_3$) δ: 0.88 (t, J = 6.8 Hz, 6H, –CH_3), 1.25-1.76 (m,

56H, –CH_2–), 3.89 (t, J = 6.42 Hz, 4H, –OCH_2–), 6.81 (s,

4H, phenyl-H) ppm; HRMS (FAB) calcd for C$_{38}$H$_{70}$O$_2$

(M$^+$): 558.54, found: 558.42.

2,5-Bis(bromomethyl)-1,4-bis(hexadecyloxy)benzene (14). To a suspension of

13 (15 mmol) and paraformaldehyde (45 mmol) in glacial acetic acid (60 mL),

33% HBr in acetic acid (11.5mL) was added and heated at 70 °C for 4 h. After

cooling to room temperature, the reaction mixture was poured into cold water. The

precipitated product was filtered and washed several times with water and dried in

a vacuum oven to give 14 in good yield.
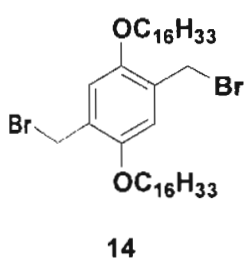
Yield: 90%; mp: 99-100 °C; FT-IR (KBr) v_{max}: 547, 690,

721, 864, 1002, 1031, 1045, 1190, 1211, 1228, 1255,

1315, 1396, 1409, 1448, 1471, 1508, 2850, 2916 cm^{-1}; ^{1}H

NMR (300 MHz, CDCl$_3$) δ: 0.88 (t, J = 6.59 Hz, 6H,

–CH_3), 1.25-1.82 (m, 56H, –CH_2–), 3.98 (t, J = 6.38 Hz,

4H, –OCH_2–), 4.52 (s, 4H, –CH_2Br), 6.85 (s, 2H, phenyl-

H) ppm; ^{13}C NMR (CDCl$_3$, 75 MHz) δ: 14.33, 22.92,

26.31, 28.94, 29.58, 29.82, 29.92, 32.15, 69.29, 114.93, 127.78, 150.91 ppm; HRMS (FAB) calcd for $C_{40}H_{72}Br_2O_2$ (M$^+$): 742.39, found: 742.47.

2,5-Bis(acetylmethyl)-1,4-bis(hexadecyloxy)benzene (15). A solution of **14** (10.4 mmol), potassium acetate (31.3 mmol) and tetrabutylammonium bromide (TBAB) (0.5 mg) in a mixture of acetonitrile (100 mL) and chloroform (50 mL) was refluxed for 12 h. The resulting solution was then poured into water and extracted with chloroform. The organic layer was separated, washed several times with water, dried over anhydrous Na_2SO_4 and concentrated to give **15** in high yield.
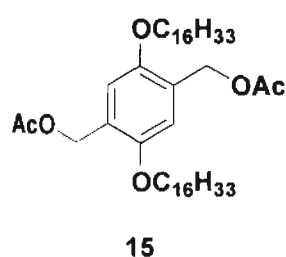
Yield: 88%; mp: 85-86 °C; FT-IR (KBr) v_{max}: 647, 721, 875, 927, 960, 1001, 1018, 1074, 1190, 1217, 1238, 1257, 1315, 1357, 1379, 1394, 1429, 1465, 1516, 1720, 2848, 2918 cm^{-1}; ^{1}H NMR (300 MHz, CDCl$_3$) δ: 0.88 (t, J = 6.57 Hz, 6H, -CH_3), 1.25-1.77 (m, 56H, -CH_2-), 2.09 (s, 6H, -CO-CH_3), 3.93 (t, J = 6.39 Hz, 4H, -OCH_2-), 5.13 (s, 4H, -CH_2OAc), 6.87 (s, 2H, phenyl-H) ppm; HRMS (FAB) calcd for $C_{44}H_{78}O_6$ (M$^+$): 702.58, found: 702.62.

2,5-Bis(hydroxymethyl)-1,4-bis(hexadecyloxy)benzene (16). KOH (5 N) in methanol (20 mL) was added to a solution of **15** (6 mmol) in distilled THF (60 mL), the reaction mixture was then refluxed for 4 h. After checking the completion of reaction by TLC, the solvent was evaporated under reduced pressure. The residue was suspended in THF (50 mL) and trifluoroacetic acid (TFA) was added to this solution to adjust the pH around 2. The solvent was then removed and the solid residue was extracted with chloroform and washed several times with water until the washings stayed neutral. The organic layer was dried over anhydrous Na_2SO_4 and concentrated to give **16** as a white solid.
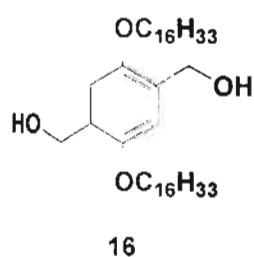
Yield: 90%; mp: 104-105 °C; FT-IR (KBr) v_{max}: 647, 717, 802, 875, 1004, 1053, 1072, 1207, 1259, 1392, 1419, 1454, 1469, 1506, 2848, 2914, 2953, 3358 cm^{-1}; ^{1}H NMR (300 MHz, $CDCl_3$) δ: 0.88 (t, J = 6.46 Hz, 6H, –CH_3), 1.26-1.8 (m, 56H, –CH_2–), 3.98 (t, J = 6.46 Hz, 4H, –OCH_2–), 4.66 (s, 4H, –CH_2OH), 6.84 (s, 2H, phenyl-H) ppm; HRMS (FAB) calcd for $C_{40}H_{74}O_4$ (M^+): 618.56, found: 618.41.

OC$_{16}$H$_{33}$

HO — OH

OC$_{16}$H$_{33}$

16

2,5-Bis(hexadecyloxy)benzene-1,4-dialdehyde (17). A suspension of **16** (4.49 mmol) and pyridinium chlorochromate (PCC) (1.98 mmol) in dichloromethane (200 mL) was stirred at room temperature for 3 h. The reaction mixture was

directly transferred onto the top of a short silica gel column (100-200 mesh) and the fluorescent product **17** was then eluted with chloroform.
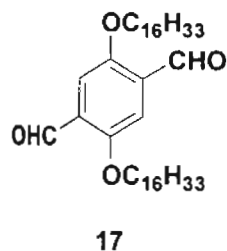
Yield: 92%; mp: 87-88 °C; FT-IR (KBr) v_{max}: 695, 717, 881, 960, 989, 1014, 1035, 1062, 1128, 1157, 1215, 1280, 1390, 1427, 1467, 1492, 1680, 2848, 2916 cm^{-1}; ^{1}H NMR (300 MHz, CDCl$_3$) δ: 0.88 (t, J = 6.57 Hz, 6H, –CH_3), 1.25-1.85 (m, 56H, –CH_2–), 4.08 (t, J = 6.45 Hz, 4H, –OCH_2–), 7.42 (s, 2H, phenyl-H), 10.51 (s, 2H, –CHO) ppm; ^{13}C NMR (75 MHz, CDCl$_3$) δ: 14.11, 22.68, 26.00, 29.05, 29.31, 29.35, 29.54, 29.57, 29.65, 29.68, 31.92, 69.26, 111.63, 114.40, 129.29, 155.24, 189.46 ppm; HRMS (FAB) calcd for $C_{40}H_{70}O_4$ (M^+): 614.53, found: 614.42.

2,5-Bis(hexadecyloxy)-1,4-bis[(2,5-hexadecyloxy-4-formyl)phenylenevinylene] benzene (19). A suspension of the bisbromomethyl derivative **14** (1 mmol) and triphenylphosphine (2.1 mmol) in dry benzene (15 mL) was refluxed for 4 h. The solvent was then removed and the resulting triphenylphosphonium salt **18** was dissolved in dichloromethane (50 mL) along with the bisaldehyde **17**. To this, lithium ethoxide solution (2.5 mL, 1.0 M in ethanol) was added dropwise at room temperature and stirred for 15 minutes. The reaction mixture was then poured into

aqueous solution of HCl. The organic layer was separated, washed with water and concentrated. The residues, after the removal of the solvents, contained both E- and Z-isomers. A solution of this isomeric mixture and iodine (500 mg) in dichloromethane (50 mL) was stirred at room temperature overnight. The dark brown solution was then diluted with dichloromethane, washed several times with $Na_2S_2O_3$ solution and water. The organic layer was then dried over anhydrous Na_2SO_4 and concentrated. The crude product was then chromatographed on a silica gel column (100-200 mesh), eluting with a mixture of hexane and chloroform (1:1) to give **19** as a yellow solid.

19
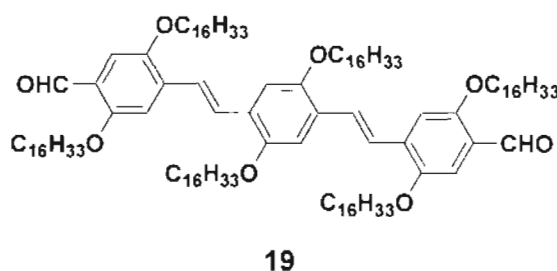
Yield: 71%; mp: 95-96 °C; FT-IR (KBr) v_{max}: 721, 802, 966, 1024, 1068, 1103, 1124, 1205, 1263, 1342, 1390, 1423, 1465, 1520, 1595, 1678, 2848, 2920 cm^{-1}; ^{1}H NMR (300 MHz, CDCl$_3$) δ: 0.85-0.88 (m, 18H, $-CH_3$), 1.24-1.87 (m, 168H, $-CH_2-$), 4.01-4.12 (m, 12H, $-OCH_2-$), 7.14 (s, 2H, phenyl-*H*), 7.20 (s, 2H, phenyl-*H*), 7.32 (s, 4H, phenyl-*H*), 7.50 (d, *J* = 17.04 Hz, 2H, vinyl-*H*), 7.60 (d, *J* = 16.74 Hz, 2H, vinyl-*H*), 10.44 (s, 2H, $-CHO$) ppm; ^{13}C NMR (75 MHz, CDCl$_3$) δ: 14.09, 22.67, 26.10, 26.20, 29.20, 29.30, 29.42, 29.51, 29.71, 31.93,

69.10, 69.18, 69.40, 110.11, 110.50, 110.81, 123.22, 124.12, 126.90, 127.43, 134.90, 150.71, 151.31, 156.24, 189.13 ppm; MALDI-TOF MS (MW = 1780.95): m/z = 1781.17 $[M]^+$.

2,5-Bis(hexadecyloxy)-1,4-bis[(2,5-hexadecyloxy-4-hydroxymethyl)phenylene-vinylene]benzene (20). The bisaldehyde **19** (0.2 mmol) was dissolved in a mixture of methanol (5 mL) and dichloromethane (35 mL). To this solution, $NaBH_4$ (0.4 mmol) was added and stirred at room temperature for 30 minutes. The reaction mixture was poured into water and extracted with dichloromethane. The organic layer was dried over anhydrous Na_2SO_4 and concentrated to give the corresponding bisalcohol derivative **20** as a yellow solid.

20
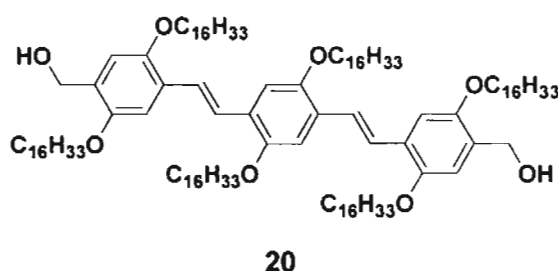
Yield: 92%; mp: 113-114 °C; FT-IR (KBr) ν_{max}: 851, 965, 1011, 1068, 1202, 1259, 1341, 1388, 1418, 1460, 1511, 2845, 2918, 3381 cm^{-1}. ^{1}H NMR (300 MHz, CDCl$_3$) δ: 0.85-0.88 (m, 18H, $-CH_3$), 1.25-1.83 (m, 168H, $-CH_2-$), 2.30 (br, 2H, $-OH$), 3.97-4.04 (m, 12H, $-OCH_2-$), 4.68 (s, 4H, $-CH_2OH$), 6.86 (s, 2H, phenyl-H), 7.13 (d, J = 7.53 Hz, 4H, vinyl-H), 7.46 (s, 4H, phenyl-H) ppm; ^{13}C NMR (75 MHz, CDCl$_3$) δ: 14.10, 22.69, 26.21, 26.26, 28.70, 28.95, 29.37,

29.57, 29.58, 29.72, 31.93, 62.31, 68.57, 69.49, 69.70, 109.10, 110.73, 114.00, 122.69, 123.33, 127.25, 127.35, 129.29, 150.64, 151.05 ppm; MALDI-TOF MS (MW = 1785.12): m/z = 1785.55 $[M]^+$.

Ethyl-2-(diethoxyphosphoryl)acetate (21). Compound **21** was prepared by reacting ethyl bromoacetate (8.98 mmol) with 2.0 mL of triethyl phosphite at 100 °C for 10 h. The unreacted triethyl phosphite was removed under reduced pressure to give **21** as a colorless liquid.
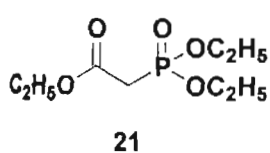
Yield 95%; FT-IR (neat) v_{max}: 661, 744, 975, 1055, 1116, 1163, 1211, 1255, 1369, 1392, 1442, 1477, 1510, 1734, 2872, 2908, 2937, 3018 cm^{-1}; ^1H NMR (300 MHz, CDCl$_3$) δ: 1.27-1.38 (m, 9H, $-CH_3$), 3.22 (d, J = 21.57 Hz, 2H, $-CH_2P=O$), 4.03-4.26 (m, 4H, $-OCH_2-$) ppm; HRMS (FAB) calcd for $C_8H_{17}O_5P$ (M^+): 224.08, found: 224.16.

Preparation of OPV1. The bisalcohol derivative **20** of the corresponding bisaldehyde **19** (0.1 mmol) was dissolved in dry chloroform. Acetic anhydride (0.3 mmol) and catalytic amount of 4-dimethylaminopyridine (DMAP) were added to this solution. The reaction mixture was stirred at room temperature for 12 h under argon atmosphere. After checking the completion of the reaction by TLC, the reaction mixture was poured into water and then extracted with chloroform. The

organic layer was separated, washed several times with water, dried over anhydrous Na_2SO_4 and concentrated, followed by column chromatography (hexanes/chloroform, 3:1) over silica gel (100-200 mesh). The pure **OPV1** was obtained as a greenish yellow solid.

OPV1
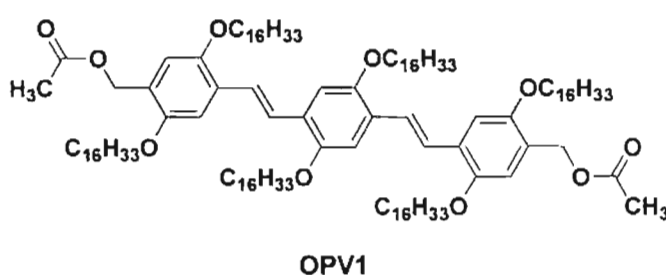
Yield: 63%; mp: 94-95 °C; FT-IR (KBr) v_{max}: 717, 804, 854, 962, 1024, 1068, 1213. 1240, 1348, 1382, 1423, 1462, 1510, 1608, 1741, 2746, 2848, 2918, 3053 cm^{-1}; ^1H NMR (300 MHz, $CDCl_3$) δ: 0.85-0.88 (m, 18H, $-CH_3$), 1.25-1.83 (m, 168H, $-CH_2-$), 2.11 (s, 6H, $-CO-CH_3$), 3.98-4.04 (m, 12H, $-OCH_2-$), 5.15 (s, 4H, $-CH_2O-$), 6.89 (s, 2H, phenyl-*H*), 7.13 (d, *J* = 5.10 Hz, 4H, vinyl-*H*), 7.45 (s, 4H. phenyl-*H*) ppm; ^{13}C NMR (75 MHz, $CDCl_3$) δ: 14.32, 21.33, 22.90, 26.39. 26.43, 26.53, 29.58, 29.69, 29.77, 29.88, 29.93, 31.36, 32.14, 62.08, 69.68. 69.91, 109.78, 110.83, 115.34, 125.56, 126.75, 127.38, 129.51, 151.18, 152.28, 152.37, 171.13 ppm; MALDI-TOF MS (MW= 1869.05): *m/z* = 1869.34 [*M*]⁺.

Preparation of OPV2. To a solution of the phosphonate of ethyl bromoacetate, **21** (1.12 mmol), and the bisformyl derivative **19** (0.56 mmol) in 35 mL THF, NaH

(3.7 mmol) was added carefully under argon atmosphere. The reaction mixture was then heated at 70 °C with stirring. After 8 h the reaction mixture was cooled and THF was removed under reduced pressure. The resultant residue was extracted with chloroform, and washed several times with saturated brine and water. The organic layer was dried over anhydrous Na_2SO_4 and concentrated. The crude product was subjected to column chromatography (hexanes/chloroform, 3:1) over silica gel (100-200 mesh) that gave the pure **OPV2** as an orange solid.

OPV2
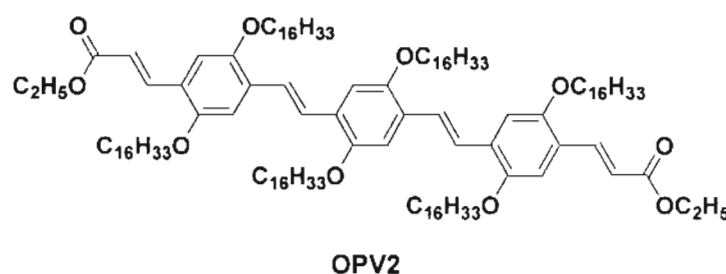
Yield: 71%; mp: 98-99 °C; FT-IR (KBr) v_{max}: 668, 860, 963, 1082, 1175, 1212, 1253, 1351, 1424, 1475, 1506, 1600, 1636, 1724, 2856, 2934 cm^{-1}; ^1H NMR (300 MHz, $CDCl_3$) δ: 0.85-0.89 (m, 18H, $-CH_3$), 1.24-1.86 (m, 174H, $-CH_2-$), 3.97-4.07 (m, 12H, $-OCH_2-$), 4.23-4.30 (q, $J = 7.10$ Hz, 4H, $-COOCH_2-$), 6.48-6.54 (d, $J = 16.09$ Hz, 2H, vinyl-*H*), 7.03 (s, 2H, phenyl-*H*), 7.14 (s, 4H, phenyl-*H*), 7.46 (d, $J = 16.62$ Hz, 2H, vinyl-*H*), 7.54 (d, $J = 16.41$ Hz, 2H, vinyl-*H*), 7.99 (d, $J = 16.09$ Hz, 2H, vinyl-*H*) ppm; ^{13}C NMR (75 MHz, $CDCl_3$) δ: 14.12, 14.36, 22.69, 26.21, 26.30, 29.38, 29.47, 29.53, 29.67, 29.72, 31.92, 60.28, 69.20, 69.39, 110.09, 110.60, 112.31, 115.89, 117.86, 123.19, 124.93,

127.38, 130.52, 139.74, 150.62, 151.17, 152.49, 167.58 ppm; MALDI-TOF MS (MW= 1921.13): m/z = 1921.88 $[M]^+$.

General Procedure for the Preparation of OPV3 and OPV4. A mixture of the bisformyl derivative **19** (0.56 mmol), the required active methylene compound **22** or **23** (1.23 mmol), NH$_4$OAc (~20 mg), and acetic acid (5 mL) in toluene (30 mL) were stirred at 80 °C for 4 h. The solvent was removed under reduced pressure, the residue was extracted with chloroform and washed several times with water. The organic layer was dried over anhydrous Na$_2$SO$_4$ and concentrated to give the corresponding OPV derivatives. Further purification was done by repeated precipitation from chloroform by adding methanol.

OPV3
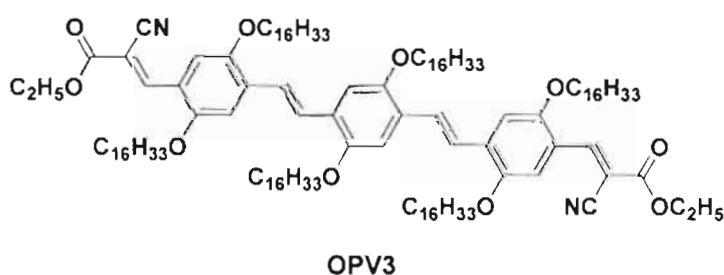
Red solid: yield: 95%; mp: 78-79 °C; FT-IR (KBr) ν_{max}: 719, 763, 802, 854, 960, 1024, 1049, 1091, 1165, 1213, 1240, 1294, 1365, 1394, 1429, 1467, 1506, 1571, 1726, 2214, 2848, 2916, 2956 cm^{-1}; ^{1}H NMR (300 MHz, CDCl$_3$) δ: 0.85-0.88 (m, 18H, –C*H*$_3$), 1.24-2.05 (m, 174H, –C*H*$_2$–), 4.07-4.09 (m, 12H, –OC*H*$_2$–), 4.34-4.41 (q, J = 6.95 Hz, 4H, –COOC*H*$_2$–), 7.16 (s, 4H, phenyl-*H*), 7.51 (d, J = 16.40 Hz, 2H, vinyl-*H*), 7.63 (d, J = 16.38 Hz, 2H, vinyl-*H*), 7.98 (s,

2H, phenyl-*H*), 8.78 (s, 2H, −C*H*=(CO$_2$C$_2$H$_5$)(CN)) ppm; ^{13}C NMR (75 MHz,

CDCl$_3$) δ: 14.32, 14.44, 22.90, 26.33, 26.46, 26.53, 29.46, 29.59, 29.69, 29.74,

29.95, 32.15, 62.49, 69.38, 69.59, 100.14, 109.78, 110.93, 111.88, 116.95,

120.37, 123.34, 127.12, 127.73, 134.74, 148.82, 150.74, 151.63, 154.08, 163.46

ppm; MALDI-TOF MS (MW= 1985.17): *m/z* = 1985.43 [*M*]$^+$.

OPV4
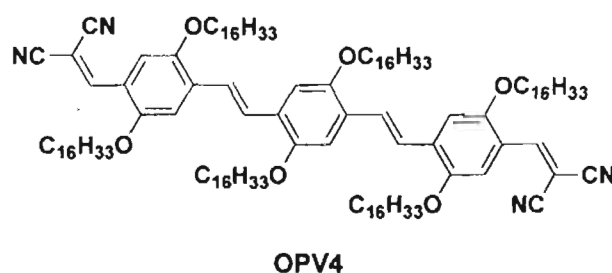
Dark red solid; yield: 95%; mp: 100-101 °C; FT-IR (KBr) v_{max}: 607, 715, 804,

854, 966, 1024, 1095, 1213, 1259, 1292, 1361, 1427, 1463, 1504, 1566, 2223,

2850, 2920, 2953 cm^{-1}; ^{1}H NMR (300 MHz, CDCl$_3$) δ: 0.85-0.88 (m, 18H,

−C*H$_3$*), 1.24-1.86 (m, 168H, −C*H$_2$*−), 3.97-4.06 (m, 12H, −OC*H$_2$*−), 7.14 (s, 4H,

phenyl-*H*), 7.51 (d, *J* = 16.71 Hz, 2H, vinyl-*H*), 7.66 (d, *J* = 16.60 Hz, 2H,

vinyl-*H*) 7.82 (s, 2H, phenyl-*H*), 8.26 (s, 2H, −C*H*=(CN)$_2$) ppm; ^{13}C NMR (75

MHz, CDCl$_3$) δ: 14.22, 22.77, 23.57, 24.43, 26.25, 26.39, 28.48, 29.24, 29.45,

29.60, 32.00, 69.12, 69.25, 69.38, 79.54, 109.32, 110.47, 111.61, 113.46,

113.96, 119.58, 123.03, 127.56, 127.98, 136.27, 150.59, 151.54, 153.55, 162.17

ppm; MALDI-TOF MS (MW= 1877.04): m/z = 1877.15 [*M*]$^+$.

2.5.2. Description of Experimental Techniques

Optical Measurements. Electronic absorption spectra were recorded on a Shimadzu UV-3101 PC NIR scanning spectrophotometer and the emission spectra were recorded on a SPEX-Fluorolog F112X spectrofluorimeter. Temperature dependent studies were carried out in a 1 cm quartz cuvette with a thermistor directly attached to the wall of the cuvette holder. Optical studies in the gel state were carried out in a 1 mm quartz cuvette. Emission spectra in the gel state were recorded using the front face geometry. Fluorescence lifetimes were measured using IBH (FluoroCube) time-correlated picosecond single photon counting (TCSPC) system. Solutions were excited with a pulsed diode laser (375, 405 and 440 nm) <100 ps pulse duration with a repetition rate of 1 MHz. The detection system consists of a microchannel plate photomultiplier (5000U-09B, Hamamatsu) with a 38.6 ps response time coupled to a monochromator (5000M) and TCSPC electronics (DataStation Hub including Hub-NL, NanoLED controller and preinstalled Fluorescence Measurement and Analysis Studio (FMAS) software). The fluorescence lifetime values were determined by deconvoluting the instrument response function with biexponential decay using DAS6 decay analysis software. The quality of the fit has been judged by the fitting parameters such as χ^2 (<1.2) as well as the visual inspection of the residuals.

Quantum Yield Measurements. Fluorescence quantum yields of OPV (Φ_s) are reported either relative to quinine sulfate ($\Phi_r = 0.546$ in 0.1 N H_2SO_4) or Rhodamine 6G ($\Phi_r = 0.9$ in ethanol). The experiments were done using optically matching solutions and the quantum yield is calculated using equation 2.3,[22]

$$\Phi_s = \Phi_r \, (A_rF_s/A_sF_r) \, (\eta_s^2/\eta_r^2) \qquad \text{- - - - (2.3)}$$

where, A_s and A_r are the absorbance of the sample and reference solutions respectively at the same excitation wavelength, F_s and F_r are the corresponding relative integrated fluorescence intensities and η is the refractive index of the solvent.

Calculation of Average Lifetime. Average lifetime, $<\tau>$ of the biexponential decay is calculated using equation 2.4,[22]

$$<\tau> = (\alpha_1 \tau_1^2 + \alpha_2 \tau_2^2)/(\alpha_1 \tau_1 + \alpha_2 \tau_2) \qquad \text{- - - - (2.4)}$$

where α is the amplitude and τ is the corresponding lifetime of the decay components.

Gelation Studies. The gelation studies were carried out as per reported procedures.[17a,b] A typical procedure for gelation studies is as follows: A weighed amount of the compound in an appropriate solvent (1 mL) was placed in a glass vial (1 cm diameter), which was sealed and heated until the compound was dissolved. The solution was allowed to cool to room temperature and the gel

formation was confirmed by the failure of the transparent soft mass to flow by inverting the glass vial. The reversibility of the gelation was confirmed by repeated heating and cooling. The critical gelator concentration (CGC) is determined from the minimum amount of gelator required for the formation of gel at room temperature.

Gel Melting Temperature (T_{gel}) Determination. The thermotropic behavior of the gels formed by **OPV1-3** was investigated by dropping ball method.[17a,b] In dropping ball method, a steel ball (150 mg) was placed on the top of a 1 mL volume gel in a sealed glass vial. Then the gels were slowly heated, while the position of the ball on the top of gel is continuously observed, until the gel no longer bears the ball. The temperature at which the ball reaches the bottom of vial is taken as the sol-gel phase transition temperature (T_{gel}).

Atomic Force Microscopy (AFM) Studies. AFM images were recorded under ambient conditions using a Digital Instrument Multimode Nanoscope IV operating in the tapping mode regime. Micro-fabricated silicon cantilever tips (MPP-11100-10) with a resonance frequency of 299 kHz and a spring constant of 20-80 Nm^{-1} were used. The scan rate varied from 0.5 to 1 Hz. AFM section analysis was done offline. Samples for the imaging were prepared by drop casting the toluene solution of **OPV1-4** (5 x 10^{-5} M) on freshly cleaved mica surface. Blank experiments with neat solvent on mica sheet were carried out to eliminate the possibility of any artifacts, prior to the measurements of the samples. AFM height

and phase image analyses of several samples of each OPV solutions at different

scanning areas were carried out to check the uniform formation of supramolecular

structures.

2.6. References

1. (a) S. R. Forrest, *Nature* **2004**, *428*, 911. (b) J. M. Tour, *Molecular Electronics: Commercial Insights, Chemistry, Devices, Architectures and Programming*, World Scientific: River Edge, New Jersey, **2003**. (c) R. L. Carroll, C. B. Gorman, *Angew. Chem., Int. Ed.* **2002**, *41*, 4378.

2. F. J. M. Hoeben, P. Jonkheijm, E. W. Meijer, A. P. H. J. Schenning, *Chem. Rev.* **2005**, *105*, 1491.

3. (a) S. R. Marder, *Chem. Commun.* **2006**, 131. (b) S. R. Marder, B. Kippelen, A. K.-Y. Jen, N. Peyghambarian, *Nature* **1997**, *388*, 845.

4. (a) A. C. Grimsdale, K. Müllen, *Angew. Chem., Int. Ed.* **2005**, *44*, 5592. b) A. Kraft, A. C. Grimsdale, A. B. Holmes, *Angew. Chem., Int. Ed.* **1998**, *37*, 402. (c) *Electronic Materials: The Oligomer Approach* (Eds.: K. Müllen, G. Wegner), VCH: Weinheim, **1998**. (d) K. Müllen, *Pure Appl. Chem.* **1993**, *65*, 89.

5. (a) J. Roncali, *Acc. Chem. Res.* **2000**, *33*, 147. (b) R. E. Martin, F. Diederich, *Angew. Chem., Int. Ed.* **1999**, *38*, 1350. (c) J. M. Tour, *Chem. Rev.* **1996**, *96*, 537.

6. (a) U. Scherf, *Top. Curr. Chem.* **1999**, *201*, 163. (b) T. Maddux, W. Li, L. Yu, *J. Am. Chem. Soc.* **1997**, *119*, 844. (b) J. Gierschner, J. Cornil, H.-J. Egelhaaf, *Adv. Mater.* **2007**, *19*, 173.

7. (a) H. Meier, B. Mühling, A. Oehlhof, S. Theisinger, E. Kirsten, *Eur. J. Org. Chem.* **2006**, 405. (b) H. Meier, *Angew. Chem., Int. Ed.* **2005**, *44*, 2482 and references cited therein. (c) H. Meier, J. Gerold, H. Kolshorn, B. Mühling, *Chem. –Eur. J.* **2004**, *10*, 360. (d) H. Meier, J. Gerold, D. Jacob, *Tetrahedron Lett.* **2003**, *44*, 1915. (e) H. Meier, J. Gerold, H. Kolshorn, W. Baumann, M. Bletz, *Angew. Chem., Int. Ed.* **2002**, *41*, 292. (f) H. Meier, D. Ickenroth, *Eur. J. Org. Chem.* **2002**, 1745. (g) V. Gebhardt, A. Bacher, M. Thelakkat, U. Stalmach, H. Meier, H.-W. Schmidt, D. Haarer, *Adv. Mater.* **1999**, *11*, 119. (h) H. Meier, U. Stalmach, H. Kolshorn, *Acta Polym.* **1997**, *48*, 379 and references cited therein.

8. (a) T. Izumi, S. Kobashi, K. Takimiya, Y. Aso, T. Otsubo, *J. Am. Chem. Soc.* **2003**, *125*, 5286. (b) T. Takahashi, K. Takimiya, T. Otsubo, Y. Aso, *Org. Lett.* **2005**, *7*, 4313.

9. (a) Y. Yamaguchi, T. Ochi, T. Wakamiya, Y. Matsubara, Z.-i. Yoshida *Org. Lett.* **2006**, *8*, 717. (b) Y. Yamaguchi, T. Tanaka, S. Kobayashi, T. Wakamiya, Y. Matsubara, Z.-i. Yoshida, *J. Am. Chem. Soc.* **2005**, *127*, 9332.

10. (a) C.-L. Li, S.-J. Shieh, S.-C. Lin, R.-S. Liu, *Org. Lett.* **2003**, *5*, 1131. (b) M. S. Wong, Z. H. Li, Y. Tao, M. D'Iorio, *Chem. Mater.* **2003**, *15*, 1198. (c) H. Detert, D. Schollmeyer, E. Sugiono, *Eur. J. Org. Chem.* **2001**, 2927. (d) L. P. Candeias, G. H. Gelinck, J. J. Piet, J. Piris, B. Wegewijs, E. Peeters, J. Wildeman, G. Hadziioannou, K. Müllen, *Synth. Met.* **2001**, *119*, 339. (e) B. Strehmel, A. M. Sarker, J. H. Malpert, V. Strehmel, H. Seifert, D. C. Neckers, *J. Am. Chem. Soc.* **1999**, *121*, 1226.

11. (a) K.-H. Schweikart, M. Hanack, L. Lüer, D. Oelkrug, *Eur. J. Org. Chem.* **2001**, 293. (b) S. E. Döttinger, M. Hanack, J. L. Segura, E. Steinhuber, M. Hohloch, A. Tompert, D. Oelkrug, *Adv. Mater.* **1997**, *9*, 233.

12. (a) J. L. Segura, N. Martín, *J. Mater. Chem.* **2000**, *10*, 2403. (b) C. W. Spangler, *J. Mater. Chem.* **1999**, *9*, 2013. (c) P. F. Van Hutten, V. V. Krasnikov, G. Hadziioannou, *Acc. Chem. Res.* **1999**, *32*, 257. (d) A. Greiner, B. Bolle, P. Hesemann, J. M. Oberski, R. Sander, *Macromol. Chem. Phys.* **1996**, *197*, 113.

13. (a) S.-J. Chung, M. Rumi, V. Alain, S. Barlow, J. W. Perry, S. R. Marder, *J. Am. Chem. Soc.* **2005**, *127*, 10844. (b) M. Albota, D. Beljonne, J.-L. Brédas, J. E. Ehrlich, J.-Y. Fu, A. A. Heikal, S. E. Hess, T. Kogej, M. D. Levin, S. R. Marder, D. McCord-Maughon, J. W. Perry, H. Röckel, M. Rumi, G. Subramaniam, W. W. Webb, S.-L. Wu, C. Xu, *Science* **1998**, *281*, 1653.

14. (a) H. Detert, V. Schmitt, *J. Phys. Org. Chem.* **2004**, *17*, 1051. (b) B. Strehmel, A. M. Sarker, H. Detert, *ChemPhysChem* **2003**, *4*, 249.

15. (a) H. Y. Woo, B. Liu, B. Kohler, D. Korystov, A. Mikhailovsky, G. C. Bazan, *J. Am. Chem. Soc.* **2005**, *127*, 14721. (b) M. Barzoukas, M. Blanchard-Desce, *J. Chem Phys.* **2000**, *113*, 3951.

16. (a) A. P. H. J. Schenning, E. W. Meijer, *Chem. Commun.* **2005**, 3245. (b) M. Van der Auweraer, F. C. De Schryver, *Nat. Mater.* **2004**, *3*, 507. (c) A. P. H. J. Schenning, P. Jonkheijm, F. J. M. Hoeben, J. van Herrikhuyzen, S. C. J. Meskers, E. W. Meijer, L. M. Herz, C. Daniel, C. Silva, R.T. Phillips, R.H. Friend, D. Beljonne, A. Miura, S. De Feyter, M. Zdanowska, H. Uji-i, F. C. De Schryver, Z. Chen, F. Würthner, M. Mas-Torrent, D. den Boer, M.

Durkut, P. Hadley, *Synth. Met.* **2004**, *147*, 43. (d) E. W. Meijer, A. P. H. J. Schenning, *Nature* **2002**, 419, 353.

17. (a) V. K. Praveen, S. J. George, A. Ajayaghosh, *Macromol. Symp.* **2006**, *241*, 1. (b) S. J. George, A. Ajayaghosh, *Chem. –Eur. J.* **2005**, *11*, 3217. (c) A. Ajayaghosh, S. J. George, *J. Am. Chem. Soc.* **2001**, *123*, 5148.

18. (a) A. Ajayaghosh, C. Vijayakumar, R. Varghese, S. J. George, *Angew. Chem., Int. Ed.* **2006**, *45*, 456. (b) A. Ajayaghosh, R. Varghese, S. J. George, C. Vijayakumar, *Angew. Chem., Int. Ed.* **2006**, *45*, 1141. (c) S. J. George, A. Ajayaghosh, P. Jonkheijm, A. P. H. J. Schenning, E. W. Meijer, *Angew. Chem., Int. Ed.* **2004**, *43*, 3422. (d) R. Varghese, S. J. George, A. Ajayaghosh, *Chem. Commun.* **2005**, 593.

19. (a) Q. Miao, M. Lefenfeld, T.-Q. Nguyen, T. Siegrist, C. Kloc, C. Nuckolls, *Adv. Mater.* **2005**, *17*, 407. (b) J. Reichwagen, H. Hopf, A. Del Guerzo, C. Belin, H. Bouas-Laurent, J.-P. Desvergne, *Org. Lett.* **2005**, *7*, 971. (c) S. Yao, U. Beginn, T. Gress, M. Lysetska, F. Würthner, *J. Am. Chem. Soc.* **2004**, *126*, 8336. (d) J.-i. Mamiya, K. Kanie, T. Hiyama, T. Ikeda, T. Kato, *Chem. Commun.* **2002**, 1870. (e) O. Gronwald, S. Shinkai, *J. Chem. Soc. Perkin. Trans.* 2 **2001**, 1933.

20. For reviews of low molecular weight organogels, see: (a) *Molecular Gels, Materials with Self-Assembled Fibrillar Networks* (Eds.: R. G. Weiss, P. Terech), Kluwer Press: Dordrecht, The Netherlands, **2005**. (b) N. M. Sangeetha, U. Maitra, *Chem. Soc. Rev.* **2005**, *34*, 821. (c) A. Ajayaghosh, S. J. George, A. P. H. J. Schenning, *Top. Curr. Chem.* **2005**, *258*, 83. (d) P. Terech, R. G. Weiss, *Chem. Rev.* **1997**, *97*, 3133.

21. (a) B. Wang, M. R. Wasielewski, *J. Am. Chem. Soc.* **1997**, *119*, 12. (b) A. W. van der Made, R. H. van der Made, *J. Org. Chem.* **1993**, *58*, 1262.

22. J. R. Lakowicz, *Principles of Fluorescence Spectroscopy* (2nd ed.), Kluwer Academic/Plenum Publishers: New York, **1999**.

23. E. Zojer, D. Beljonne, T. Kogej, H. Vogel, S. R. Marder, J. W. Perry, J.-L. Brédas, *J. Chem. Phys.* **2002**, *116*, 3646.

24. K.-Y. Peng, S.-A. Chen, W.-S. Fann, *J. Am. Chem. Soc.* **2001**, *123*, 11388.

25. (a) P. Jonkheijm, F. J. M. Hoeben, R. Kleppinger, J. van Herrikhuyzen, A. P. H. J. Schenning, E. W. Meijer, *J. Am. Chem. Soc.* **2003**, *125*, 15941. (b) J. J. Apperloo, R. A. J. Janssen, P. R. L. Malenfant, J. M. J. Fréchet, *Macromolecules* **2000**, *33*, 7038.

26. P. Samori, V. Francke, T. Mangel, K. Müllen, J. P. Rabe, *Opt. Mater.* **1998**, *9*, 390.

27. A. Ajayaghosh, C. Vijayakumar, V. K. Praveen, S. S. Babu, R. Varghese, *J. Am. Chem. Soc.* **2006**, *128*, 7174.

28. M. Lal, S. Pakatchi, G. S. He, K. S. Kim, P. N. Prasad, *Chem. Mater.* **1999**, *11*, 3012.

Chapter 3

Self-Assembled π-Organogels as Donor Scaffolds for Selective and Thermally Gated Fluorescence Resonance Energy Transfer (FRET)
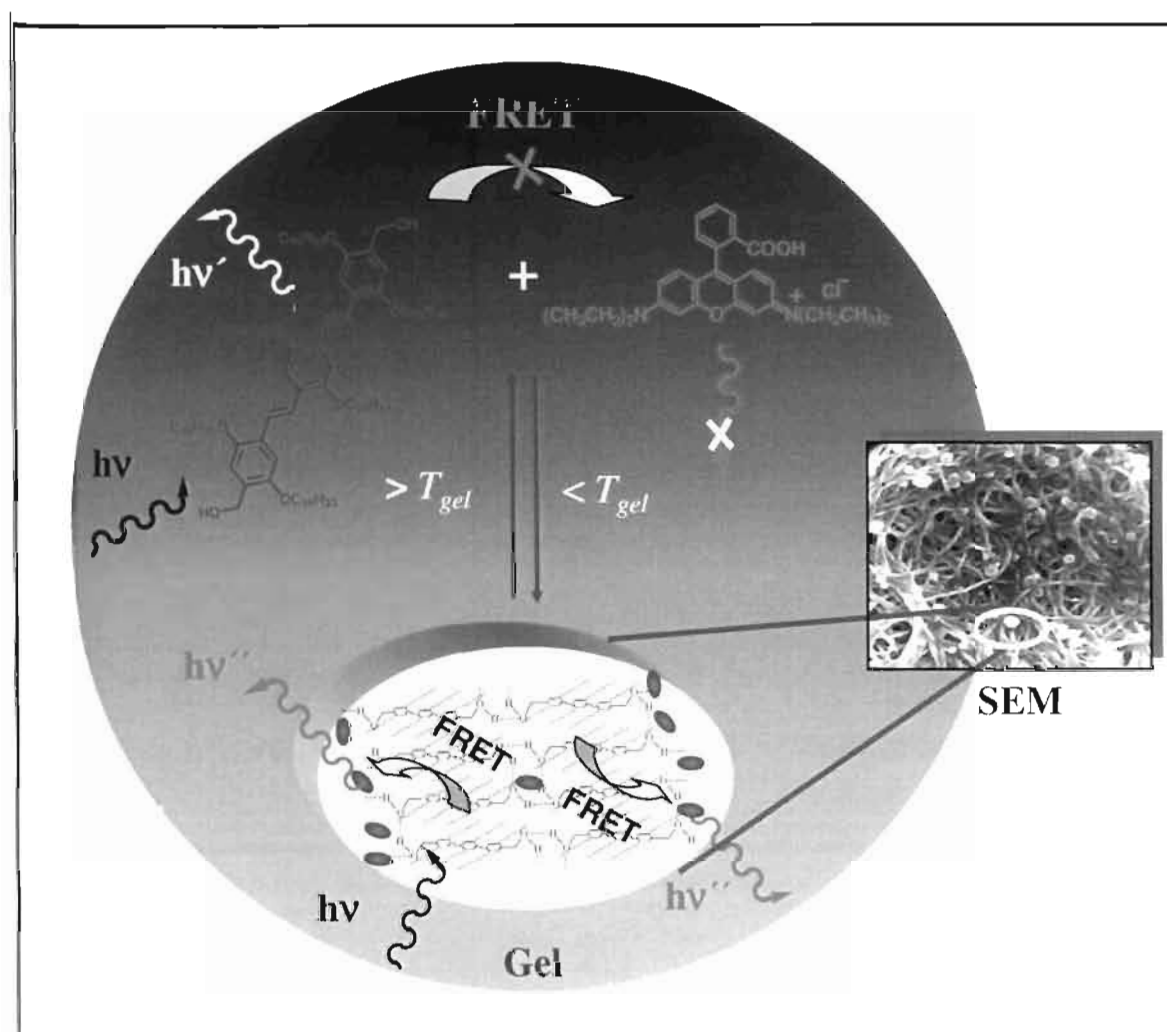
3.1. Abstract

Self-assembled organogels of a few tailor made oligo(p-phenylenevinylene)s (OPVs) have been prepared and used as supramolecular donor scaffolds to study the fluorescence resonance energy transfer (FRET) to a suitable acceptor. In nonpolar solvents, FRET occurs with nearly 63-81% efficiency, exclusively from the self-assembled OPVs to entrapped Rhodamine B, resulting in the quenching of the donor emission with concomitant formation of the acceptor emission at 625 nm. The efficiency of FRET is considerably influenced by the ability of the OPVs to form the self-assembled aggregates and hence could be controlled by structural variation of the molecules, and polarity of the solvent. Most importantly, FRET could be controlled by temperature as a result of the thermally reversible self-assembly process. The FRET efficiency was significantly enhanced (ca. 90%) in a xerogel film of the **OPV1** which is dispersed with relatively less amount of the acceptor (33 mol%), when compared to that of the aggregates in dodecane gel. These results indicate that energy transfer occurs exclusively from the self-assembled donor and not directly from the individual donor molecules. The present study illustrates that the self-assembly of chromophores facilitates temperature and solvent controlled FRET within π-conjugated nanostructures.

3.2. Introduction

Photoinduced energy transfer is one of the fundamental processes of natural photosynthetic systems and has been a subject of numerous studies. Supramolecular organization of chromophores[1] play a crucial role in facilitating energy and electron transfer processes in natural light harvesting assemblies.[2] On the other hand, these processes have become extremely important in the field of organic based optoelectronic materials,[3] particularly in the emerging field of supramolecular electronics.[4] Among several strategies adopted for chromophore organization, the use of H-bonded supramolecular assemblies need special mention in the context of the present work.[5] In recent years, a number of H-bonded donor-acceptor systems have been reported for energy transfer studies in which the self-assembly is restricted to the formation of dimeric or trimeric complexes.[6,7] Therefore, creation of higher order supramolecular assemblies of nano- to micrometer length scale is important when electron or energy transport processes are addressed. In this context, energy transfer within chromophore based organogelators has been of great interest.[8,9]

Linear π-conjugated systems, particularly oligo(*p*-phenylenevinylene)s (OPVs) are known to be efficient energy donors to different acceptors. For example, Heeger, Bazan, Swager, Schanze, Armaroli and others have shown fluorescence resonance energy transfer (FRET) from functionalized linear π-conjugated systems to suitable acceptors.[10-16] The research groups of Meijer and

Janssen have extensively studied the energy transfer processes in H-bonded OPV self-assemblies.[17]
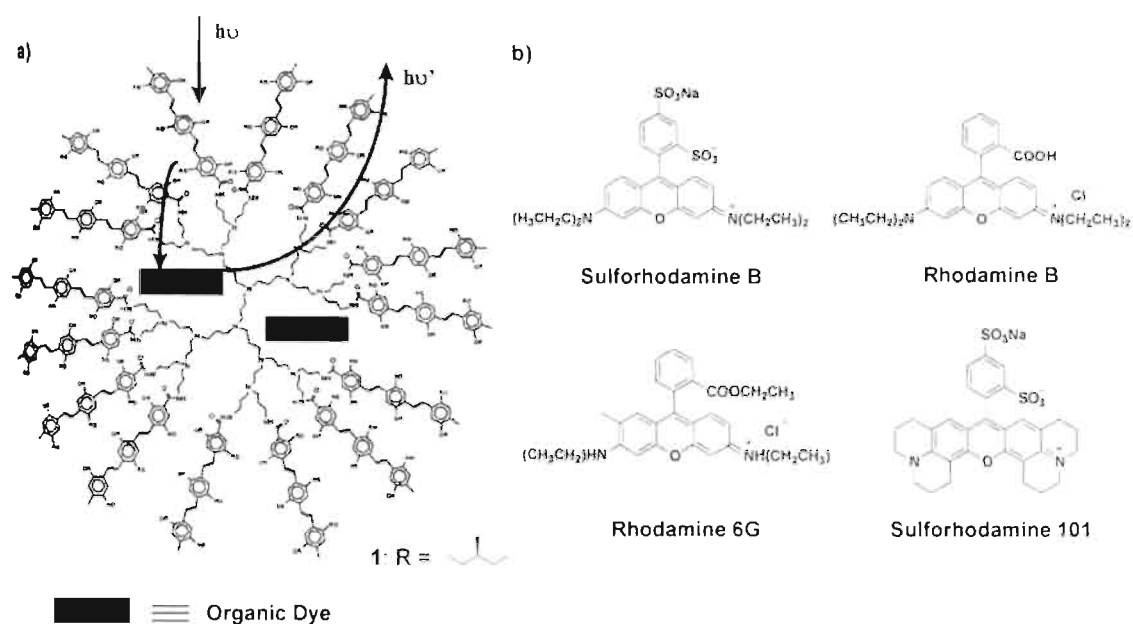

FIGURE 3.1. a) Schematic representation of energy transfer in amphiphilic OPV dendrimer encapsulated with an organic dye. b) Molecular structure of organic dyes used to tune the emission wavelength of OPV dendrimer (1). (adapted from ref. 18)

Energy transfer from OPV functionalized poly(propylene imine) dendrimer (1) to different encapsulated organic dyes has been demonstrated by Meijer and co-workers (Figure 3.1).[18] Owing to the amphiphilic nature, the OPV functionalized dendrimers function as hosts, capable of extracting water soluble organic dyes into the organic phase. The resulted host-guest system showed energy transfer from the peripheral OPV units to the encapsulated dye molecules with 40% efficiency. Energy transfer studies in thin films showed efficient quenching of the OPV emission with 90% efficiency. Such an increase in

efficiency of energy transfer process is attributed to the orientation and better spectral overlap between the donor and acceptor molecules in films.

Recently, Stupp and coworkers have demonstrated energy transfer in nanostructured OPV/silicate hybrid film, loaded with Rhodamine B.[15b] The amphiphilic OPV molecules 2a-d (Chart 3.1), in which the hydrophilic segment of the molecules interact with precursors of silica and self assemble into ordered phase during the solvent evaporation. Detailed X-ray diffraction (XRD), optical and IR spectroscopic studies of OPV/Silicate films showed that OPV domains in the hybrid film are separated by silicate layers having limiting thickness. In order to study how the order parameters of hybrid films affects the efficiency of energy transfer process, a Rhodamine B derivative 3 (Chart 3.1) is covalently grafted into the inorganic silicate domains of the 2a/silicate film (Figure 3.2a). The energy transfer process is found to be highly efficient as quenching of OPV fluorescence is observed with the acceptor concentration as low as 0.5 mol%. Comparison of the energy transfer studies in an amorphous 2a/poly(2-hydroxyethyl methacrylate) film with that of 2a/silicate films showed better efficiency for the latter. Figure 3.2b shows the photograph of 2a/polymer film and 2a/silicate films in the presence of 2 mol% of the acceptor which showed good red fluorescence of 3 from 2a/silicate film. This is attributed to the shorter distance between donors and acceptors and also to efficient energy migration within the organic domains of 2a/silicate film.
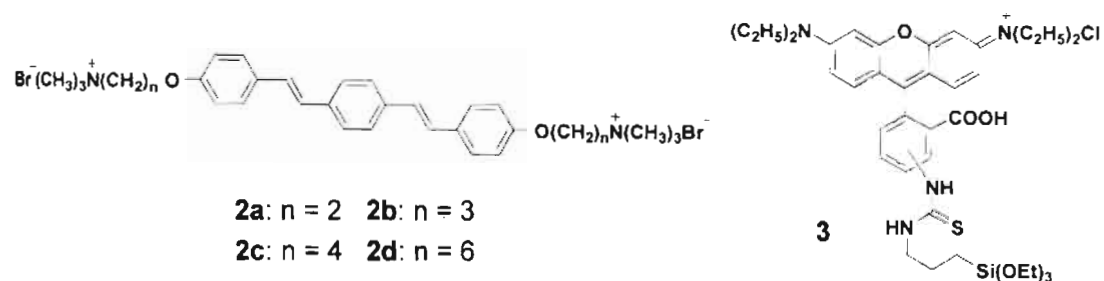
CHART 3.1.
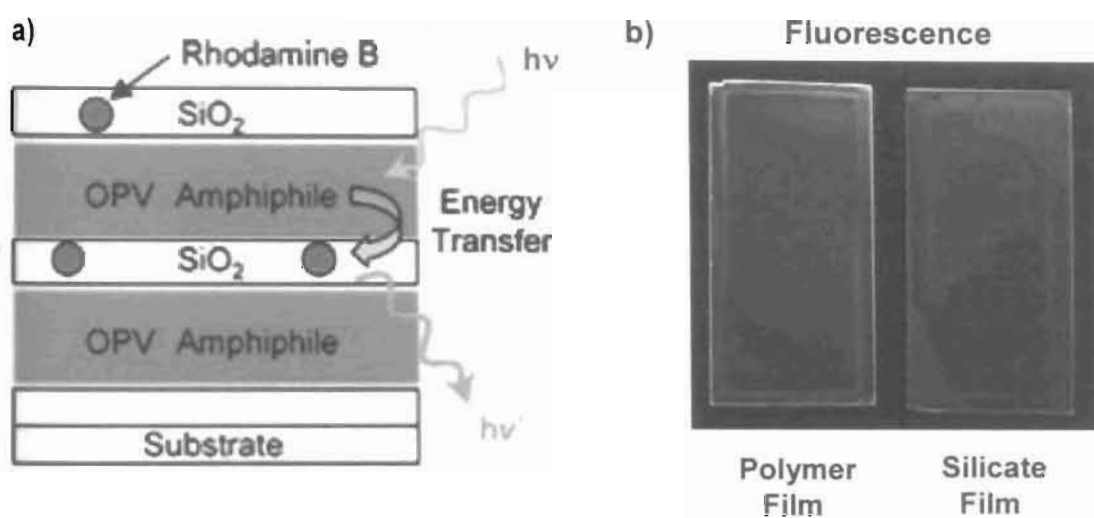
FIGURE 3.2. a) Schematic representation of the energy transfer process in oligo(*p*-phenylenevinylene) amphiphile **2a**/silicate hybrid films when doped with the Rhodamine B derivative **3**. b) Photographs of oligo(*p*-phenylenevinylene) amphiphile **2a**/poly(2-hydroxyethyl methacrylate) film (left) and **2a**/silicate film (right) from precursor solutions containing 2 mol% of Rhodamine B derivative **3** under UV irradiation (λ_{ex} = 365 nm). (adapted from ref. 15b)

FIGURE 3.3. a) Chemical structure of PPE-polyNIPA copolymer (4) and Rhodamine B functionalized polyNIPA polymer (5). b) Fluorescence spectra of thermally induced coprecipitates of 4 and 5 on a filter paper. Concentration of 4 is fixed (0.12 mg/mL) and that of 5 is varied from 0.00625 to 0.05 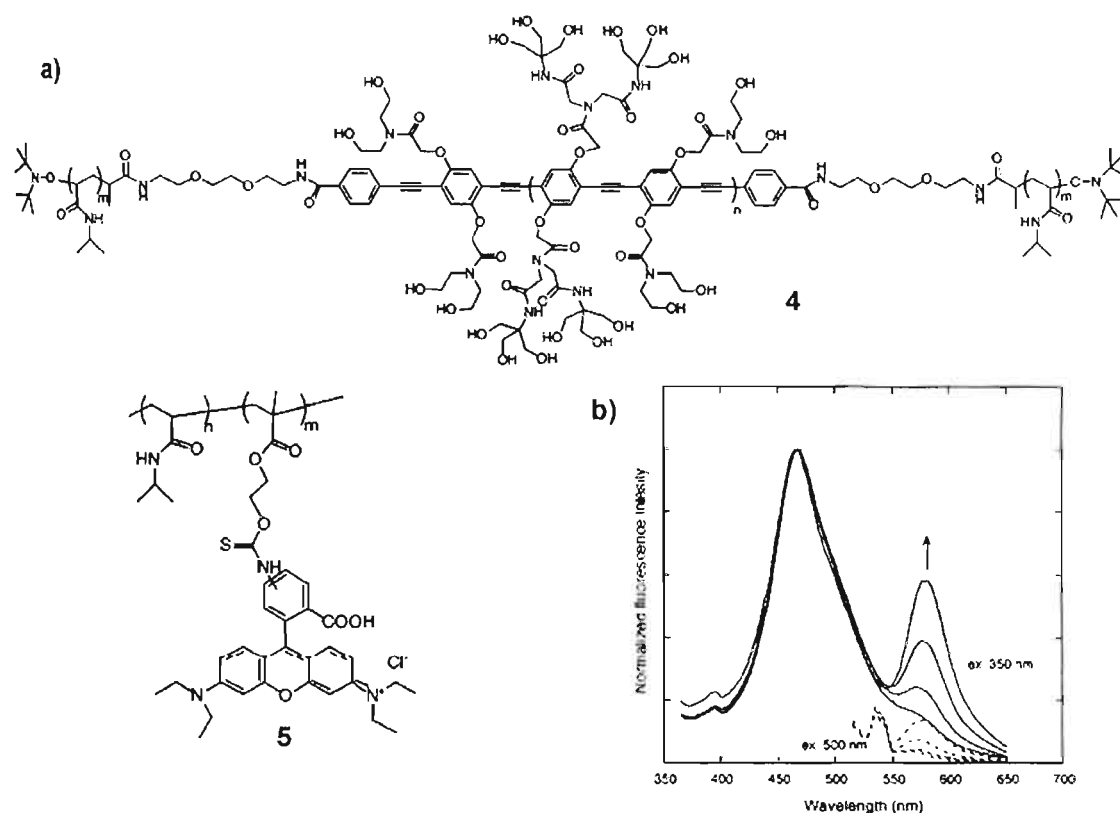mg/mL. PPE unit of polymer 4 is the principal absorbing group with 350 nm excitation; Rhodamine B is selectively excited with excitation at 500 nm. (adapted from ref. 11c)

An interesting example related to energy transfer from π-conjugated molecules to organic dyes was reported by Kuroda and Swager.[11c] They have synthesized a thermally responsive block polymer of poly(phenylenethynylene) (PPE) and poly(N-isopropylacrylamide) (polyNIPA) (4). Emission studies of co-precipitates prepared from polymer 4 and a Rhodamine B dye-labeled polyNIPA polymer (5) revealed energy transfer from the PPE segment to the dye due to the

localization of the dye in the vicinity of the PPE segments of the polymer **4**. Detailed studies showed that energy transfer from PPE unit (λ_{ex} = 350 nm) to the Rhodamine B brings about >5-fold increase in the acceptor fluorescence (λ_{em} = 580 nm) when compared to that by selective excitation of the acceptor unit at 500 nm (Figure 3.3b).

The present study demonstrates the use of supramolecular architectures of OPV organogels as energy donor scaffolds for FRET to encapsulated acceptors. OPVs which are functionalized with H-bonding groups and long alkyl side chains form stable organogels with good optical properties.[19,20] It is observed that the emission of OPVs is significantly shifted towards long wavelength region as a result of the gelation.[19c] This property of self-assembled OPVs make them ideal energy donor scaffolds to suitable acceptors that facilitate FRET processes.[21] In the present chapter, we describe the details of our investigation on the use of a few OPV self-assemblies as FRET donors to an entrapped organic dye (Rhodamine B).[22] The structures of the donors and the acceptor under investigation are shown in Figure 3.4.
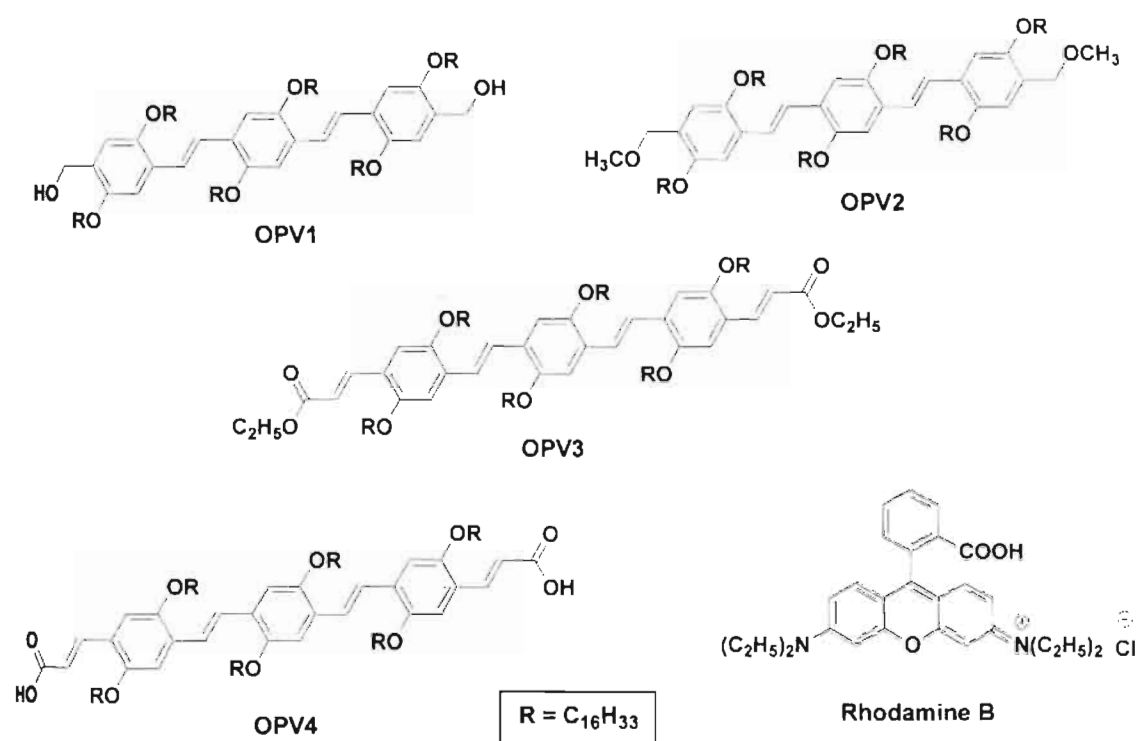
FIGURE 3.4. Molecular structures of the OPV donors and the acceptor under investigation.

3.3. Results and Discussion

3.3.1. Synthesis of OPVs

The synthesis and characterization of **OPV1** and **OPV3** is described in the previous chapter. **OPV2**, the hydroxyl protected derivative of **OPV1** was prepared by adapting a simple methylation procedure using methyl iodide and NaH as base in 95% yield (Scheme 3.1).[19c] Base hydrolysis of **OPV3** followed by acidification using trifluoroacetic acid afforded **OPV4** in a quantitative yield (Scheme 3.2). All the OPV derivatives under investigation were characterized by IR, ^{1}H NMR, ^{13}C NMR, and MALDI-TOF analysis.
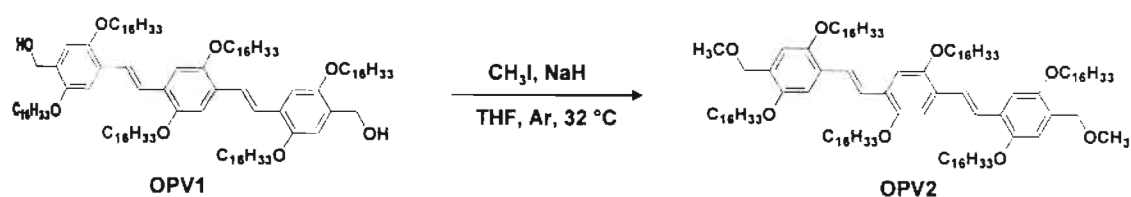
SCHEME 3.1. Synthesis of the hydroxyl protected OPV derivative.
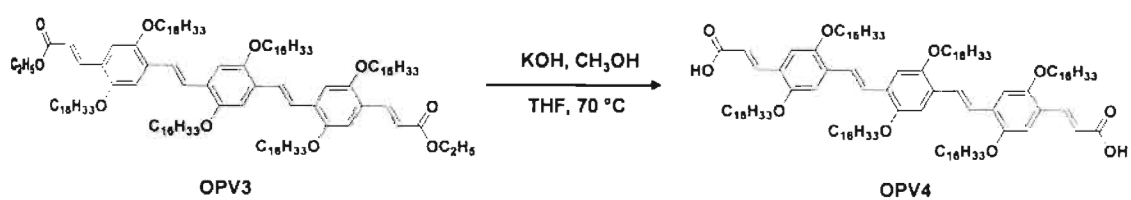
SCHEME 3.2. Synthesis of the OPV acid derivative.

3.3.2. Absorption and Emission Properties

The electronic absorption and emission properties of OPVs are ideal tool to monitor the self-assembling process. The photophysical data of the OPVs under investigation are presented in Table 3.1. The most important feature of the gelation of OPVs is the self-assembly induced modulation of the optical properties. The absorption and emission spectra of a dodecane solution of **OPV1** (1×10^{-5} M) at 20 °C showed a broad absorption with a shoulder at 467 nm and a broad emission between 500-700 nm (Figure 3.5). Upon increasing the temperature to 65 °C the absorption and emission maxima are shifted towards the short wavelength with significant increase in the intensity. On the other hand, the spectra in dodecane at

TABLE 3.1. Optical Properties and Energy Transfer Efficiencies of **OPV1-4**.

Compound	Solvent	Absorption λ_{max} (nm)	Emission λ_{max} (nm)	Φ_f	Energy transfer efficiency (%)
OPV1	chloroform	407	463, 490	0.73[a]	-
	cyclohexane	401, 468	454, 476, 527, 561	0.20[b]	63[c]
	dodecane	404, 467	537, 567	0.23[b]	72[d]
OPV2	chloroform	408	464, 496, 533	0.71[a]	-
	cyclohexane	401	452, 480, 520	0.66[a]	10[c]
	dodecane	394, 465	517, 552	0.34[b]	63[d]
OPV3	chloroform	450	527, 562	0.94[b]	-
	cyclohexane	438	506, 540, 589	0.67[b]	-
	dodecane	427, 515	530, 568, 620	0.58[b]	69[d]
OPV4	chloroform	448	534, 562	0.90[b]	-
	cyclohexane	470, 515	508, 545	0.69[b]	-
	dodecane	475, 517	588	0.21[b]	81[d]

[a]Fluorescence quantum yields were determined using quinine sulphate as the standard (Φ_f = 0.546 in 0.1 N H_2SO_4), ±5% error. [b]Fluorescence quantum yields were determined using Rhodamine 6G (Φ_f = 0.9 in ethanol), ±5% error. [c]In cyclohexane-chloroform (16:1). [d] In dodecane-chloroform (16:1).

20 °C were more or less identical to those of the casted films. Thus temperature and solvent dependent spectral changes indicates the aggregation of **OPV1** in dodecane. Moreover the similarity of the spectra in the aggregated state and in the film state indicate that extend of aggregation and the chromophore packing may be

more or less identical in both cases. In cyclohexane at room temperature, **OPV1** showed a broad emission with several maxima at 454, 476, 527 and 561 nm, the relative intensities of which are dependent upon temperature and concentration (Figure 3.5b, doted lines). This observation indicates the possibility of more than one co-existing species in cyclohexane.

FIGURE 3.5. a) Absorption and b) emission spectra of **OPV1** under different conditions. In chloroform (- ·· -), cyclohexane (·····), dodecane at 20 °C (——), dodecane at 65 °C (- · - ·) and in the solid state (– – –). In all experiments concentration of **OPV1** is 1 x 10^{-5} M and the excitation wavelength is 380 nm.

Insight to the effect of structural variation of the OPVs on the self-assembly properties could be obtained by comparing the optical properties of **OPV2-4** with those of **OPV1**. Absorption spectrum of **OPV2** in cyclohexane showed only a slight difference from that in chloroform which is relatively weak when compared to the changes for **OPV1** (Figure 3.6a). However, the absorption spectrum in
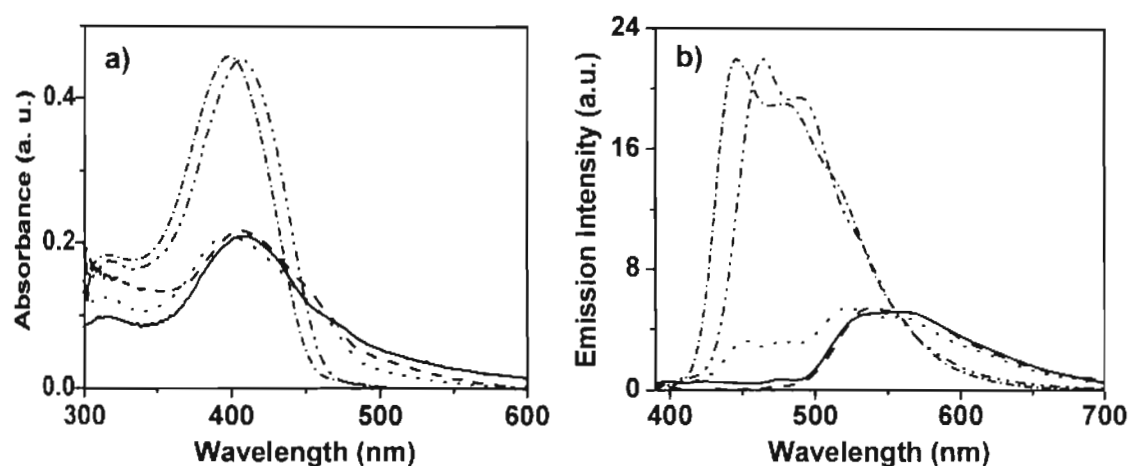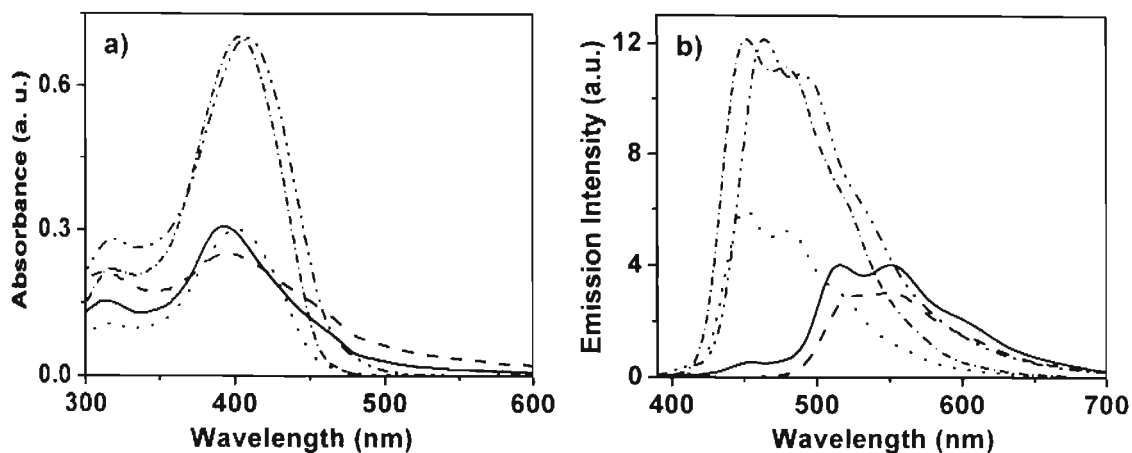
FIGURE 3.6. a) Absorption and b) emission spectra of OPV2 under different conditions. In chloroform (- ·· -), cyclohexane (·····), dodecane at 20 °C (——), dodecane at 65 °C (- · - ·) and in the solid state (– – –). In all experiments concentration of OPV2 is 1 x 10⁻⁵ M and the excitation wavelength is 380 nm.

dodecane showed considerable difference with a maximum at 394 nm, which is blue shifted by 14 nm with a shoulder at 465 nm when compared to that in chloroform (λ_{max} = 408 nm). In contrast to the observation of OPV1 the emission spectra of OPV2 in chloroform and in cyclohexane showed a marginal difference between the two (Figure 3.6b). These observations indicate a weak self-assembly of OPV2 in cyclohexane, which could be due to the lack of H-bonding interactions. However, in dodecane the emission spectrum is completely red shifted with two long wavelength maxima at 517 and 552 nm and matches with the film state spectra. Similar observations were made in the case of OPV3 also (Figure 3.7). The absorption and emission spectra of OPV3 in cyclohexane revealed the weak self-assembly character of this molecule in this solvent. This

observation is similar to that of **OPV2**. However, in dodecane **OPV3** showed a broad absorption spectra with a shoulder band at 515 nm while the emission spectra is found to be red shifted with two long wavelength maxima at 530 and 568 nm (Figure 3.7). These optical features indicate the formation of **OPV3** self-assembly in dodecane.

FIGURE 3.7. a) Absorption and b) emission spectra of **OPV3** under different conditions. In chloroform (- ·· -), cyclohexane (·····), dodecane at 20 °C (——), dodecane at 65 °C (- · - ·) and in the solid state (– – –). In all experiments concentration of **OPV3** is 1 X 10⁻⁵ M and the excitation wavelength is 410 nm.

Due to the presence of additional vinylic double bonds, the absorption and emission properties of **OPV3** and **OPV4** in cyclohexane and dodecane is found to be red shifted towards the long wavelength region when compared to that of **OPV1** and **OPV2**. Comparison of the absorption properties of **OPV1-3** in dodecane at 20 °C with that of **OPV4** revealed that the contribution from the long wavelength absorbing shoulder band is more prominent in the latter case (Figure 3.8a). In addition, the emission spectrum of **OPV4** in dodecane at 20 °C is found

to be broad when compare to that of other OPVs (Figure 3.8b). Similar observations were made in the case of **OPV4** in cyclohexane. These observations indicate the strong tendency of **OPV4** to aggregate in nonpolar a solvent, which is facilitated by the hydrogen bond assisted strong π-π interaction between the OPV chromophores. This is justified from the similarities between the optical properties of **OPV4** in dodecane at 20 °C with that of casted films. However, at higher temperature (65 °C) due to the breaking of the self-assembly, the absorption and emission spectra of **OPV4** in dodecane are shifted towards shorter wavelength with significant increase in intensity. Under this condition the optical features of **OPV4** matches with that in chloroform solution.
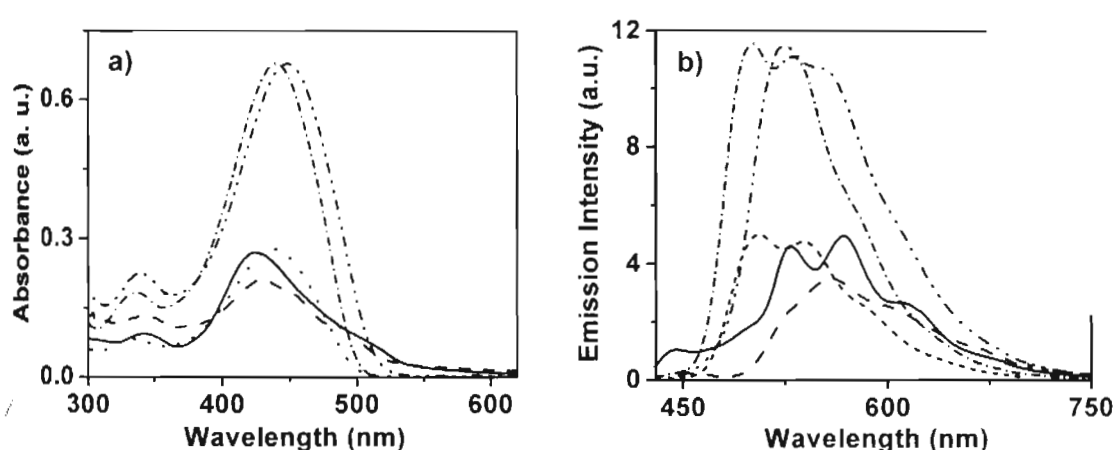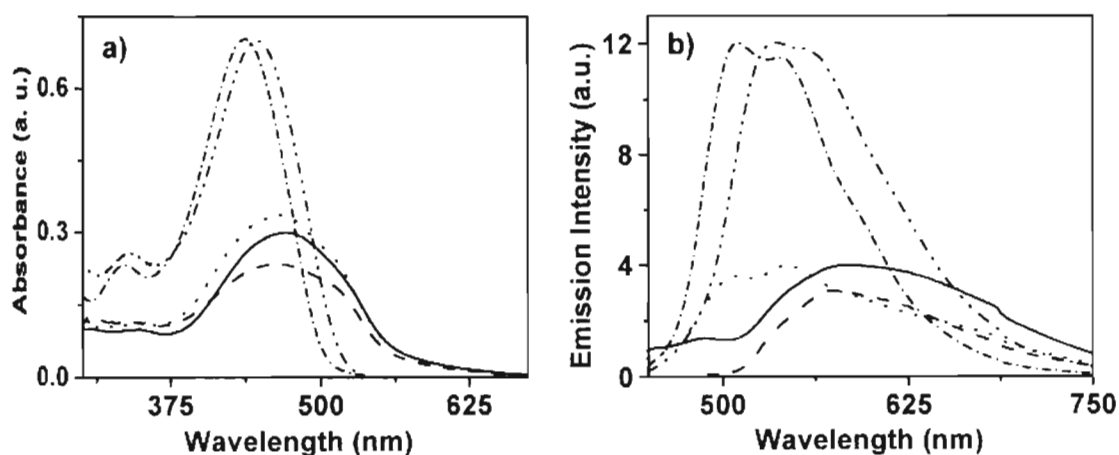

FIGURE 3.8. a) Absorption and b) emission spectra of **OPV4** under different conditions. In chloroform (- ·· -), cyclohexane (·····), dodecane at 20 °C (——), dodecane at 65 °C (- · · - ·) and in the solid state (– – –). In all experiments concentration of **OPV4** is 1 X 10⁻⁵ M and the excitation wavelength is 460 nm.

In order to get insight into the nature and stability of the OPV self-assemblies, detailed temperature dependent absorption studies were conducted.

Plots of the fraction of aggregates (α) versus temperature (Figure 3.9) exhibit

sigmoidal type transitions within short temperature range in the case of **OPV1-3**,

which indicate a co-operative self-assembly process.[19c,23] However, in the case of

OPV4 a broad transition is observed for a wide temperature range. The carboxylic

acid groups of **OPV4** participate in two-point linear H-bonding interactions

leading to the formation of one dimensional supramolecular polymeric aggregates

(Figure 3.10). They subsequently undergo π-stacking, resulting in higher order

structures that show better stability than the self-assemblies of **OPV1-3**. These

polymeric aggregates break at relatively higher temperatures in a noncooperative

way as evident from the aggregate to monomer transition curve which could be the

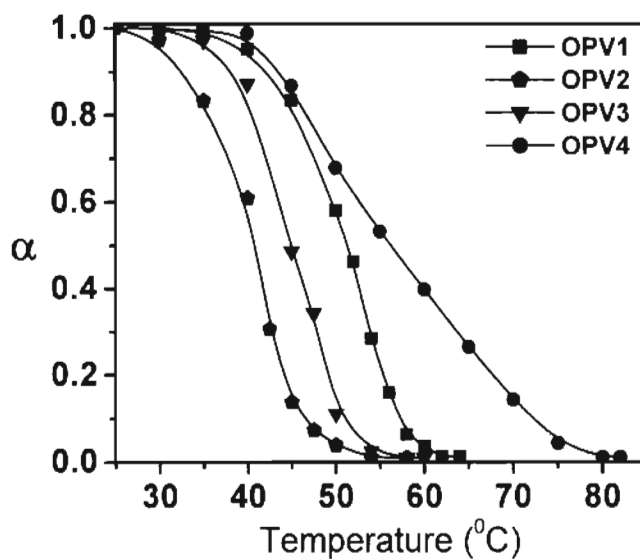reason for the broad transition in Figure 3.9.[23b]

FIGURE 3.9. Stability of the OPV self-assemblies [1 x 10⁻⁵ M] in dodecane obtained from plots of aggregate fraction (α) versus temperature. The data points were obtained from the variable temperature absorption spectral changes at 470 nm (**OPV1**), 465 nm (**OPV2**) 513 nm (**OPV3**) and 517 nm for **OPV4**.
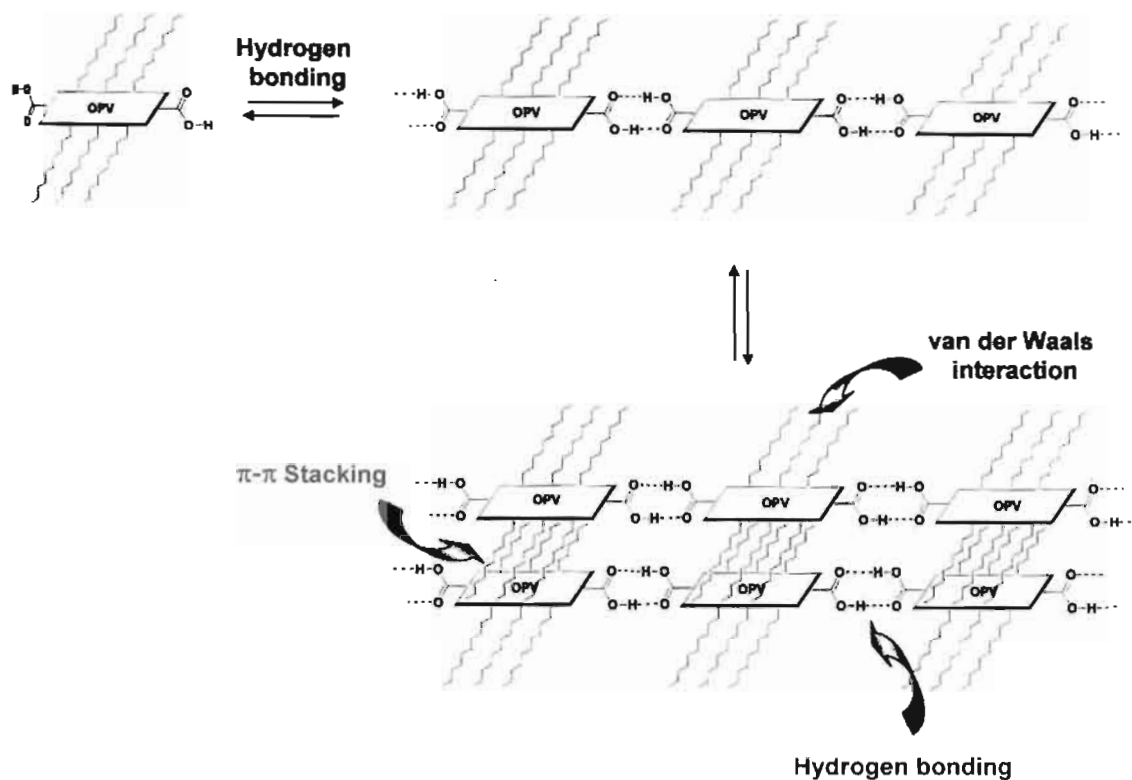
FIGURE 3.10. Schematic representation showing the H-bond and π-π stack assisted formation of supramolecular polymeric aggregates of **OPV4** in dodecane.

3.3.3. Fluorescence Resonance Energy Transfer (FRET) Studies

We have chosen Rhodamine B for the FRET studies since it is known to be a good energy acceptor from excited OPVs.[15b,18] The emission spectra of **OPV1-4** in cyclohexane or dodecane showed significant overlap with the absorption spectrum of Rhodamine B. The absorption spectra of **OPV1-4** $(1.01 \times 10^{-5}$ M) in the presence of Rhodamine B $(8.38 \times 10^{-5}$ M) in cyclohexane-chloroform or dodecane-chloroform (16:1) exhibited their individual spectral characteristics, revealing the absence of any ground state interaction between the donor and the acceptor molecules. The emission spectrum of **OPV1** and the absorption spectrum

of Rhodamine B in cyclohexane-chloroform (16:1) and dodecane-chloroform (16:1) are shown in Figure 3.11. The corresponding spectra of **OPV2** are shown in Figure 3.12.

FIGURE 3.11. a) Emission spectrum of **OPV1** (– – –) and absorption spectrum of Rhodamine B (——) in cyclohexane-chloroform (16:1), λ_{ex} = 380 nm. b) The corresponding spectra in dodecane-chloroform (16:1).

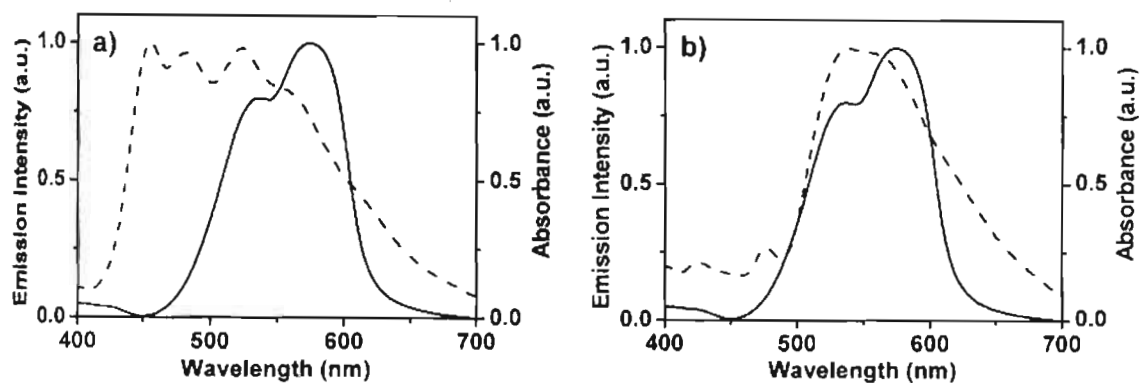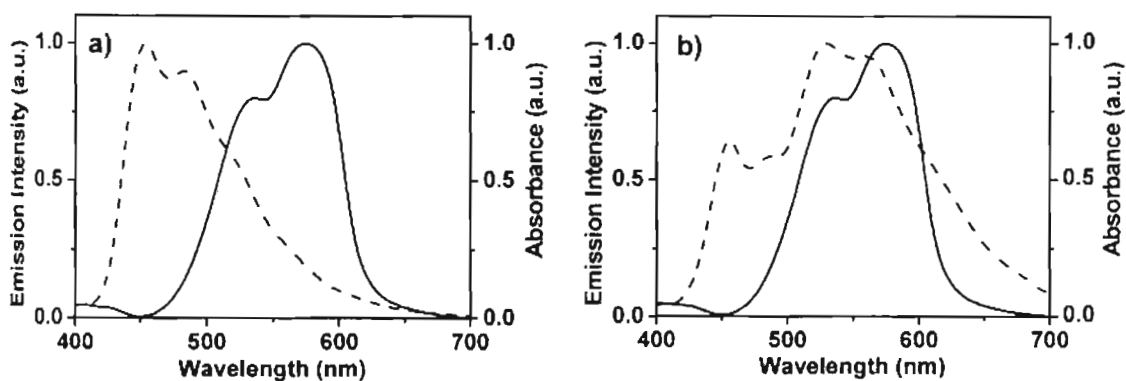**FIGURE 3.12.** a) Emission spectrum of **OPV2** (– – –) and absorption spectrum of Rhodamine B (——) in cyclohexane-chloroform (16:1), λ_{ex} = 380 nm. b) The corresponding spectra in dodecane-chloroform (16:1).

The fluorescence spectra of **OPV1** (1.01 x 10^{-5} M) in cyclohexane-chloroform (16:1) showed a broad emission corresponding to both monomeric and

FIGURE 3.13. Emission spectra of **OPV1** [1.01 x 10⁻⁵ M] in the absence (——) and in the presence (----) of Rhodamine B [8.38 x 10⁻⁵ M]. a) In cyclohexane-chloroform (16:1) λ_{ex} = 380 nm. b) Selective excitation of **OPV1** self-assembly at 470 nm in cyclohexane-chloroform (16:1). Emission of Rhodamine B (– – –) in the absence of **OPV1**, on excitation at 380 nm is shown for a comparison. The inset shows the emission of the acceptor on indirect excitation at 470 nm (■) and direct excitation at 535 nm (▲).

assembled **OPV1** is selectively quenched (ca. 63%) with concomitant emission at

625 nm, indicating the occurrence of FRET from the self-assembled donor to the

acceptor. The emission between 400-480 nm of the molecularly dissolved OPVs was virtually unaffected indicating that FRET is not feasible from molecular OPVs. Direct excitation of a solution of Rhodamine B (8.38×10^{-5} M) at 380 nm in the absence of OPVs showed a negligible fluorescence at 625 nm. When the self-assembled species were selectively excited at 470 nm in the presence of Rhodamine B, 63% quenching of the **OPV1** emission could be observed (Figure 3.13b). The inset of Figure 3.13a shows a comparison of the emission of optically matching solutions of Rhodamine B upon direct ($\lambda_{ex} = 535$ nm) excitation with that of indirect excitation ($\lambda_{ex} = 470$ nm) in the presence of OPV nanotapes. The enhanced dye emission on indirect excitation when compared to that of the direct excitation indicates that the fluorescence quenching is not due to a trivial energy transfer but due to FRET from the OPV self-assembly to Rhodamine B.[10d,11c,24]

FRET from the self-assembled OPVs to the entrapped Rhodamine B is strongly influenced by the solvent used for inducing the self-assembly. For example, the emission spectrum of **OPV1** in dodecane-chloroform (16:1) is completely shifted towards the long wavelength region indicating efficient self-assembly of the molecules. Excitation at 380 nm in the presence of Rhodamine B showed nearly 72% quenching of the OPV emission (Figure 3.14a). Figure 3.14b shows the plot of the relative fluorescence intensity of Rhodamine B and **OPV1** against their molar ratio in dodecane-chloroform and in cyclohexane-chloroform, which showed an enhanced efficiency in the former case.
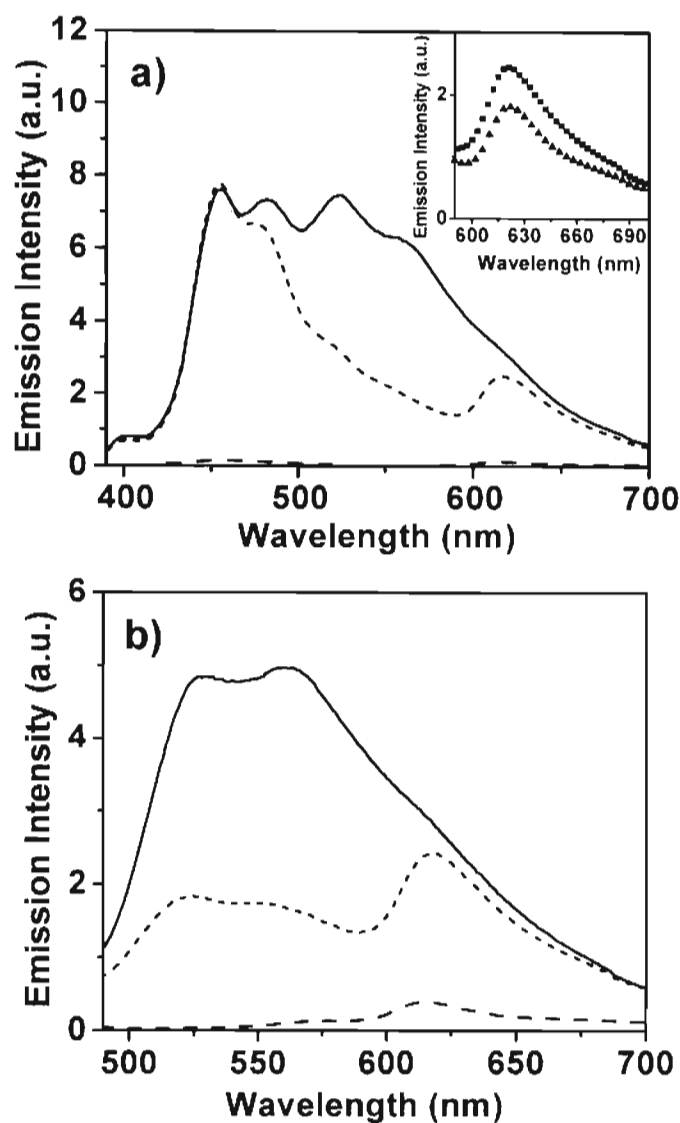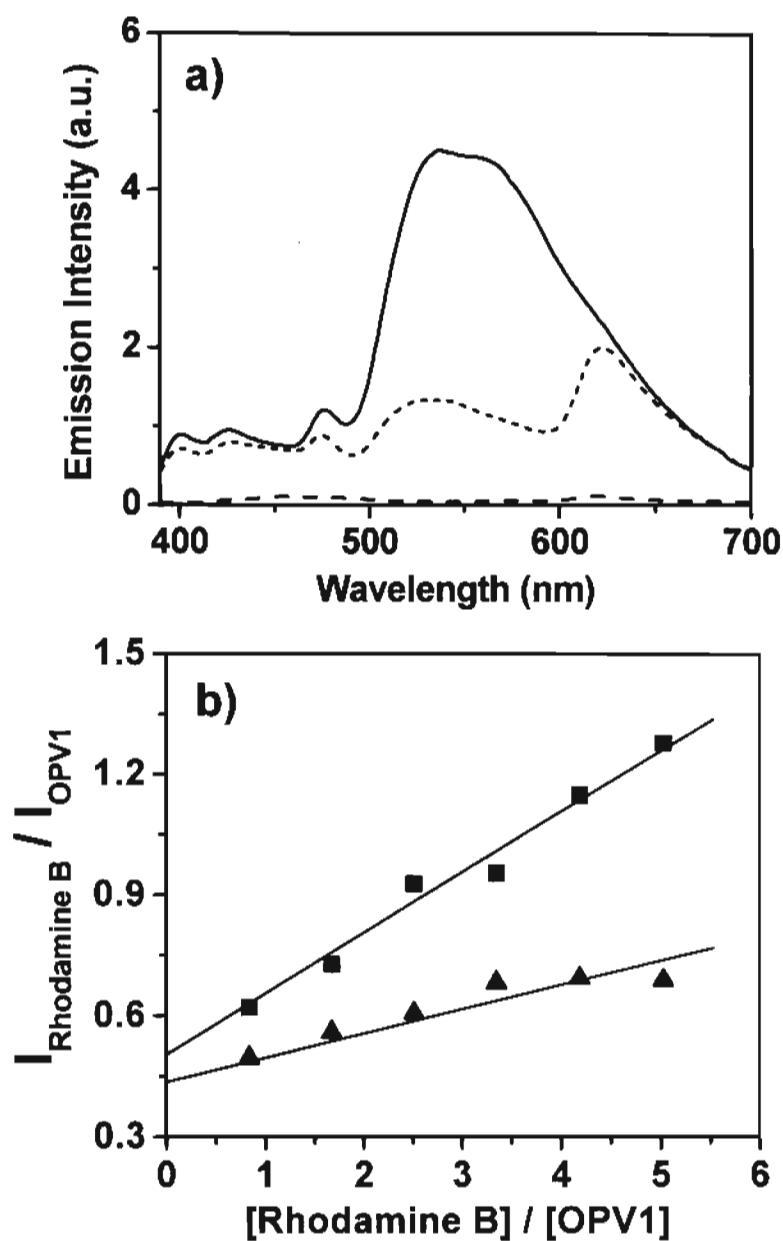
FIGURE 3.14. a) Emission spectra of **OPV1** [1.01 x 10^{-5} M] in the absence (———) and in the presence (-----) of Rhodamine B [8.38 x 10^{-5} M] in dodecane-chloroform (16:1, λ_{ex} = 380 nm). The emission of Rhodamine B in the absence of **OPV1**, on excitation at 380 nm (– – –) is shown for a comparison. b) Effect of solvents on the dependence of the relative fluorescence intensities against the molar ratio of the acceptor and the donor upon excitation at 380 nm. (■) In dodecane-chloroform (16:1) and (▲) in cyclohexane-chloroform (16:1).
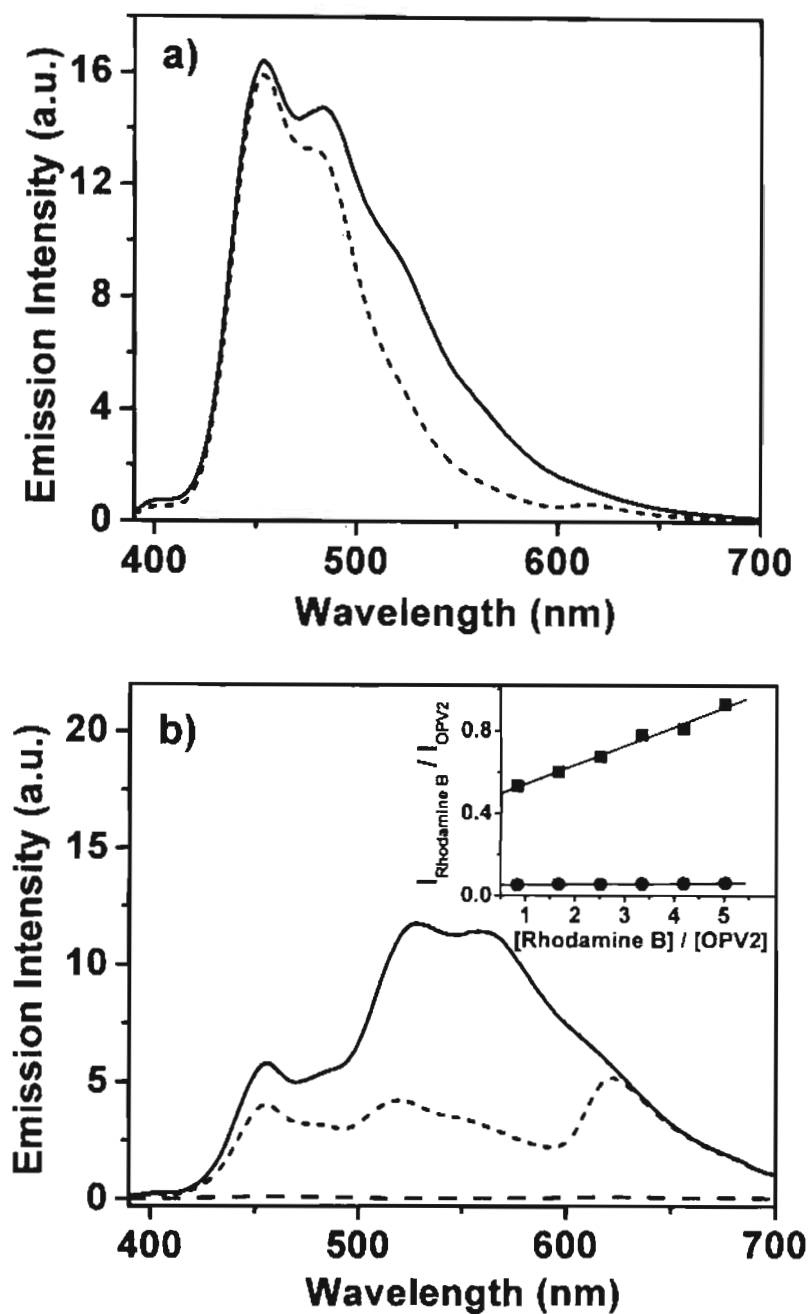
FIGURE 3.15. Emission spectra of **OPV2** [1.01 x 10⁻⁵ M] (a) in cyclohexane-chloroform (16:1) and (b) in dodecane-chloroform (16:1) in the absence (——) and in the presence (-----) of Rhodamine B [8.38 x 10⁻⁵ M]. Fluorescence of Rhodamine B (– – –) in the absence of **OPV2** on excitation at 380 nm is also shown. Inset of Figure 3.15b shows the effect of solvents on the dependence of relative fluorescence intensities of the acceptor and the donor against their molar ratio in cyclohexane: chloroform (●) and in dodecane-chloroform (■).

Excitation of **OPV2** in the presence of Rhodamine B in cyclohexane-chloroform (16:1) shows a marginal quenching of the emission indicating that FRET is not efficient (ca. 10%) due to the weak self-assembly (Figure 3.15a). However, in dodecane-chloroform, the emission of **OPV2** is significantly quenched when excited at 380 nm (Figure 3.15b). A comparison of the relative emission of the acceptor and the donor against the corresponding concentrations shows better FRET efficiency in dodecane-chloroform. Although **OPV2** showed considerable energy transfer to Rhodamine B (ca. 63%) in dodecane-chloroform (16:1), the efficiency was relatively low in cyclohexane-chloroform (16:1) when compared to that of the strongly self-assembling **OPV1** under identical conditions. These observations support the fact that the ability of the donor to form the self-assembly, which in turn is a solvent dependent process, is crucial for the efficient energy transfer process.

Results of the FRET studies of **OPV3** and **OPV4** in dodecane-chloroform (16:1) are shown in Figure 3.16 and 3.17 respectively. In this solvent, the emission of **OPV3** showed fairly good overlap with the absorption of Rhodamine B (Figure 3.16a). Detailed fluorescence quenching studies of **OPV3** (1.01 x 10^{-5} M, λ_{ex} = 410 nm) showed that in the presence of 8.38 x 10^{-5} M of Rhodamine B, the energy transfer occurs in 69% efficiency (Figure 3.16b).
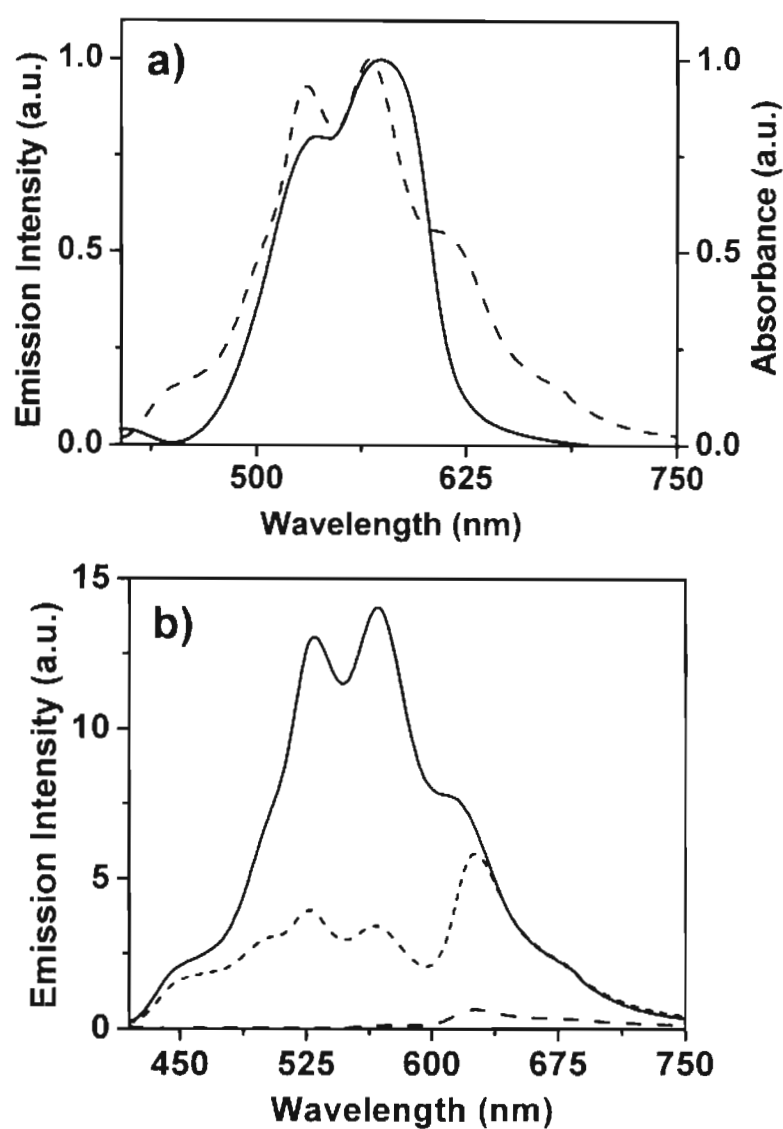
FIGURE 3.16. a) Spectral overlap between the emission spectrum of **OPV3** (– – –) and the absorption spectrum of Rhodamine B (—). b) Emission spectra of **OPV3** [1.01 x 10⁻⁵ M] in the absence (—) and in the presence of Rhodamine B [8.38 x 10⁻⁵ M] (-----). The emission of Rhodamine B alone (– – –) is shown for a comparison. All studies were conducted in dodecane-chloroform (16:1) and λ_{ex} = 410 nm.
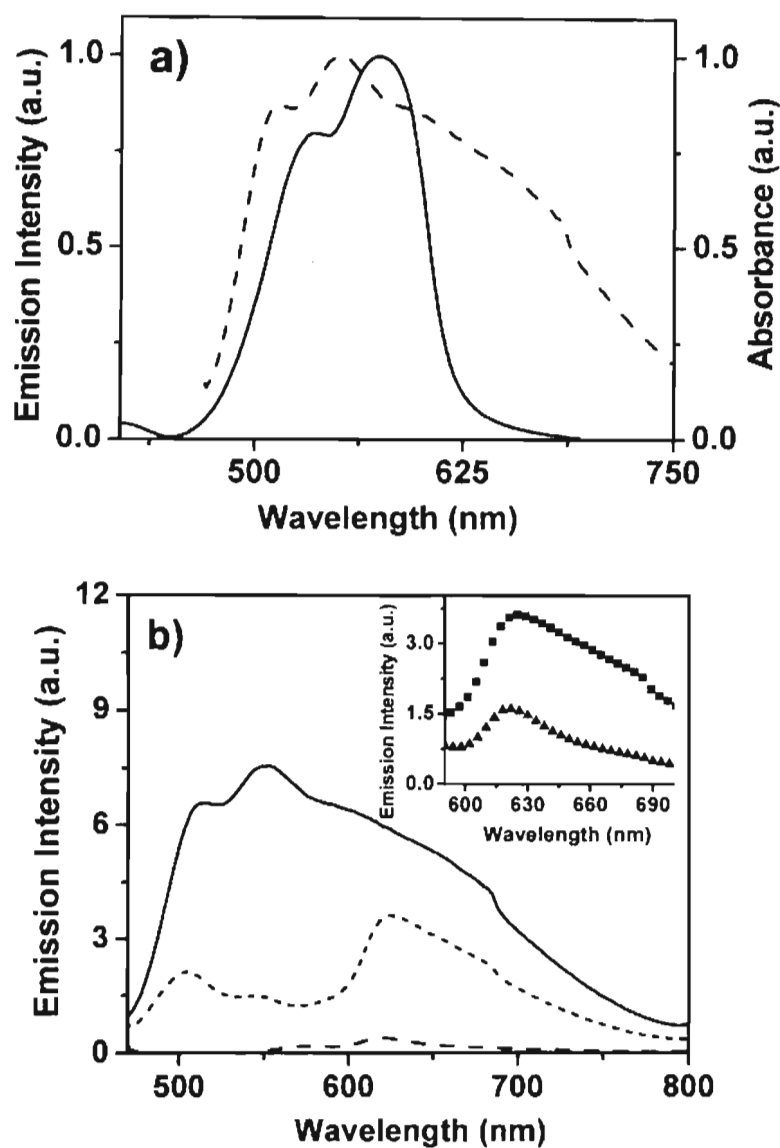
FIGURE 3.17. a) Spectral overlap between the emission spectrum of **OPV4** (– – –) and the absorption spectrum of Rhodamine B (—). b) **OPV4** emission [1.01 x 10⁻⁵ M] in the absence (—) and in the presence of Rhodamine B [4.19 x 10⁻⁵ M] (----), λ_{ex} = 460 nm. The emission of Rhodamine B alone (– – –) is shown for a comparison. Inset of the Figure 3.17b shows the emission of the dye on indirect (λ_{ex} = 460 nm) (■) and direct excitation (λ_{ex} = 535 nm) (▲). All studies were conducted in dodecane-chloroform (16:1).

Addition of Rhodamine B into **OPV4** (1.01 x 10⁻⁵ M) in dodecane-chloroform (16:1) showed nearly 81% quenching of the fluorescence of the latter

when excited at 460 nm. The concomitant formation of the Rhodamine B emission

at 625 nm gets saturated at 4.19 x 10^{-5} M concentration of the acceptor (Figure

3.17b). Excitation of Rhodamine B alone at the same wavelength did not show

significant emission. Comparison of the Rhodamine emission upon direct

excitation at 535 nm and indirect excitation at 460 nm in the presence of **OPV4**

indicates that the FRET emission is nearly three times more intense than that of

the emission from direct excitation (Figure 3.17b inset). Noticeably, in this case

four times excess of the acceptor is sufficient for the maximum quenching of the

self-assembly emission when compared to the eight times excess of the acceptor as

in the cases of **OPV1-3**.

FIGURE 3.18. Plots of relative fluorescence intensities against the molar ratio of the acceptor and the donor. **OPV1** (●), **OPV2** (■), **OPV3** (♦) and **OPV4** (▲).
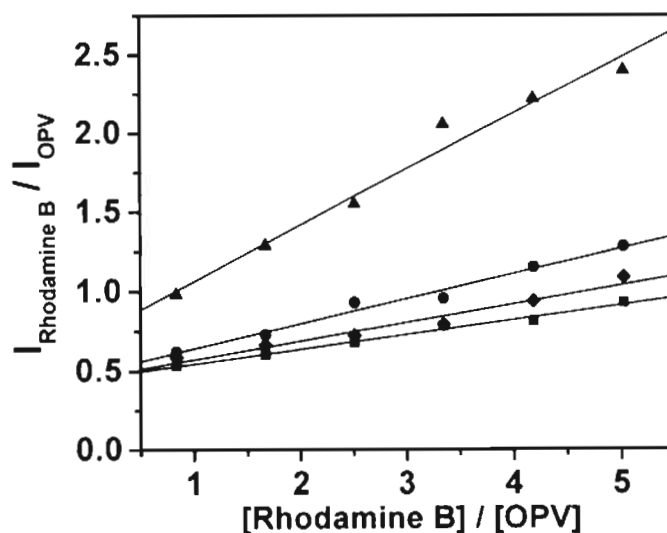
A comparison of the relative fluorescence intensities of Rhodamine B with

different OPVs against the respective molar ratios (Figure 3.18), revealed a

maximum FRET efficiency for **OPV4**. The better FRET efficiency of **OPV4** with relatively less amount of the acceptor indicates the better interaction between the donor and the acceptor when compared to the results of **OPV1-3**.
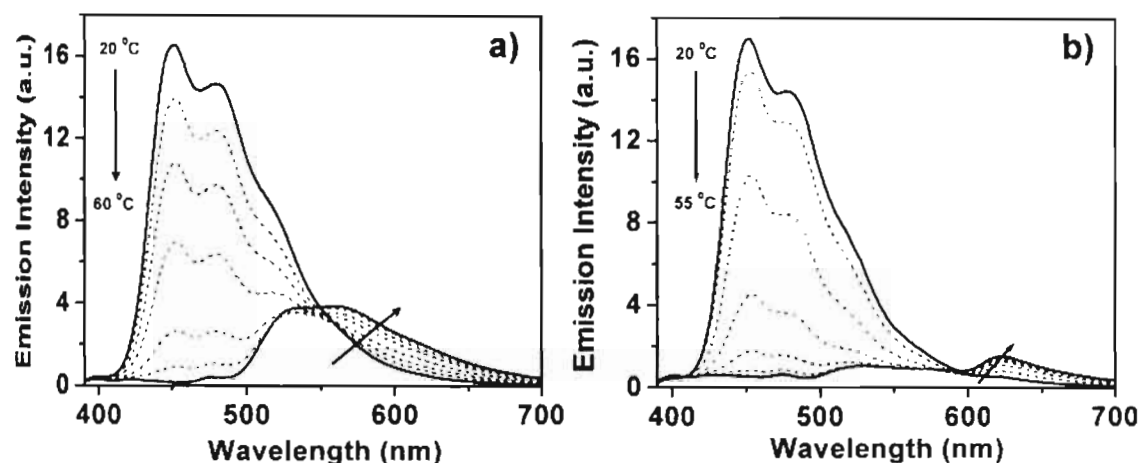
FIGURE 3.19. Temperature dependent emission spectra of **OPV1** [1.01 x 10⁻⁵ M] a) in the absence and b) in the presence of Rhodamine B [8.38 x 10⁻⁵ M] in dodecane-chloroform (16:1). The weak emission of the self-assembly around 500-600 nm in Figure 3.19b indicates the thermally gated energy transfer to Rhodamine B. Emission spectra at 25 °C and 60 °C is highlighted with black solid line.

A unique feature of the present system is the thermal control on the FRET process. This is clear from the temperature dependent emission changes of **OPV1** in the absence and in the presence of Rhodamine B (Figure 3.19). When cooled from 60-20 °C in dodecane-chloroform (16:1), the intensity of the emission maximum of **OPV1** at 452 nm is decreased and shifted to the region of 530-570 nm due to the self-assembly of the molecules (Figure 3.19a). However, while cooling from 60-20 °C in the presence of Rhodamine B, the emission maximum of **OPV1** is directly gated toward 625 nm, bypassing the emission of the self-

assembled species at 530-570 nm (Figure 3.19b). Since the energy transfer between the donor and the acceptor is usually independent of temperature, the observed thermal gating of FRET emission is the result of the thermoreversible breaking and making of the self-assembly which in turn thermally modulate the spectral features of the donor self-assembly.

One of the major limitations of the present system is the noncompatibility of the cationic acceptor with the OPV self-assembly in nonpolar solvents. Therefore, the major portion of the acceptor gets aggregated in the gel medium. These aggregates may not be in contact with the self-assembled donors. Moreover, the emission of the aggregated acceptor is very weak when compared to that of the monomer. Therefore, the intensity of the acceptor emission as a result of FRET in dodecane or cyclohexane is weak. However, this problem could be solved partially by performing the FRET experiments in xerogel films. In the xerogel film, the **OPV1** emission is completely shifted to the long wavelength region around 530 and 560 nm, corresponding to the self-assembled species (Figure 3.20a). Upon excitation of a Rhodamine B dispersed xerogel film of **OPV1** (1:2 molar ratio, 33 mol% of the acceptor) at 380 nm, the emission at 530-560 nm is almost completely quenched and the emission of the dye at 625 nm could be observed (Figure 3.20a). In this case, the intensity of the acceptor emission at 625 nm is enhanced nearly 6-fold when compared to that on direct excitation at 535 nm even though the dye concentration is only 33 mol% (Figure 3.20b). The insets of Figure

3.21a show the emission colors of the self-assembled **OPV1** film in the absence (greenish yellow) and in the presence of Rhodamine B (red).

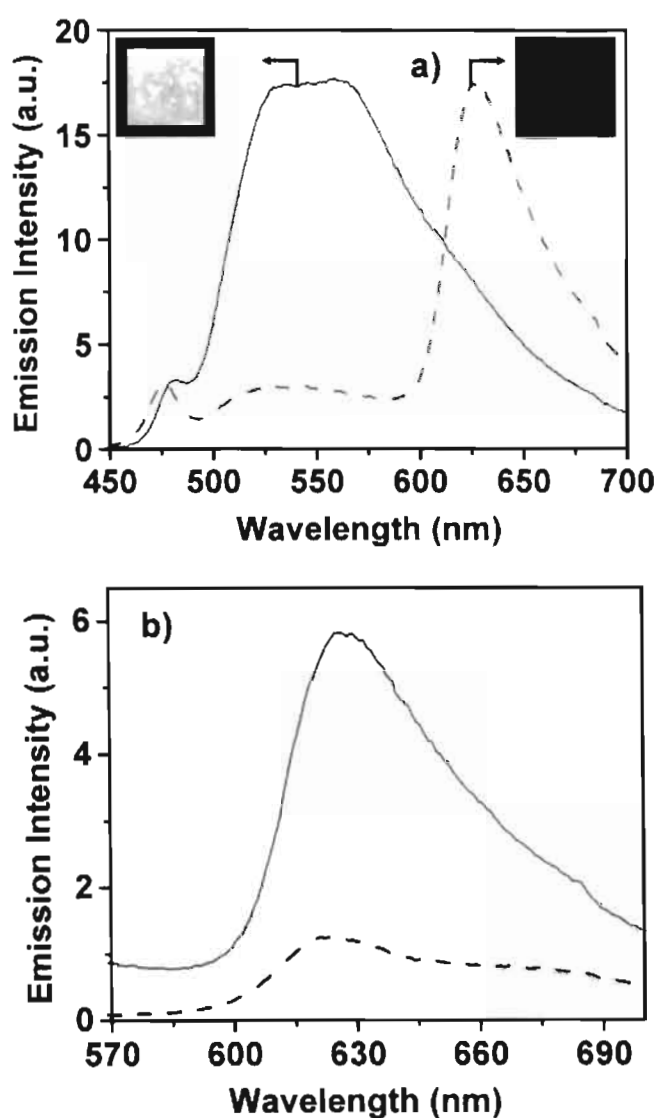**FIGURE 3.20.** a) Emission from the xerogel film of **OPV1** in the absence ( ) and in the presence of Rhodamine B (– – –) (33 mol%) upon excitation at 380 nm. Emission colors of **OPV1** and **OPV1**+Rhodamine B films under UV light (365 nm) are shown in the inset of Figure 3.20a. b) Comparison of the emission of Rhodamine B (——) at indirect excitation (380 nm) and direct excitation at 535 nm (– – –).

3.3.4. Morphological Studies

Scanning electron microscope (SEM) analysis of the **OPV1** gel revealed the formation of entangled tape-like structures (Figure 3.21a). When Rhodamine B is loaded in small amounts in the gel state of **OPV1** in cyclohexane-chloroform phase separated aggregates of the former could be seen (Figure 3.21b). A drop cast film in the presence of excess amount of Rhodamine B from cyclohexane-chloroform reveals that the acceptor is uniformly aggregated around the supramolecular tapes (Figure 3.22c).
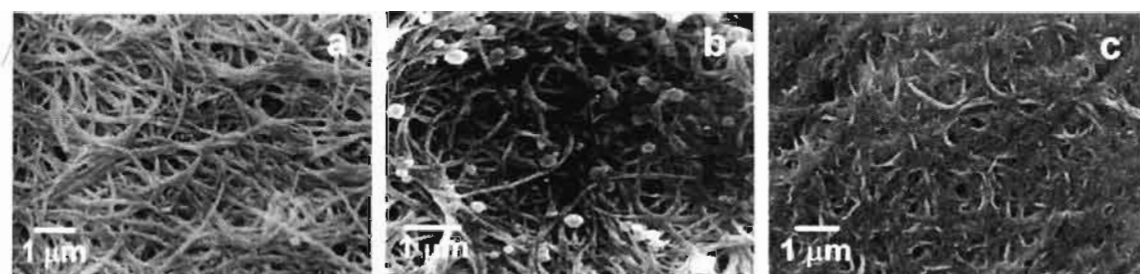
FIGURE 3.21. SEM pictures of **OPV1**. a) Gel in cyclohexane, b) gel in the presence of Rhodamine B and c) a drop cast film in the presence of Rhodamine B.

The atomic force microscope (AFM) analysis of **OPV1** indicates the formation of supramolecular tapes of 5-15 nm thickness with 36-176 (± 10) nm width and several micrometers in length (Figure 3.22a). Addition of Rhodamine B indicates the localization of the latter around the tapes (Figure 3.22b). In addition, the phase separated aggregates of the dye is also seen in the AFM picture (Figure 3.22c). Interestingly, **OPV4** showed the formation of interconnected short linear

tapes of 1-2 µm in length, 54-84 (± 1) nm in width and 3 ± 0.5 nm in height (Figure 3.22d). These structures are considerably different from those of the entangled nanotapes of **OPV1**. The AFM pictures indicate that in the presence of Rhodamine dye, individual fibers of **OPV4** are agglomerated along the edge as seen in Figure 3.23e. Interestingly, the AFM height profiles reveal that the thickness and the width of the individual tapes do not vary considerably before and after the addition of the dye. This means that the presence of the dye does not disturb the original morphology of the OPVs, rather the aggregated dye tend to localize on the polar edges of the tapes.

Based on the morphological analysis, the plausible arrangement of the Rhodamine dye entrapped OPV self-assembly is shown in Figure 3.23. The two edges along the axis of the self-assembled OPV tapes are polar due to free carboxylic acid or hydroxyl groups on which the Rhodamine dye is localized. This is clear from the AFM pictures which reveal that most of the dye molecules are aggregated between tapes when the solvent is dried off before the image analysis. The energy transfer occurs preferably to the dye aggregates which are in contact with the self-assembled tapes. This could be the reason that excess amount of the dye is needed for the efficient quenching of the self-assembled OPV emission in cyclohexane and dodecane gel. However, in the case of the dye doped xerogel film, the dye molecules are in close contact with the OPV nanotapes, which could be within the Förster radii. This could be the reason for the enhanced efficiency of
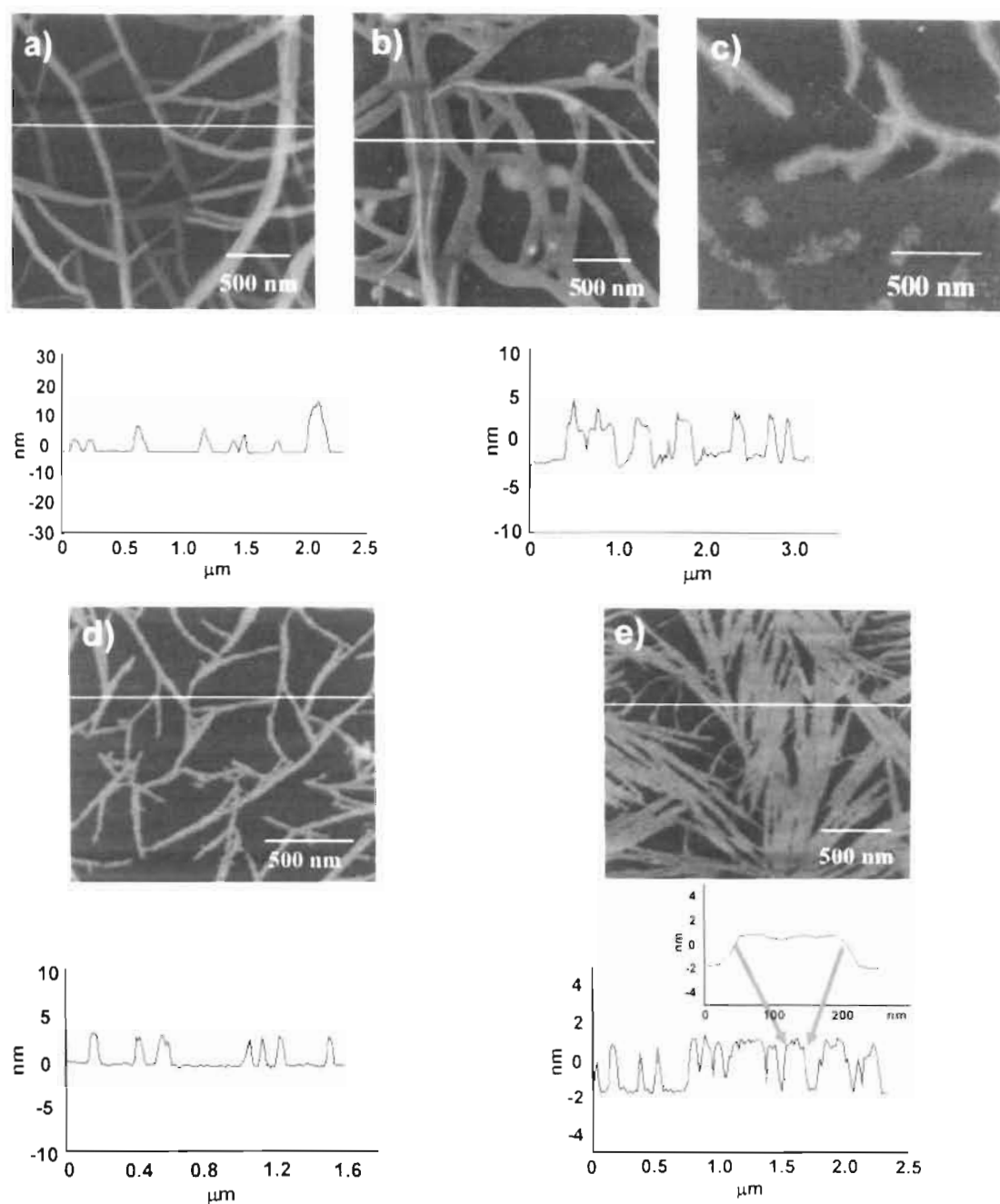
FIGURE 3.22. Taping mode AFM height images and the corresponding section analysis of (a) **OPV1**, (b and c) **OPV1**+Rhodamine B, (d) **OPV4** and (e) **OPV4** + Rhodamine B. The section analysis of a, b, d, e are also shown. In all experiments [OPV] = 5 x 10^{-5} M and [Rhodamine B] = 2 x 10^{-4} M in dodecane-chloroform (16:1).

FRET in the case of the self-assembled film even at low dye concentrations when compared to that in the organogel state.
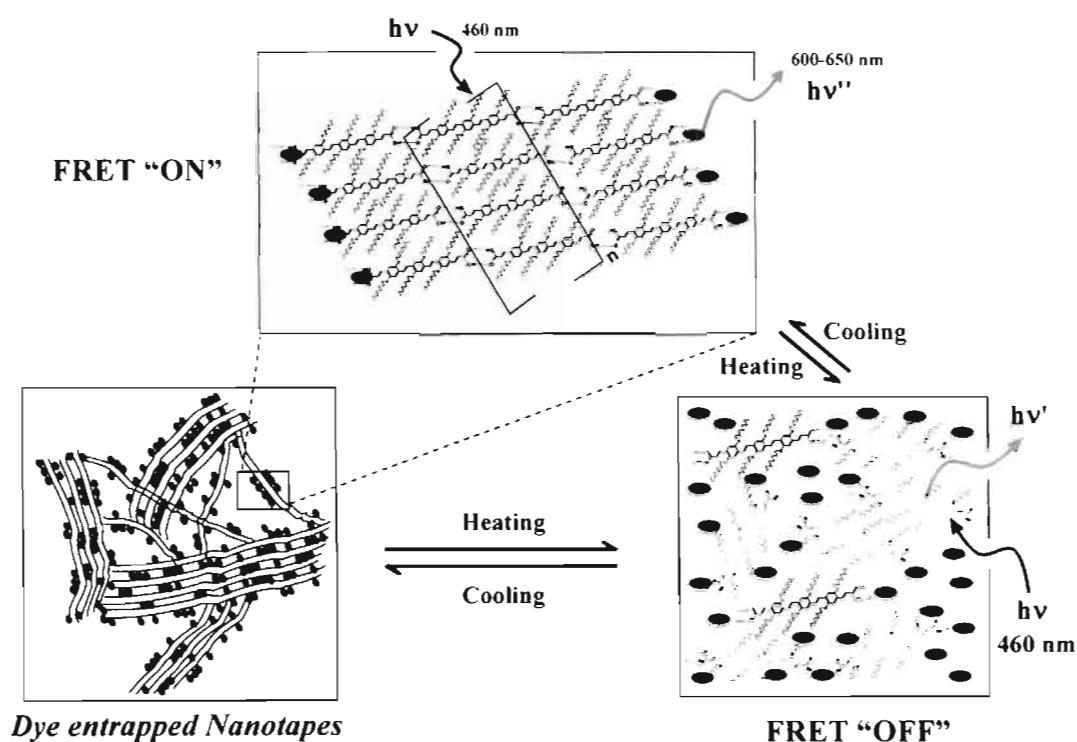
FIGURE 3.23. A cartoon representation of the self-assembly induced FRET from **OPV4** to Rhodamine B.

3.4. Conclusions

We have demonstrated the use of self-assembled OPV nanotapes as donor scaffolds to achieve FRET to entrapped Rhodamine B. The FRET efficiency depends upon the ability of the OPVs to form self-assemblies which is strongly influenced by the end functional groups as well as the solvent. The edges of the H-bonded nanotapes are polar due to the presence of free $-CO_2H$ or $-OH$ groups

where the acceptor molecules are preferably localized. FRET occurs exclusively from the self-assembled OPVs to the physically attached acceptors and not from the individual donor molecules. More importantly, since FRET occurs exclusively from the self-assembled molecules, it could be thermally controlled by the reversible self-assembly process. FRET is found to be more efficient in a xerogel film when compared to that of the self-assembly in dodecane or cyclohexane gel.

3.5. Experimental Section

3.5.1. Synthesis and Characterization

The details of the melting point, FT-IR, ^{1}H NMR and ^{13}C NMR and MALD-TOF instruments are described in the experimental section (section 2.5.1) of Chapter 2.

Preparation of OPV2.[19c] The bisalcohol **OPV1** (0.1 mmol) was dissolved in dry THF (25 mL). To this solution NaH (0.3 mmol) in dry THF (10 mL) was added in portions followed by the addition of methyl iodide (0.3 mmol) while cooling. The reaction mixture was stirred for 12 h and poured into water and then extracted with dichloromethane. Concentration of the organic layer followed by column chromatography (hexane/chloroform, 3:1) over silica gel (100-200 mesh) gave the pure product **OPV2** as a yellow solid.

OPV2
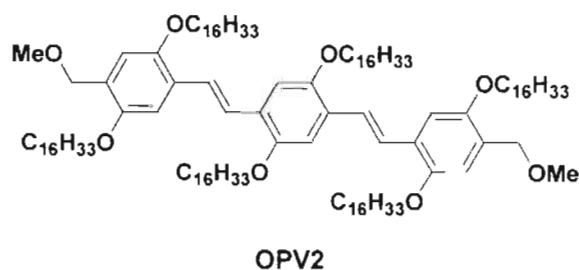
Yield: 95%; mp: 99-100 °C; FT-IR (KBr) v_{max}: 846, 955, 1011, 1068, 1094, 1125, 1202, 1248, 1336, 1382, 1418, 1465, 1511, 2850, 2923 cm^{-1}; ^{1}H NMR (300 MHz, CDCl$_3$) δ: 0.85-0.89 (m, 18H, –CH$_3$), 1.25-1.85 (m, 168H, –CH$_2$), 3.45 (s, 6H, –OCH$_3$), 3.97-4.05 (m, 12H, –OCH$_2$), 4.51 (s, 4H, –CH$_2$OCH$_3$), 6.96 (s, 2H, phenyl-H), 7.11 (s, 2H, phenyl-H), 7.14 (s, 2H, phenyl-H), 7.39-7.45 (m, 4H, vinyl-H) ppm; ^{13}C NMR (75 MHz, CDCl$_3$) δ: 14.04, 22.68, 26.20, 26.62, 28.70, 28.95, 29.34, 29.71, 29.69, 31.91, 58.4, 68.32, 69.27, 69.52, 109.46, 110.68, 113.63, 123.29, 126.92, 127.28, 127.42, 150.70, 151.05 ppm; MALDI-TOF MS (MW = 1813.03): m/z = 1813.55 $[M]^+$.

Preparation of OPV4. KOH (5 N) in methanol (40 mL) was added to a solution of **OPV3** (0.75 mmol) in THF (50 mL). The reaction mixture was refluxed at 70 °C for 4 h. The solvent was then evaporated, and the residue was suspended in THF (50 mL). Trifluoroacetic acid was added to adjust the pH around 2. The solvent was then evaporated and the solid residue was washed with cold water until the washings stayed neutral. Finally, the solid was washed with cold (ice bath) THF and dried in a vacuum oven to get **OPV4** as a red solid.
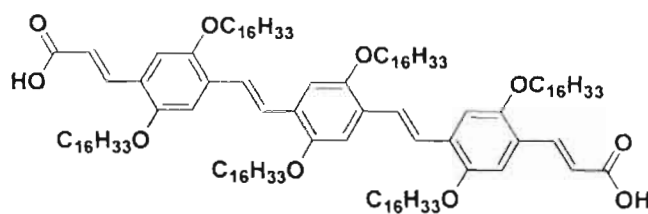
OPV4

Yield: 93%; mp: 203-205 °C; FT-IR (KBr) v_{max}: 725, 855, 1046, 1206, 1258, 1429, 1470, 1506, 1594, 1625, 1687, 2856, 2924, 3441 cm^{-1}; ^{1}H NMR (300 MHz, CDCl$_3$) δ: 0.80-0.83 (m, 18H, $-CH_3$), 1.17-1.79 (m, 168H, $-CH_2-$), 3.96-4.08 (m, 12H, $-OCH_2-$), 6.46 (d, J = 15.07 Hz, 2H, vinyl-H), 6.96 (s, 2H, phenyl-H), 7.08 (s, 4H, phenyl-H), 7.39 (d, J = 16.01 Hz, 2H, vinyl-H), 7.46 (d, J = 16.11 Hz, 2H, vinyl-H), 8.00 (d, J = 15.09 Hz, 2H, vinyl-H) ppm; ^{13}C NMR (75 MHz, d_8-THF) δ: 13.6, 22.71, 26.31, 28.41, 28.95, 29.21, 29.42, 29.53, 29.59, 29.67, 29.92, 31.42, 70.20, 111.09, 112.60, 113.31, 119.86, 122.19, 125.92, 128.32, 140.01, 151.07, 152.11, 153.19, 167.49 ppm; MALDI-TOF MS (MW$^-$ 1865.02): m/z = 1865.31 $[M]^+$.

3.5.2. Description of Experimental Techniques

Optical Measurements. The details of UV/Vis absorption spectrophotometer and spectrofluorimeter are described in the section 2.5.2 of Chapter 2. Fluorescence spectra of optically dilute solutions were recorded from 390-800 nm at the excitation wavelengths of 380, 410, 460 and 470 nm. Fluorescence spectra of the xerogel films were recorded using the front face geometry.

Quantum Yield Measurements. Fluorescence quantum yields of molecularly dissolved OPV molecules upon excitation at 380 nm are reported relative to quinine sulfate ($\Phi_f = 0.546$), whereas the quantum yields of the self-assembled molecules are reported relative to Rhodamine 6G ($\Phi_f = 0.9$). The experiments were done using optically matching solutions and the quantum yield is calculated using equation 3.1.[25]

$$\Phi_f = \Phi_r (A_r F_s / A_s F_r)(\eta_s^2 / \eta_r^2) \qquad \text{- - - - } (3.1)$$

where, A_s and A_r are the absorbance of the sample and reference solutions, respectively at the same excitation wavelength, F_s and F_r are the corresponding relative integrated fluorescence intensities and η is the refractive index of the solvent.

General Procedure for Energy Transfer Studies. Energy transfer experiments were carried out in cyclohexane-chloroform or dodecane-chloroform solvent mixtures (16:1). Samples for the FRET studies were prepared by adding appropriate concentration of the dye in 0.2 mL chloroform to 3 mL cyclohexane or dodecane solution of the OPVs. Energy transfer studies in the film form was performed by drop casting a film of the appropriate OPV containing 10-33 mol% of Rhodamine B from cyclohexane-chloroform. The film was dried in a vacuum oven before recording the emission spectra. The efficiency of energy transfer was

estimated from the donor fluorescence quenching profiles by using the equation 3.2.[25]

$$\text{Efficiency of energy transfer} = 1 - \left(\frac{I_{DA}}{I_D} \right) \quad \text{- - - - (3.2)}$$

where I_D and I_{DA} are emission intensities of the donor in the absence and presence of the acceptor, respectively.

Scanning Electron Microscopy (SEM) Studies. Gel samples for the SEM analysis were prepared by dissolving the required amount of OPV in cyclohexane. Into this known quantities of Rhodamine B in chloroform is injected and the solution was heated and cooled to room temperature. Sheared gels were placed on sample studs and coated with gold by ion sputtering. SEM pictures were obtained either on a JEOL 5600 LV scanning electron microscope with an accelerating voltage of 10 kV.

Atomic Force Microscopy (AFM) Studies. The details of AFM instrument is described in the section 2.5.2 of Chapter 2. Samples for the AFM imaging were prepared by drop casting the dodecane-chloroform (16:1) solution at the required compositions of donor and acceptor on freshly cleaved mica. Blank experiments with neat solvents on mica sheet were carried out to eliminate the possibility of any artifacts, prior to the measurements of the samples. AFM height and phase image analyses of three different samples of each OPV solutions at different

scanning areas were carried out. The actual size of the self-assemblies were estimated by subtracting the tip broadening factor from the measured size.[26] The radius of the tips (Veeco probes, MPP-11100-10) is taken as 12.5 nm. For **OPV1**, the measured height of the tapes is 5-15 nm and the calculated tip broadening is 24 ± 10 nm. Therefore the actual width of the tapes is estimated by subtracting the broadening factor from the measured width (60-200 nm) which is 36-176 ± 10 nm. Similarly, for **OPV3** the apparent height of the tapes is 3 ± 0.5 nm and the calculated tip broadening is 16 ± 1 nm, hence the actual width is 54-84 (± 1) nm.

3.6. References

1. For recent reviews on supramolecular organization of chromophores, see: (a) F. J. M. Hoeben, P. Jonkheijm, E. W. Meijer, A. P. H. J. Schenning, *Chem. Rev.* **2005**, *105*, 1491. (b) *Supramolecular Dye Chemistry* (Ed. F. Würthner), Topics in Current Chemistry, Springer Berlin: New York, *258*, **2005**.

2. (a) W. Kühlbrandt, D. N. Wang, *Nature* **1991**, *350*, 130. (b) W. Kühlbrandt, *Nature* **1995**, *374*, 497. (c) G. McDermott, S. M. Prince, A. A. Freer, A. M. Hawthornthwaite-Lawless, M. Z. Papiz, R. J. Cogdell, N.W. Isaacs, *Nature* **1995**, *374*, 517. (d) X. Hu, A. Damjanović, T. Ritz, K. Schulten, *Proc. Natl. Acad. Sci. U. S. A.* **1998**, *95*, 5935. (e) *Energy Harvesting Materials* (Ed.: D. L. Andrews), World Scientific: Singapore, **2005**.

3. For reviews, see: (a) R. L. Carroll, C. B. Gorman, *Angew. Chem., Int. Ed.* **2002**, *41*, 4378. (b) S. R. Forrest, *Nature* **2004**, *428*, 911. (c) A. C. Grimsdale, K. Müllen, *Angew. Chem., Int. Ed.* **2005**, *44*, 5592.

4. (a) E. W. Meijer, A. P. H. J. Schenning, *Nature* **2002**, *419*, 353. (b) M. Van Der Auweraer, F. C. De Schryver, *Nat. Mater.* **2004**, *3*, 507. (c) Ph. Leclère, M. Surin, P. Jonkheijm, O. Henze, A. P. H. J. Schenning, F. Biscarini, A. C. Grimsdale, W. J. Feast, E. W. Meijer, K. Müllen, J. L. Brédas, R. Lazzaroni, *Eur. Polym. J.* **2004**, *40*, 885. (d) A. P. H. J. Schenning, E. W. Meijer, *Chem. Commun.* **2005**, 3245.

5. A. Ajayaghosh, S. J. George, A. P. H. J. Schenning, *Top. Curr. Chem.* **2005**, *258*, 83 and references therein.

6. For reviews on H-bonded assemblies based energy transfer systems, see: (a) M. D. Ward, *Chem. Soc. Rev.* **1997**, *26*, 365. (b) L. S. Sánchez, N. Martín, D. M. Guldi, *Angew. Chem., Int. Ed.* **2005**, *44*, 5374.

7. (a) S. Encinas, N. R. M. Simpson, P. Andrews, M. D. Ward, C. M. White, N. Armaroli, F. Barigelletti, A. Houlton, *New J. Chem.* **2000**, *24*, 987. (b) S. Rau, B. Schäfer, S. Schebesta, A. Grüßing, W. Poppitz, D. Walther, M. Duati, W. R. Browne, J. G. Vos, *Eur. J. Inorg. Chem.* **2003**, 1503. (c) J. Otsuki, K. Iwasaki, Y. Nakano, M. Itou, Y. Araki, O. Ito, *Chem. –Eur. J.* **2004**, *10*, 3461.

8. For reviews of low molecular weight organogels, see: (a) P. Terech, R. G. Weiss, *Chem. Rev.* **1997**, *97*, 3133. (b) N. M. Sangeetha, U. Maitra, *Chem. Soc. Rev.* **2005**, *34*, 821. (c) *Molecular Gels, Materials with Self-Assembled Fibrillar Networks* (Eds.: R. G. Weiss, P. Terech), Kluwer Press: Dordrecht, **2005**.

9. For light harvesting organogels, see: (a) T. Sagawa, S. Fukugawa, T. Yamada, H. Ihara, *Langmuir* **2002**, *18*, 7223. (b) T. Nakashima, N.

Kimizuka, *Adv. Mater.* **2002**, *14*, 1113. (c) K. Sugiyasu, N. Fujita, M. Takeuchi, S. Yamada, S. Shinkai, *Org. Biomol. Chem.* **2003**, *1*, 895. (d) J. B. Beck, S. J. Rowan, *J. Am. Chem. Soc.* **2003**, *125*, 13922. (e) K. Sugiyasu, N. Fujita, S. Shinkai, *Angew. Chem., Int. Ed.* **2004**, *43*, 1229. (f) S. Yamaguchi, I. Yoshimura, T. Kohira, S.-i. Tamaru, I. Hamachi, *J. Am. Chem. Soc.* **2005**, *127*, 11835. (g) J.-H. Ryu, M. Lee, *J. Am. Chem. Soc.* **2005**, *127*, 14170. (h) A. Del Guerzo, A. G. L. Olive, J. Reichwagen, H. Hopf, J.-P. Desvergne, *J. Am. Chem. Soc.* **2005**, *127*, 17984. (i) M. Montalti, L. S. Dolci, L. Prodi, N. Zaccheroni, M. C. A. Stuart, K. J. C. Van Bommel, A. Friggeri, *Langmuir* **2006**, *22*, 2299.

10. (a) M. Stork, B. S. Gaylord, A. J. Heeger, G. C. Bazan, *Adv. Mater.* **2002**, *14*, 361. (b) B. S. Gaylord, A. J. Heeger, G. C. Bazan, *J. Am. Chem. Soc.* **2003**, *125*, 896. (c) B. Liu, B. S. Gaylord, S. Wang, G. C. Bazan, *J. Am. Chem. Soc.* **2003**, *125*, 6705. (d) S. Wang, B. S. Gaylord, G. C. Bazan, *J. Am. Chem. Soc.* **2004**, *126*, 5446. (e) B. Liu, G. C. Bazan, *J. Am. Chem. Soc.* **2006**, *128*, 1188.

11. (a) D. T. McQuade, A. H. Hegedus, T. M. Swager, *J. Am. Chem. Soc.* **2000**, *122*, 12389. (b) J. Zheng, T. M. Swager, *Chem. Commun.* **2004**, 2798. (c) K. Kuroda, T. M. Swager, *Macromolecules* **2004**, *37*, 716.

12. (a) C. Tan, E. Atas, J. G. Müller, M. R. Pinto, V. D. Kleiman, K. S. Schanze, *J. Am. Chem. Soc.* **2004**, *126*, 13685. (b) J. G. Müller, E. Atas, C. Tan, K. S. Schanze, V. D. Kleiman, *J. Am. Chem. Soc.* **2006**, *128*, 4007.

13. (a) N. Armaroli in *Fullerenes: From Synthesis to Optoelectronic Properties* (Eds.: D. M. Guldi, N. Martin), Kluwer Academic Publishers: Dordrecht,

2002, pp. 137. (b) N. Armaroli, G. Accorsi, Y. Rio, J.-F. Nierengarten, J.-F. Eckert, M. J. Gómez-Escalonilla, F. Langa, *Synth. Met.* **2004**, *147*, 19 and references therein. (c) M. Gutierrez-Nava, G. Accorsi, P. Masson, N. Armaroli, J.-F. Nierengarten, *Chem. –Eur. J.* **2004**, *10*, 5076. (d) F. Langa, M. J. Gómez-Escalonilla, J.-M. Rueff, T. M. F. Duarte, J.-F. Nierengarten, V. Palermo, P. Samori, Y. Rio, G. Accorsi, N. Armaroli, *Chem. –Eur. J.* **2005**, *11*, 4405. (e) N. Armaroli, G. Accorsi, J. N. Clifford, J.-F. Eckert, J.-F. Nierengarten, *Chem. –Asian. J.* **2006**, *1*, 564.

14. (a) Y.-J. Cheng, T.-Y. Hwu, J.-H. Hsu, T.-Y. Luh, *Chem. Commun.* **2002**, 1978. (b) Y.-J. Cheng, T.-Y. Luh, *Chem. –Eur. J.* **2004**, *10*, 5361. (c) C.-H. Chen, K.-Y. Liu, S. Sudhakar, T.-S. Lim, W. Fann, C.-P. Hsu, T.-Y. Luh, *J. Phys. Chem. B* **2005**, *109*, 17887.

15. (a) D. Oelkrug, A. Tompert, J. Gierschner, H.-J. Egelhaaf, M. Hanack, M. Hohloch, E. Steinhuber, *J. Phys. Chem. B* **1998**, *102*, 1902. (b) K. Tajima, L.-s. Li, S. I. Stupp, *J. Am. Chem. Soc.* **2006**, *128*, 5488.

16. (a) D. M. Guldi, A. Swartz, C. Luo, R. Gómez, J. L. Segura, N. Martín, *J. Am. Chem. Soc.* **2002**, *124*, 10875. (b) F. Giacalone, J. L. Segura, N. Martín, J. Ramey, D. M. Guldi, *Chem. –Eur. J.* **2005**, *11*, 4819.

17. For OPV H-bonded energy transfer systems, see refereces 22 to 27 in Chapter 1.

18. A. P. H. J. Schenning, E. Peeters, E. W. Meijer, *J. Am. Chem. Soc.* **2000**, *122*, 4489.

19. (a) A. Ajayaghosh, S. J. George, *J. Am. Chem. Soc.* **2001**, *123*, 5148. (b) R. Varghese, S. J. George, A. Ajayaghosh, *Chem. Commun.* **2005**, 593. (c) S. J. George, A. Ajayaghosh, *Chem. –Eur. J.* **2005**, *11*, 3217.

20. (a) S. J. George, A. Ajayaghosh, P. Jonkheijm, A. P. H. J. Schenning, E. W. Meijer, *Angew. Chem., Int. Ed.* **2004**, *43*, 3422. (b) A. Ajayaghosh, R. Varghese, S. J. George, C. Vijayakumar, *Angew. Chem., Int. Ed.* **2006**, *45*, 1141.

21. A. Ajayaghosh, S. J. George, V. K. Praveen, *Angew. Chem., Int. Ed.* **2003**, *42*, 332.

22. For a review on encapsulation of organic dyes, see: E. Arunkumar, C. C. Forbes, B. D. Smith, *Eur. J. Org. Chem.* **2005**, 4051.

23. (a) P. Jonkheijm, F. J. M. Hoeben, R. Kleppinger, J. van Herrikhuyzen, A. P. H. J. Schenning, E. W. Meijer, *J. Am. Chem. Soc.* **2003**, *125*, 15941. (b) F. J. M. Hoeben, A. P. H. J. Schenning, E. W. Meijer, *ChemPhysChem* **2005**, *6*, 2337.

24. L. A. J. Chrisstoffels, A. Adronov, J. M. J. Fréchet, *Angew. Chem., Int. Ed.* **2000**, *39*, 2163.

25. J. R. Lakowicz, *Principles of Fluorescence Spectroscopy* (2nd ed.), Kluwer Academic/Plenum Publishers: New York **1999**.

26. P. Samori, V. Francke, T. Mangel, K. Müllen, J. P. Rabe, *Opt. Mater.* **1998**, *9*, 390.

Chapter 4

Molecular Wire Encapsulated π-Organogels: A New Design of Efficient Supramolecular Light Harvesting Antenna
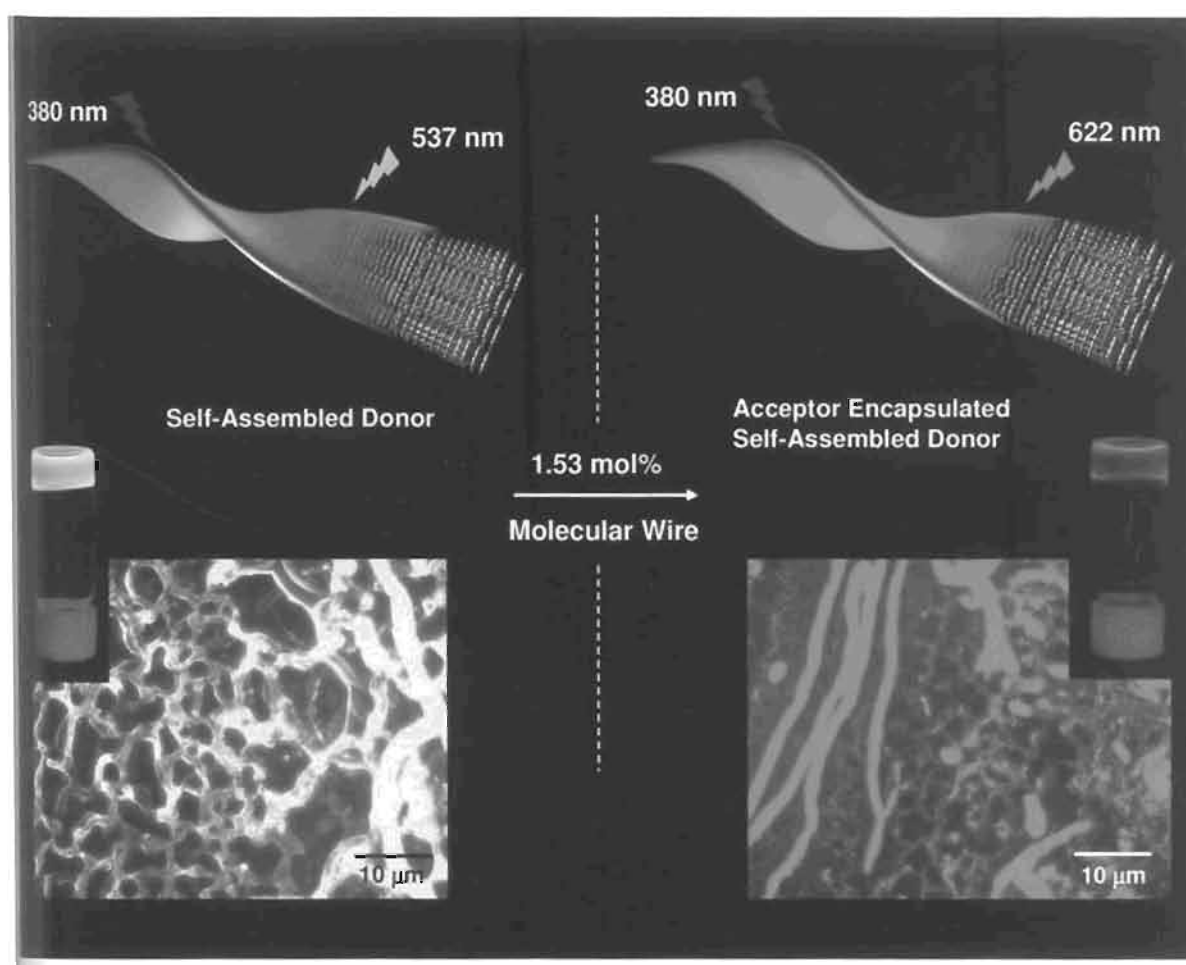
4.1. Abstract

*An efficient supramolecular light harvesting antenna is developed by encapsulating a semiconducting molecular wire within the self-assembled donor scaffold of a π-organogel. In this design a gel forming oligo(p-phenylenevinylene) derivative **OPV1** is used as the energy transfer donor and a copolymer of phenylenevinylene and pyrrolylenevinylene (**PYPV**, average molecular weight (M_n) of ~ 4358 g/mol, polydispersity index = 1.12) as the acceptor. Steady state and time resolved emission studies showed that at very low concentration (< 1.6 mol%), the molecular wire functions as an excellent excitation energy trap (k_{ET} = 2.99 x 10^9 s^{-1}) when self-aligned within the donor self-assembly in the gel state. Detailed time resolved studies provided evidence for fast energy migration along the donor scaffold (k_{EM} = 1.28 x 10^{10} s^{-1}) which facilitates the funneling of the excitation energy from a long distance of the donor scaffold to a few encapsulated molecular wires. Temperature controlled breaking of the gel self-assembly leads to variation in energy transfer efficiency and change in the emission color. Energy transfer is efficient from the donor (OPV) self-assembly to the molecular wires in the gel state. A quantitative evaluation of the energy migration and energy transfer processes is presented.*

4.2. Introduction

Excitation energy transfer from donors to acceptors separated by a distance 'R' occurs through Dexter, Förster or trivial radiative transfer mechanisms.[1] Dexter transfer is a wave-function overlap that has exponential distance dependence within ~ 1 nm range whereas Förster transfer is a near-field resonant dipole-dipole interaction with a distance dependence of 'R^{-6}' and cover a greater range of ~10 nm. In contrast, the radiative energy transfer process is a simple reabsorption of the emitted photon by a suitable fluorophore and covers the longest range. However, the probability of radiative transfer is usually low and the directionality cannot be controlled. For efficient energy transfer from donors to acceptors at distances of > 10 nm, fast energy migration is required, especially in the presence of very low concentrations of the acceptor molecules.[2-7] Such systems are examples of light harvesting antennae.

Design of systems capable of directional energy transfer between several chromophore units is a subject of much attention. Use of chromophore functionalized polymers,[8] dendrimers,[9] and encapsulation of organic dyes in Zeolite L crystals[10] are shown to be effective for this purpose. Recently a new strategy based on orientation of a semiconducting polymer, poly[2-methoxy-5-(2'-ethylhexyloxy)-1,4-phenylene vinylene] (1, MEH-PPV) in mesoporous silica has been introduced by Schwartz, Tolbert and co-workers (Figure 4.1).[11] In this case energy flow along single polymer chains into the oriented, periodic component of

the composite material. The driving force for this energy flow arises from changes in polymer conformation; the short conjugation-length polymer segments outside the silica framework have a higher energy than the long conjugation-length polymer segments encapsulated within the channels. As a result, energy migration in this composite system produces a spontaneous increase in luminescence polarization with minimal decrease in fluorescence energy. Thus, nanometer-scale positional control achieved through host-guest chemistry and the sensitive optical properties of MEH-PPV (1) can be combined to control energy flow. Moreover, the strategy also allow to separate the role of interchain versus intrachain energy transfer in conjugated polymers, providing valuable information for the optimization of polymer-based optoelectronic devices.

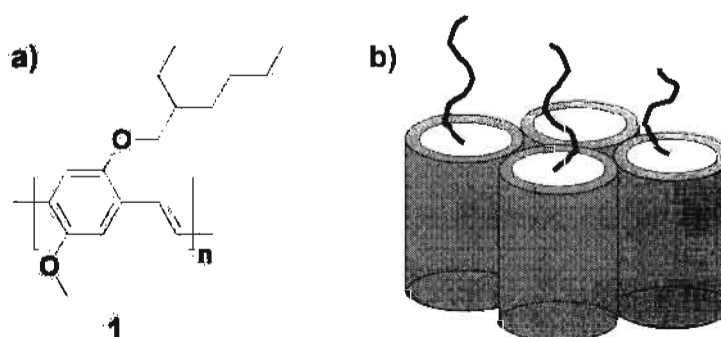FIGURE 4.1. a) Chemical structure of MEH-PPV (1). b) Cartoon representation of semiconducting polymers encapsulated mesoporous silica composite materials. (adapted from ref. 11)

Förster energy transfer mechanism in blends of conjugated materials is widely exploited for the design of organic light-emitting diodes.[2-5] This strategy offers several advantages that makes their use as a more attractive option. For

example, the strategy based on energy transfer will ensure enhanced electro-optical properties in the blends of conjugated materials by reducing the concentration dependent quenching effect of photoluminescence. Another important aspect is that the emission properties of the blends can be effectively tuned towards different regions of visible spectrum by using suitable combinations of host-guest conjugated materials. The efficiency of the energy transfer process in certain blends is such that total transfer can be achieved even at a very low concentration of guest molecules.[2-5] This is mainly due to the shorter donor-acceptor distances achieved in blends. According to the Förster theory the rate of energy transfer depends upon average donor acceptor distance 'R' (equation 4.1),[1,12]

$$k_{ET} = \frac{1}{\tau_D} \left(\frac{R_0}{R} \right)^6 \qquad ---- (4.1)$$

where τ_D is the lifetime of the donor in the absence of the acceptor, R_0 is the Förster distance, at which the energy transfer rate (k_{ET}) is equal to the decay rate of the donor in the absence of acceptor (τ_D^{-1}).

There are several reports in the literature concerning energy transfer in polymer-polymer or polymer-dye blends which suggest discrepancies with the Förster theory.[3-5] This deviation is partly due to the fact that the R^{-6} dependence arises from considerations of the dipole-dipole interaction between two isolated

molecules. This type of molecule-molecule interaction is unlikely to take place in polymer blends since the donor groups are not isolated but distributed along polymer chains. At the same time, the polymer chains may be arranged to form aggregates (refer to them as *surfaces*) where the acceptor molecules are embedded. A more appropriate description should account not only point-point dipole interactions but also point-surface or surface-surface interactions.

These different types of interactions lead to variations of the functional dependences in equation 4.1 as Hill et al., have demonstrated.[4b] They have studied the energy transfer between two LB films of poly(9,9-dioctylfluorene) (**2**, PFO) and poly(9,9-dioctylfluorene-*co*-benzothiadiazole) (**3**, PFO-BT) in which an energy transfer dependence $k_{ET} \propto R^{-2}$ is obtained. In polymer-polymer blends however, the difficulty arises from the random distribution of the donor and acceptor chromophores. Hence, estimation of the average donor-acceptor separation becomes extremely complicated.
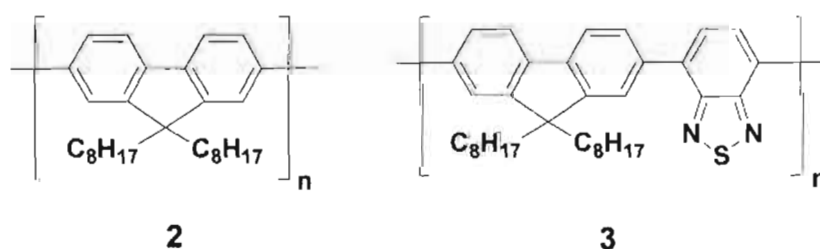

2   **3**

CHART 4.1.

Alternatively, polymer-dye blends offers a simplified insight to the problem.[4a] For example, in the blends of poly(9,9-dioctylfluorene) (2, PFO) and Nile Red (4), each Nile Red molecules is homogeneously distributed in the bulk polymer, occupying the volume of a hard sphere. This approximation leads to a dependence on the donor-acceptor separation $k_{ET} \propto R^{-3}$ which differs significantly from the point-point dipole interaction described by $k_{ET} \propto R^{-6}$. The R^{-3} dependence is, however, in agreement with the expression expected for a dipole-surface type interaction. This observation is explained by considering the aggregation of Nile red (4) molecules in the bulk. The clustering of the Nile Red (4) may lead to a screening of surface-dipole interactions surrounding the cluster, leading to an effective point-single surface interaction (Figure 4.2).

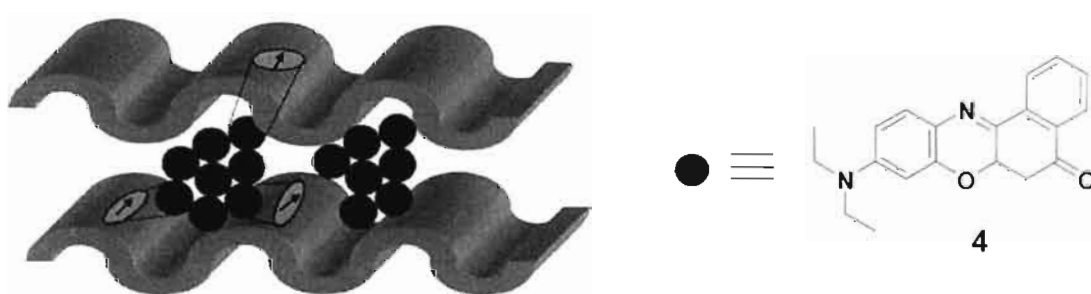FIGURE 4.2. Proposed energy transfer scenario in PFO (2)-Nile Red (4) blends. Two aggregates (represented by clustered spheres), appear embedded between two polymer planes. The chromophore groups in the PFO (2) chains (arrows enclosed in ovals) interact only with the nearest acceptor dipoles (arrows enclosed in circles) due to partial screening of the more distant dipoles contained in the aggregate. (adapted from ref. 4a)

Exciton migration and energy transfer process in π-conjugated polymers and conjugated polyelectrolytes (CPEs) has generated considerable interests among chemists.[6,13] It has been found that many ionic species quench the fluorescence of oppositely charged CPEs with extremely high sensitivity. This effect has been termed as "amplified quenching" or "superquenching".[13] The amplified quenching effect has been demonstrated to arise with quenchers that operate either by electron or energy transfer. The effect has been attributed to at least two features unique to the CPE-ionic quencher systems, namely, ion pairing between CPE chains and the oppositely charged quencher species and ultrafast intrachain diffusion of the exciton within the CPE.[14] Detailed studies showed that CPEs aggregates in aqueous solution and the amplified quenching effect is enhanced further in the aggregates.[14a,15] This observation suggests that interchain exciton diffusion may also play a role in amplified quenching. In order to address this issue recently Kleiman, Schanze and co-workers have carried out detailed energy transfer studies between sulfonate-substituted poly(phenyleneethynylene) (**5**) donor to a series of cationic cyanine dye acceptors, **6-8** (Chart 4.2).[6]

The steady-state and time-resolved fluorescence experiments revealed that the energy transfer quenching in the **5**-cyanine complexes occurs on two different time scales. The first one is a fast process occurring within the time scale of $\tau_1 < 4$ ps, (rate, $k_1 > 0.25$ ps^{-1}) and the second one is comparatively slow and has a rate comparable to the natural decay rate of the singlet exciton $\tau_2 \approx 20\text{-}1000$ ps ($k_2 \approx$

0.05–0.001 ps⁻¹). The energy transfer pathways in the 5-cyanine complexes are depicted in Figure 4.3.
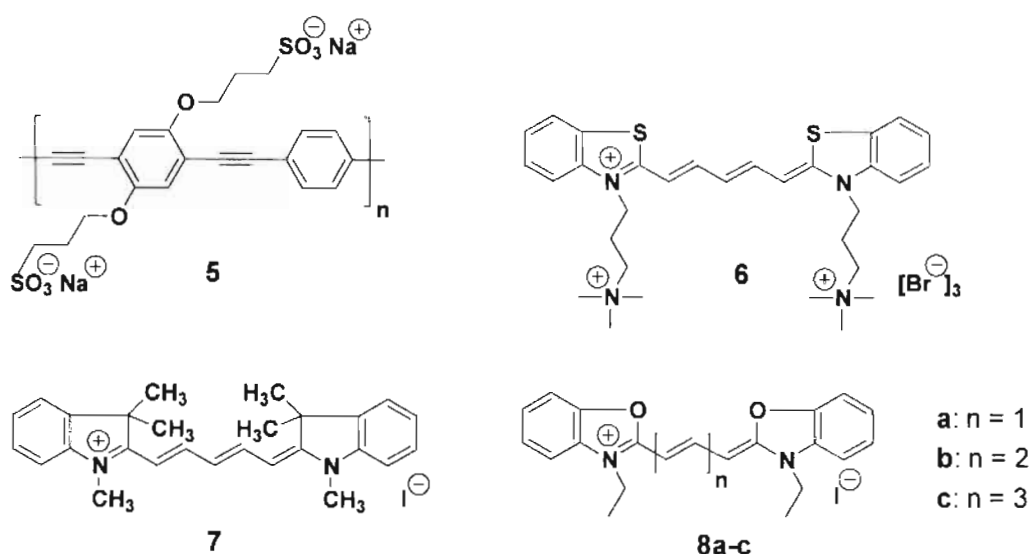

CHART 4.2.

In the presence of very low concentration of the dye molecules, polymer exists mainly as isolated ones (Figure 4.3a). In this situation a fraction of polymer excitons generated at a site near to the quenching radius of the dye binding site (i.e., an exciton produced in the dark region around the dye in Figure 4.3a) experience a rapid quenching (i.e., within 4 ps) due to a very fast energy transfer process. Whereas the exciton initially produced at a site distant from the prompt quenching radius of the dye are quenched more slowly due to the requirement for exciton diffusion along the chain (Figure 4.3a). At higher dye concentration polymer aggregation occurs and the possibility of interchain diffusion becomes significant (Figure 4.3b). Polymer aggregation significantly increases the

probability that an exciton will be produced within close proximity to a bound dye which increases the contributions of intra and interchain exciton diffusion to the overall quenching process.
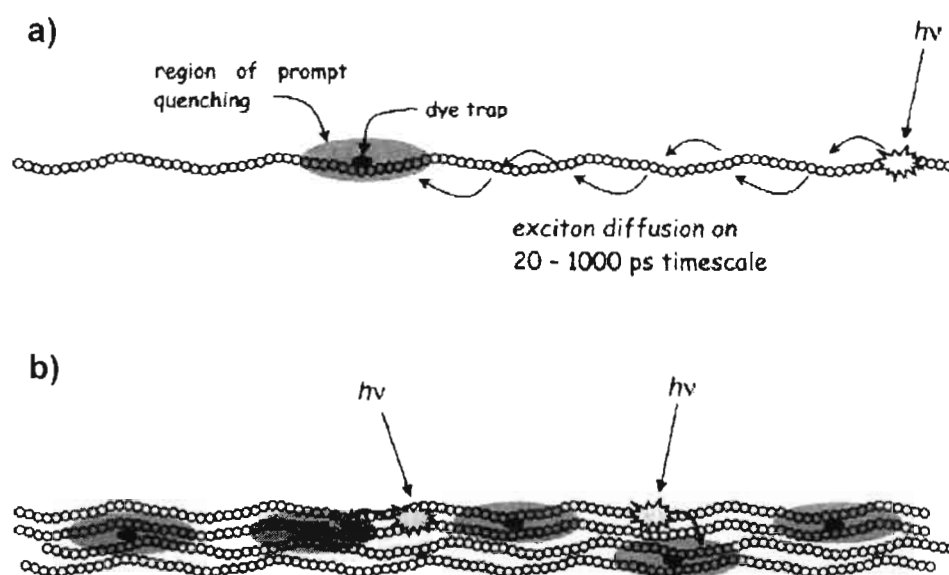

FIGURE 4.3. Cartoon depicting the processes involved in quenching of the exciton by complexed dye. a) Low dye concentrations result in unaggregated polymer chain. The gray ellipse represents the prompt quenching region. b) High dye concentrations result in aggregation of polymer chains. (adapted from ref. 6b)

In the previous chapter we have discussed the importance of supramolecular self-assembly in the energy transfer process between OPV donors and encapsulated acceptors.[16] In this context, the challenge is the design of acceptors which are compatible with the donor self-assembly, resulting in co-assembled aggregates and gels. In the present chapter we demonstrate that the encapsulation of an organic semiconducting molecular wire within an organogel scaffold facilitate fast exciton funneling and efficient energy transfer. We have

chosen a gel forming oligo(*p*-phenylenevinylene) derivative[17] **OPV1** as the energy transfer donor and a copolymer of phenylenevinylene and pyrrolylenevinylene (**PYPV**) as the acceptor (Figure 4.4). This donor-acceptor system is selected in view of their favorable self-assembly, absorption and emission properties which are ideal for energy transfer.
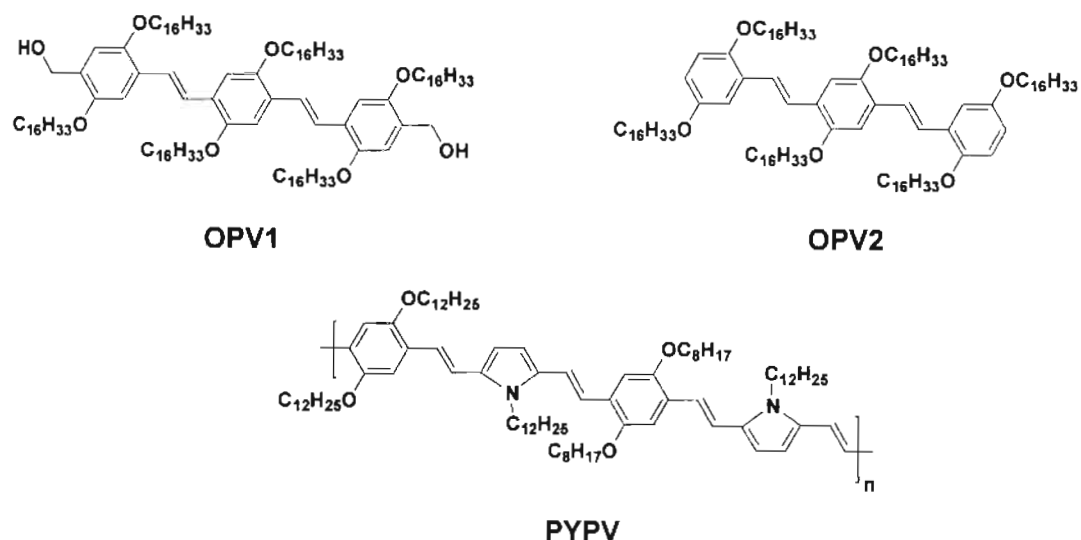

FIGURE 4.4. Molecular structures of the donors and the acceptor used in the present study.

4.3. Results and Discussion

4.3.1. Synthesis of Donor and Acceptor Molecules

Synthesis and characterization of **OPV1** is described in Chapter 2 of the thesis. Synthesis of the model derivative **OPV2**, is accomplished by adapting a known literature procedure.[17b] The phenylenevinylene-*co*-pyrrolylenevinylene oligomer (**PYPV**) was prepared as per Scheme 4.2. The bispyrrole derivative **16** was prepared by the Wittig-Horner-Emmons reaction of the bisphosphonate **15a**

and the N-doecylpyrrole-2-carbaldehyde (**11**) using NaH in a 64% yield.[18] The required N-dodecylpyrrole-2-carbaldehyde (**11**) was prepared by the Vilsmeier formylation of the N-dodecylpyrrole (**10**) in a 78% yield using a reported procedure (Scheme 4.1).[18]
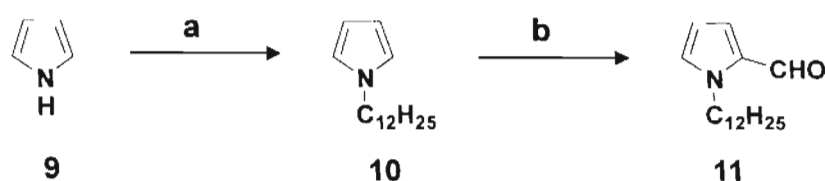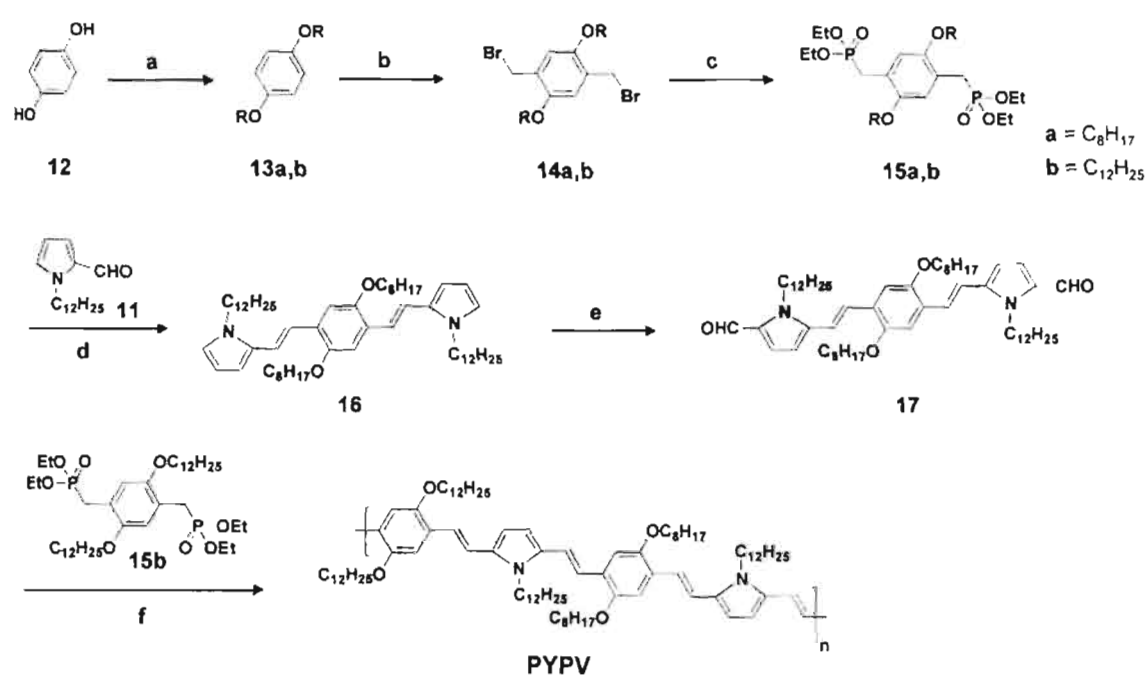

SCHEME 4.1. Reagents and conditions: a) 1-Bromododecane, potassium *t*-butoxide, THF, 27 °C, 21 h (88%). b) DMF, POCl₃, 5-10 °C, 45 min (78%).

The bisphosphonate derivatives (**15a,b**), were prepared by starting from hydroquinone **12** as reported earlier.[18] The dialkoxyhydroquinone **13a,b** were bromomethylated with 33% HBr in acetic acid under sonication to get the bisbromomethyl derivatives in 90% yields, which on reaction with triethyl phosphite gave the corresponding bisphosphonate derivatives (**15a,b**) (Scheme 4.2).

The oligomer **PYPV** was prepared by the Wittig-Horner olefination procedure (Scheme 4.2). For this purpose, the bispyrrole **16** was converted to the corresponding bisformyl derivative **17** by Vilsmeier formylation (62% yield).[18c] After column chromatographic purification, the formylated derivative **17** was characterized by spectral analysis. Reaction of the bisaldehyde **17** with the bisphosphonate **15b** in THF using NaH as base turned the initial green

fluorescence of the reaction mixture to red on progress of the reaction. The deep red solution obtained was concentrated and the oligomer was purified by repeated precipitation by adding methanol into a dichloromethane solution. The product is obtained as a dark red solid in a 53% yield.

SCHEME 4.2. Reagents and conditions: a) alkyl bromide, NaOH, DMF, 100 °C, 24 h (**13a**: 75%, **13b**: 65%). b) Paraformaldehyde, 33% HBr in CH$_3$COOH, glacial CH$_3$COOH, sonication, 4 h (**14a**: 90%, **14b**: 96%). c) P(OEt)$_3$, 100 °C, 12 h (**15a,b**: 90%). d) **15a**, NaH, THF, 70 °C, 10 h (64 %). e) DMF, POCl$_3$, 1,2-dichlorobenzene 0 °C, 3 h (62%). f) **17**, NaH, THF, 70 °C, 26 h (53 %).

The molecular weight of **PYPV** was determined by gel permeation chromatography (GPC) after calibration with standard polystyrene. Number average molecular weight (M_n) was 4358 with a polydispersity index of 1.12. ^{1}H NMR spectrum of **PYPV** showed the required resonance peaks of the aromatic and vinylic protons (δ 6.60-7.40 ppm), –NCH$_2$– and –OCH$_2$– protons at δ 4.04

and 4.47 ppm, respectively and the aliphatic protons (δ 0.85-1.90 ppm). In addition, ^{1}H NMR spectrum of **PYPV** showed weak resonance peaks at δ 9.46, corresponding to the terminal –CHO group. The all *trans* conformation of **PYPV** is established from the FT-IR spectral analysis. The absorption corresponding to the C–H out-of-plane vibration mode of the *trans*-vinylic group at 964 cm^{-1} is very strong when compared to the C–H out-of-plane mode of the *cis*-vinylic group at 863 cm^{-1}.[19]

4.3.2. Photophysical Properties of the OPV Self-Assemblies

The most important feature of the gelation of OPVs is the self-assembly induced modulation of the optical properties which strongly depend upon the solvents, variation in temperature and concentrations.[17] Figure 4.5 shows the variable temperature absorption and emission spectra of **OPV1**-cyclohexane gel (4 x 10^{-4} M). The temperature dependent absorption and fluorescence spectra of the **OPV1**-cyclohexane gel showed a transition from the self-assembled species to the molecularly dissolved species as the temperature is increased from 10-70 °C (Figure 4.5). For example, the intensity of the absorption maximum at 400 nm was increased upon increasing the temperature, with concomitant decrease in the intensity of the shoulder band at 463 nm through an isosbestic point at 433 nm (Figure 4.5a). Similarly, in the fluorescence spectra (λ_{ex} = 380 nm), the intensity of the broad red shifted emission between 500-700 nm decreases with the

simultaneous increase in the intensity of the emission bands at 456 nm and 479 nm (Figure 4.5b) when the temperature is increased from 10-70 °C.
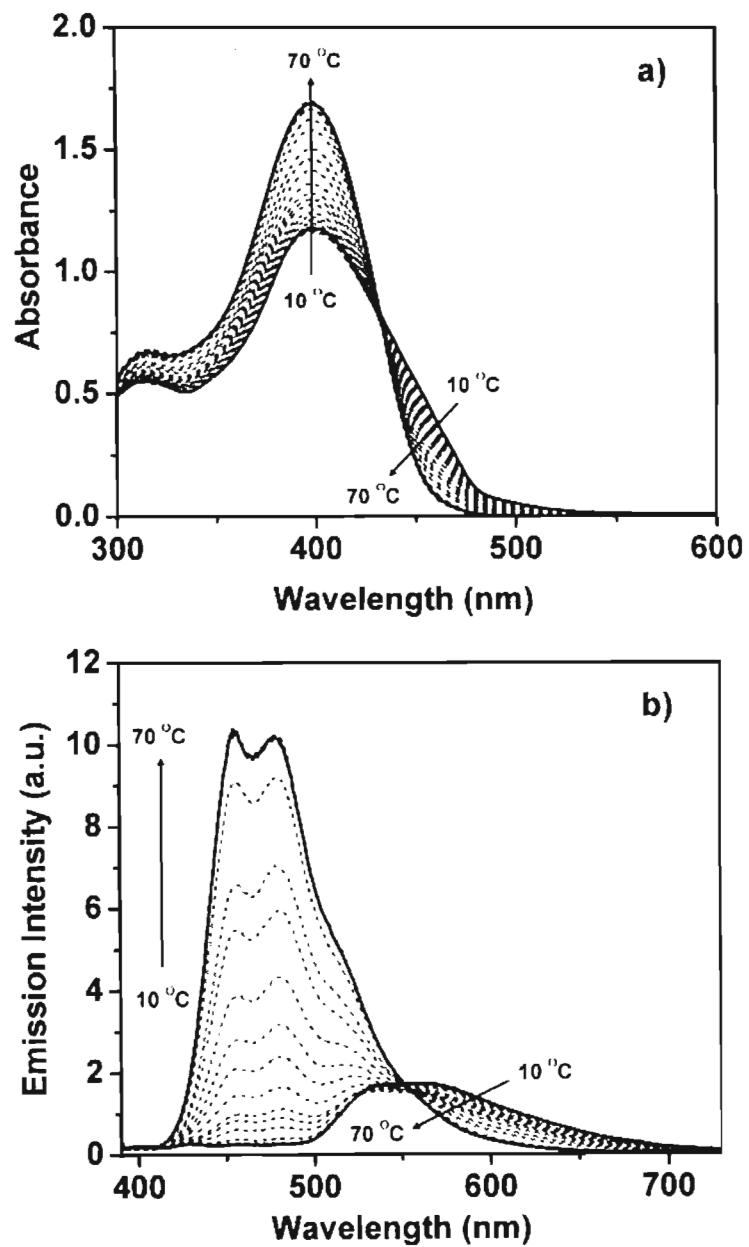

FIGURE 4.5. Temperature dependent a) absorption and b) fluorescence spectra (λ_{ex} = 380 nm) of **OPV1** cyclohexane gel [4 x 10^{-4} M], l = 1 mm. Spectra at 10 °C and 70 °C are highlighted with black solid line.

The large red shift in the emission spectra during the self-assembly of **OPV1** indicates the delocalization of the exciton across the self-assembly.[17b,20] In order to gain insight into the dynamics of the exciton migration between **OPV1** aggregates within the gel, detailed time-resolved anisotropy measurements were conducted. The two predominant pathways for the loss of anisotropy of organized donors are either by rotational motion or by energy migration.[1a,21] In the case of the self-assembled **OPV1** gel, fluorescence depolarization by rotational motion is least favoured and hence energy migration is the feasible pathway.[21c,22] Exciton migration within **OPV1** aggregates leads to loss of memory of the initial excitation polarization eventually resulting in no difference between the intensities of the emitted light which is polarized either parallel $(I_{\parallel})$ or perpendicular $(I_{\perp})$ to that of the excitation source. The time-dependent anisotropy r (t) in such a case is determined by the equation 4.2,[1a]

$$r \text{ (t)} = [I_{\parallel}(\text{t}) - G \, I_{\perp}(\text{t})] \, / \, [I_{\parallel}(\text{t}) + 2G \, I_{\perp}(\text{t})] \qquad \text{- - - - (4.2)}$$

where G is an experimentally determined correction factor for the instrumental anisotropy. Figure 4.6 shows the fluorescence anisotropy decay of the **OPV1** gel. The initial anisotropy value (r_0) is 0.32 with a decay time τ_r = 78 ps which rapidly lose the anisotropy memory and plateau at r_{∞} = 0.04. The anisotropy decay time τ_r renders an estimate of the rate of the energy migration (k_{EM}) from higher to the lower energy state which is found to be 1.28×10^{10} s^{-1}. The extremely fast

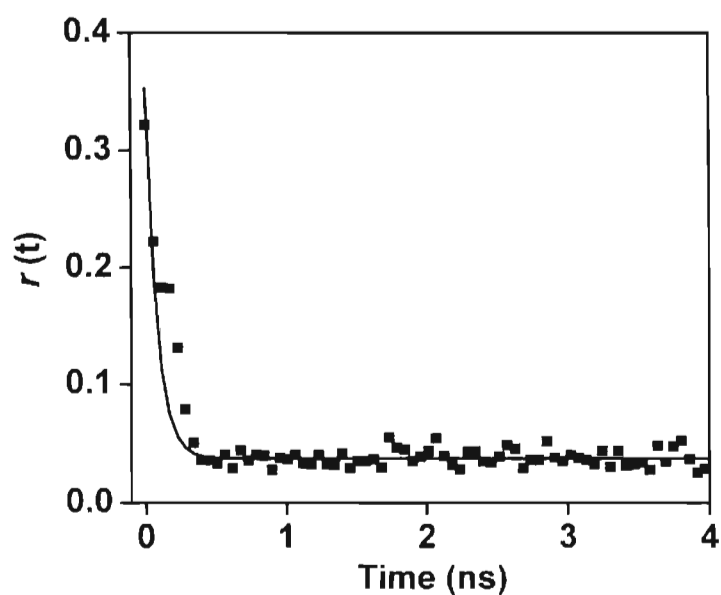depolarization is an indication of the fast interchromophore singlet exciton migration.[21]

FIGURE 4.6. Time-resolved anisotropy decay (scattered symbols) and the fit (solid line) for the **OPV1**-cyclohexane gel [4 x 10^{-4} M], emission monitored at 537 nm. Path length of the cell, l = 1 mm, λ_{ex} = 375 nm.

The time resolved emission spectra (TRES) of **OPV1** gel in cyclohexane (4 × 10^{-4} M) at different time scales after 375 nm excitation are shown in Figure 4.7. At short time scales after excitation, recombination of excitons exhibited a broad emission with a shoulder at short wavelength region. With increase in time after excitation, the intensity of the shoulder bands in the short wavelength region is decreased with a red-shift of the emission. The spectrum obtained after 336 ps was almost identical to the steady state emission of the **OPV1** gel. The rapid decay of the higher energy shoulder bands and the dynamic red-shift of the emission within

short time scale are attributed to exciton migration from lower order aggregates (higher energy sites) to higher order aggregates (lower energy sites) of the self-assembled **OPV1** gel.[5b,20b,23]
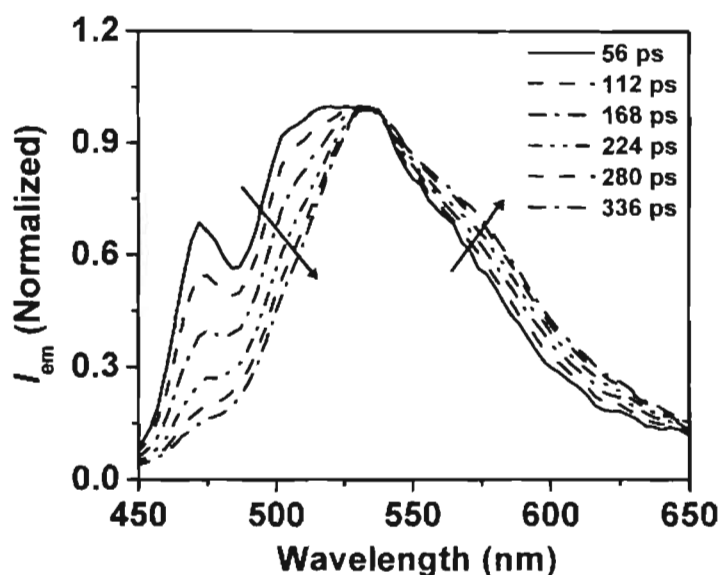

FIGURE 4.7. Time-resolved emission spectra of **OPV1**-cyclohexane gel [4 x 10^{-4} M], l = 1 mm, λ_{ex} = 375 nm.

The wavelength dependence of the emission decay of **OPV1** in the gel state is shown in Figure 4.8 which provides further evidence for energy migration. The emission at 478 nm decays faster than the higher wavelength (lower energy) emission and contains a fast decay component (79 ps). The lifetime decay monitored at 536 nm is apparently biexponential whereas the decay monitored at 574 nm emission is found to be multiexponential with a growth component (100 ps). Such delayed growth (Fig. 4.8 inset) within the initial short time scales

indicates migration of exctions from higher to the lower energy sites and the population of the excited states of the latter.[20b,23b]
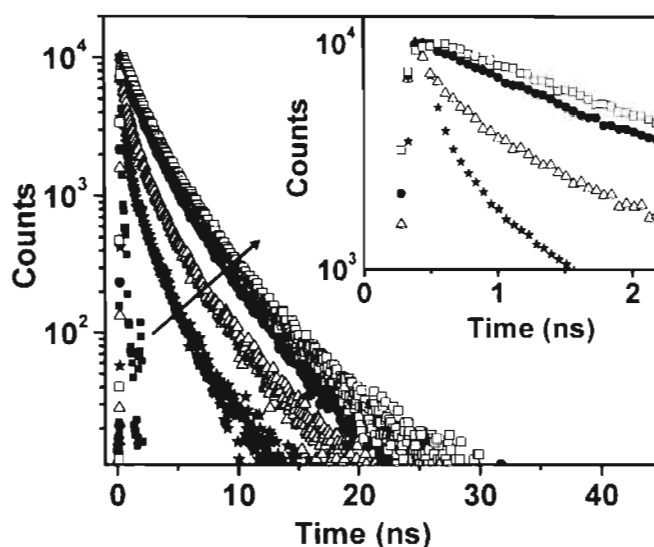

FIGURE 4.8. Emission decay curves of **OPV1**-cyclohexane gel [4 × 10⁻⁴ M] monitored at different wavelengths. The inset shows initial growth in the emission decay of **OPV1** gel within short time scales, monitored at different wavelengths after excitation. IRF (■), 478 nm (★), 504 nm (△), 536 nm (♦), 574 nm (□). l = 1 mm, λ_{ex} = 375 nm.

4.3.3. Morphological Studies of the PYPV Encapsulated Gels

Encapsulation of **PYPV** within the **OPV1** self-assembly is achieved by dissolving small quantities of the former (0-1.53 mol%) in a cyclohexane solution of the latter (1.12 x 10⁻³ M). The solution was heated to 70 °C and kept under room temperature to form a self-supporting soft gel. The scanning electron microscope (SEM) and atomic force microscope (AFM) analyses of the gel before and after the addition of **PYPV** revealed that the encapsulation of the molecular wire could not induce any significant morphological changes to the self-assembly

(Figure 4.9 and 4.10 respectively). In both cases the molecules self-assemble to form entangled tape-like architectures which bundle to form microsized soft organogel in cyclohexane.
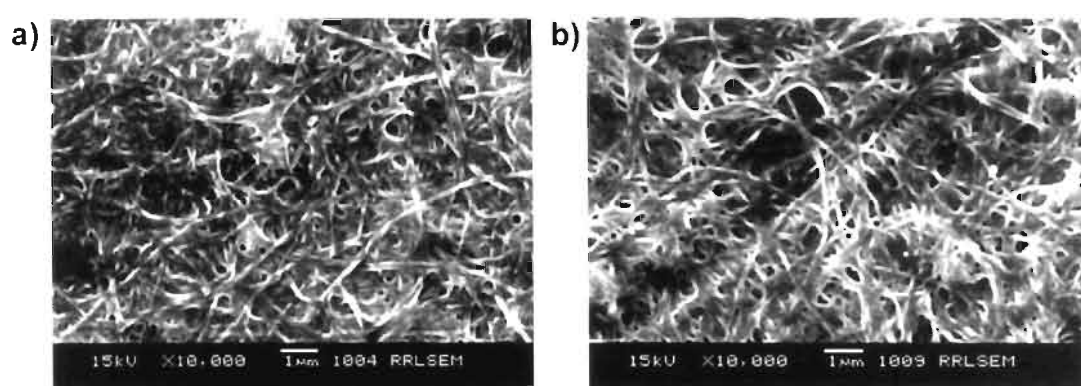

FIGURE 4.9. SEM picture of **OPV1-** cyclohexane [1.12 × 10⁻³ M] gel a) in the absence and b) presence of **PYPV** (1.53 mol%).
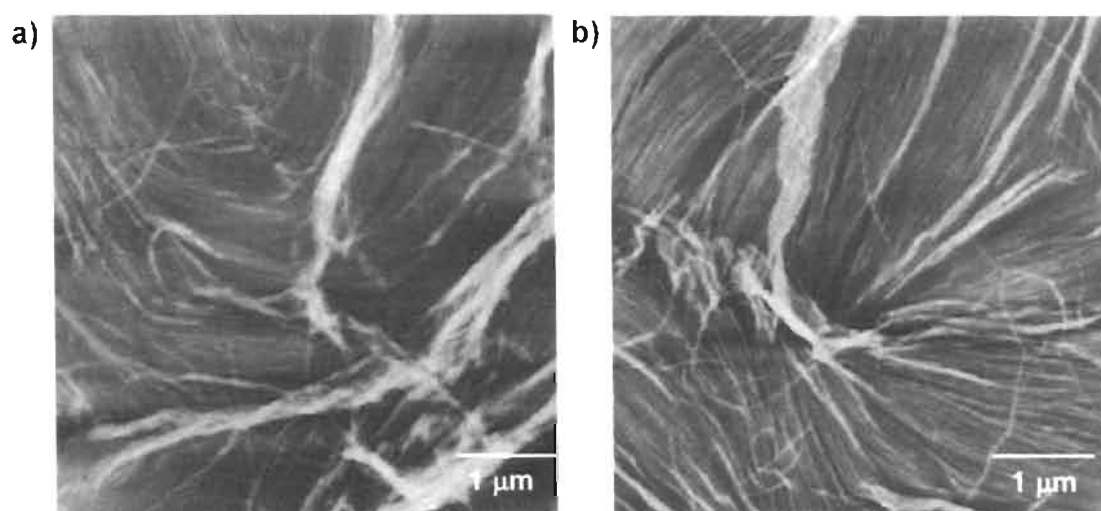

FIGURE 4.10. Tapping mode AFM images of **OPV1** [5 × 10⁻⁵ M] in cyclohexane a) in the absence and b) presence of **PYPV** (1.53 mol%) on mica surface (Z scale is 100 nm).

These structures are formed by the π-stacking of the hydrogen bonded supramolecular polymeric architectures having molecular weights of several kilodalton (kDa).[7b] A crude estimation of the molecular weight is as follows. A 10 × 10 nm area in a monolayer packing of the self-assembled tape has roughly 114 **OPV1** molecules. Each **OPV1** has a molecular weight of 1784.98 g/mol. Therefore the overall molecular weight of the self-assembly could be ca. 203 kDa which means that each self-assembled tape has a huge molecular weight. The chromophores are packed perpendicular to the growth of the long axis of the tapes (Figure 4.11).[7b] Gel melting studies of **OPV1**-cyclohexane gel (1.12×10^{-3} M) in the presence and in the absence of the acceptor **PYPV** showed that the gel stability has been marginally decreased by the encapsulation. The gel melting temperature of **OPV1** gel is found to be 70 °C which upon addition of **PYPV** (1.53 mol%) decreased to 60 °C.
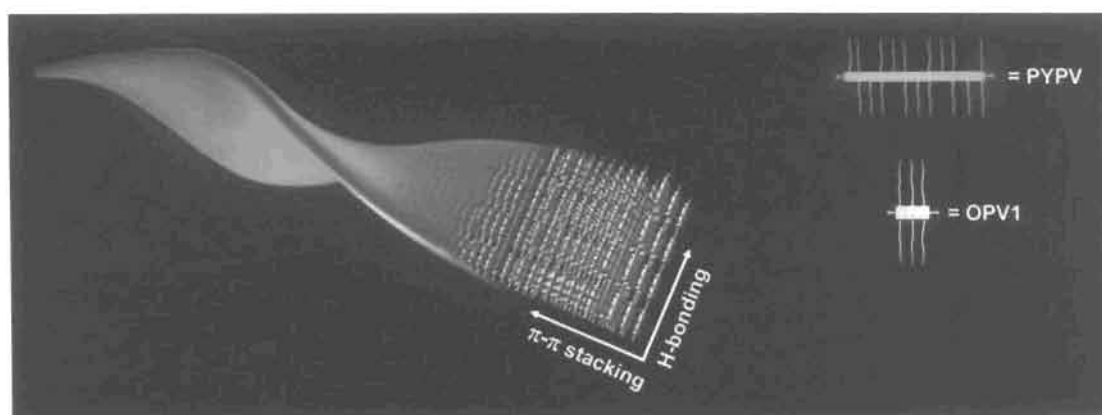
FIGURE 4.11. A cartoon representation of the **PYPV** encapsulated **OPV1** tape.

Molecular modeling studies of **PYPV** having a molecular weight of 4200 g/mol showed nonplanar geometry having kinks at different locations with an average length of 8 nm. There can be six benzene and six pyrrole units in a single **PYPV** chain, arranged in an alternate fashion (Figure 4.12).

FIGURE 4.12. Energy minimized structure of the molecular wire **PYPV** having a molecular weight of 4200 g/mol (TITAN software, Wavefunction, Inc). For computation, the alkyl side chains in the **PYPV** structure were replaced with methyl groups.

FIGURE 4.13. Cartoon representation of a completely encapsulated single molecular wire (**PYPV**) within **OPV1** gel.

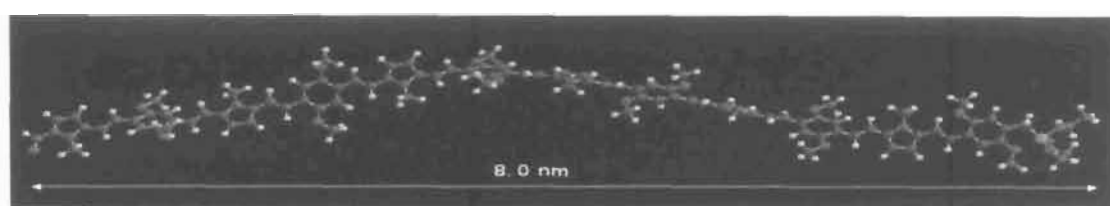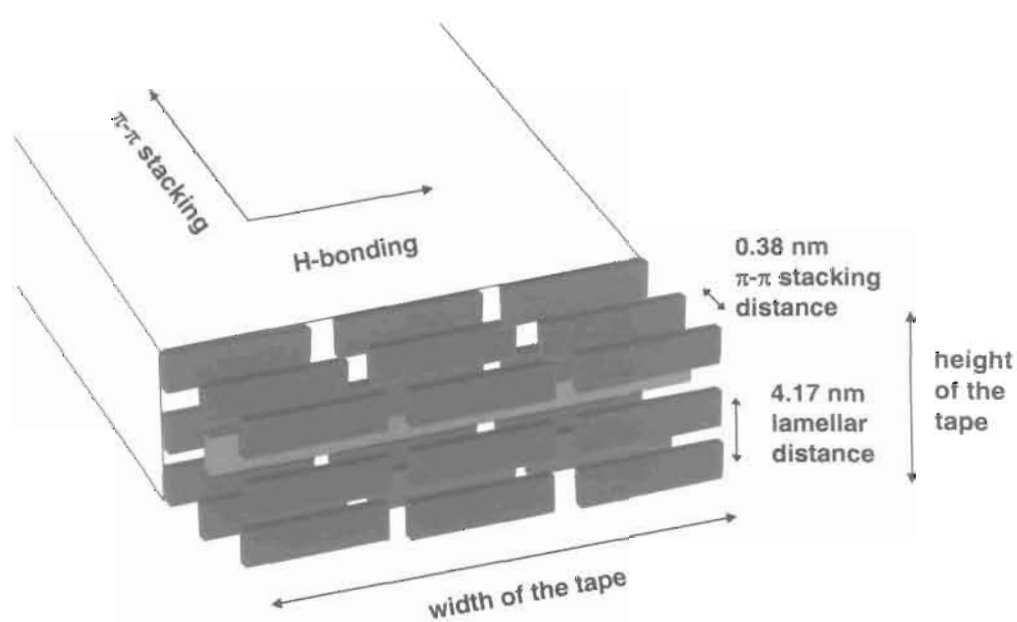However, the encapsulated molecular wire may have the possibility to exist in a planar conformation which may enhance the effective conjugation length. In principle, each **PYPV** molecule of ca. 8 nm in length could be wrapped by nearly six **OPV1** donors within the π-stacking distance, three each on both sides (Figure 4.13). Similarly, there can be a total of six donors, three each on the top and in the bottom. This means that each encapsulated molecular wire is in the immediate vicinity of nearly twelve donors. In addition, there could be another twelve donors around the acceptor thus making a total of nearly 24 donors within the Förster radius of each **PYPV**, which can facilitate effective transfer of the excitation energy, harvested from a long distance of the donor scaffold.

4.3.4. Fluorescence Resonance Energy Transfer (FRET) Studies

In the present system the emission from the self-assembled **OPV1** donor molecules showed considerable overlap with the absorption of the acceptor. The spectral overlap integral $J(\lambda)$ of the donor emission and the acceptor absorption was calculated using the equation 4.3,[1]

$$J(\lambda) = \frac{\int_0^\infty F_D(\lambda) \, \varepsilon_A(\lambda) \, \lambda^4 \, d\lambda}{\int_0^\infty F_D(\lambda) \, d\lambda} \quad \text{- - - - (4.3)}$$

where $F_D(\lambda)$ is the fluorescence intensity of the donor in the wavelength range λ to $\lambda + \Delta\lambda$, $\varepsilon_A(\lambda)$ is the extinction coefficient of the acceptor at λ. The spectral overlap

integral for the **OPV1** donor emission and **PYPV** acceptor absorption is $J(\lambda) =$ 5.83×10^{15} $M^{-1}cm^{-1}nm^4$.

Another essential criterion for a good donor acceptor energy transfer system is that the acceptor should have minimum absorption in the excitation wavelength of the donor. In the case of **OPV1-PYPV** system the donor is excited at 380 nm where **PYPV** molecules have minimum absorption (Figure 4.14) thereby minimizing the contribution from direct excitation of acceptor molecules in the overall efficiency of energy transfer. These features indicate that the present donor-acceptor system satisfies the necessary conditions for an efficient light harvesting system.
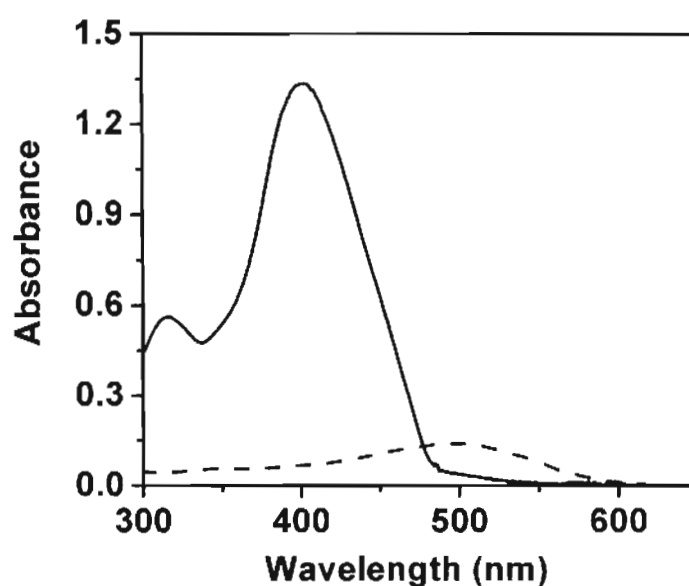

FIGURE 4.14. Absorption spectra of **OPV1** gel [4 x 10^{-4} M] (——) and that of **PYPV** [6.12 x 10^{-6} M] (- - -) in cyclohexane.

The simple way to visualize energy transfer is the direct observation of the emission colors of the gel before and after the encapsulation of the acceptor (Figure 4.15a and b inset). Fluorescence microscopy images of the gel fibers show bright yellow emission which turn into red upon encapsulation of **PYPV** (Figure 4.15a and b).

a)   **b)**   1.53 mol %   PYPV   10 μm   10 μm
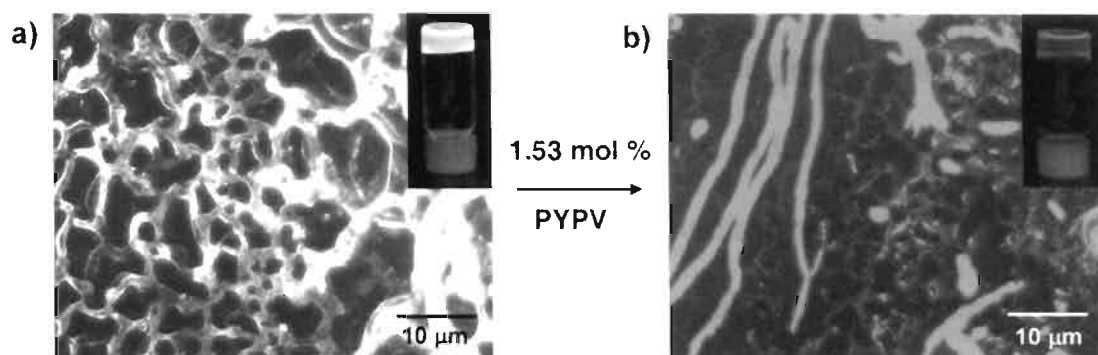
FIGURE 4.15. Fluorescence microscopy images of the drop-casted **OPV1**-cyclohexane gel [1.12 × 10⁻³ M] a) in the absence and b) presence of **PYPV** (1.53 mol%), inset shows photograph of the gel under respective condition when illuminated at 365 nm.

In Figure 4.16a the fluorescence spectra of **OPV1** (1×10^{-5} M) in the absence and presence of **PYPV** in cyclohexane ($\lambda_{ex} = 380$ nm) is shown. In the absence of **PYPV**, **OPV1** exhibited a broad emission with a maximum at 537 nm and another band at 567 nm, which is characteristic of the self-assembled OPV aggregates. When **PYPV** (1.15 mol%) is added into the self-assembly of **OPV1**, the intensity of the emission corresponding to the self-assembled species is decreased (ca. 73%) while the emission corresponding to the **PYPV** is appeared at around 622 nm. Direct excitation of a blank solution of **PYPV** (1.15 mol%) in the

absence of **OPV1** at 380 nm showed negligible fluorescence. This observation clearly indicates that the emission of **PYPV** is the result of FRET from OPV self-assembly to **PYPV**.

The compatibility of **PYPV** with the OPV self-assembly in nonpolar solvent allowed us to extend the energy transfer studies into the gel phase. Figure 4.16b shows the emission spectra of **OPV1** (4×10^{-4} M) and a mixture of **OPV1** and **PYPV** in the gel phase. **OPV1** has a broad emission in the gel phase with maxima at 537 and 565 nm. The observed emission is predominantly from the self-assembled OPV and the contribution of the emission from monomeric species is negligible. When excited at 380 nm in the presence of **PYPV** (1.53 mo%) emission maxima of the **OPV1** in the gel phase was completely quenched (ca. 94%) with the formation of strong fluorescence corresponding to **PYPV** (λ_{max} = 622 nm). Direct excitation of **PYPV** (1.53 mol%) in cyclohexane at 380 nm resulted in negligible emission indicating that the intense red emission of **PYPV** in the **OPV1** gel is due to excitation energy transfer. A 38 nm red shift in the energy transfer emission of the encapsulated **PYPV** is observed when compared to the emission upon direct excitation. This observation indicates that the encapsulated **PYPV** has better conjugation and the energy transfer emission from the acceptor with extended conjugation also contributes to the observed emission spectrum.
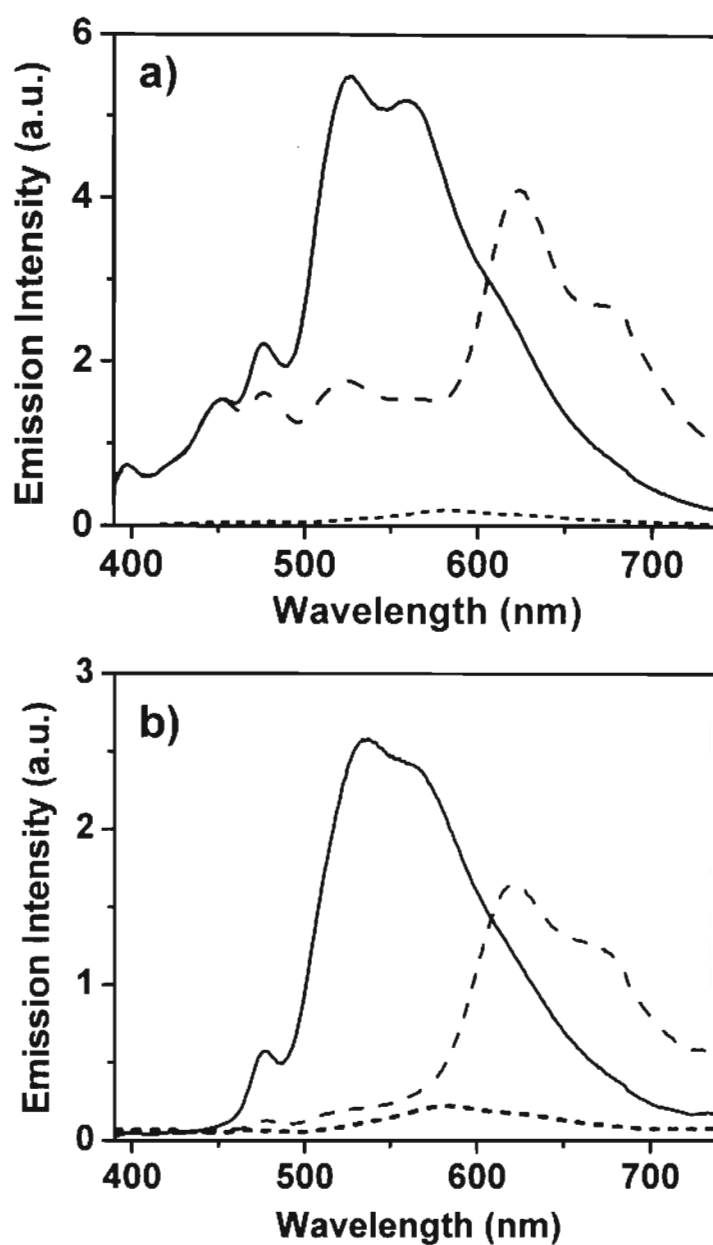
FIGURE 4.16. FRET quenching of fluorescence of **OPV1** in the presence of oligomer **PYPV**, λ_{ex} = 380 nm. Emission spectra of **OPV1** in the absence (——) and in the presence (– – –) of **PYPV**. Emission of **PYPV** (-----) in the absence of **OPV1**, on excitation at 380 nm is shown for a comparison. a) In cyclohexane solution **[OPV1]** = 1 x 10^{-5} M, **[PYPV]** = 1.15 mol% (l = 1 cm). b) In cyclohexane gel state **[OPV1]** = 4 x 10^{-4} M, **[PYPV]** = 1.53 mol% (l = 1 mm).

Figure 4.17 shows the relative fluorescence intensities of **PYPV** and **OPV1** when plotted against their molar ratio. The I_{emPYPV} /I_{emOPV1} value is a measure of the energy transfer efficiency,[16a,24] and the values obtained in the gel phase is greater than that in the solution state. In the solution state, the emission ratio exhibited a slow increase which plateau when the molar ratio reached ~ 1 x 10^{-2}. However, in the gel phase the emission ratio showed remarkable increment with increase in the molar ratio. When the ratio reached to 1.53 x 10^{-2}, the emission from the **OPV1** is completely quenched. The apparent efficiency of energy transfer estimated from the OPV fluorescence quenching profile was 94% for the gel phase and 73% for the solution. These results indicate that in the gel phase the energy transfer process is highly efficient.
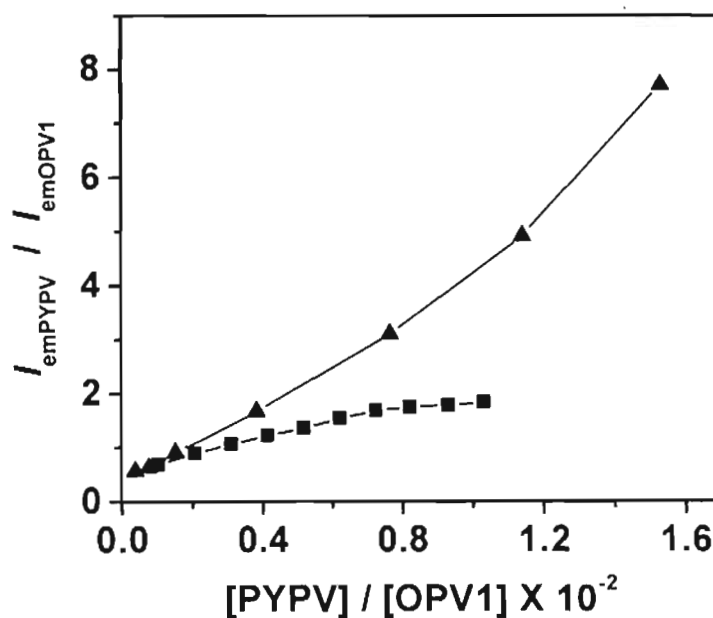

FIGURE 4.17. Plots of the relative fluorescence intensities against the molar ratio of **PYPV** and **OPV1** in cyclohexane gel (▲) and solution state (■).

The fluorescence decay profiles of **OPV1** gel in cyclohexane (4×10^{-4} M) in the presence of different amounts of **PYPV** are shown in Figure 4.18. In the absence of **PYPV**, **OPV1** gel exhibited biexponential decay with lifetimes $\tau_1 = 1.62$ ns (49%) and $\tau_2 = 4.43$ ns (51%). Shortening of the decay lifetimes of **OPV1** is observed with increase in the **PYPV** concentration. In the presence of 1.53 mol% of **PYPV**, **OPV1** exhibited fast biexponential decay with time constants of $\tau_1 = 0.72$ ns (56%) and $\tau_2 = 2.22$ ns (44%). Such shortening of the decay lifetimes of the donor in the presence of an acceptor provides evidence for nonradiative energy transfer and rules out the possibility of trivial (radiative) energy transfer (emission-reabsorption) mechanism.[2,4a,7b,25]

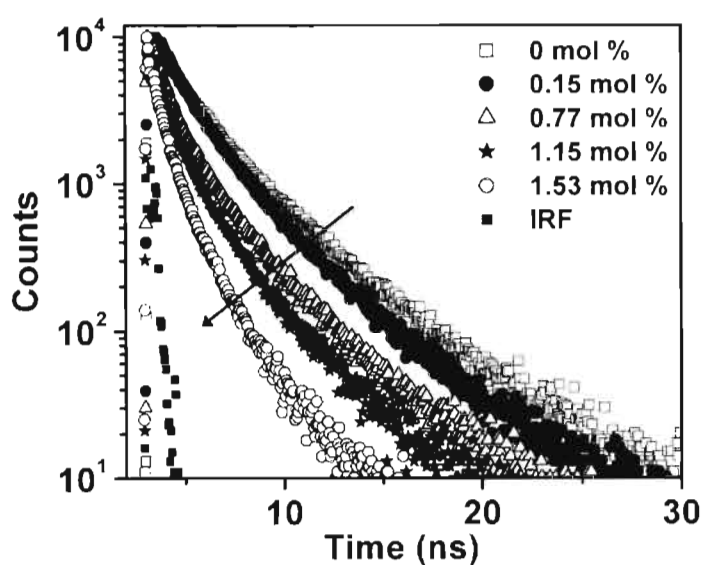

FIGURE 4.18. Fluorescence decay curves of **OPV1** cyclohexane gel [4×10^{-4} M] ($l = 1$ mm) with varying concentration of **PYPV** (0-1.53 mol%), emission monitored at 537 nm, $\lambda_{ex} = 375$ nm.

An estimate of the rate of energy transfer k_{ET} could be possible from the steady state fluorescence quenching data and the excited state lifetimes of the donor (τ_D) according to the equation 4.4 assuming that the observed quenching is due to energy transfer,[1a,26]

$$k_{ET} = [Q_{max}-1] / \tau_D \qquad \text{- - - (4.4)}$$

where $Q_{max} = I_D/I_{DA}$, is the maximum quenching observed in the fluorescence titration studies, I_D and I_{DA} are emission intensities of donor in the absence and presence of the acceptor. The average lifetime of the biexponential decay of the **OPV1** gel is calculated $<\tau> = 3.69$ ns.[1a] In the presence of 1.53 mol% of **PYPV**, the value of k_{ET} obtained is 2.99 ns^{-1}. The high energy transfer efficiency of **PYPV** encapsulated **OPV1** gel at very low concentration of the former is attributed to the fast exciton migration along the self-assembled tapes.[2-7,22,27a]

It is important to note that the self-organization of the donor-acceptor chromophores in the gel state is crucial for the energy transfer.[16,22,24,27,28] In order to study this aspect we extended the energy transfer studies to **OPV1** in chloroform and **OPV2** in cyclohexane, in which both the OPV derivatives exist as the monomeric species.[17] Steady state emission studies showed that even though significant spectral overlap is observed between the emission of the OPV donors with the absorption of acceptor **PYPV** (Table 4.1), energy transfer quenching of the donor emission is very marginal (Figure 4.19 and 4.20). In order to confirm the above mentioned observation we have carried out detailed lifetime studies of the
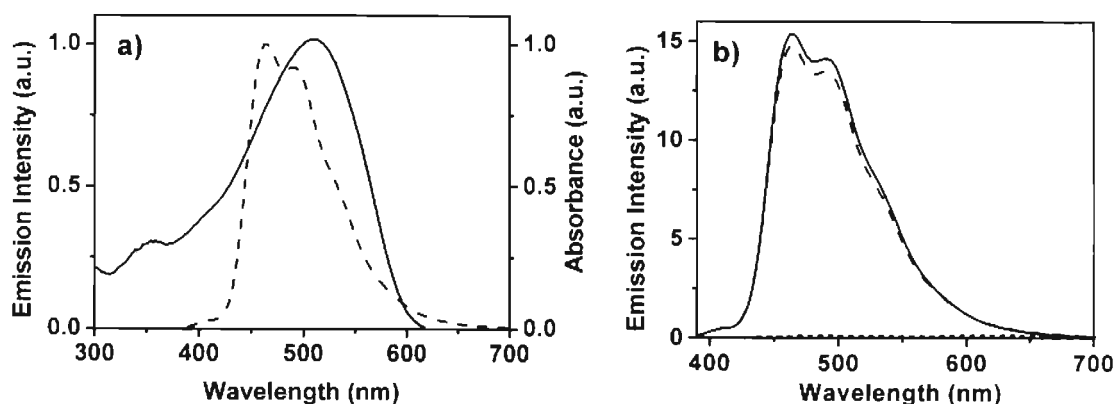
FIGURE 4.19. a) Spectral overlap of the emission of **OPV1** donor (– – –) and the absorption of **PYPV** (——) in chloroform. b) FRET quenching of the fluorescence of **OPV1** (———) in chloroform [1 × 10⁻⁵ M] in the presence of **PYPV** (1.15 mol%) (– – –). Fluorescence of **PYPV** alone (-----) is also shown for a comparison (l = 1 cm, λ_{ex} = 380 nm).
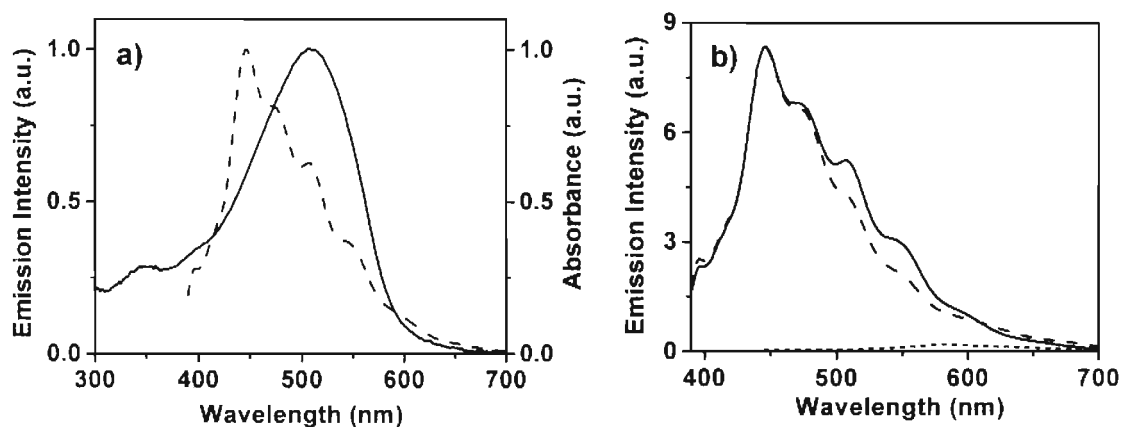
FIGURE 4.20. a) Spectral overlap of the emission of **OPV2** donor (– – –) and the absorption of **PYPV** (——) in cyclohexane. b) FRET quenching of the fluorescence of **OPV2** (———) in cyclohexane [1 × 10⁻⁵ M] in the presence of **PYPV** (1.15 mol%) (– – –). Fluorescence of **PYPV** alone (-----) is also shown for a comparison (l = 1 cm, λ_{ex} = 380 nm).

donors in the absence and presence of the acceptor **PYPV**. Lifetime studies showed no shortening of the decay profiles of the donor fluorescence even in the presence of maximum loading of the acceptor. These observations clearly indicate

that OPV donor molecules fail to bring about the energy transfer when they exist as monomeric species. Moreover, these results substantiate the importance of gel scaffold in organizing the donor-acceptor chromophores for efficient light harvesting process.

Table 4.1. Spectral overlap integrals and results of lifetime studies of **OPV1-2** under different experimental conditions.

Experimental condition	Spectral Overlap integral $J(\lambda)$ $M^{-1}cm^{-1}nm^4$	Life time values in ns	
		In the absence of PYPV	**In the presence of PYPV**
OPV1 in chloroform	1.02×10^6	1.55 (100%)	1.55 (100%)
OPV2 in cyclohexane	5.67×10^{15}	1.57 (100%)	1.54 (100%)

4.3.5. Temperature Dependent Energy Transfer Studies

An interesting feature of the present light harvesting system is the remarkable temperature dependency of the energy transfer efficiency and the consequent change in the emission color (Fig. 4.21). At 10 °C, excitation of the **PYPV** (1.53 mol%) encapsulated **OPV1** gel in cyclohexane (4×10^{-4} M) resulted in a strong red fluorescence at 622 nm. Interestingly, as the temperature is increased the intensity of 622 nm emission is decreased and a broad emission between 440 nm to 700 nm is formed. Surprisingly, at 54 °C a white emission was visible which upon further heating changed into blue (λ_{em} = 454 nm) emission of

the isotropic **OPV1** molecules. At 54 °C the self-assembly partially breaks into aggregates and single molecules. Energy transfer occurs partly to the molecular wire resulting in red emission along with the residual emission from self-assembled species and the emission of the single molecules. This leads to the presence of the fundamental RGB emission leading to white light when excited at 365 nm. Thus with increase in temperature, the red emission changes to blue through white in a reversible fashion like a chameleon.
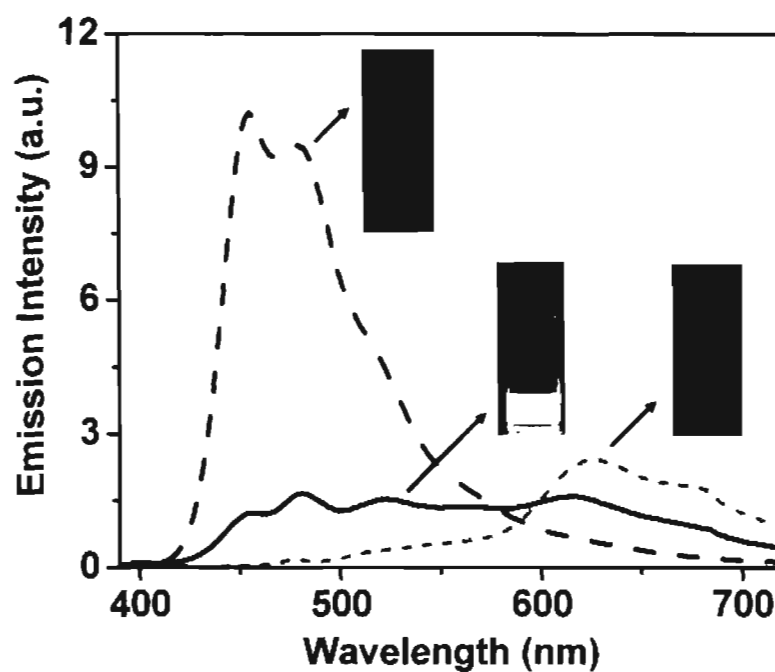

Figure 4.21. Temperature-dependence of energy transfer between **OPV1** [4 × 10^{-4} M] and **PYPV** (1.53 mol%) in cyclohexane gel (l = 1 mm, λ_{ex} = 380 nm). Emission spectrum at 10 °C (····), 54 °C (——) and 70 °C (– – –). Inset of the figure shows the emission under respective conditions upon illumination with a UV light (365 nm).

4.4. Conclusions

In conclusion we have demonstrated the design of an organic supramolecular light harvesting antenna by encapsulating an energy accepting molecular wire into an energy donating π-organogel scaffold. The encapsulated molecular wire (**PYPV**) is an efficient excitation energy trap when aligned with the donor in the gel state. Energy transfer is feasible only in the case of the gel and occurs exclusively from the donor (OPV) self-assembly to the molecular wires. These results are expected to open up further research interests in supramolecular light harvesting assemblies.

4.5. Experimental Section

4.5.1. Synthesis and Characterization

The details of melting point, FT-IR, ^{1}H NMR and ^{13}C NMR and MALDI-TOF instruments are described in the experimental section (section 2.5.1) of Chapter 2. Gel Permeation Chromatography (GPC) was carried out on a Shimadzu LC-8A GPC system equipped with a refractive index detector. Calibrations were done with standard polystyrene samples. Tetrahydrofuran (THF) was used as the eluent at a flow rate of 1 mL min^{-1} at 25 °C.

N-dodecylpyrrole (10). To a solution of potassium *tert*-butoxide (200 mmol) in dry THF (200 mL), pyrrole (**9**, 190 mmol) was added and stirred for 3 h to give a dark brown slurry of potassium pyrrole salt. To this, 18-crown-6 (18 mmol) was

added and stirred for 15 min. To the reaction mixture, 1-bromododecane (216

mmol) was added in dropwise and the stirring was continued for further 18 h. The

precipitated inorganic salt was filtered off and the solvent was removed under

reduced pressure. The reaction mixture was then extracted with dichloromethane

and washed several times with saturated brine and water. The organic layer was

then dried over anhydrous Na_2SO_4 and the solvent was removed by evaporation.

The crude product was then chromatographed on a silica gel column (100-200

mesh), using petroleum ether as the eluent. The product **10** is obtained as a brown

liquid.
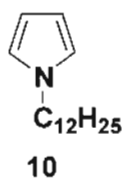
Yield: 88%; FT-IR (neat) v_{max}: 721, 1091, 1285, 1451,

1500, 1541, 2394, 2863 cm^{-1}; ^{1}H NMR (300 MHz,

CDCl$_3$) δ: 0.88 (t, J = 6.63 Hz, 3H, $-CH_3$), 1.18-1.76 (m,

20H, $-CH_2-$), 3.84 (t, J = 7.19 Hz, 2H, $-NCH_2-$), 6.12 (t,

J = 2.03 Hz, 2H, pyrrole-H), 6.63 (t, J = 2.02 Hz, 2H,

pyrrole-H) ppm; ^{13}C NMR (75 MHz, CDCl$_3$) δ: 13.93,

22.52, 26.67, 29.06, 29.29, 29.47, 29.59, 31.47, 31.68,

49.46, 107.70, 120.23 ppm; HRMS (FAB) calcd for

$C_{16}H_{29}N$ (M$^+$): 235.23, found: 235.69.

N-dodecylpyrrole-2-carboxaldehyde (11). To a solution of dry DMF (279.7

mmol) and POCl$_3$ (69.9 mmol) kept at 5-10 °C, N-dodecylpyrrole (**10**, 75 mmol)

in dry DMF (7 mL) was added slowly with stirring. The mixture was then stirred

at 10 °C for 45 min and then poured into crushed ice. The clear solution at 20-30

°C was neutralized with aqueous NaOH. The mixture was boiled for one minute.

The solution was then extracted with diethyl ether and the organic layer was dried

over anhydrous Na_2SO_4. Removal of the solvent gave a viscous liquid, which was

chromatographed over silica gel (100-200 mesh) using a mixture of petroleum

ether and ethyl acetate (95:5) to give N-dodecylpyrrole-2-carboxaldehyde, **11**.
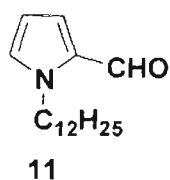
Yield: 78 %; FT-IR (neat) v_{max}: 744, 765, 1031, 1077,

1219, 1372, 1409, 1485, 1532, 1659, 1678, 2725, 2862,

2934 cm^{-1}; ^{1}H NMR (300 MHz, $CDCl_3$) δ: 0.85 (t, J =

6.61 Hz, 3H, $-CH_3$), 1.18-1.76 (m, 18H, $-CH_2-$), 4.29 (t,

J = 7.23 Hz, 2H, $-NCH_2-$), 6.19-6.21 (m, 1H, pyrrole-H),

6.90-6.93 (m, 2H, pyrrole-H), 9.52 (s, 1H, $-CHO$) ppm;

^{13}C NMR (75 MHz, $CDCl_3$) δ: 14.04, 22.64, 26.48, 29.29,

29.47, 29.59, 31.32, 31.89, 49.07, 109.37, 124.61, 131.09,

131.38, 179.12 ppm; HRMS (FAB) calcd for $C_{17}H_{29}NO$

(M^+): 263.22, found: 263.78.

Hydroquinone Dialkyl Ether Derivatives (13a and 13b). The hydroquinone

dialkyl ether derivatives **13a** and **13b** were synthesized by a procedure used for the

synthesis of 1,4-bis(hexadecyloxy)benzene derivative which is described in the section 2.5.1 of Chapter 2. Details of the analytical data are given below.

1,4-Bis(octyloxy)benzene (13a)
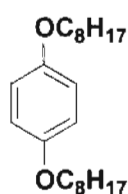
Yield: 75%; mp: 55-56 °C; FT-IR (KBr) v_{max}: 723, 820, 1040, 1108, 1225, 1285, 1385, 1455, 1500, 2859, 2954 cm^{-1}; ^{1}H NMR (300 MHz, CDCl$_3$) δ: 0.88 (t, J = 6.9 Hz, 6H, –CH_3), 1.29-1.85 (m, 24H, –CH_2–), 3.92 (t, J = 6.50 Hz, 4H, –OCH_2–), 6.82 (s, 4H, phenyl-H) ppm; ^{13}C NMR (75 MHz, CDCl$_3$) δ: 14.07, 22.61, 26.64, 29.42, 29. 46, 31.82, 68.72, 115.41, 127.52, 153.01 ppm; HRMS (FAB) calcd for C$_{22}$H$_{38}$O$_2$ (M$^+$): 334.29, found: 334.36.

OC$_8$H$_{17}$

OC$_8$H$_{17}$

13a

1,4-Bis(dodecyloxy)benzene (13b)
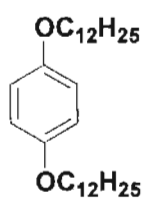
Yield: 65%; mp 74-75 °C; FT-IR (KBr) v_{max}: 718, 821, 1029, 1110, 1242, 1396, 1468, 1510, 2851, 2905 cm^{-1} ; ^{1}H NMR (300 MHz, CDCl$_3$) δ: 0.90 (t, J = 6.89 Hz, 6H, –CH_3), 1.2-1.4 (m, 40H, –CH_2–), 3.90 (t, J = 6.42 Hz, 4H, –OCH_2–), 6.85 (s, 4H, phenyl-H) ppm; ^{13}C NMR (75 MHz, CDCl$_3$) δ: 14.07, 22.72, 26.12, 29.35, 29.43, 29.62, 31.90, 68.71, 115.48, 127.63, 153.22 ppm; HRMS (FAB)

OC$_{12}$H$_{25}$

OC$_{12}$H$_{25}$

13b

calcd for $C_{30}H_{54}O_2$ (M$^+$): 446.41, found: 446.36.

General Procedure for the Preparation of 2,5-Bis(bromomethyl)-1,4-bis(alkyloxy)benzene (14).[18] To a suspension of the appropriate hydroquinone dialkyl ether derivatives (**13a** or **13b**, 10 mmol) in glacial acetic acid (35 mL), paraformaldehyde (30.25 mmol) was added and sonicated for 10 min. To this mixture, 33% HBr in acetic acid (31.12 mmol) was added and sonicated for 3 h. After a further addition of 5 mL glacial acetic acid followed by sonication for 30 min, the reaction mixture was poured into cold water. The precipitated product was filtered and dried to give the appropriate derivatives **14a** and **14b** in high yields.

2,5-Bis(bromomethyl)-1,4-bis(octyloxy)benzene (14a)
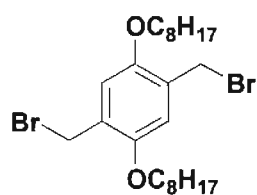
14a

Yield: 90%; mp 85-86 °C; FT-IR (KBr) v_{max}: 720, 865, 1040, 1118, 1224, 1268, 1309, 1408, 1470, 1516, 2860, 2950 cm^{-1}; ^{1}H NMR (300 MHz, CDCl$_3$) δ: 0.88 (t, J = 6.45 Hz, 6H, $-CH_3$), 1.29-1.85 (m, 24H, $-CH_2-$), 3.98 (t, J = 6.33 Hz, 4H, $-OCH_2-$), 4.52 (s, 4H, $-CH_2Br$), 6.84 (s, 2H, phenyl-H) ppm; ^{13}C NMR (75 MHz, CDCl$_3$) δ: 14.02, 22.61, 26.03, 29.32, 31.84, 69.03, 114.61, 127.52, 150.61 ppm; HRMS (FAB) calcd for $C_{24}H_{40}Br_2O_2$ (M$^+$): 518.14, found: 519.34.

2,5-Bis(bromomethyl)-1,4-bis(dodecyloxy)benzene (14b)
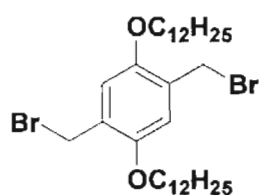
Yield: 96%; mp 88-89 °C; FT-IR (KBr) v_{max}: 723, 885, 1028, 1110, 1229, 1310, 1411, 1464, 1503, 2857, 2912 cm^{-1}; ^{1}H NMR (300 MHz, CDCl$_3$) δ: 0.89 (t, J = 6.30 Hz, 6H, –CH_3), 1.22-1.81 (m, 40 H, –CH_2–), 3.97 (t, J = 6.40 Hz, 4H, –OCH_2–), 4.52 (s, 4H, –CH_2Br), 6.86 (s, 2H, phenyl-H); ^{13}C NMR (75 MHz, CDCl$_3$) δ: 14.01, 22.70, 26.10, 29.32, 29.41, 29.60, 31.90, 69.12, 114.81, 127.63, 157.21 ppm; HRMS (FAB) calcd for C$_{32}$H$_{56}$Br$_2$O$_2$ (M$^+$): 630.26, found: 630.58.

General Procedure for the Preparation of 2,5-Bis(alkyloxy)-1,4-bis(benzyl)-phosphonates (15a and 15b). Compounds **15a** and **15b** were prepared by the reaction of 2,5-bis(bromomethyl)-1,4-bis(alkyloxy)benzene derivatives (**14**) (10 mmol) with 5 mL triethyl phosphite at 100 °C for 12 h. The unreacted triethyl phosphite was removed under reduced pressure.[18] The products obtained was used as such for further reactions.

2,5-Bis(octyloxy)-1,4-bis(benzyl)phosphonate (15a)

Yield: 90 %; FT-IR (neat): v_{max} 832, 967, 1027, 1217, 1397, 1515, 2880, 2969 cm^{-1}; ^{1}H NMR (300 MHz, CDCl$_3$) δ: 1.01 (t, J = 7.30 Hz, 6H, –CH_3), 1.31-1.90
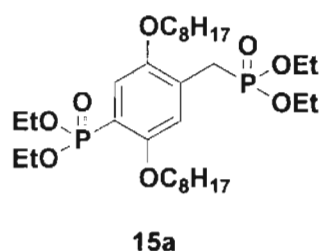
(m, 36H, $-CH_2-$), 3.31 (d, J = 21.00 Hz, 4H, $-CH_2-$P=O), 4.01-4.32 (m, 12H, $-OCH_2-$), 6.85 (s, 2H, phenyl-*H*) ppm; ^{13}C NMR (75 MHz, CDCl$_3$) δ: 14.01, 16.20, 16.23, 16.28, 16.31, 22.59, 25.24, 26.06, 27.10, 29.18, 29.32, 29.37, 29.40, 31.74, 61.71, 61.79, 61.83, 61.87, 61.91, 68.93, 114.85, 119.30, 119.37, 150.32 ppm; HRMS (FAB) calcd for C$_{32}$H$_{60}$O$_8$P$_2$ (M$^+$): 634.38, found: 634.73.

2,5-Bis(dodecyloxy)-1,4-bis(benzyl)phosphonate (15b)
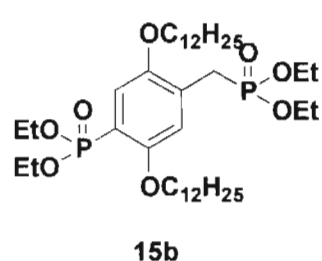
Yield: 90%; FT-IR (neat) v_{max}: 738, 968, 1033, 1219, 1472, 1510, 2861, 2934 cm^{-1}; ^{1}H NMR (300 MHz, CDCl$_3$) δ: 0.88 (t, J = 6.80 Hz, 6H, $-CH_3$), 1.21-1.75 (m, 52H, $-CH_2-$), 3.22 (d, J = 21.18 Hz, 4H, $-CH_2-$P=O), 3.92-4.02 (m, 12H, $-OCH_2-$), 6.9 (s, 2H, phenyl-*H*) ppm; ^{13}C NMR (75 MHz, CDCl$_3$) δ: 14.02, 16.23, 16.24, 16.32, 22.607, 25.21, 26.01, 27.13, 29.23, 29.32, 29.42, 29.51, 29.62, 31.83, 61.89, 61.94, 61.91, 68.92, 114.80, 119.31, 150.31 ppm; HRMS (FAB) calcd for C$_{40}$H$_{76}$O$_8$P$_2$ (M$^+$): 746.50, found: 747.10.

1,4-Bis{[(1-dodecyl)pyrrol-2-yl]vinyl}2,5-dioctyloxybenzene (16)[18]

A suspension of NaH (30 mmol) in THF (20 mL) was added slowly to a solution of the 2,5-bis(octyloxy)-1,4-bis(benzyl)phosphonate (**15a**, 5 mmol) and N-dodecyl pyrrole-2-carboxaldehyde (**11**, 10 mmol) in THF (40 mL). After refluxing for 10 h the highly fluorescent reaction mixture was cooled and THF was removed under reduced pressure to give a pasty residue. The residue was suspended in water and extracted with dichloromethane. The organic layer was washed with brine and dried over anhydrous Na₂SO₄. Removal of the solvent gave the crude product, which was further purified by column chromatography using a mixture of petroleum ether and ethyl acetate (9:1). The pure compound **16** was obtained as a greenish yellow solid.

16
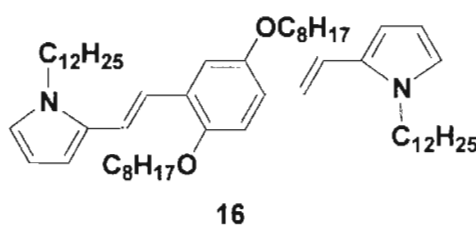
Yield: 64%; mp 91-92 °C; FT-IR (KBr) ν_{max}: 778, 962, 1509, 1094, 1295, 1360, 1392, 1490, 1628, 1656, 2863, 2931 cm⁻¹; ¹H NMR (300 MHz, CDCl₃) δ: 0.87 (t, J = 6.7 Hz, 12H, –CH_3), 1.24-1.79 (m, 64H, –CH_2–), 3.95 (t, J = 6.63 Hz, 4H, –NCH_2–), 4.01 (t, J = 7.0 Hz, 4H, –OCH_2–), 6.14 (m, 2H, pyrrole-*H*), 6.48 (d, J = 4.05 Hz, 2H, pyrrole-*H*), 6.66 (d, J = 4.02 Hz, 2H, pyrrole-*H*), 6.95 (s, 2H, phenyl-*H*), 7.06 (d, J = 15.66 Hz, 2H, vinyl-*H*), 7.09 (d, J = 15.56 Hz, 2H,

vinyl-*H*) ppm; ^{13}C NMR (75 MHz, CDCl$_3$) δ: 14.10, 22.67, 26.28, 26.87, 29.64, 29.28, 29.34, 29.45, 31.57, 31.09, 47.08, 69.45, 106.44, 108.13, 111.19, 117.79, 121.43, 122.40, 126.54, 132.09, 150.91 ppm. HRMS (FAB) calcd for C$_{58}$H$_{96}$N$_2$O$_2$ (M$^+$): 852.74, found: 852.69.

1,4-Bis{[(1-dodecyl-5-formyl)pyrrol-2-yl]vinyl}2,5-dioctyloxy benzene (17)

To a solution of **16** (0.5 mmol) in 1,2-dichlorobenzene (25 mL) at 0 °C, Vilsmeier reagent which was prepared by the slow addition of POCl$_3$ (1.4 mmol) into a flask containing DMF (5.8 mmol) at 0 °C, was added. The mixture was stirred at 0 °C for 3 h and poured into crushed ice. The clear solution was heated at 20-30 °C and then neutralized with sodium acetate. The mixture was boiled for one minute and cooled. The solution was then extracted with diethyl ether and the organic layer was dried over anhydrous Na$_2$SO$_4$. Removal of the solvent gave a viscous liquid, which was purified by column chromatography using a mixture of petroleum ether and ethyl acetate (8:2). The pure compound **17** was obtained as a yellow solid.
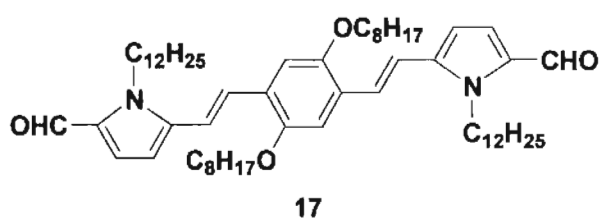

17

Yield: 62%; mp: 78-79 °C; FT-IR (KBr) ν$_{max}$: 784, 963, 1036, 1228, 1394, 1460, 1507, 1659, 2846, 2925 cm^{-1}; ^{1}H NMR (300 MHz, CDCl$_3$) δ: 0.86 (t, *J* =

6.60 Hz, 12H, –C*H₃*), 1.26-1.90 (m, 64H, –C*H₂*–), 4.06 (t, *J* = 6.44 Hz, 4H,

–NC*H₂*–), 4.47 (t, *J* = 7.15 Hz, 4H, –OC*H₂*–), 6.58 (d, *J* = 4.09 Hz, 2H, pyrrole-

H), 6.60 (d, *J* = 3.99 Hz, 2H, pyrrole-*H*), 6.99 (s, 2H, phenyl-*H*), 7.19 (d, *J* =

16.01 Hz, 2H, vinyl-*H*), 7.36 (d, *J* = 16.12 Hz, 2H, vinyl-*H*), 9.47 (s, 2H,

–C*H*O) ppm; ^{13}C NMR (75 MHz, CDCl₃) δ: 14.34, 23.08, 26.60, 27.04, 29.72,

29.81, 30.05, 31.91, 32.21, 32.33, 45.19, 69.31, 108.09, 112.28, 117.62, 124.95,

127.01, 127.99, 132.96, 141.46, 152.01, 178.35 ppm; HRMS (FAB) calcd.

$C_{60}H_{96}N_2O_4$ (M⁺): 908.74, found: 908.52.

Preparation of PYPV. A suspension of NaH (3.36 mmol) in THF (5 mL) was

added carefully to a solution of the bisphosphonate **15b** (0.56 mmol) and the

bisformyl derivative **17** (0.56 mmol) in THF (25 mL). After refluxing for 26 h the

highly fluorescent reaction mixture was cooled and THF was removed under

reduced pressure. The resultant residue was then extracted with dichloromethane

and washed several times with saturated brine and water. The organic layer was

dried over anhydrous Na₂SO₄ and the solvent was removed. The product thus

obtained was purified by repeated precipitation by adding methanol to a

dichloromethane solution which gave the oligomer **PYPV** as dark red solid.

PYPV
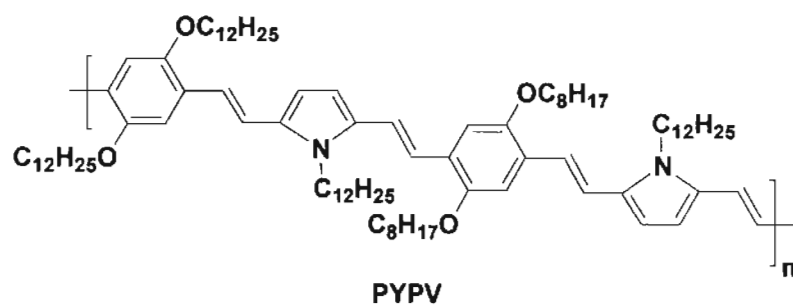
Yield: 53%; FT-IR (KBr) ν_{max}: 863, 964, 1036, 1142, 1208, 1401, 1500, 1653, 2853, 2925 cm^{-1}; ^{1}H NMR (300 MHz, CDCl$_3$) δ: 0.87 (br, –CH_3), 1.24-1.88 (m, –CH_2–), 4.04 (br, –NCH_2–), 4.47 (br, –OCH_2–), 6.61 (br, pyrrole-H), 6.93-7.40 (m, phenyl-H and vinyl-H), 9.46 (s, trace, terminal –CHO) ppm; M_n = 4358, M_w / M_n = 1.12 by GPC.

Preparation of OPV2. The title compound was prepared by Wittig-Horner reaction according to a reported procedure.[17b]

OPV2
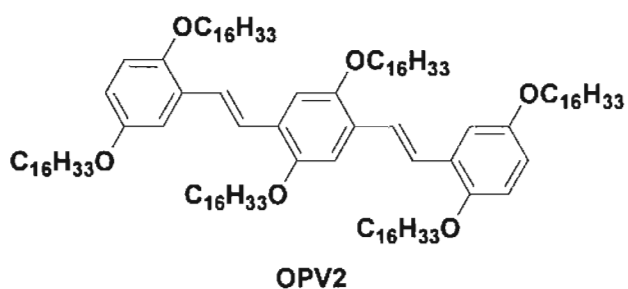
Yield: 90%; mp 106-107 °C; FT-IR (KBr) ν_{max}: 847, 965, 1074, 1223, 1254, 1347, 1398, 1429, 1465, 1506, 2840, 2923 cm^{-1}. ^{1}H NMR (300 MHz, CDCl$_3$) δ: 0.86-0.89 (m, 18H, –CH_3), 1.26-1.85 (m, 168H, –CH_2–), 3.94-4.04 (m, 12H, –OCH_2–), 6.71-6.87 (m, 4H, phenyl-H), 7.06-7.18 (m, 4H, phenyl-H), 7.34-7.42

(m, 4H, vinyl-*H*) ppm; ^{13}C NMR (75 MHz, CDCl$_3$) δ: 14.09, 22.68, 26.12, 26.22, 26.28, 29.36, 29.48, 29.58, 29.63, 29.71, 31.92, 68.63, 69.54, 110.79, 112.24, 113.41, 114.00, 127.41, 128.32, 129.29, 150.93, 151.55, 153.34 ppm; MALDI-TOF MS (MW = 1724.93): *m/z* = 1724.58 [*M*]$^+$.

4.5.2. Description of Experimental Techniques

Optical Measurements. The details of UV/Vis absorption spectrophotometer, spectrofluorimeter and time-correlated picosecond single photon counting (TCSPC) system are described in the section 2.5.2 of Chapter 2. Fluorescence lifetime, time resolved anisotropy and time resolved emission spectra (TRES) were measured using IBH (FluoroCube) TCSPC system. For the TRES measurements, the decay curves were measured at multiple emission wavelengths (450 to 650 nm) to construct a 3D dataset of counts versus time versus wavelength. Using the Fluorescence Measurement and Analysis Studio (FMAS) software, this 3D dataset was then sliced orthogonally to the time axis to produce 2D spectra of counts versus wavelength to visualize how the emission spectrum evolves during the fluorescence lifetime.

General Procedure for Energy Transfer Studies. Energy transfer studies were carried out by mixing appropriate volumes of OPVs from a stock solution to a cyclohexane solution of **PYPV**. The overall concentration of OPVs is maintained either at 4 x 10^{-4} M or 5 x 10^{-5} M depending upon the experimental condition

while the amount of **PYPV** varied from 0-1.53 mol%. For energy transfer studies in gel state, the donor and the acceptor molecules were mixed and heated to 70 °C. The solution was slowly cooled to room temperature to form the gel. The energy transfer was monitored by recording the emission of OPVs in the absence and presence of **PYPV** after excitation of OPVs at 380 nm.

Atomic Force Microscopy (AFM) Studies. The details of AFM instrument are described in the section 2.5.2 of Chapter 2. Samples for the imaging were prepared by drop casting the cyclohexane solution at the required compositions of **OPV1** (5 x 10^{-5} M) and **PYPV** (1.53 mo%) on freshly cleaved mica. Blank experiments with neat solvent on mica sheet were carried out to eliminate the possibility of any artifacts, prior to the measurements of the samples. AFM height and phase image analyses of several samples of each OPV solutions at different scanning areas were carried out to get better views of the supramolecular structures.

Scanning Electron Microscopy (SEM) Studies. Gel samples for the SEM analysis were prepared by dissolving the required amount of **OPV1** (1.12 × 10^{-3} M) in cyclohexane. Into this, 1.53 mol% of **PYPV** is added and the solution was heated and cooled to room temperature. Sheared gels were placed on sample studs and coated with gold by ion sputtering. SEM pictures were obtained on a JEOL 5600 LV scanning electron microscope with an accelerating voltage of 10 kV.

Fluorescent Microscopic Studies. Fluorescent microscopic images were recorded on a Leica-DMIR2 Optical Microscope using UV light (340-380 nm) as the excitation source. Samples were prepared by drop casting cyclohexane solution (concentration of the donor was kept at 1.12×10^{-3} M and concentration of the acceptor varied from 0-1.53 mol%) on a glass slide followed by slow evaporation.

4.6. References

1. (a) J. R. Lakowicz, *Principles of Fluorescence Spectroscopy* (2nd ed.), Kluwer Academic/Plenum Publishers: New York **1999**. (b) N. J. Turro, *Modern Molecular Photochemistry*, University Science Books: Sausalito, **1991**.

2. (a) M. A. Wolak, J. S. Melinger, P. A. Lane, L. C. Palilis, C. A. Landis, J. Delcamp, J. E. Anthony, Z. H. Kafafi, *J. Phys. Chem. B* **2006**, *110*, 7928. (b) L. C. Palilis, J. S. Melinger, M. A. Wolak, Z. H. Kafafi, *J. Phys. Chem. B* **2005**, *109*, 5456. (c) M. A. Wolak, B.-B. Jang, L. C. Palilis, Z. H. Kafafi, *J. Phys. Chem. B* **2004**, *108*, 5492.

3. (a) E. Hennebicq, G. Pourtois, G. D. Scholes, L. M. Herz, D. M. Russell, C. Silva, S. Setayesh, A. C. Grimsdale, K. Müllen, J.-L. Brédas, D. Beljonne, *J. Am. Chem. Soc.* **2005**, *127*, 4744. (b) E. J. W. List, C. Creely, G. Leising, N. Schulte, A. D. Schluter, U. Scherf, K. Müllen, W. Graupner, *Chem. Phy. Lett.* **2000**, *325*, 132. (c) E. J. W. List, C. Creely, G. Leising, N. Schulte, A. D. Schluter, U. Scherf, K. Müllen, W. Graupner, *Synth. Met.* **2001**, *119*, 659. (d)

S. Tasch, E. J. W. List, O. Ekström, W. Graupner, G. Leising, P. Schlichting, U. Rohr, Y. Geerts, U. Scherf, K. Müllen, *Appl. Phy. Lett.* **1997**, *71*, 2883.

4. (a) J. Cabanillas-Gonzalez, A. M. Fox, J. Hill, D. D. C. Bradley, *Chem. Mater.* **2004**, *16*, 4705. (b) J. Hill, S.Y. Heriot, O. Worsfold, T.H. Richardson, A.M. Fox, D.D.C. Bradley, *Synth. Met.* **2003**, *139*, 787. (c) A. R.; Buckley, M. D. Rahn, J. Hill, J. Cabanillas-Gonzalez, A. M. Fox, D. D. C. Bradley, *Chem. Phys. Lett.* **2001**, *339*, 331. (d) G. Cerullo, S. Stagira, M. Zavelani-Rossi, S. De Silvestri, T. Virgili, D. G. Lidzey, D. D. C. Bradley, *Chem. Phys. Lett.* **2001**, *335*, 27. (e) T. Virgili, D. G. Lidzey, D. D. C. Bradley, *Adv. Mater.* **2000**, *12*, 58.

5. (a) H. Wiesenhofer, D. Beljonne, G. D. Scholes, E. Hennebicq, J.-L. Brédas, E. Zojer, *Adv. Funct. Mater.* **2005**, *15*, 155. (b) K. Brunner, J. A. E. H. van Haare, B. M. W. Langeveld-Voss, H. F. M. Schoo, J. W. Hofstraat, A. van Dijken, *J. Phys. Chem. B* **2002**, *106*, 6834.

6. (a) J. G. Müller, E. Atas, C. Tan, K. S. Schanze, V. D. Kleiman, *J. Am. Chem. Soc.* **2006**, *128*, 4007. (b) C. Tan, E. Atas, J. G. Müller, M. R. Pinto, V. D. Kleiman, K. S. Schanze, *J. Am. Chem. Soc.* **2004**, *126*, 13685.

7. (a) F. J. M. Hoeben, I. O. Shklyarevskiy, M. J. Pouderoijen, H. Engelkamp, A. P. H. J. Schenning, P. C. M. Christianen, J. C. Maan, E. W. Meijer, *Angew. Chem., Int. Ed.* **2006**, *45*, 1232. (b) F. J. M. Hoeben, L. M. Herz, C. Daniel, P. Jonkheijm, A. P. H. J. Schenning, C. Silva, S. C. J. Meskers, D. Beljonne, R. T. Phillips, R. H. Friend, E. W. Meijer, *Angew. Chem., Int. Ed.* **2004**, *43*, 1976.

8. S. E. Webber, *Chem. Rev.* **1990**, *90*, 1469.

9. (a) M.-S. Choi, T. Yamazaki, I. Yamazaki, T. Aida, *Angew. Chem., Int. Ed.* **2004**, *43*, 150. (b) V. Balzani, P. Ceroni, M. Maestri, V. Vicinelli, *Curr. Opin. Chem. Biol.* **2003**, *7*, 657. (c) S. Hecht, J. M. J. Fréchet, *Angew. Chem., Int. Ed.* **2001**, *40*, 74. (d) A. Adronov, J. M. J. Fréchet, *Chem. Commun.* **2000**, 1701. (e) C. Devadoss, P. Bharathi, J. S. Moore, *J. Am. Chem. Soc.* **1996**, *118*, 9635.

10. (a) G. Calzaferri, S. Huber, H. Maas, C. Minkowski, *Angew. Chem., Int. Ed.* **2003**, *42*, 3732. (b) C. Minkowski, G. Calzaferri, *Angew. Chem., Int. Ed.* **2005**, *44*, 5325.

11. T.-Q. Nguyen, J. Wu, V. Doan, B. J. Schwartz, S. H. Tolbert, *Science* **2000**, *288*, 652.

12. T. Förster, *Ann. Phys.* **1948**, *2*, 55.

13. (a) D. Whitten, L. Chen, R. Jones, T. Bergstedt, P. Heeger, D. McBranch, In *Optical Sensors and Switches*; V. Ramamurthy, K. S. Schanze, Eds.; Marcel Dekker, New York, **2001**, p 189. (b) Q. Zhou, T. M. Swager, *J. Am. Chem. Soc.* **1995**, *117*, 12593.

14. (a) B. S. Harrison, M. B. Ramey, J. R. Reynolds, K. S. Schanze, *J. Am. Chem. Soc.* **2000**, *122*, 8561. (b) L. Chen, D. W. McBranch, H.-L. Wang, R. Helgeson, F. Wudl, D. G. Whitten, *Proc. Natl. Acad. Sci. U. S. A.* **1999**, *96*, 12287.

15. (a) M. R. Pinto, B. M. Kristal, K. S. Schanze, *Langmuir* **2003**, *19*, 6523. (b) C. Tan, M. R. Pinto, K. S. Schanze, *Chem. Commun.* **2002**, 446. (c) L. H. Chen, S. Xu, D. McBranch, D. Whitten, *J. Am. Chem. Soc.* **2000**, *122*, 9302.

16. (a) V. K. Praveen, S. J. George, R. Varghese, C. Vijayakumar, A. Ajayaghosh, *J. Am. Chem. Soc.* **2006**, *128*, 7542. (b) A. Ajayaghosh, S. J. George, V. K. Praveen, *Angew. Chem., Int. Ed.* **2003**, *42*, 332.

17. (a) V. K. Praveen, S. J. George, A. Ajayaghosh, *Macromol. Symp.* **2006**, *241*, 1. (b) S. J. George, A. Ajayaghosh, *Chem. −Eur. J.* **2005**, *11*, 3217. (c) A. Ajayaghosh, S. J. George, *J. Am. Chem. Soc.* **2001**, *123*, 5148.

18. (a) J. Eldo, A. Ajayaghosh, *Chem. Mater.* **2002**, *14*, 410. (b) M. Büschel, A. Ajayaghosh, J. Eldo, J. Daub, *Macromolecules* **2002**, *35*, 8405. (c) J. Eldo, E. Arunkumar, A. Ajayaghosh, *Tetrahedron Lett.* **2000**, *41*, 6241.

19. R. M. Silverstein, F. X. Webster, *Spectroscopic Identification of Organic Compounds* (6th ed.) Wiley-VCH: Weinheim, **1997**.

20. (a) P. Jonkheijm, F. J. M. Hoeben, R. Kleppinger, J. van Herrikhuyzen, A. P. H. J. Schenning, E. W. Meijer, *J. Am. Chem. Soc.* **2003**, *125*, 15941. (b) K.-Y. Peng, S.-A. Chen, W.-S. Fann, *J. Am. Chem. Soc.* **2001**, *123*, 11388.

21. (a) L. M. Herz, C. Daniel, C. Silva, F. J. M. Hoeben, A. P. H. J. Schenning, E. W. Meijer, R. H. Friend, R. T. Phillips, *Phys. Rev. B* **2003**, *68*, 045203/1. (b) J. Gierschner, H.-J. Egelhaaf, D. Oelkrug, *Synth. Met.* **1997**, *84*, 529. (c) H.-J. Egelhaaf, J. Gierschner, D. Oelkrug, *Synth. Met.* **1996**, *83*, 221.

22. M. Montalti, L. S. Dolci, L. Prodi, N. Zaccheroni, M. C. A. Stuart, K. J. C. Van Bommel, A. Friggeri, *Langmuir* **2006**, *22*, 2299.

23. (a) L. M. Herz, C. Silva, R. T. Philips, S. Setayesh, K. Müllen, *Chem. Phys. Lett.* **2001**, *347*, 318. (b) A. Watanabe, T. Kodaira, O. Ito, *Chem. Phys. Lett.* **1997**, *273*, 227.

24. T. Nakashima, N. Kimizuka, *Adv. Mater.* **2002**, *14*, 1113.

25. A. Ajayaghosh, C. Vijayakumar, V. K. Praveen, S. S. Babu, R. Varghese, *J. Am. Chem. Soc.* **2006**, *128*, 7174.

26. (a) A. M. Ramos, S. C. J. Meskers, E. H. A. Beckers, R. B. Prince, L. Brunsveld, R. A. J. Janssen, *J. Am. Chem. Soc.* **2004**, 126, 9630. (b) E. E. Neuteboom, E. H. A. Beckers, S. C. J. Meskers, E. W. Meijer, R. A. J. Janssen, *Org. Biomol. Chem.* **2003**, *1*, 198. (c) E. H. A. Beckers, P. A. van Hal, A. P. H. J. Schenning, A. El-ghayoury, E. Peeters, M. T. Rispens, J. C. Hummelen, E. W. Meijer, R. A. J. Janssen, *J. Mater. Chem.* **2002**, *12*, 2054.

27. (a) A. Del Guerzo, A. G. L. Olive, J. Reichwagen, H. Hopf, J.-P. Desvergne, *J. Am. Chem. Soc.* **2005**, *127*, 17984. (c) J.-H. Ryu, M. Lee, *J. Am. Chem. Soc.* **2005**, *127*, 14170. (d) S. Yamaguchi, I. Yoshimura, T. Kohira, S.-i. Tamaru, I. Hamachi, *J. Am. Chem. Soc.* **2005**, *127*, 11835.

28. (a) K. Sugiyasu, N. Fujita, S. Shinkai, *Angew. Chem., Int. Ed.* **2004**, *43*, 1229. (b) J. B. Beck, S. J. Rowan, *J. Am. Chem. Soc.* **2003**, *125*, 13922. (c) T. Sagawa, S. Fukugawa, T. Yamada, H. Ihara, *Langmuir* **2002**, *18*, 7223.

List of Publications

1. Gelation Assisted Light Harvesting via Selective Energy Transfer from Oligo(*p*-phenylenevinylene)-Based Self-Assembly to an Organic Dye.

    A. Ajayaghosh, S. J. George, V. K. Praveen

    Angew. Chem., Int. Ed. **2003**, *42*, 332–335.

2. Evolution of Nano- to Microsized Spherical Assemblies of a Short Oligo(*p*-phenyleneethynylene) into Superstructured Organogels.

    A. Ajayaghosh, R. Varghese, V. K. Praveen, S. Mahesh

    Angew. Chem., Int. Ed. **2006**, *45*, 3261–3264.

3. Self-Location of Acceptors as "Isolated" or "Stacked" Energy Traps in a Supramolecular Donor Self-Assembly: A Strategy to Wavelength Tunable FRET Emission.

    A. Ajayaghosh, C. Vijayakumar, V. K. Praveen, S. S. Babu, R. Varghese

    J. Am. Chem. Soc. **2006**, *128*, 7174–7175.

4. Self-Assembled π-Nanotapes as Donor Scaffolds for Selective and Thermally Gated Fluorescence Resonance Energy Transfer (FRET).

    V. K. Praveen, S. J. George, R. Varghese, C. Vijayakumar, A. Ajayaghosh

    J. Am. Chem. Soc. **2006**, *128*, 7542–7550.

5. Self-assembled Fibrillar Networks of Oligo(*p*-phenylenevinylene) Based Organogelators.

    V. K. Praveen, S. J. George, A. Ajayaghosh

    Macromol. Symp. **2006**, *241*, 1–8.

6. Vesicles to Helical Nanotubes: An Unprecedented "Sergeant and Soldiers" Effect in the Self-assembly of Oligo(*p*-phenyleneethynylene)s.

    A. Ajayaghosh, R. Varghese, S. Mahesh, V. K. Praveen

    Angew. Chem., Int. Ed. **2006**, *45*, 7729–7732.

7. Quadrupolar π-Gels: Sol-Gel Tunable Red-Green-Blue (RGB) Emission in Donor-Acceptor Type Oligo(*p*-phenylenevinylene)s.

    A. Ajayaghosh, V. K. Praveen, S. Srinivasan, R. Varghese

    Adv. Mater. **2007**, *19*, 411–415.

8. π-Organogels of Self-Assembled *p*-Phenylenevinylenes: Soft Materials with Distinct Size, Shape and Functions.

    A. Ajayaghosh, V. K. Praveen (Submitted to *Acc. Chem. Res.*).

9. Encapsulation of Molecular Wires in π-Organogels: A New Design of Efficient Supramolecular Light Harvesting Antennae with Color Tunable Emission.

    A. Ajayaghosh, V. K. Praveen, C. Vijayakumar, S. J. George (Submitted).

Posters Presented at Conferences

1. Oligo(*p*-phenylenevinylene) Derived Organogels: A Novel Class of Self-Assembled Nanostructures *via* Noncovalent Interactions.

    S. J. George, V. K. Praveen, A. Ajayaghosh

    4th CRSI National Symposium in Chemistry, NCL, Pune, February 01–03, 2002, Poster No. 53, (Best Poster Award).

2. Energy Harvesting Organogels: Selective Energy Transfer from OPV Based Self-assembly to Rhodamine B.

    S. J. George, V. K. Praveen, A. Ajayaghosh

    5th CRSI National Symposium in Chemistry, Chennai, February 07–09, 2003, Poster No. 94.

3. Novel Organogelators Derived from Oligo(*p*-phenylenevinylene) Self-Assembly.

    S. J. George, V. K. Praveen, A. Ajayaghosh

3rd International Symposium on Recent Trends in Photochemical Sciences, Trivandrum, January 05–07, 2004, Poster No. 39.

4. Fluorescent Oligo(*p*-phenylenevinylene) Gels *via* Cooperative Dipolar and π-Stacking Interactions.

    V. K. Praveen, S. J. George, A. Ajayaghosh

    6th CRSI National Symposium in Chemistry, IIT Kanpur, February 06–08, 2004, Poster No. 93.

5. Oligo(*p*-phenylenevinylene) Derived π-Electronic Organogels: A Novel Class of Functional Macromolecular Self-assemblies.

    V. K. Praveen, S. J. George, A. Ajayaghosh

    MACRO 2004, Fourth International Conference on Polymers for Advanced Technologies, Trivandrum, December 14–17, 2004, Poster No. 19.

6. Self-Assembled Helical Nanostructures of Gel Forming π-Conjugated Molecules: A Novel Approach to Optoelectronic Modulation and Light Harvesting.

    S. J. George, V. K. Praveen, R. Varghese, C. Vijayakumar, A. Ajayaghosh

    Indo-US Frontiers of Science Symposium, IISc Banglore, January 09–11, 2005, Poster No. 06.

7. Organic Semiconductor Based Molecular Wires as Energy Trap in the Design of Organogel Derived Light Harvesting Assembly.

    V. K. Praveen, A. Ajayaghosh

    7th CRSI National Symposium in Chemistry, February 04–06, 2005, IACS Kolkata, Poster No. 164.

8. Molecular Wires as Energy Trap in the Design of Organogel Derived Light Harvesting Assembly.

    V. K. Praveen, A. Ajayaghosh

1st Jawaharlal Nehru Centre (JNC) Research Conference on Chemistry of Materials, Quilon, October 01–03, 2005, Poster No. 20.

9. The "Sergeant and Soldiers" Approach in Chirality Induction and Amplification in Co-assembled π-Gels: Helicity Inversion and Stereo-mutation.

   R. Varghese, C. Vijayakumar, V. K. Praveen, A. Ajayaghosh

   8th CRSI National Symposium in Chemistry, IIT-Bombay, Mumbai, February 03–05, 2006, Poster No. 89.

10. Oligo(p-phenylenevinylene) Derived Light Harvesting π-Gels.

    V. K. Praveen, A. Ajayaghosh

    2nd National Organic Symposium Trust (NOST) Symposium for Research Scholars, ICG, Jaipur, October 11–14, 2006, Oral Presentation No. 48

11. Molecular Self-Assemblies as Energy Donor Scaffolds for Light Harvesting: A Rational Approach to Wavelength Tunable FRET Emission.

    C. Vijayakumar, V. K. Praveen, S. S. Babu, A. Ajayaghosh

    2nd Jawaharlal Nehru Centre (JNC) Research Conference on Chemistry of Materials, Quilon, October 29–31, 2006, Poster No. 18.

12. Quadrupolar π-Gels: Sol-Gel Tunable Red-Green-Blue (RGB) Emission in Donor- Acceptor Type Oligo(p-phenylenevinylene)s.

    V. K. Praveen, S. Srinivasan, R. Varghese, A. Ajayaghosh

    National Seminar on Frontiers in Organic Chemistry, University of Calicut, January 11–12, 2007, Poster No. 10, (Best Poster Award).